OPTIMISATION OF THE PERFORMANCE CHARACTERISTICS OF Cu-Al-Mo THIN FILM RESISTORS

MARTIN BIRKETT

A thesis submitted in partial fulfilment
of the requirements of the
University of Northumbria at Newcastle
for the degree of
Doctor of Philosophy

Research undertaken at
TT Electronics - Welwyn Components Ltd
Bedlington, Northumberland, UK

August 2009

Abstract

This thesis presents a novel approach to the manufacture of thin film resistors using a new low resistivity material of copper, aluminium and molybdenum, which under industrially achievable optimised process conditions, is shown to be capable of producing excellent temperature coefficient of resistance (TCR) and long term stability properties.

Previous developments in the field of thin film resistors have mainly centred around the well established resistive materials such as nickel-chromium, tantalum-nitride and chromium-silicon-monoxide. However recent market demands for lower value resistors have been difficult to satisfy with these materials due to their inherent high resistivity properties.

This work focuses on the development and processing of a thin film resistor material system having lower resistivity and equal performance characteristics to that of the well established materials.

An in depth review of thin film resistor materials and manufacturing processes was undertaken before the electrical properties of a binary thin film system of copper and aluminium were assessed. These properties were further enhanced through the incorporation of a third doping element, molybdenum, which was used to reduce the TCR and improve the electrical stability of the film.

Once the desired chemical composition was established, the performance of the film was then fine tuned through optimisation of critical manufacturing process stages such as sputter deposition, heat treatment and laser adjustment.

The results of these investigations were then analysed and used to generate a set of optimum process conditions, suitable for repeatedly producing thin film resistors in the 1 to 10Ω resistance range, to tolerances of less than ±0.25% and TCR values better than ±15ppm/^{o}C.

Contents

List of Figures

List of Tables

List of Symbols

Symbol	Definition	Unit
Upper case symbols		
B	experimental width of XRD peak	°
D	grain size	nm
G	trim gain	
K	Scherrer constant	
L	crystallite size	nm
PV	pre trim resistanve vlaue	Ω
R	grain boundary reflection co-efficient	
R_e	end resistance	Ω
R_i	initial resistance	Ω
Rs	sheet resistance	Ω/□
R_{TT}	trim target resistance value	Ω
T_c	condensation temperature	°C
TCR	temperature coefficient of resistance	ppm/°C
TCR_{av}	average TCR measured between 20° and 70°C	ppm/°C
TCR_{ex}	extended TCR measured between -55° and 125°C or 155°C	ppm/°C
T_m	melting temperature	°C
T_s	substrate temperature	°C
Lower case symbols		
b	XRD instrument resolution	°
d	film thickness	nm
h	surface roughness	nm
h_{cr}	critical thickness	nm
k	process parameters or factors	
l	film length	mm
p	specularity coefficient	
tc	treatment combinations	
w	film width	mm

Greek symbols

l	wavelength and mean free path (MFP)	nm
β	real width of XRD peak	°
θ	Bragg angle	°
ρ	resistivity	μΩcm
ρ_f	film resistivity	μΩcm
ρ_{gr}	grain boundary resistivity	μΩcm
ρ_o	bulk resistivity	μΩcm
ρ_r	residual resistivity	μΩcm
ρ_{sr}	surface roughness resistivity	μΩcm
ρ_{ss}	surface scattering resistivity	μΩcm
ρ_t	thermal resistivity	μΩcm
σ	conductivity	Sm^{-1}

Acknowledgements

Many people have helped me throughout the course of this project, and I would like to take this opportunity to thank some of them.

Firstly many thanks must go to my principle supervisor Dr Roger Penlington for his invaluable knowledge, guidance and encouragement and also his willingness to always make time for me.

I would also like to thank my other academic supervisors; Professor Nicola Pearsall, Dr Kian Tan and Dr Alasdair Wilson for their continued support and expert advice.

I acknowledge the School of Engineering for the analysis facilities that have been made available to me and in particular would like to thank Bob Best for his technical advice and help with SEM measurements.

Thanks to Welwyn Components Ltd for supporting this project and to all my colleagues in the Resistor Business Unit, including my industrial supervisor Dr Jason Brooker, for his help and encouragement along the way.

I also gratefully acknowledge the Royal Commission for the Exhibition of 1851 for the Industrial Fellowship award and the financial support it has brought to the project.

Finally I would like to thank my family, and in particular my wife, Sarah, for her continued support, tolerance and encouragement.

Declaration

I declare that the work contained in this thesis has not been submitted for any other award and that it is all my own work unless otherwise stated. This work was done in collaboration with TT Electronics – Welwyn Components Ltd, Northumberland.

Name:

Signature:

Date:

Excerpts from this work have been presented and published as follows:

1. Birkett, M, Brooker, J, Penlington, R, Wilson, A, Tan, K, (2006), "Effects of Annealing on the Electrical Properties of NiCr vs AlCu Thin Film Resistors prepared by DC Magnetron Sputtering", *Proceedings of the 20th Annual Capacitor and Resistor Technology Symposium, CARTS Europe 2006*, Bad Homburg, Germany, pg307-316.

2. Birkett, M, Brooker, J, Penlington, R, Wilson, A, Tan, K, (2007), "Electrical Characterisation of AlCuMo Thin Films Prepared by DC Magnetron Sputtering", *Proceedings of the 34th International Conference on Metallurgical Coatings and Thin Films, ICMCTF 2007, San Diego, USA,* pgTS-18.

3. Birkett, M & Oxley, S (2008), Invited Tutorial – "Discrete Resistor Technologies and Potential Future Improvements", *Proceedings of the 22nd Annual Capacitor and Resistor Technology Symposium, CARTS Europe 2008*, Helsinki, Finland, pg115-140.

4. Birkett M, Brooker J, Penlington R, Wilson W, Tan K, (2008), "Electrical Characterisation of AlCuMo Thin Films Prepared by DC Magnetron Sputtering", *IET Science, Measurement and Technology*, 2 (5), pg304-309.

To my daughter, Heidi Eve

born 27th of October 2007

Chapter 1

Introduction

1.1 INTRODUCTION

Nearly forty years ago the following statements were published:

> "*Most film-resistor requirements can be met with films having sheet resistance (Rs) in the range 10 to 1,000Ω/□. Resistors below 10Ω are rarely needed, whereas resistors with values in the MΩ range can be realised through the use of very long path lengths. There remains, however, a limited, but urgent, need for films with Rs greater than 1,000Ω/□, and much of current research on thin film resistors is devoted to finding a solution to this problem"* (Maissel, L & Glang, R, 1970), [1].

Indeed, it was not long until a solution to this problem of higher Rs was developed in the form of chromium silicon monoxide (Cr/30-50wt.%SiO [114]) thin film resistors. However the earlier part of this statement is no longer valid and one trend, which has continued to grow over recent years, is the need for thin film discrete resistors in the 100mΩ to 10Ω range.

Resistors possessing low resistivity and a small temperature co-efficient of resistance (TCR), which assure low and stable values of resistance over a wide temperature range, are of great importance in the microelectronics industry [2]. Their demand is largely fuelled by the need to measure the flow of current in electronic systems, which is becoming increasingly widespread. Reasons for this include the growth of battery-powered portable products, increasing concern to minimize energy usage, and the spread of electrically actuated systems in cars. In this context, measuring a current means converting it to a voltage, which may then be compared with a threshold, digitised or otherwise processed by a current sense circuit. There are several solutions for doing this, including current transformers, hall-effect sensors and magnetoresistive sensors. However, the simplest and, in many cases, lowest cost method is to employ Ohm's law in the form of a current sense resistor [314].

Traditionally this type of application has largely been met with resistor technologies such as wirewound, metal strip, electroless or thick film resistors where resistance is easily reduced through increasing the bulk of the metal alloy element or its chemical composition. However the downfall of all of these technologies is that they do not possess good electrical performance such as tight resistance tolerance and temperature coefficient of resistance (TCR), or good long term resistance stability.

Conventionally when this level of performance is required, thin film resistors must be employed. However thin film resistors below 10Ω are inherently difficult and expensive to manufacture and can regularly result in excessive scrap rates in batch manufacture. Two of the most costly process stages are the deposition and subsequent laser adjustment to target value of the thin film.

1.2 BACKGROUND

Typical process flows for both axial-leaded and surface mount (SMD) thin film devices are illustrated in Figures 1.1a and 1.1b respectively.

(1) Blank Al_2O_3 rods

(2) Deposit metal film

(3) Fit termination caps

(4) Laser adjust film

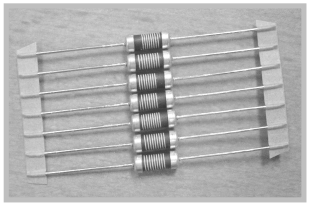

(5) Weld termination leads

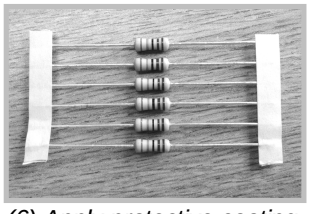

(6) Apply protective coating

Fig. 1.1a Axial-leaded process flow.

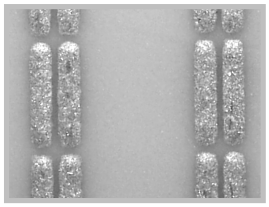

(1) Apply terminations to Al_2O_3 substrate

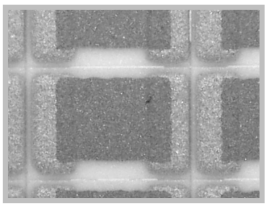

(2) Deposit metal film

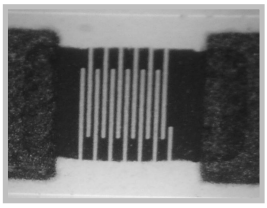

(3) Laser adjust film

(4) Apply protective coating

(5) Singulate chips

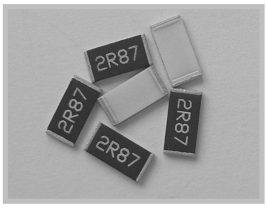

(6) Apply outer terminations

Fig. 1.1b SMD process flow.

In general thin film resistors are manufactured by depositing a sub-micron (µm) layer of metal alloy or ceramic/metallic (cermet) material onto a ceramic substrate and then

heat treating it to obtain the required TCR and pre-value resistance [3]. This pre-value is then adjusted to target value by removing part of the metal film to increase its length, usually by a laser or abrasive cutting wheel [4]. Outer terminations are then applied and the component is encapsulated in a protective coating.

Nickel chromium (Ni/20-50wt.%Cr) is widely regarded as a good all round film as it can cover the whole pre-value resistance range of around 1 to 1000Ω/□ [5]. Although this is perfect for values in the middle of the range, problems with film thickness can arise at the two extremes, low film thickness for high resistance values and high film thickness for low resistance values.

At the high end, typically 1000Ω/□, the film can become very thin and patchy and break down under voltage load. This problem may be overcome through the use of a higher resistivity cermet film such as CrSiO, which produces a thicker film for the same ohmic value [6-7]. This gives better overload properties but in practical use it can suffer from inferior resistance stability and TCR to that of NiCr [8].

However at the thicker film, low resistance range, typically 1 to 10Ω/□, there has been little improvement and NiCr remains the preferred film [9]. Currently there exist a number of problems with this range, all of which are related to the increased film thickness.

Firstly, as increase in film thickness and hence reduction in resistance is proportional to sputtering time, it can take in excess of 15 hours to deposit a batch of standard 0.25 watt axial resistors to a pre-value of ≤1Ω/□ and uses up approximately 30% of the NiCr sputtering target. In comparison to achieve a value of say 100Ω/□ using the same standard sputtering conditions, this figure may only be approximately 1 hour and uses less than 2% of the amount of expensive target material.

More problems can arise at laser adjust; where the increased film thickness is more difficult to cut and a reduction in machine output is often the only option. Furthermore, perhaps equally as problematic is the reduced trim gain associated with low resistance parts which can result in large increases in the resistance distribution of the batch. Trim gain (G) can be defined as follows:

$$G = \frac{R_{TT}}{PV} \qquad \textit{Equation 1.1}$$

Where ‘PV’ is the measured ohmic value of the deposited pre-value resistor and ‘R_{TT}’ is the target ohmic value to which the deposited pre-value is laser adjusted.

Trim gain is also related to the overall length of the laser trim. As the trim length and thus the resistor length increases, so do its measured resistance 'R_{TT}' and thus the trim gain 'G' through Equation 1.1.

For example a typical 0.25 watt axial resistor with a target value of 10Ω would be adjusted from a 1Ω pre-value, which is the lowest value that can currently be deposited using NiCr, giving a trim gain of 10. In comparison a resistor in a higher value band, say 220KΩ, which would normally be adjusted from a pre-value of approximately 200Ω, would have a trim gain of 1100 and thus a considerably longer trim length.

The main reason trim gain and hence the length of the kerf have such a great effect on resistance distribution is due to the pulsed power output and switching off time of the laser adjusting machine. Using its pulsed power output, the laser adjusts the resistor by melting a series of holes in the metal film, which overlap one another creating a continuous cut path. Once the pre-value has been trimmed to its target value the laser automatically switches off.

However as the laser beam is pulsed, it must complete its last whole pulse before it switches off, i.e. it is not possible to have half a pulse. Therefore the target value may lie in the middle of the last pulse, i.e. too much metal film has been removed and the resistance of the part is too high.

If the resistor has a low trim gain and therefore a shorter kerf length, then this minute difference in length caused by the switching off time of the laser will account for a much greater percentage of the overall kerf length and hence the resistance distribution of the batch will be wider.

There are methods to improve this situation such as increasing the overlap of the pulses or reducing the laser beam diameter, but these always come at a cost of reduced trim speed or inferior resistor stability performance.

At present, poorly understood process attributes at the early manufacturing stages have negative quality impacts during later processing activities such as the laser adjustment of the resistance value.

At this stage few researchers have sought to identify and develop a suitable low resistance metal film for this application. Indeed resistor manufacturers worldwide appear to have accepted NiCr as the preferred film and are prepared to trade off the problems associated with its increased thickness at low resistance values in order to attain its excellent resistance stability, TCR properties and thermal characteristics[5,9-11].

1.3 RESEARCH AIMS AND OBJECTIVES

The aims of this research are as follows:

1. Identify a thin film system based on copper and aluminium which has processing and performance characteristics equal to that of NiCr, however possessing features such as lower resistivity and higher deposition rate values.

2. Process thin films of copper and aluminium with additions of molybedum and analyse their electrical performance characteristics against those of the well established NiCr alloy.

3. Generate a set of optimum process conditions, suitable for repeatedly producing copper-aluminium-molybdenum (CuAlMo) thin film resistors to the required specification.

The objectives of this work are to:

1. Conduct a comprehensive literature review and develop a critical understanding of the materials and process stages involved in the manufacture of thin film resistors and establish their inter-relationships.

2. Manufacture thin film resistors of CuAlMo and assess their key electrical performance characteristics against the following specification requirements [12]:

Resistance range:	1 - 10Ω
TCR_{av} (20ºC to 70ºC):	0 ± 25ppm/ºC
Resistance stability (1000hrs at UCT):	<0.5%
Tolerance of resistance:	±0.25%

3. Develop an in-depth understanding of appropriate analytical procedures including methods of characterisation of metal films as well as relevant experimental design techniques and employ these to critically investigate the characteristics of CuAlMo thin film resistors, particularly the complex interactions of the deposition, heat treatment and laser trimming process stages on their performance.

4. Manufacture batches of CuAlMo thin film resistors under these optimised conditions and conduct long term reliability testing to approve the product for full scale production.

1.4 THESIS OUTLINE

CHAPTER 1: This chapter gives an overview of the important electrical characteristics of thin film resistors, followed by an in-depth literature review of material systems used in their manufacture.

CHAPTER 2: Potential material systems for use in the manufacture of low resistivity resistors are reviewed in more detail, before a combination of Cu and Al is identified as a system worthy of a full investigation. The electrical properties of sputter deposited CuAl films are investigated across the full composition range using a purpose built multi section sputtering target. Following heat treatment in both air and N_2, films are found to have acceptable sheet resistance and stability properties, but are unsuitable for commercialisation as the TCR is too positive.

CHAPTER 3: The focus of the work in this chapter is to dope the CuAl films with small quantities of Mo and Si to reduce the positive TCR. Mo is found to be the most successful of the two elements and by fine tuning its incorporation within the sputtering target, films with negative as-grown TCR properties are produced, whilst limiting the affect of increased resistivity. Following heat treatment, the TCR value can be raised to near zero and long term stability of the films is found to improve.

CHAPTER 4: The purpose of this chapter is to analyse the chemical composition of the CuAlMo resistor films using several techniques, to allow specification and subsequent manufacture of a composite sputtering target. The thicknesses of the films are also measured using a number of methods to allow accurate calculation of the film resistivity. Once manufactured, films are sputtered from the composite target and compared directly with those produced using the sectioned development target. The Mo content is found to be high in the composite target and films sputtered from it, resulting in more negative TCR properties. However this discrepancy is overcome by annealing the films at higher temperatures.

CHAPTER 5: This chapter is concerned with the sputtering and heat treatment stages of the thin film resistor manufacturing process. A suitable experimental design is employed to study the effects of varying the levels of key sputtering and heat treatment process parameters on the electrical properties of the films. Once the optimum conditions have been determined, the structural and chemical transformations taking place within the films are investigated and related to subsequent changes in the electrical properties.

CHAPTER 6: An introduction to the types of conduction mechanisms present in continuous thin metal films is presented. These theories are then applied experimentally to the CuAlMo thin films to determine the variation in the dominating conduction mechanisms with increasing film thickness and to give an approximation of fundamental film properties such as bulk conductivity and the mean free path of conduction electrons.

CHAPTER 7: This chapter is concerned with optimising the laser adjustment stage of the thin film resistor manufacturing process. An introduction to the laser trimming process is given before a suitable experimental design is selected to study the effects of varying key laser trim parameters on the electrical performance of the CuAlMo films. Once determined, the optimum laser conditions are used to trim CuAlMo films to various trim gains using two trim patterns; the L cut and the serpentine cut. The stability of the film is then further improved by employing a two stage adjustment technique incorporating a heat stabilisation process.

CHAPTER 8: The purpose of this chapter is to assess the manufacturability and long term reliability of batches of CuAlMo resistors manufactured under the optimised process conditions. Three separate batches of CuAlMo films are sputtered and heat treated before being laser trimmed to target values in the range 1.5 to 10Ω. These parts are then processed to the end of line where they are final measured to tolerances of ±0.10 and ±0.25%. Once complete the batches are subjected to environmental testing against BS CECC specifications.

CHAPTER 9: In this chapter the main conclusions from the research are drawn and a number of recommendations for further work in the area are suggested.

1.5 ORIGINAL CONTRIBUTIONS

The research carried out in this work has resulted in the following contributions to knowledge:

- The development of a new thin film material system of CuAlMo for use in the manufacture of low value resistors with negative as-grown TCR properties.
- Optimisation of sputtering and subsequent heat treatment process stages to produce CuAlMo films with defined electrical properties.
- A preliminary investigation into the dominant conduction mechanisms which influence the resistivity of the CuAlMo thin films with increasing film thickness.
- Optimisation of the laser trimming process, using two stage adjustment techniques to produce CuAlMo film resistors to target values of 1 to 10Ω and tolerance limits of ±0.1%.
- Manufacture of production size batches of CuAlMo thin film resistors under these optimised process conditions with end of line yields in excess of 90%.
- Successful approval testing of these batches of CuAlMo thin film resistors to BS CECC specifications.

These contributions are supported by a number of publications as detailed in the declarations section on page XIX.

1.6 INTRODUCTION TO THIN FILM RESISTOR MATERIALS

The development of thin metal film resistors dates back to at least around 1920 [13]. Thin film technology was used because it offers enhanced performance and reliability over that of metal composition and wirewound type resistors.

As well as possessing a suitable sheet resistance and TCR, films must be sufficiently stable so that any changes in resistance during their operating life can be reliably expected not to exceed a pre-specified value. Moreover the resistor must be able to be manufactured to this specification at a realistic cost.

1.6.1 Basic Electrical Properties

Sheet resistance, Rs

The resistance of a thin film resistor is directly proportional to the resistivity, ρ, and inversely proportional to the thickness, d, of the thin film material. It is usual to use the sheet resistance of the film, Rs, which is defined as ρ/d to describe thin film resistors [14-15]:

$$esistance = \frac{resistivty \times length}{thickness \times width} \qquad W = \frac{rl}{dw}$$

However, $\frac{l}{w} = \square$ (No. of squares in the film pattern)

Hence, $$Rs = \frac{W}{R} = \frac{r}{d}$$ *Equation 1.2*

Temperature co-efficient of resistance, TCR

A parameter equally as important as sheet resistance is the temperature co-efficient of resistance, (TCR), of the film. TCR describes the change in resistance of the film with change in its temperature dR(T)/dT. However, as dR(T)/dT is nearly constant for most metal films it is common practice to use an average TCR parameter [16]:

$$TCR_{av} = \frac{1}{R_i}\frac{R_e - R_i}{T_e - T_i} \times 10^6 \, ppm/^{\circ}C$$ *Equation 1.3*

Where R_i is the initial resistance at temperature T_i and R_e is the end resistance at temperature T_e Typical values of T_i and T_e are 20ºC and 70ºC respectively.

However using the above approach and assuming that resistance changes linearly as a function of temperature is not strictly valid for thin film resistors. Errors can arise from the ‘composite TCR’ effect of conductor materials which are measured in series with

the resistor element. For this reason a more accurate method of defining the TCR of the resistor is to measure its change in resistance over the extremes of its operating range, typically -55ºC to +125ºC for surface mount devices and -55ºC to +155ºC for axial leaded components [17]. This parameter is generally referred to as 'Extended TCR' and denoted as TCR_{ex} [18-19].

Resistance stability, ΔΩ/Ω

Resistance stability or reliability is basically a measure of the change in resistance of the film against a certain specification over a period of time. There are a number of conditions under which the reliability of the component can be tested such as dc load, dry heat or humidity, a full discussion of which is presented in chapter 8.

The severity of the effects of a test condition on the resistor depends greatly upon film thickness. For thicker films the resistance value is inherently lower and hence the dc load voltage that can be applied will also be lower. Moreover, humidity is also likely to have less effect on a more robust thicker film.

Perhaps the most convenient and universal test condition is that of dry heat (temperature) as the test can be performed by simply storing the film in an oven. Dry heat stability tests generally entail measuring the change in the resistance value of the film, ΔΩ, following storage at the upper category temperature, usually 155ºC for axial resistors and 125ºC for surface mount resistors, for a period of 1000hrs:

$$DW / W = \frac{R_e - R_i}{R_i} \times 100\% \qquad \textit{Equation 1.4}$$

Where R_i is the initial resistance and R_e is the end resistance following storage.

1.6.2 Materials Systems

Materials used in the manufacture of thin film resistors typically require resistivities in the range 100-2,000 μΩcm and a TCR of ±50ppm/ºC. However, owing to their mechanical structure, bulk metals and alloys cannot have resisitivities much in excess of the lower limit of this range and TCR is usually large and positive (see Table 1.1).

Metal or alloy	Resistivity (μΩcm)	TCR (ppm/ºC)
Aluminium	2.7	4200
Chromium	12.9	4500
Copper	1.7	4300
Molybdenum	5.7	4600
Nickel	7.3	6500
Tantalum	13.5	3800
Ni 80% / Cr20%	100	170

Table 1.1 – Electrical properties of some bulk metals and alloys [20].

Conversely, bulk semiconductors can readily satisfy these resistivity requirements, but this is usually at the cost of a very negative TCR.

Fortunately when deposited in thin film form most metals produce resistivity values which are much greater than that when in bulk form and frequently without acquiring a large positive TCR. There are a number of mechanisms which can produce this phenomenon as illustrated in Table 1.2.

Description	Mechanism for resistivity increase	effect on TCR
Ultra thin film	Conduction electron scattering	→ 0
Insulating phase	Inter grain barriers	→ - ∞
Porous film	Construction resistance	→ - ∞
Trapped gas	Impurity scattering	→ 0
Discontinuous	Particle separation	→ 0
Double layer	TCRs cancel	→ 0
New structure	Fewer carriers	→ 0

Table 1.2 – Mechanisms causing metal films to have resistivities greater than the bulk [21].

The thin film material systems available for resistor manufacture can therefore largely be divided into three main groups, depending upon the conduction mechanism present:

1. Metal alloys
2. Single metal systems
3. Cermets (metal-insulator)

Metal Alloys

Metals are known to have a periodic crystal structure at low temperatures which provides a regular field for mobile electrons to flow [20]. Any distortions in this periodic nature of the lattice will distort the flow of electrons and thus increase its resistivity. This distortion can be caused by a number of defect types; lattice dislocations, contamination due to foreign atoms or atoms interstitially located within the lattice or non-stoichiometric ratio of constituents. Resistance can also be increased on a temporary basis due to lattice distortions caused by vibration increases with temperature; hence the reason TCR is generally positive for all metals.

By alloying metals, the lattice distortions are dissolved in one another thus increasing the resistivity of the solution. In general the resistivity rises with increasing impurity concentration, reaching a maximum for an alloy concentration of approximately 50% impurity [22].

By far the most successful of the metal alloy systems used in the manufacture of bulk material resistors is nickel chromium, or nichrome, with a composition of NiCr 80:20

wt.%. Due to its high resistivity, low TCR and widespread commercial availability it seemed an obvious candidate for the development of thin film resistors during the 1960's.

Over the years there have been a number studies undertaken on the properties of nichrome thin film resistors [23-35]. Work has focused on the effects of varying substrate materials and process parameters on the electrical performance and structural properties of the fixed composition NiCr 80:20 binary alloys.

The properties of films deposited onto alumina [23-25], mylar [24], glass [24-31], NaCl crystal [30-31], silicon nitride coated silicon [32-33] and silicon nitride coated GaAs [34-35] have all been studied. Although many of these substrates are desirable for analytical purposes, in general it was found that alumina substrates were the most suitable for the fabrication of thin film resistors due to their superior power handling capabilities [24].

By varying deposition parameters such as pressure, power and substrate temperature [35] films with sheet resistances of 10 to 1000Ω/□, and TCR in the range +50 to +250ppm/ºC could be achieved. Subsequent annealing of these films led to typical long term stability figures of better than 0.5% [32]. Optimum annealing conditions were found to be in the range 200 to 600ºC for 1.5 to 6 hours in air ambient [23-25, 24]. Although treatment at similar temperatures under vacuum [28], in nitrogen [31] and forming gas [32] atmospheres have all been shown to produce reasonable values of TCR, it appears that a subsequent oxidation of the film in air ambient is essential if good long term stability of the film is to be realised [30].

In general, depositing the nichrome alloy in thin film form increased the resistivity and subsequently reduced TCR when compared to its bulk counterpart. Even to this day thin films of NiCr 80:20 still receive a substantial amount of interest in both resistor and strain gauge applications [29-30].

By the mid 1970's, demand was increasing for thin film resistors with improved electrical performance over that achievable with NiCr 80:20 alloys. It was soon discovered that the TCR of the film could be reduced by increasing the chromium content in the film [36-45].

However, due to vapour pressure differences between Ni and Cr (0.25×10^{-3} Torr and 1.8×10^{-3} Torr at 1300ºC respectively [1]), it was very difficult to control the composition of the film during evaporation and this led to use of sputtering and in particular d.c. magnetron sputtering for the reliable and repeatable production of thin film NiCr resistors [39].

A plot of TCR and resistivity against chromium content for NiCr films deposited on oxidized silicon wafers is shown in Figure 1.2.

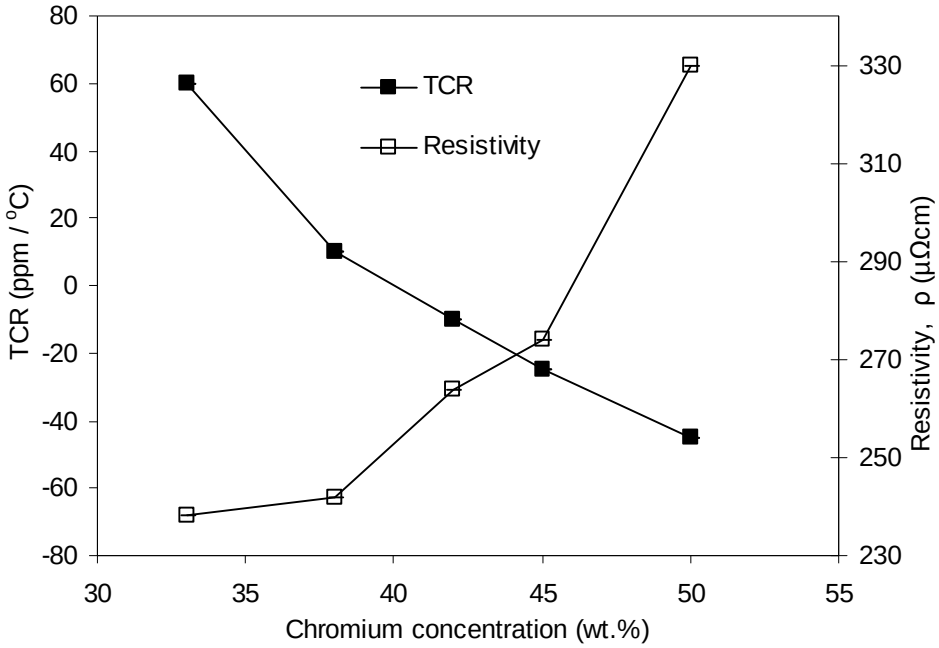

Fig. 1.2 – Variation of TCR and resistivity in NiCr films as a function of chromium concentration [44].

As can be seen the TCR steadily decreases with increase in chromium content in the film, passing the zero line at approximately 40wt.%. Conversely the resistivity rises with increase in chromium content having a value of around 250μΩcm at the point of zero TCR.

This marked change against the properties of 80:20 alloy are due mainly to two reasons; firstly the decrease in grain size of the film as the Cr content increased leading to a more amorphous structure having higher resistivity [43] and secondly the higher quantity of chromium oxide (Cr_2O_3) formation with negative TCR in the film [41]. The occurrence of amorphous and crystalline metastable phases are related to characteristics such as a large immiscibility gap between the two solid solutions (nickel fcc and chromium fcc solid solution), the existence of a relatively deep eutectic point and the presence of complex tetrahedral close-packed structures [37].

As chromium has a higher chemical affinity with oxygen than does nickel, then as its ratio in the film increases so does the amount of chromium oxide formed with residual oxygen in the deposition chamber [46]. In fact this mechanism led to a number of studies whereby oxygen was deliberately introduced into the deposition chamber to reactively sputter the NiCr film [46-51]. Partial pressures in the range 2-6% reactive oxygen in the

inert argon atmosphere were reported to give further increases in the content of chromium oxide in the film and hence a lower TCR [49].

There are a number of studies which report a near zero TCR for films with chromium content in the range 30 to 60wt.%, both sputtered in argon and mixed argon/oxygen environments. It seems that in addition to film composition, accurate TCR control can be also be achieved through varying the deposition temperature and annealing treatment used. For films with negative as grown TCR, annealing in the temperature range 300 to 350ºC appears to be essential if a near zero TCR is to be achieved [41, 49]. It also appears that this annealing can be carried out in the deposition chamber by increasing the film temperature either through heating of the substrate or through increased deposition power [39, 45]. However all of these methods rely on the same mechanisms such as grain growth and reduction of impurities to reduce resistivity and in turn increase TCR.

In addition to the desirable change in the TCR properties of the film, increasing the chromium concentration of the film and sputtering in an oxygen partial pressure can also improve the long term resistance stability of the film. Some research shows that stability figures as low as 0.3% change following 1000hrs at 155ºC are not untypical for films sputtered in an oxygen partial pressure of $3x10^{-5}$ torr [50].

Again the reason for this improved performance is attributed to the increase in chromium oxide formation at the surface of the film. As the chromium oxide grows it forms a protective passivation layer, similar to aluminium oxide, which protects the film from further attack [38, 52].

Once it was realised that the addition of a third element, oxygen, into the film could give improvements in resistance stability, a number of investigations were carried on doping or modifying the NiCr alloy with a third element incorporated into the sputtering target itself.

Probably the most widely documented of these elements is aluminium [53-56]. Additions of aluminium were proven to stabilise the film and reduce the TCR to values around zero [55]. Three regions have been found in the NiCrAl composition which result in highly stable resistive films with a very low TCR; one with less than 3at.% Al, one with 28-32 at.% Al and one with 45-60at.% Al. The role of aluminium is reported to be to stabilise the amorphous structure and state of ordering of the atoms in the deposited nickel chromium film. This can lead to stability figures of better than 0.08% following 1000hrs storage in air at 155ºC [54]. Moreover the addition of aluminium allows thin film resistors with lower sheet resistances in the range below 10Ω/□ to be produced [5].

Of the other elements which have been proven to improve the performance of NiCr films, Silicon is perhaps the most widely documented [57-63]. Additions of around 5 to 10wt.% Si can produce films with TCRs of ±20ppm/ºC and long term resistance stability of better than 0.05%. It is assumed that the improved thermal stability of the NiCrSi film is due to the diffusion limiting effect of silicon [58].

Not satisfied with the performance of ternary film compositions, there have also been several studies investigating the effect of adding two extra elements to the NiCr alloy to form quaternary composition films. Thin film resistors based on the Evanohm, Ni-Cr-Cu-Al alloy are the most popular and have been reported to possess very low TCRs of ±10ppm/ºC [64-67].

Apart from NiCr the most popular metal alloy system used in the production of thin film resistors is probably copper nickel. Cu-45wt.% Ni alloy, known as “constantan” is a typical material of low resistivity around 50 to 60μΩcm and with a low TCR value of less than +50ppm/ºC [68-75]. CuNi was reported to be the main film used at Philips Electrical in the manufacture of low value resistors below 10Ω. Films were deposited having resistivities below 50μΩcm making it suitable for low ohmic applications. However the lower limit for the sheet resistivity of the sputtered CuNi films was 1Ω/□ [5].

In order to produce thicker films of CuNi with even lower resistivities, electroless deposition is required. Films of up 10μm in thickness are achievable producing CuNi films possessing resistivities of around 40μΩcm. Following post deposition stabilisation the TCR of the films shifted to near zero. However the electroless deposition rate of the alloy was reported to be remarkably slow [70].

Single Metal Systems

As is evident for the nickel chromium films discussed above, the resistivity of the thin film is usually dominated by the background gases which are incorporated into the film during the deposition process, rather than the resistivity of the source material itself. With this realisation the focus of many researchers turned to the use of single metal systems as problems such as alloy composition control and fractionation could be automatically eradicated.

By far the most widely documented of the single metal systems is tantalum, reactively deposited in nitrogen to produce tantalum nitride (TaN) [76-96]. The as-deposited resistivity of pure tantalum is close to that of bulk tantalum (13μΩcm). However when reactively sputtered in a nitrogen atmosphere the tantalum and nitrogen atoms combine to form a nitride which is trapped in the growing film. As shown in Figure 1.3, this nitride produces an increase in resistivity and subsequent decrease in TCR [80].

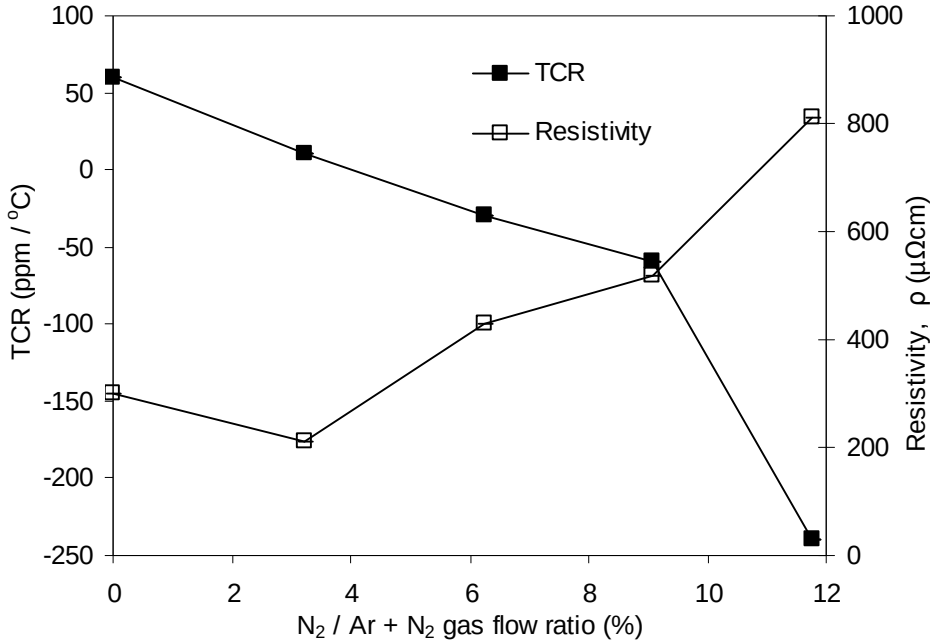

Fig. 1.3 – Variation of TCR and resistivity in TaN films as a function of nitrogen flow rate [80].

As can be seen TaN possesses similar electrical properties to that of NiCr and is generally used in the same mid-range area of resistor manufacture. However the intrinsic properties of linear TCR and physio-chemical inertness made TaN thin film material superior to the more popular NiCr for thin film resistors [76] and the mass production of TaN thin film resistors by magnetron sputtering with sheet resistivity of 50-100Ω/□ and TCR of about -80ppm/ºC was announced in the early 1980's [77].

Since that date, results reported on the electrical properties of TaN thin films have varied quite considerably. However a number of more recent investigations have suggested that its properties are indeed very similar to that of NiCr, with films sputtered to thicknesses of between 300-1000nm possessing resistivities of 100-450μΩcm and giving sheet resistances of around 10 to 1000Ω/□ and TCR values of around -50 to -100ppm/ºC. Again post deposition stabilisation at around 200 to 400ºC in both air and N_2 atmospheres was reported to produce films with TCR's of -5 to +5 ppm/ºC and a resistance stability of better than 0.1% [78-80].

Although these properties made TaN one of the main thin film systems adopted by resistor manufacturers world wide, it was felt there was still room for improvement. As with NiCr, development would come in the form of a third element to produce a ternary system. There were two main issues with TaN; its negative as deposited TCR and the need to further improve its stability for precision resistor applications.

The first issue was tackled with the addition of copper [97-99]. By varying the Cu concentration in a TaNCu sputtering target, as-deposited films of 150μΩcm with near zero TCR were produced. The films could then be stabilised using a rapid heat treatment method to reduce processing time.

To further improve resistance stability, as with NiCr the incorporation of aluminium was used [100-105]. Reports showed that additions of 35-60wt.% of Al to TaN could produce films of sheet resistance 50-600Ω/□ with long term resistance stabilities of better than 0.05% [100]. Investigations were also conducted for binary systems of TaAl, with sheet resistance of around 150-300μΩcm resulting. However the elimination of nitrogen from the film appeared to result in inferior stabilities of around 0.3% [101-102].

Cermets

Electron conduction is greatly impeded by a potential barrier in the path of the flow and although the energy of the electron may be less than the barrier height there is a finite probability that the electron will pass the barrier. This form of conduction is called tunnelling and is an extremely useful mechanism for the production of high resistivity materials [3].

One way in which potential barriers are produced, and hence the resistance of the film is increased, is by the precipitation of background gas impurities at grain boundaries. It therefore seemed a logical step to try and include these impurities deliberately in the sputtering target instead of accidentally in the background gases. In the case of a cermet, a heterogeneous mixture of ceramic insulator and conductive metal material is formed producing the potential barrier, hence the name cermet. As the inclusion of ceramic, an insulator, has the effect of increasing resistance, cermet films usually find application at the higher sheet resistance values >1kΩ/□.

Although a number of metal-insulator combinations such as WSiO [106], TiCrAlO [8] and CrAlSiO [107] have been studied in film form, by far the most successful to date has been the chromium-silicon monoxide (CrSiO) system [6-7, 14, 108-119]. Its main use in thin film resistor manufacture is in the 1k to 10kΩ/□ range where standard alloy films such as NiCr and TaN are too thin. However, although CrSiO produces a thicker, more robust film at these higher ohmic ranges, its resistance stability and TCR are far inferior to that of the alloy and single metal systems [6].

1.7 SUMMARY

From the previous review it can be concluded that there are primarily four material systems currently used in the manufacture of thin film resistors. A summary of the basic electrical properties of these films is presented in Table 1.3

Film type	r (mWcm)	Rs (W/□)	d (nm)	TCR (ppm/°C)	DΩ/Ω (%)	Deposition method	Stabilisation temp (°C)	Stabilisation time (hrs)
NiCr NiCrO NiCrSi NiCrAl NiCrCuAl	100-500	10-1000	10-500	<5	0.1 0.01 0.08	sputtering	200-400	2-5
CuNi	50 40	1-50 0.08	500 5000	<15	0.15	sputtering electroless	100-800	1-3
Ta TaN TaNAl	100-450	10-1000	300-1000	<10	0.3 0.1 0.05	sputtering	200-400	2-5
CrSiO		1-10k		<25		sputtering	200-600	2-5

Table 1.3 – Electrical properties of thin film resistor material systems.

1.) Alloys of nickel and chromium either in binary form or with small additions of doping elements such as aluminium or silicon are used in the mid-range of sheet resistance from approximately 10 to 1000Ω/□ and possess excellent TCR and long term stability properties.

2.) Alloys of copper and nickel find use in the lower sheet resistance range of around 1 to 50Ω/□ but have inferior stability properties to those of NiCr.

3.) Single metal systems of tantalum, reactively sputtered in nitrogen are also used in the same mid-range sheet resistance area as nickel chromium, but possess slightly worse TCR and stability properties. The main advantage of TaN is in its corrosion resistance under humid conditions, meaning it usually finds use in the high reliability military and aerospace applications.

4.) Ceramic metallic systems of chromium silicon monoxide are used when higher sheet resistances in the kilohm range are required. TCR and stability are poor in comparison to the alloy and single metal systems, however the inherent high resistivity properties of the cermet systems mean they continue to find widespread application.

Chapter 2

Binary Thin Film Composition Selection

2.1 INTRODUCTION

As detailed in chapter 1, the main objective of this work was to investigate the electrical properties and performance of thin metal film systems which have lower resistivity than that of NiCr and can be deposited to sheet resistances of <1Ω/□ at preferably faster rates. From the material systems currently available for the manufacture of thin film resistors, perhaps the most suitable candidate to meet this objective is copper nickel 45/55wt%.

When sputtered from a commercially available constantan alloy target, thin films possessing desirable electrical properties such as a resistivity of ≤50μΩcm, TCR down to +15ppm/ºC and an adequate long term stability of resistance of better than 0.5% are achievable. It would therefore appear to be the obvious choice for the successful manufacture of thin film resistors of low sheet resistance.

However there have already been a number of reviews for this material [68-75] and it seems that the lower range of sheet resistance is restricted to around 1Ω/□ when deposited by the PVD method. This figure is similar to that reported for nickel chromium [3] and is a result of the maximum film thicknesses achievable for these materials by the sputtering technique. There has also been work undertaken to reduce this sheet resistance figure by electroless deposition of copper-nickel films of increased thickness, but this resulted in a subsequent increase in film stress and hence inferior electrical stability [70].

Although alloys of copper nickel may not be ideally suited to this application it can be postulated that it is the inclusion of copper, with its intrinsic low resistivity and high sputter yield properties, which is largely responsible for the reported low sheet resistivity of the film. Table 2.1 shows some important electrical and atomic properties of the individual metals discussed in chapter 1.

Metal symbol	Sputter yield at 500eV Ar+ (atom/ion)	Resistivity at 20ºC (μΩcm)	TCR (0-100ºC) (ppm/ºC)	Atomic radius (nm)	Covalent radius (nm)
Cu	2.0	1.69	4300	0.135	0.132
Al	1.0	2.67	4500	0.125	0.121
Ni	1.1	6.9	6800	0.135	0.124
Cr	1.3	13.2	2140	0.140	0.139

Table 2.1 – Electrical and atomic properties of individual metals [168, 310].

In addition to copper-nickel, two other potential alloys employing the low resistivity copper element are copper-chromium and copper-aluminium. Copper-chromium has received limited attention in the application of thin film resistors [120]. Schuman et al,

1993, investigated the electrical properties of CuCr 53/47at.% alloy thin films sputtered onto both Al_2O_3 and oxidised Si substrates. Films were found to have low internal stress characterised by a TCR close to zero, a long term stability of around 0.1% and a resistivity of 60-80μΩcm. Following heat treatment in the increased temperature range of 300-500^oC the resistivity of the films was reduced to around 30μΩcm, however TCR and stability was worse and increased stress was apparent in the films.

There has also been limited research conducted for alloys of copper-aluminium in the application of thin film resistors [121]. Bashev et al, 1990, investigated the electrical properties of CuAl thin films sputtered from a multiple section target made of small sections of Cu and Al. Binary films across the full composition range of 0 to 100at.% Al were investigated and it was found that a composition of approximately CuAl 60/40at.% yielded a near zero TCR with a sheet resistance of ≈ 7Ω/□. Following post deposition annealing at 90ºC in air, the formation of the Cu_9Al_4 γ_2 phase was apparent with a wide range of homogeneity and good long term stability of resistance was achieved. Bashev concluded that thin films of CuAl could find use as low value thin film resistors, however there appears to have been no published research in this area since this recommendation.

There have however been several reports on the structural and electrical properties of the copper-aluminium thin film system in various other applications [122-146]. The most prominent of these in recent years is the work of Draissia and Debili and co-workers [122-128]. They too found the stable γ_2 phase to exist in the 40-60at.% Cu region but also discovered an unexpected Cu_3Al phase with similar stable properties.

Although it appears that there has been limited work carried out for concentrated copper-aluminium thin films, there have been numerous studies undertaken to understand the electrical behaviour of dilute copper-aluminium films [147-166]. Traditionally thin films of aluminium containing up to 4at.% copper found widespread usage in the semiconductor industry for the purpose of line interconnects. Additions of copper have been shown to reduce electromigration by up to two orders of magnitude [159].

However with the ever increasing demand for smaller semiconductor devices the line width of interconnects has been forced to reduce, meaning that the resistance has increased, causing reduced current handling and signal processing speeds. In order to improve this situation a material with lower resistivity than aluminium was required and copper was the obvious candidate.

Although it was soon realised that films of pure copper possessed the required low electrical resistivity, their reliability was far inferior to their aluminium predecessor due to the poor oxidation resistance of the copper. However by adding aluminium in small amounts up to 10at.% to the copper bulk, the self passivating properties of the aluminium can be utilised to improve reliability without having too much effect on the resistivity of the film [165-166].

As it appears that there has been little or no further research into thin films of copper-aluminium for use as resistors since the work of Bashev et al suggested its suitability in 1990, and also due to the promising stability and reliability properties already established through its use in the semiconductor industry it would seem a viable option to investigate the suitability of thin films of copper and aluminium for use as low ohmic value resistors.

2.2 EXPERIMENTAL

2.2.1 Substrate Preparation

The substrate materials used were as-fired 96% Al_2O_3 for electrical measurements and borosilicate glass for structural and dimensional characterisation. Both substrate types were 0.635mm thick and were supplied in a standard 70mm x 60mm plate form to suit automatic processing equipment.

To allow accurate resistance measurement of the films once deposited, 15µm thick palladium silver (97/3wt.%) terminations were screen printed onto the Al_2O_3 substrates followed by an overglaze mask to produce the resistor matrix pattern. This mask could then be removed with a light solvent wash after deposition revealing the resistor pattern, consisting of ten individual four-terminal designs per substrate as shown in Figure 2.1.

This design allowed accurate measurement of the resistor using the four-probe, or Kelvin, method. With reference to Figure 2.1, this technique involves passing a current, I, from an adjustable source through the film using probes I_1 and I_2 and then sensing the potential difference, V, developed between probes V_1 and V_2 with a high impedance voltmeter. This measurement of voltage in the absence of any current in the electric circuit of the voltmeter removes the effect of the potential drops across the resistances of probes V_1 and V_2 to the sample and the current carrying wires [171].

The resistance meters used in this investigation were a Wavetek model 1271 and an Agilent model 3458A unless otherwise stated. Both of these meters have accuracies of better than ±20ppm across all resistance ranges used.

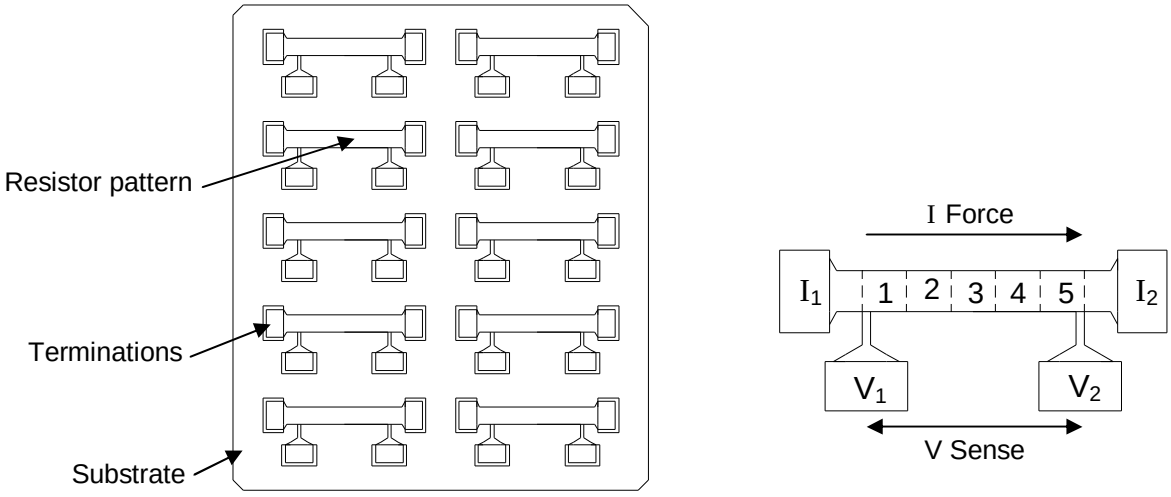

Fig. 2.1 – Resistor test substrate pattern (60 x 70mm).

2.2.2 Sputtering Target Construction

In order to investigate the electrical properties over the full range of copper-aluminium compositions, a multiple section sputtering target consisting of eighteen interchangeable sections was manufactured as shown in Figure 2.2.

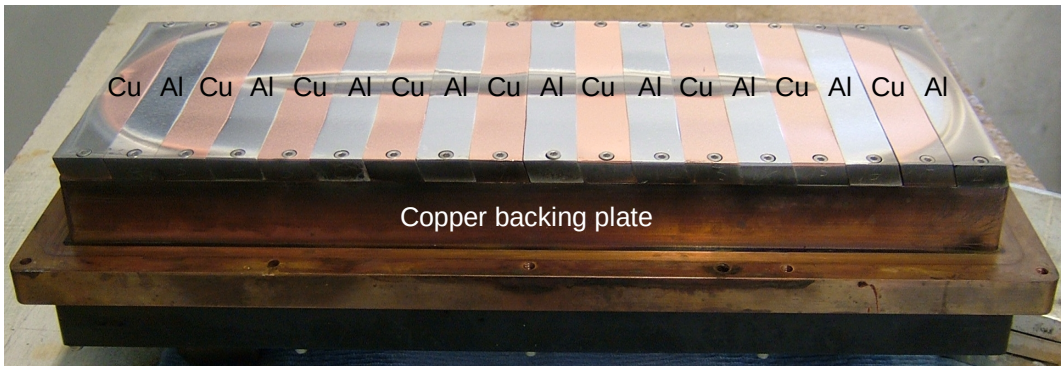

Fig. 2.2 – Multi-section sputtering target and magnetron cathode assembly.

The eighteen target pieces are fastened to the copper backing plate with stainless steel bolts, there is also a copper membrane (hidden from view) between the target and backing plate to allow for any errors in surface flatness and to improve electrical and thermal contact between the two parts. The backing plate is in turn bolted to an aluminium housing to form a water cooling jacket for the target, in which the magnetron is also housed. To prevent through sputtering of the backing plate, which could eventually breakthrough into the water jacket, the edges of the target pieces are machined at an angle of 20º. Moreover, sputtering of the stainless steel mounting bolts is guarded against by a rectangular dark shield which sits in front of the target once mounted in the plant.

This arrangement allowed the target composition by area to be adjusted by around 5.5%. Hence the following nineteen compositions, % by area, could be sputtered:

Area.% Cu	100	94	89	83	78	72	67	61	56	50	44	39	33	28	22	17	11	6	0
Area.% Al	0	6	11	17	22	28	33	39	44	50	56	61	67	72	78	83	89	94	100

Table 2.2 – Possible CuAl sputtering target compositions.

2.2.3 Composition Selection

To obtain an initial impression of the electrical properties of varying CuAl thin film ratios, samples were sputtered using the following target compositions, see Table 2.3. A set of samples were also sputtered from the standard NiCrMo 45/45/10wt.% target to be used as a control to assess the CuAl film properties against.

Run No.		**1**	**2**	**3**	**4**	**5**	**6**	**7**	**8**
Target area.%	**Al**	0	17	33	50	67	83	100	NiCrMo
	Cu	100	83	67	50	33	17	0	

Table 2.3 – Cu-Al target compositions investigated.

2.2.4 Deposition Method

Once the target had been assembled to the desired composition it was fitted into the deposition plant. The plant employed was a Circuit Processing Apparatus 900 (CPA) load locked magnetron sputtering plant which had been modified to give full automatic computer control. A schematic diagram of the plant is shown in Figure 2.3.

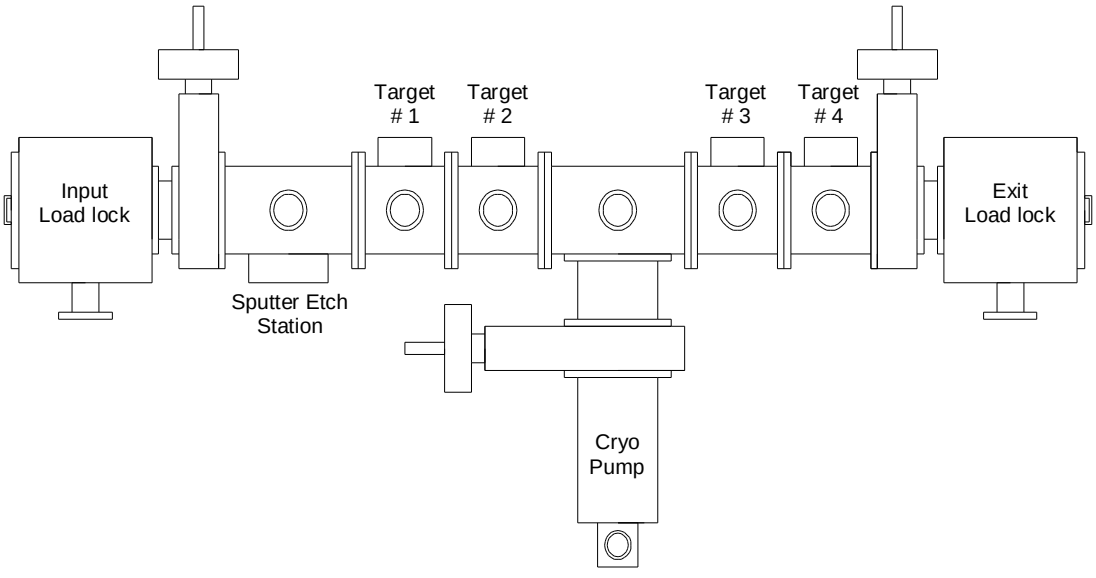

Fig. 2.3 – Schematic representation of the CPA sputtering plant.

In this system, argon atoms are excited to a plasma state by applying a d.c. voltage between the target (cathode biased) and the substrates (anode). The film properties are controlled by varying the substrate feed (deposition time), power level, and argon pressure.

The basic sample manufacturing process is as follows:

1. *Configure sputtering target for required CuAl composition*
2. *Place 3 off Al_2O_3 substrates and 1 off glass slide onto stainless steel sputtering pallet and load into input load lock magazine.*
3. *Evacuate full chamber to better than $1x10^{-7}$ Torr base pressure*
4. *Switch on pallet drive and adjust speed to 4cm/min*
5. *Switch on Ar flow and set to $35cm^3$/sec*
6. *Adjust throttle valve to give pressure of $3.5x10^{-3}$ Torr*
7. *Switch on target power supply and pre-sputter for 30mins at 1.5kW d.c.*
8. *Lower pallet onto drive chains*
9. *Pallet automatically stops at sputter etch station and substrates are plasma cleaned for 5mins at 500W R.F.*
10. *Pallet then continues on drive chain under the target where the substrates are deposited with the sputtered target material for » 5mins at 1.5kW d.c.*
11. *Pallet then enters output load lock magazine and is allowed to cool for 30mins*
12. *Switch off pallet drive and power supplies*
13. *Vent plant to atmosphere with N_2 and remove pallet from output load lock.*
14. *Remove substrates from pallet and clean off mask with light alcohol wash.*
15. *Repeat steps 1 to 14 until all trials are complete.*

2.2.5 Film Stabilisation

Following deposition samples from each trial were stabilised for 5 hours at 200, 300, 400 and 500°C in both air and N_2 atmospheres. The equipment used was a Hedinair HT3 nitrogen oven and the accuracy across the temperature range 150 to 550ºC was found to be $\leq \pm 5$ºC.

2.3 CHARACTERISATION OF FILMS

2.3.1 Chemical Composition Analysis

The composition of the film samples sputtered on to the glass slides were analysed using an FEI Quanta 200, Scanning Electron Microscope (SEM) coupled with Energy Dispersive X-ray analysis (EDX). The films were examined at five areas on the surface, and were then fractured and a further five areas were analysed on the cross section. The composition was found to be homogeneous and did not vary by more than ±2at.% across the 10 areas of analysis for all samples studied. The mean film composition from each deposition run is shown in Table 2.4 along with the starting composition of the sputtering target.

Run No.		1	2	3	4	5	6	7	8 - NiCrMo Control
Target	**Al**	0	12.8	26.1	41.8	59.3	77.8	100	49.8/44.2/6.0
at.%	**Cu**	100	87.2	73.9	58.2	40.7	22.2	0	
Film	**Al**	0	7.1	15.4	27.0	42.9	64.4	100	51.0/43.5/5.5
at.%	**Cu**	100	92.9	84.6	73.0	57.1	35.6	0	

Table 2.4 – Mean composition of the CuAl target and film samples

As can be seen there is a large discrepancy between the starting composition of the sputtering target and that of the film for all of the binary CuAl films i.e. trials 2 to 6. On average the film is rich in copper and hence deficient in aluminium by between 5 and 15at% depending on the starting composition.

There are several potential explanations for this error such as the location of the target pieces in relation to the magnetron wear ring and also the position of the test sample underneath the target. However the most likely cause of the discrepancy is due to the difference in sputtering yields obtained for the individual elements.

Sputtering yield can be defined as the average number of atoms ejected from the target per incident ion and depends on the ion incident angle, the energy of the ion, the masses of the ion and target atoms, and the surface binding energy of atoms in the target [167]. In the present case when sputtering with an Ar+ ion energy of 500eV, typical sputter yield figures for copper and aluminium are 2 and 1 atoms/ion respectively, assuming the ion incidence angle is normal (perpendicular) to the target surface. Indeed the relative ratio of sputter yields of copper to aluminium across a broad range of argon ion energies from 50eV to 100keV is approximately 2:1 [168].

If this ratio is assumed and the atomic weight of the copper in the target is doubled then the ratio of copper to aluminium is almost identical for the target and film for run numbers 2 to 6 as shown in Table 2.5. This result supports the theory that the relative sputter yields of the two elements is the main factor affecting the discrepancy in composition between the target and film samples.

Run No.		2	3	4	5	6
Target at.%	Al	12.8	26.1	41.8	59.3	77.8
	Cu x2	174.4	147.8	116.4	81.4	44.4
	Ratio Cu:Al	**13.62**	**5.66**	**2.78**	**1.37**	**0.57**
Film at.%	Al	7.1	15.4	27.0	42.9	64.4
	Cu	92.9	84.6	73.0	57.1	35.6
	Ratio Cu:Al	**13.08**	**5.49**	**2.70**	**1.33**	**0.55**

Table 2.5 – CuAl composition ratio for target and films, assuming 2:1 sputter ratio

2.3.2 Electrical Properties

As previously discussed, the three main parameters used to characterise the electrical properties of thin metal films for use as resistors are:

1. Room temperature sheet resistance, Rs, (Ω/□)
2. TCR_{av} 20/70°C, (ppm/°C)
3. Resistance Stability, ΔΩ/Ω, (%)

As Grown Electrical Properties

Figure 2.4 shows the as-grown sheet resistance and TCR_{av} properties of the CuAl films with increasing aluminium content, taken from a sample of 18 parts across the sputtering pallet. The results for the NiCrMo control are also plotted.

The as-grown sheet resistance of the film increased from a mean value of 0.06Ω/□ for the pure copper film to 1.8Ω/□ at 43at.% aluminium content. This figure then decreased to 0.3Ω/□ for the pure aluminium film. The mean TCR_{av} followed a similar but inverse trend with the TCR for the pure copper and aluminium films being large and positive at 2020 and 860ppm/ºC respectively. Once aluminium was added to the copper the TCR of the film decreased rapidly to around 500ppm/ºC at 15at.%, before falling more gradually to a minimum of -310ppm/ºC for 43at.% aluminium.

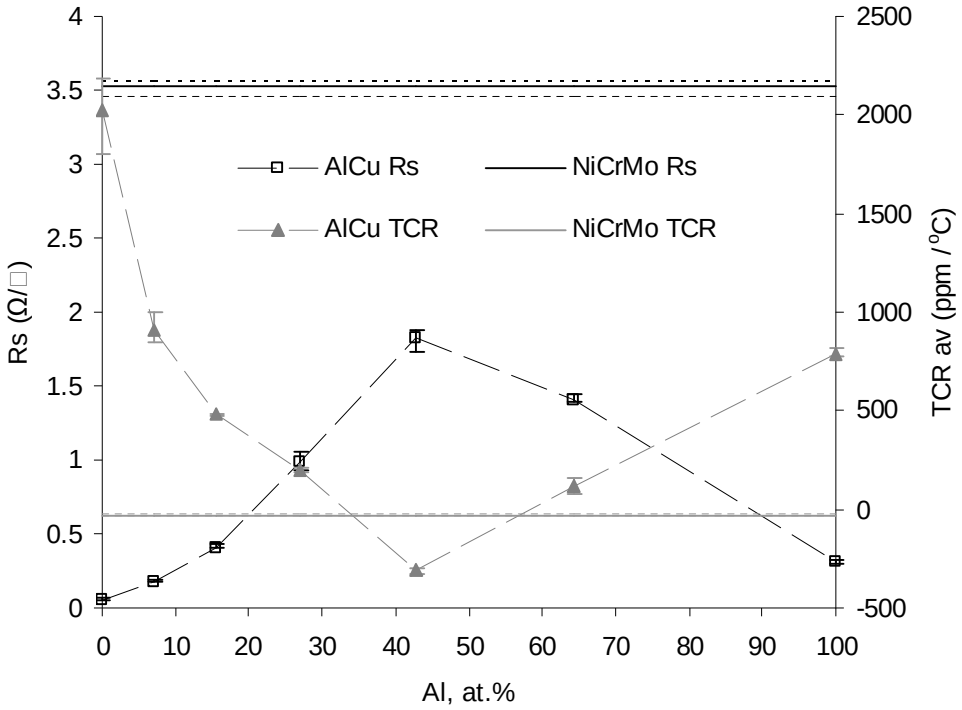

Fig. 2.4 – As grown sheet resistance and TCR_{av} properties of the CuAl and NiCrMo control films

When compared to the NiCrMo control, the sheet resistance of the CuAl films was much lower across the full range of compositions and in the worst case (43at.% Al) the value was still approximately half that of the NiCrMo sample. Although the TCR of the CuAl films were generally positive, the negative result obtained for the 43at.% Al film was encouraging as it presented the possibility of obtaining a near zero result, assuming the TCR shifted positive with increasing heat treatment temperature.

To allow further investigation of the sheet resistance and TCR results, the figures were compared with those obtained from the literature. Figure 2.5 gives a comparison of the current work and that of Bashev et al, 1990 [121]. Due to differences in sputtering conditions, the sheet resistance and TCR results have been normalised to give comparison of relative results and curve shapes. Moreover in order to replicate the processing conditions of Bashev, the experimental films were annealed for 50 hours at 90ºC in air.

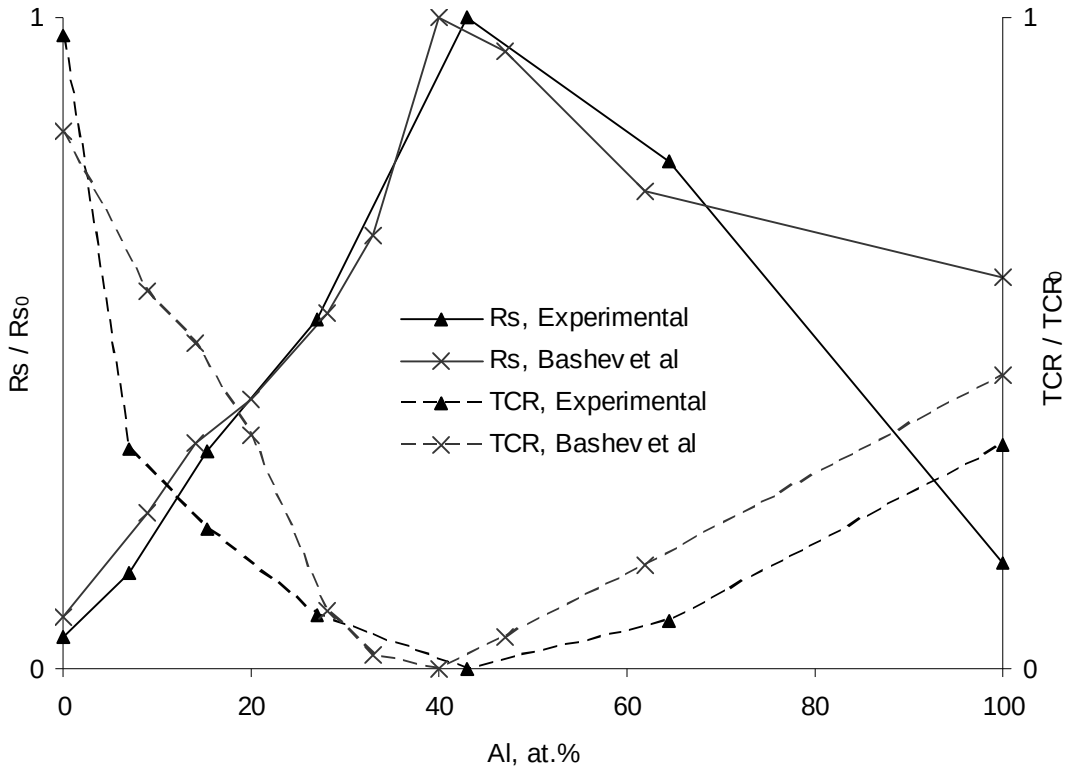

Fig. 2.5 – Comparison of mean sheet resistance and TCR properties of the CuAl films for current and previous work [121].

As can be seen the results are in reasonable agreement with similar curve shapes for both Rs and TCR plots. Perhaps the most significant variation between the results is that obtained for the pure aluminium films. The sheet resistance figure obtain by Bashev et al for the aluminium film is approximately 3.75 times greater than that obtained in the current work. Assuming that the copper and aluminium films were produced under similar conditions and again taking the sputter yield ratio to be 2:1, the ratio of sheet resistances for the current work is much closer to the ratio of bulk resistivities than that for the work of Bashev et al:

Ratio of Al:Cu Rs for Bashev et al	≈ 7.5 : 1
Ratio of Al:Cu Rs for current work	≈ 3.3 : 1
Ratio of Al:Cu r at R.T. x ratio of sputter yields (2.65/1.67) / (1/2)	= 3.2 : 1

Room temperature resistivities of copper and aluminium taken as 1.67μΩcm and 2.65μΩcm respectively [22].

To allow further comparison with the literature the film dimensions were measured and their resistivity was calculated using Equation 1.2. The film length and width were measured using a Nikon Measurescope MM-22. The thickness of the films on glass slides were measured using a SEM, the measurements were also confirmed for

several samples using a Taylor-Hobson talystep profilemeter, the film step being created with a microscope slide cover slip. Typical results for both methods are presented in Figures 2.6a and 2.6b respectively.

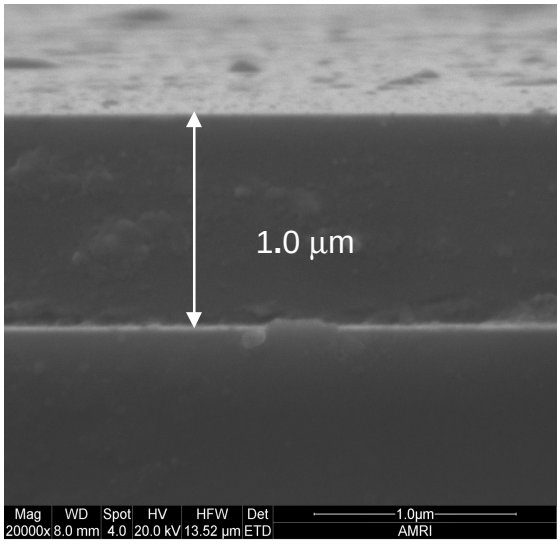

Fig. 2.6a – SEM measurement of film thickness

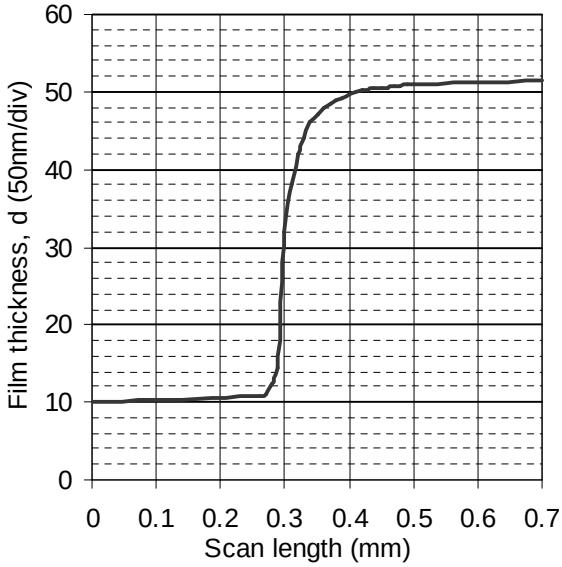

Fig. 2.6b – Profilemeter measurement of film thickness

The calculated resistivities for the as-grown experimental samples are shown in Figure 2.7.

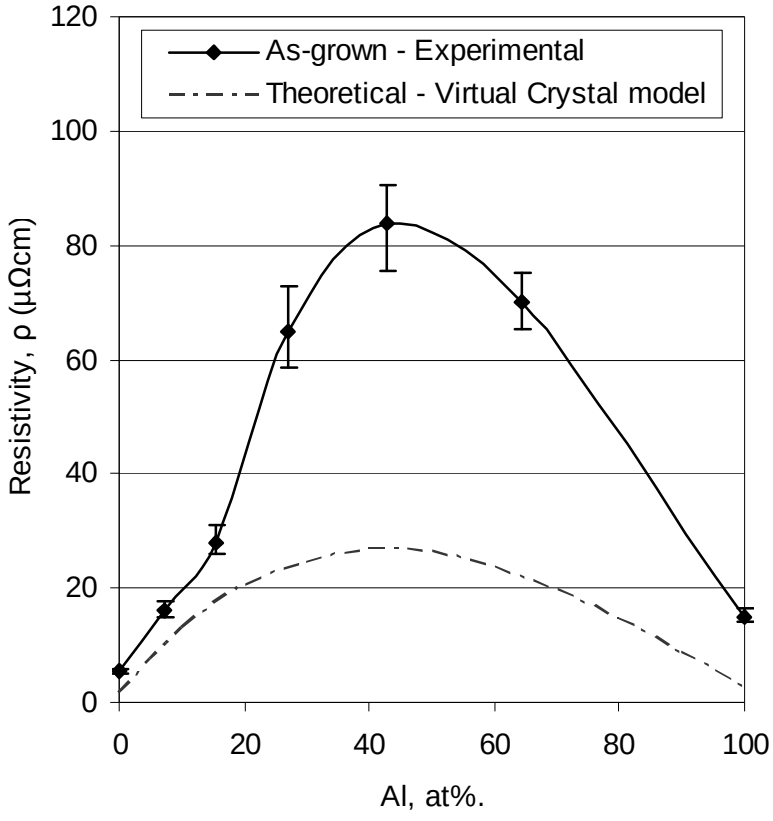

Fig. 2.7 – Experimental and theoretical resistivity plots for the CuAl system [173].

According to Matthiessen's rule for pure metals the resistivity, r, is the sum of two parts; a residual resistivity, r_r, and a thermal part r_t (see Figure 2.8):

$$r\ (total) = r_r + r_t \qquad \textit{Equation 2.1}$$

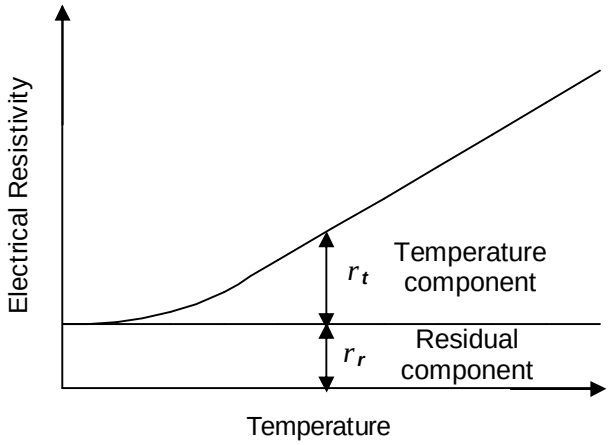

Fig. 2.8 – Resistivity versus temperature for a typical metal, Matthiessen's rule

The presence of impurities in the metal raises the residual resistivity, r_r. The increase of r_r on a single impurity can be calculated using Nordheim's rule [172]:

$$r_r(x) = Ax(1 - x) \qquad \textit{Equation 2.2}$$

Where x is the concentration of the impurity as an atomic fraction and A is a constant called the "solution resistivity coefficient". A depends on the base metal, and the impurity and material factors that can influence it include atomic sizes and crystal structure.

Equation 2.2 can also be written as follows and indicates a parabolic relationship between resistivity and impurity concentration.

$$r_r(x) = Ax - Ax^2 \qquad \textit{Equation 2.3}$$

Also when $x \perp 1$, $1 - x \approx 1$, we have:

$$r_r \gg Ax \qquad \textit{Equation 2.4}$$

This indicates a linear relationship between resistivity and impurity in a dilute solid solution alloy.

The experimental resistivity plot for the as-grown CuAl films presented in Figure 2.7, shows reasonable agreement with Nordheim's rule. It is parabolic in shape for high impurity concentration and more linear in the dilute regions in accordance with Equations 2.3 and 2.4. This result is typical of a disordered binary alloy system, the

resistivity increasing as the solute (Al) is added to the solvent (Cu) due to the increasing possibility of collisions between moving electrons and the ions constituting the crystal structure.

Although Equation 2.2 has shown good accuracy for a number of binary alloys, it relies on the two constituents being homovalent, thus the highest resistivity is always predicted at a composition of 50at%. To take into account the difference in valence between copper and aluminium a virtual crystal approximation can be employed [22]. Again the model considers only the effects of change in composition and assumes the alloy to be in a disordered state, therefore neglecting any changes in the crystal structure. The impurity resistivity r_r, for the alloy A_xB_{1-x} is given by:

$$r_r = x\,(1-x)\,[a_1 + (a_2 - a_1)x]\,|\,M\,|^2 \qquad \textit{Equation 2.5}$$

Where M is the matrix element of the difference potential (V_A-V_B) and a_1, a_2 take into account the difference in valence between the constituents A and B. The full curve calculated from Equation 2.5 for the CuAl system is plotted in Figure 2.7 and shows close similarity in shape to that obtained for the as grown samples [173]. The maximum resistivity for the experimental curve is found at around 40at.%, which again is consistent with the virtual crystal model, taking into account the difference in valence.

Perhaps the most noticeable dissimilarity between the as-grown experimental plot and the virtual crystal theoretical plot are the large differences in resistivity values. For all compositions the resistivity values for the experimental result are higher than those predicted by the model. As the model assumes a bulk disordered system and is not specifically developed for application to thin films, there are a number of potential reasons for this increase in resistivty, such as thin film size effects, formation of crystalline phases, micro-imperfections in the crystal lattice and impurity incorporation during deposition. These theories are discussed in more detail in the proceeding text.

Effect of Heat Treatment on the Electrical Properties

As discussed in chapter 1, freshly deposited thin films can exhibit instability in their physical properties during storage due to changes in their structural conditions. This is largely due to the fact that the crystal lattice of the film contains a large number of micro-imperfections in its structure such as non equilibrium vacancies. In order to remove these imperfections and thus improve the stability of the film, heat treatment is essential.

Following annealing, the structure of the film should be stable throughout its life at any temperature lower than the annealing temperature, provided interaction with any

external medium is prevented. Thus, in the case of thin film resistors, the annealing temperature used during manufacture will usually exceed the specified operating temperature of the device, in this case 125 to 155ºC.

Following deposition, samples from each trial were annealed at temperatures of 200, 300, 400 and 500ºC for 5 hrs in both air and nitrogen environments. Figures 2.9a to 2.9d show the sheet resistance and TCR_{av} properties of the CuAl films with increasing heat treatment temperature. Results obtained for the NiCrMo control are also presented. Results at each temperature are based on the measurements of a sample of 6 films taken from across the sputtering pallet.

In general, the percentage decrease in Rs with increase in temperature is similar for the CuAl films. The results of Rs obtained for films stabilised in air and N_2 are very similar, suggesting that stabilisation environment, whether air or N_2, has negligible affect on the Rs of the CuAl films.

The result for the NiCrMo control is similar to that of the CuAl films showing a decrease in Rs with increasing annealing temperature. However the result obtained for the NiCrMo films treated in air is noticeably higher than that for nitrogen. This result is most likely due to the increased formation of chromium oxide in the air atmosphere leading to an increase in resistance [46]. In terms of relative Rs, as both the NiCrMo and CuAl films decreased by similar amounts during the stabilisation process the advantage is further increased to at least 5 times for the films treated at 500^{o}C.

Figures 2.9c and 2.9d show TCR_{av} results for the different film compositions following annealing in air and N_2 respectively. It can be clearly seen that increase in stabilisation temperature results in an increase in TCR, again regardless of heat treatment environment. Possibly the most striking area of this result is the difference in TCR response to temperature between the pure elements and the alloys. As can be seen the TCR of the pure Cu and Al films rise steeply towards their bulk values and peak at values of around 4300 and 3500ppm/^{o}C respectively after stabilisation at 400^{o}C, before decreasing to final values of 4000 and 3000ppm/^{o}C following treatment at 500^{o}C. This negative shift at higher temperatures was attributed to degradation of the films.

Conversely the results obtained for the NiCrMo and CuAl alloys are relatively stable and TCR increases are more gradual. Further analysis shows that the TCR of the CuAl films moves positive quite linearly throughout the temperature range whilst that of NiCrMo remains unchanged until 300^{o}C where it then begins transition from negative to positive through the zero TCR line. This result corresponds closely to that reported for various alloys of NiCr in chapter 1.

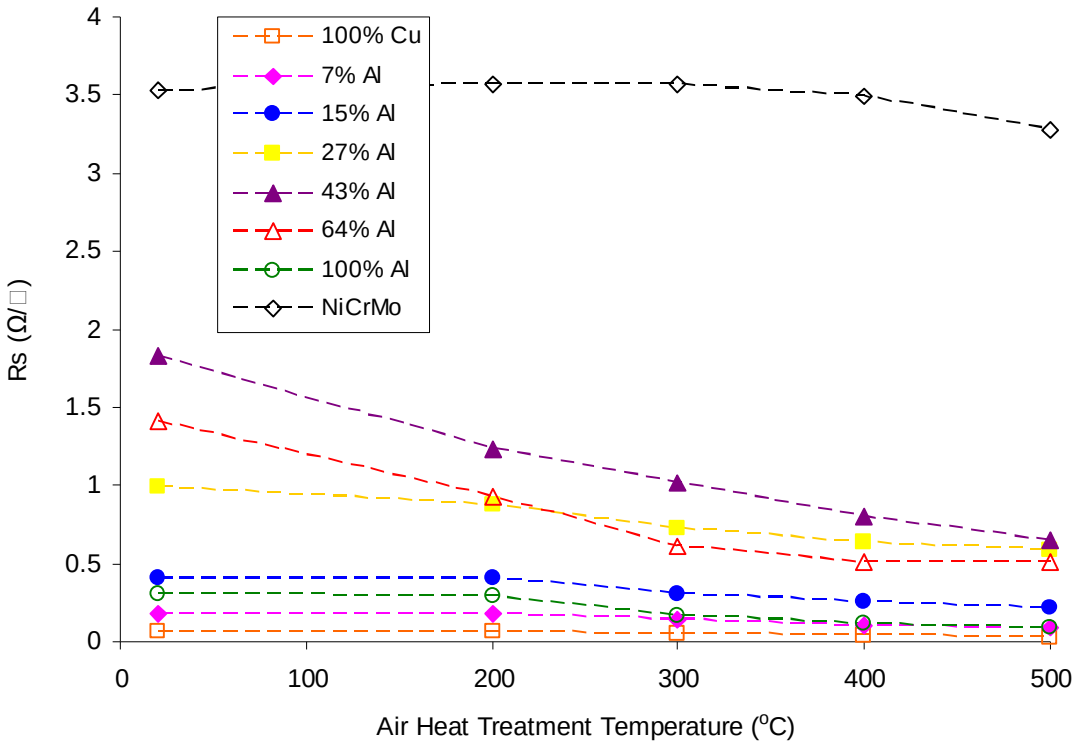

Fig. 2.9a – Sheet resistance following heat treatment in air for 5hrs at varying temperatures.

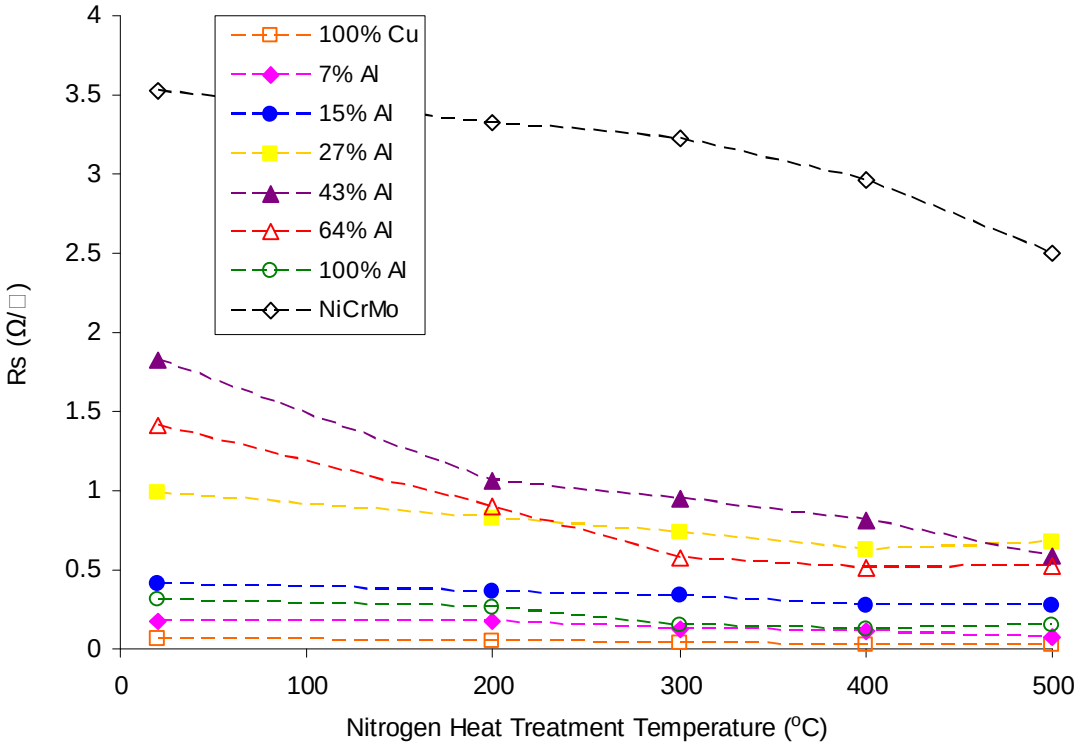

Fig. 2.9b – Sheet resistance following heat treatment in nitrogen for 5hrs at varying temperatures.

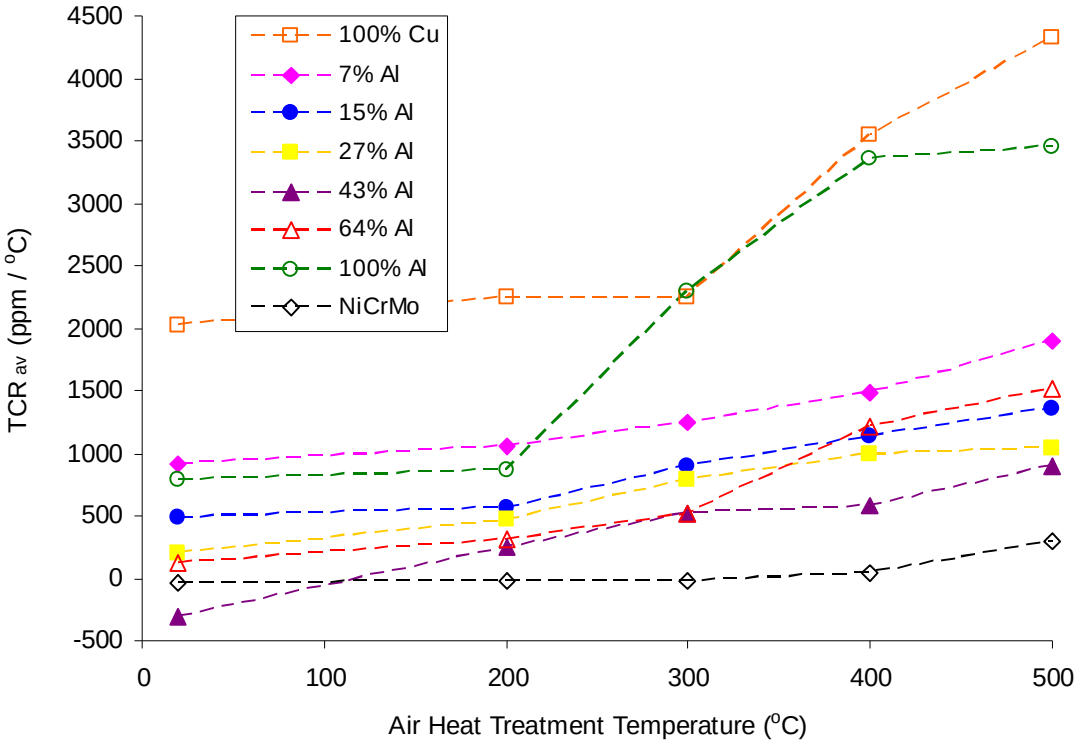

Fig. 2.9c – TCR_{av} following heat treatment in air for 5hrs at varying temperatures.

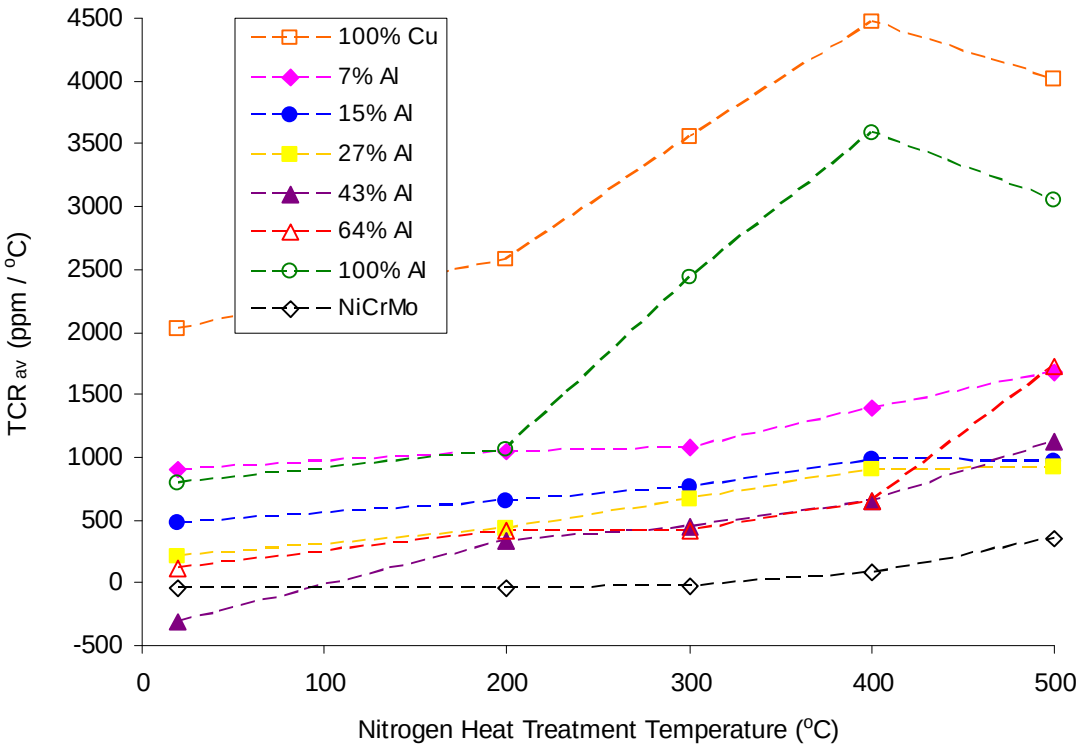

Fig. 2.9d – TCR_{av} following heat treatment in nitrogen for 5hrs at varying temperatures.

Further analysis of the results for the CuAl films shows that they all follow a very similar curvature, with the copper rich films always remaining more positive than the Al rich. One exception to this observation is the result of the 43at.% Al film, which as deposited looked promising with a TCR of around -300ppm/^{o}C. As can be seen this result soon becomes positive with a value approaching +500ppm/^{o}C following stabilisation at 300^{o}C.

Although the error bars have been excluded from Figures 2.9 for clarity, the distributions of measurements improved with increasing heat treatment temperature and in all instances were no worse than those reported for the films in the as grown state in Figure 2.4.

The general trend for all the films following heat treatment is a decrease in sheet resistance accompanied by a subsequent increase in TCR with increasing annealing temperature. This behaviour is typical of thin film resistor alloys sputtered at room temperature and subsequently annealed. The processes responsible for the changes in electrical properties can be largely divided into three categories; structural, phase and chemical modifications of the films [20]:

1. *Annealing of micro-imperfections formed during deposition*. This stage of annealing results in a decrease in the concentration of non-equilibrium point defects, redistribution of dislocations and formation and removal of small-angle grain boundaries. These processes always lead to an irreversible decrease in resistivity and subsequent increase in TCR.

2. *Recrystallisation*. This process leads to a reduction in the number of randomly orientated crystallites due to transformation of high angle grain boundaries and merging of crystallites. Again this process causes a decrease in resistivity.

3. *Chemical reactions in the solid phase*. The main process in this category is oxidation of the film in the atmosphere and always results in an increase in resistivity of the film.

It is quite normal for all the above processes to occur simultaneously and the probability of one process dominating is reliant on a number of factors such as the time and temperature of the heat treatment and also the thin film material type.

Figure 2.10 shows resistivity plots for the experimental CuAl films both as-grown and following annealing at 400ºC in nitrogen.

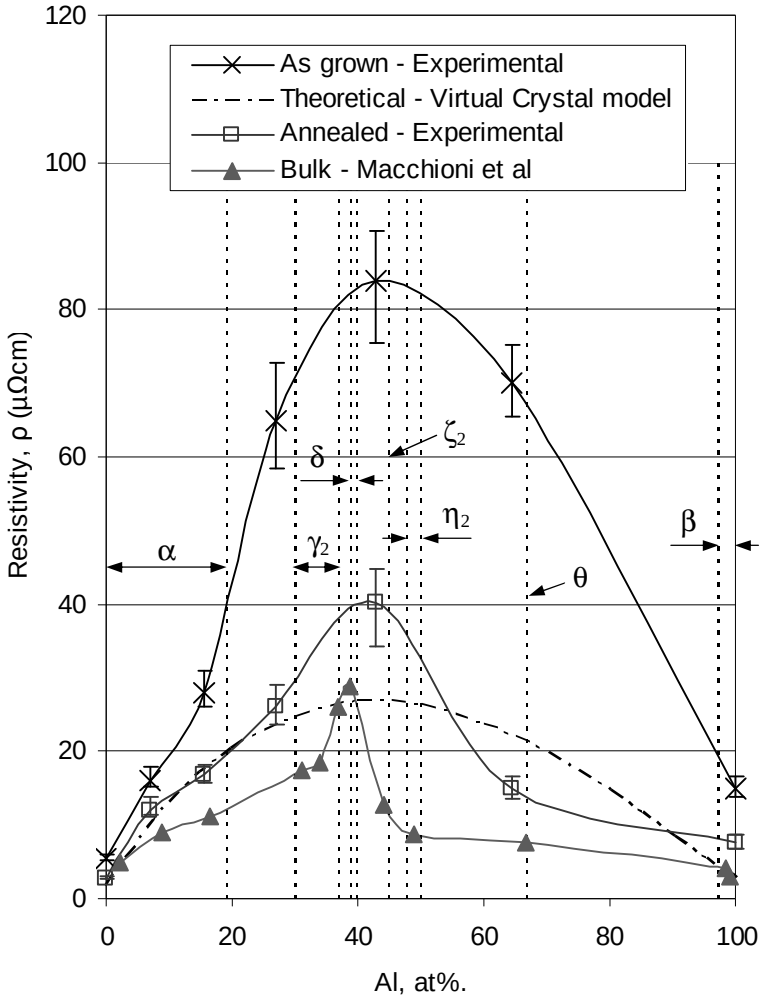

Fig. 2.10 - Experimental and theoretical resistivity plots for the CuAl system (see Table 2.6 for identification of CuAl phases)

As previously discussed the as-grown plot has a typical parabolic shape of a disordered alloy system and compares well with the theoretical model. The difference in actual values of the two plots is attributable to imperfections and impurities formed during deposition.

Once these micro-defects start to be annealed out of the film there is a considerable reduction in resistivity, as demonstrated by the 'annealed' experimental curve. However the reduction is not linear across the composition range causing a change in the shape of the plot with a distinct peak at around 40at% Al. This shape is attributable to solute interaction effects and the formation of phases of CuAl in the film and shows reasonable agreement with previous work for both thin film [174] and bulk [173] samples. For comparison the results reported by Macchioni et al [173] for bulk samples of CuAl annealed in argon, close to the maximum temperature consistent with stability as

determined from the phase diagram, are also plotted in Figure 2.10. As can be seen the shape of the plot bears close similarity to that of the current work.

As shown in Figure 2.11 the phase diagram for the copper-aluminium system is quite complex especially at the aluminium rich side [169]. In addition to the cubic solid solutions of aluminium and copper there are five stable intermediate phases in the low temperature range below 600ºC (see Table 2.6).

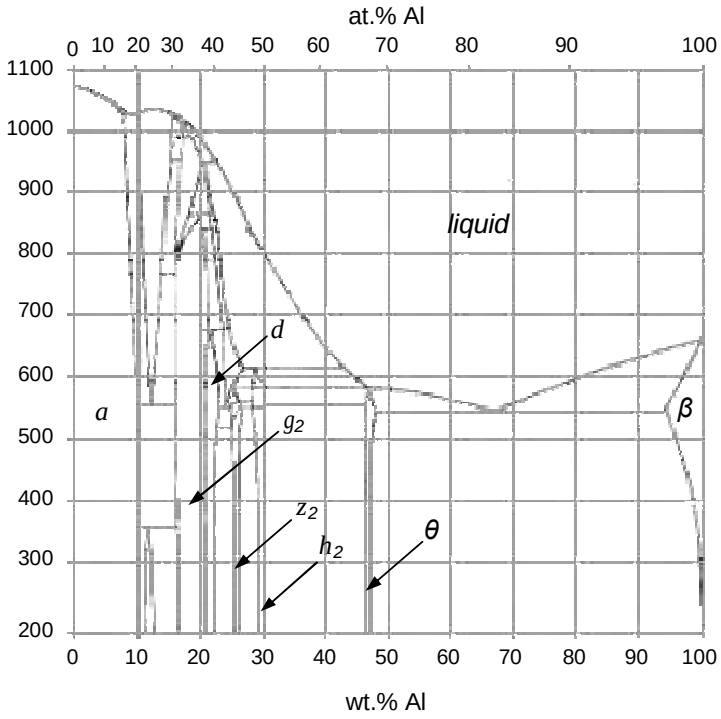

Fig. 2.11 – Copper-Aluminium phase diagram [169].

Phase	Approximate composition (at.% Al)	Lattice designation
α (Cu)	0 - 19.5	Cubic
γ_2 (Cu_9Al_4)	30 - 37	Cubic
δ (Cu_3Al_2)	39 - 40	Cubic
ζ_2 (Cu_4Al_3)	~ 45	Monoclinic
η_2 (CuAl)	48 - 50	Monoclinic
θ ($CuAl_2$)	~ 67	Tetragonal
β (Al)	97.5 - 100	Cubic

Table 2.6 – Properties of phases in the copper-aluminium system

The γ_2 and δ phases are both complex cubic structures with approximate compositions of Cu_9Al_4 and Cu_3Al_2 respectively. The γ_2 phase has a stability range of around 30 – 37at.% Al, whilst that of the δ phase is much narrower at around 40at.% Al. The remaining three phases ζ_2 η_2 and θ also have narrow stability ranges with compositions corresponding to Cu_4Al_3, CuAl and $CuAl_2$ respectively.

As shown in Figure 2.10 the resistivity plots for the annealed film and bulk samples are far from linear, the most prominent feature being the peak in resistivity for the γ_2 and δ phases at around 30-40at.% Al. The sharp increase throughout the composition range of the γ_2 phase is reported as being essentially an electronic effect associated with the γ-brass band structure and can be explained by the Jones zone formed by the (330) and (411) planes of the reciprocal lattice for a simple cubic structure [170].

Seeing that all of these planes are parallel, as the electron concentration increases the Fermi surface will make contact with all 36 zone faces provided it is spherical. This leads to a rapid decrease in the Fermi surface area and density of states at the Fermi energy. Specific heat measurements of γ-brass alloys have confirmed that this decrease takes place [175] and it therefore follows that the resistivity (r) will increase and the conductivity (σ) will decrease, due to the rapid decrease in Fermi surface (S_F) area with increasing concentration of aluminium:

$$s = \frac{1}{r} = \frac{e^2}{12p^3\mathbf{h}}\langle tu\rangle S_F \qquad \textit{Equation 2.6}$$

Where $©tu™$ is the average over the Fermi surface of the product of the relaxation time, t and carrier velocity, u. The Fermi surface can be defined as a surface of constant energy in *k*-space, where *k* is the wave vector of the electron, which separates the unfilled electron bands from the filled electron bands, at absolute zero [22]. It is important in determining the electrical properties of a metal because the current is related to changes in the occupancy of states at the Fermi surface.

The resistivity of the ζ_2, η_2 and θ phases is similar to that previously observed in polyvalent pure metals. The inconsistency between the experimental results of Macchioni et al and the theoretical resistivities for these phases is due to the fact that these are ordered electron compounds and not disordered as predicted by the virtual crystal model. Likewise the results for the γ_2 and δ phases show a reasonable fit to the theoretical curve, thus supporting the theory that these are in fact disordered systems.

Although there is evident similarity in the shape of the resistivity plots for the annealed samples for the current work and that of Macchioni et al, there is still a noticeable discrepancy in the actual values. There are a number of potential causes of this error such as sample preparation and processing conditions, however the most likely reason is due to the thin film size effects on conductivity which must be taken into account when making comparisons with data for bulk samples. This phenomenon is discussed in detail in chapter 6.

Resistance stability

To measure the stability of resistance for the CuAl samples, they were subjected to a dry heat stability test of 168hrs at 155°C in an air atmosphere. Results of resistance stability for the various film compositions following stabilisation in air and N_2 at 300°C for 5 hours are presented in Figure 2.12. All results are based on the measurement of 6 films for each chemical composition.

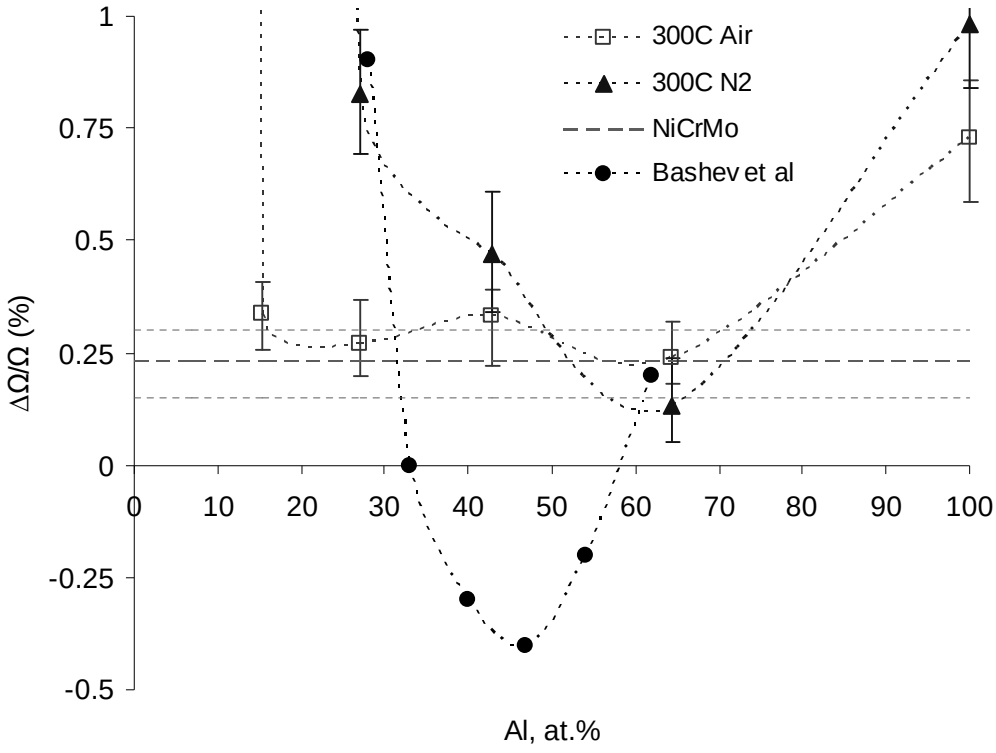

Fig. 2.12 – Resistance stability of CuAl samples following 168hrs at 155ºC in air

An initial view of the data presented in Figure 2.12 shows that the copper rich films are very unstable regardless of heat treatment regime. Although the results for these films have been excluded they were no less than +20% in all cases. The most plausible reason for these large positive shifts is oxidation of the copper rich films.

However once the aluminium content of the films begins to increase, the stability significantly improves and is no worse than 1% for films in the range ≈25 to 100at.%Al. This improvement can be largely attributed to the formation of the protective aluminium oxide layer on the surface of the film during the annealing stage which subsequently retards the rate of further oxidation and hence resistance increases. This analogy is further supported by the difference in results for the films annealed in air and nitrogen. As can be seen for films in the composition range ≈15 to 30at.%Al, the stability figures are better than 0.5% when annealed in the oxidising air atmosphere and greater than 0.75% when annealed in nitrogen.

The further improvements in stability for the mid range composition films can be attributed to the formation of the aforementioned stable CuAl phases. Results reported by Bashev et al for thin films of copper-aluminium are also presented in Figure 2.12 [121]. As can be seen excellent stability of resistance was also found in the mid range composition area and was reported to be due to the formation of the stable γ_2 phase with a wide range of homogeneity from approximately 28 to 62at.% Al. Indeed only three phases were detected over the whole composition range for the ion-plasma sputtered films: two highly-super saturated solid solutions based on Al and Cu and the γ_2 phase.

Also plotted in Figure 2.12 is the stability result for the NiCrMo control film following heat treatment at 300ºC in air. As expected changes of around 0.25% were produced for these films, which correlate closely to the findings of other researchers for NiCr films reported in chapter 1. When compared with the CuAl films annealed in air, the results for the NiCMo films are marginally better, 0.25% versus 0.4%. On average the stability of the CuAl films annealed in nitrogen are worse again, however the best result regardless of heat treatment regime is produced by the 64at.%Al film at 0.23% and 0.13% for films annealed in air and nitrogen respectively. This improvement could be due to the formation of the stable θ phase which occurs at approximately 67at.% Al and is investigated further in chapter 3.

2.4 SUMMARY

From the work conducted in this chapter it is quite evident that a binary system of copper and aluminium shows much promise in the application of thin metal film resistors.

Ultimately there are a number of detailed specifications to which a component must conform before it can be deemed 'fit for purpose' [12], the finer points of which are covered in chapter 8. However as discussed in chapter 1, in order to establish an initial impression of the performance of the films, two tests which are deemed appropriate are that of TCR_{av} (20ºC and 70ºC) and also dry heat stability (168 hours at 155^{o}C).

A summary of key electrical properties for the CuAl film samples with increasing aluminium content following heat treatment at 300ºC for 5 hours in air are presented in Figure 2.13

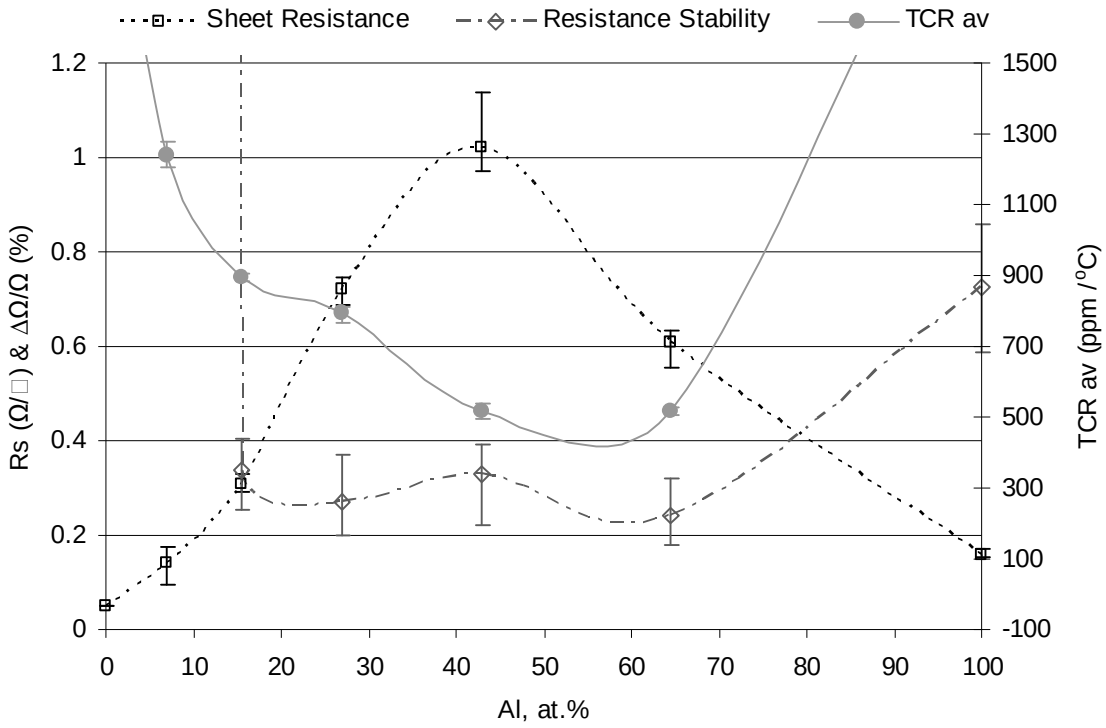

Fig. 2.13 – Key electrical properties of the CuAl thin film samples Following heat treatment in air for 5hrs at 300ºC

From the results for TCR_{av} it can be established that only the films containing ≈ 25 to 65at.% Al have as-grown values anywhere close to the specified target of ±50ppm/^{o}C. Whilst that of the Cu rich films and indeed the pure Al and Cu films is large and positive at between 500 and 2000ppm/^{o}C. This inadequacy is then further augmented following heat treatment stabilisation where TCR shifts positive with increasing temperature across the composition range and thus the near suitable TCR of the mid composition films soon deteriorates to values in excess of 400ppm/^{o}C. This trend appears to remain true regardless of annealing environment, air or nitrogen.

A similar result can be concluded for that of resistance stability, where again it appears that a minimum of around 15at.%Al is required before any adequately low figure can be established. On this occasion those films pre heat treated in an air atmosphere gave the best results with a consistent figure of 0.3% produced by films annealed at 300^{o}C.
In terms of achieving the preliminary objectives laid out in chapter 1, investigations thus far could be deemed a success. Although at this stage it is still difficult to assess the suitability of thin films of CuAl in terms of overall electrical performance it still useful to compare their fundamental electrical characteristics against those of the NiCrMo control, as ultimately it is the performance of this film which must be realised.

	Rs (Ω/□)	TCR (ppm/°C)	ΔΩ/Ω (%)
NiCrMo	3.25	-25	0.23
CuAl-43at.%	1.0	+515	0.33
CuAl-64at.%	0.6	+520	0.24

Table 2.7 – Comparison of the fundamental electrical characteristics of NiCrMo and CuAl thin film resistors stabilised at 300ºC in air.

Table 2.7 shows the results achieved for 43at%.Al and 64at%.Al films, which have the lowest TCR figures, compared to that of the NiCrMo control film sputtered and stabilised under identical conditions. As can be seen one major objective can already be satisfied in that the sheet resistance value for the CuAl film is approximately 3.5 times lower than that of NiCrMo, thus lower pre-values can be sputtered at faster rates. Moreover the stability of the CuAl films is also comparable to that of NiCrMo. However one obvious concern at this stage which must be addressed is the large positive TCR of the CuAl films.

Chapter 3

Ternary Thin Film Composition Selection

3.1 INTRODUCTION

Perhaps the most widely documented method of reducing the TCR of binary thin metal films is to introduce a third doping element into the structure to produce a ternary system.

This 'doping' element can be supplied in the sputter gas or incorporated into the target itself. Its role is to add controlled impurities into the growing metal structure giving control over TCR and in many cases resulting in additional improvements in stability. The level of doping is generally determined experimentally to give films with as grown TCR figures in the negative region, which can be subsequently shifted to near zero during heat treatment stabilisation.

In terms of 'doping' in gaseous form, oxygen and nitrogen are by far the most popular elements. Generally the reactive gas is mixed with the inert sputter gas (usually argon) at typical levels of between 1% and 20%. Once in the deposition chamber the reactive gases then form oxides and nitrides in the film which are seen as a negative TCR due to their semiconducting properties. As discussed in chapter 1 the two most popular reactively sputtered films for use as thin film resistors are TaN and CrSiO. Reports have shown that the TCR of these films is significantly reduced with increasing reactive gas content.

There does however appear to be several drawbacks associated with the reactive gas sputtering technique, the main one being accurate control of the gas flow rate and hence reproducibility of films of consistent stoichiometery. Further problems can also occur with the continuous processing of oxygen due to the build up of ozones in the pumping system which have to be routinely removed by time consuming regeneration of the system [177].

Once these negative TCR benefits were established in gaseous form, the next step for many researchers was to incorporate the doping elements as solids in the sputtering target itself. It was found that this method could match these benefits whilst also eliminating the fore-mentioned problems, thus allowing the production of films with repeatable characteristics. This transition from gas to solid allowed for the investigation of a much wider spectrum of doping elements of various ratios.

Two of the most popular of these elements are silicon and molybdenum. As silicon is a semiconductor it readily produces a negative TCR value. Molybdenum on the other hand is a metal with a large positive bulk TCR. However once in the deposition chamber Mo is known to have a high chemical affinity with residual oxygen due to its

refractory nature. This reaction leads to the formation of thin dielectric layers in the grain boundaries which are seen as a negative TCR [20].

As it was not possible to locate any literature concerned with doping of CuAl thin films, in order to try and reduce TCR, the most obvious choice was that of Si, as it has been widely reported to reduce the TCR of other metal alloy systems such as NiCr [57-63]. Moreover NiCrSi 47.5/47.5/5wt.% is one of the main thin film resistor compositions currently used at Welwyn Components Ltd.

In addition to Si, Mo is also an element in use at Welwyn Components in the NiCrMo 45/45/10wt.% composition. Although there has been limited data published for this system [311-312] it is by far the most popular in use at Welwyn Components and has been successfully used for around 20 years. Moreover Mo has been proven to be more useful at reducing the TCR of thicker low resistance NiCr films than Si [178] and its refractory nature is also known to improve stability due to the small mobility of defects at normal operating temperatures [20]. As the bulk resistivity of Mo is also lower than that of Si (5μΩcm versus 1000μΩcm [310]), it follows that its introduction into the CuAl matrix should have less effect on the conductivity of the system [224].

As each of the eighteen pieces of the CuAl sputtering target equated to approximately 6% area, a decision was made to initially try incorporations of one piece of both Si and Mo. However due to difficulties in machining matching angles on the target pieces, the eventual percentage incorporations were nearer to 6.7% area.

As concluded in chapter 2, a minimum of around 15at.% Al is required to produce CuAl films with good resistance stability following heat treatment in air. It was therefore decided to investigate the performance of the following ternary compositions.

Run No.		9	10	11	12	13	14
Target area.%	Cu	22.3	22.3	44.5	44.5	72.2	72.2
	Al	71.0	71.0	48.8	48.8	21.1	21.1
	Si	6.7	-	6.7	-	6.7	-
	Mo	-	6.7	-	6.7	-	6.7

Table 3.1 – CuAlSi and CuAlMo Target Compositions Investigated

3.2 EXPERIMENTAL AND CHARACTERISATION

All ternary film samples were manufactured and characterised under identical conditions to the binary CuAl films described in chapter 2.

3.3 RESULTS AND DISCUSSION

3.3.1 Chemical Composition Analysis

The mean composition of the film samples sputtered onto glass slides are presented in Table 3.2. The films were examined at five areas on the surface, and were then fractured and a further five areas were analysed on the cross section. The composition was found to be homogeneous and did not vary by more than ±2at.% across the 10 areas of analysis for all samples studied.

Run No.		9	10	11	12	13	14
Target at.%	Cu	29.1	28.7	53.6	52.9	79.3	78.3
	Al	65.7	64.8	41.7	41.1	16.4	16.2
	Si	5.1		4.7		4.3	
	Mo		6.5		6.0		5.5
Film at.%	Cu	37.4	34.2	61.9	58.6	80.5	78.7
	Al	57.6	57.3	33.5	34.5	15.3	15.3
	Si	4.9		4.6		4.2	
	Mo		8.5		6.9		6.0

Table 3.2 – Mean composition of the CuAlSi and CuAlMo target and thin films

As with the binary CuAl films, the content of Cu in the films is higher than that in the sputtering target and vice versa for the Al. Again this is related to the difference in sputter yields of the two elements [168] (see Table 3.3). However unlike the binary films, in this case it was not possible to directly relate the discrepancy back to the sputter yield figures. It can be postulated that this is due to the positioning of the sample substrate in the centre of the target directly beneath the single piece of Si or Mo. Indeed the content of Si and Mo in the films is reasonably close to that in the target for all except one run, number 10, and had the doping piece been more evenly spread throughout the target, the sputter yield figures suggest that their content in the films would have been lower.

Element	Sputter yield (atoms/ion)
Cu	2
Al	1
Si	0.5
Mo	0.6

Table 3.3 – Typical sputter yields of the individual elements at 500eV Ar+ at normal incidence [168].

3.3.2 Electrical Properties

As Grown Electrical Properties

Figure 3.1 shows the as-grown sheet resistance and TCR_{av} results for the various films of CuAlSi and CuAlMo. All results are based on the measurements of a sample of 18 films taken across the sputtering pallet.

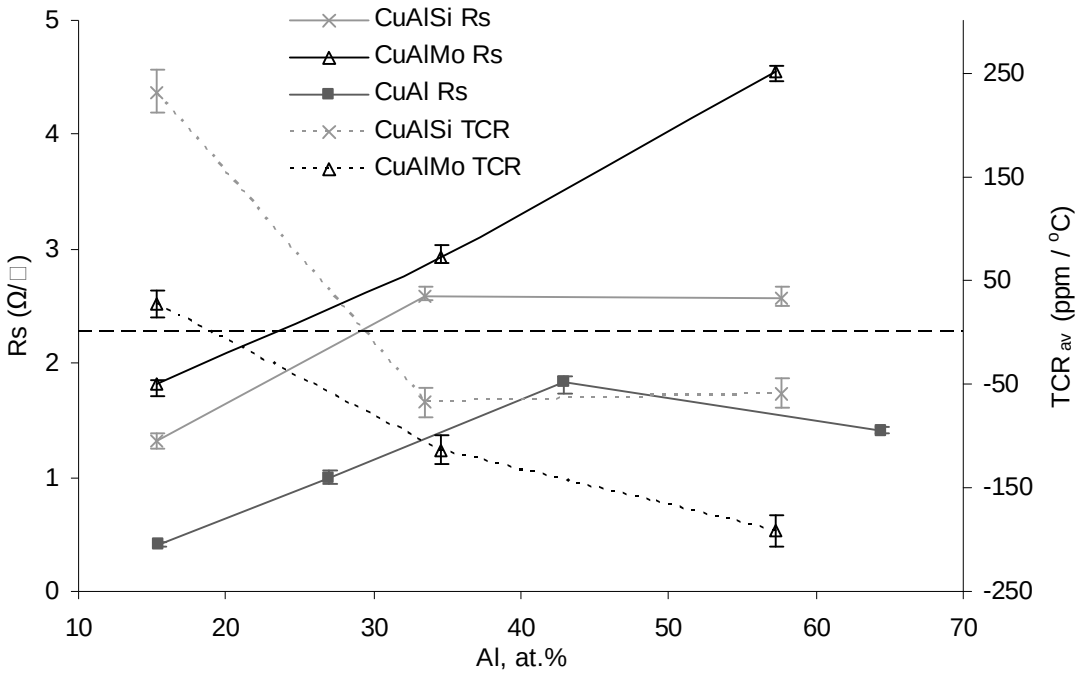

Fig. 3.1 – As grown sheet resistance and TCR for the CuAlSi and CuAlMo thin films

The addition of the Si or Mo doping element to the binary CuAl film produces the desired effect of reducing TCR across the investigated composition range and yields a negative figure for the films containing ≈ 35at.% Al and above.

However the doping has also in turn caused an increase in sheet resistance of the films. As can be seen the sheet resistance plot for the CuAlSi film follows a similar trend to the binary film and doubles in value from 1.3Ω/□ at 15at.%Al to 2.6Ω/□ at 33at.%Al, before levelling to a final value of 2.55Ω/□ at 57at.%Al. The result for the CuAlMo films is higher again and rises from 1.8Ω/□ at 15at.%Al to 2.9Ω/□ at 34at.% Al. However in this case the curve does not level off, as with the AlCuSi films, and continues to rise to a peak value of 4.55Ω/□ for the films containing 57at.% Al. This figure is higher than that measured for the NiCrMo control of 3.5Ω/□ and is obviously unacceptable.

As expected the plots for TCR follow a similar but inverse shape to the sheet resistance curves. The mean result for the CuAlSi film is positive at +230ppm/ºC for the

15at.%Al film but reduces to a negative value of -68ppm/ºC at 33at%.Al before again levelling off to a final value of -60ppm/ºC at 57at.% Al. The result for the CuAlMo film is even more negative starting at +26ppm/ºC and dropping almost linearly through -114ppm/ºC at 34at.% Al to -191ppm/ºC at 57at.% Al. These negative as-grown TCR results are encouraging and provided the opportunity to achieve a near zero TCR following heat treatment.

It is possible to explain the difference in values and shape of the resistance plots obtained for the two doping elements through their concentration in the films. With reference to Table 3.2 it can be seen that the CuAlSi films are all slightly deficient in Si across the composition range tested, when compared with the starting composition of the target. Conversely the CuAlMo films are all rich in Mo.

However as the doping element was positioned in the centre of the sputtering target directly above the substrate it would be expected that both film types would be slightly rich in concentration, especially considering the closeness in sputter yield figures for the two elements. Therefore this discrepancy is most likely related to the difference between the sputtering properties of the two materials.

In order for the dc sputtering technique, as used in this investigation, to function correctly, the target material must be an electrical conductor, i.e. a metal such as molybdenum. Simple substitution of an insulator or semiconductor, such as silicon, for the metal target is doomed to failure because of the immediate build up of surface charge of positive ions on the front side of the insulator, which prevents any further ion bombardment [167]. It is therefore common practice to employ an RF or a pulsed dc arrangement to overcome this problem.

On the other hand, it is also well documented that dc sputtering of small percentages of Si is possible when combined with alloy systems such as NiCr. Maybe the most plausible reason in this investigation is that the Si was introduced as a single solid piece in the sputtering target rather than being homogeneously mixed with the AlCu then sintered in the same way as commercial one piece NiCrSi sputtering targets are manufactured.

A closer inspection of the composition figures in Table 3.2 shows that the deviation in Si concentration in the film from the target is quite linear across the sampled range and thus the resistance plots are offset from the binary CuAl result by a fixed amount and therefore comparable in shape. The composition result for run number 10 is unusually rich in Mo, 8.5at.% in the film versus 6.5at.% in the target, and is the most plausible

reason why the CuAlMo resistance plots are linear and do not level off in the same way as the CuAl and CuAlSi results.

It is not clear why run number 10 is unusually rich in Mo but could be due to the reduced amount of high 'sputter rate' Cu present in the target in this composition, which would allow more Mo to arrive at the substrate. Perhaps the aforementioned problems associated with the dc sputtering source prevented the Si from attaining the same advantage.

Effect of Heat Treatment on the Electrical Properties

Results for sheet resistance and TCR_{av} for the CuAlSi and CuAlMo films following heat treatment in air for 5 hours at 200, 300, 400 and 500ºC are presented in Figure 3.2 and Figure 3.3 respectively. Results at each temperature are based on the measurements of a sample of 6 films taken from across the sputtering pallet.

Perhaps the most noticeable feature of the results is the step decrease in sheet resistance and coinciding increase in TCR that occurs for both film types following heat treatment stabilisation. This transformation occurs at between 200 and 300ºC for the CuAlSi films and between 300 and 400ºC for the CuAlMo films. It can be postulated that this sudden decrease in resistivity is being caused be the formation of the CuAl phases discussed in chapter 1 and that the Mo doping is able to retard their formation to higher temperatures than the Si doping. This theory is expanded upon in chapter 5.

As this step increase through the zero TCR line occurs at relatively low temperatures for the CuAlSi films the TCR may be susceptible to changes in value during subsequent manufacturing stages such as laser trim stabilisation and protection curing, which have typical settings of 200 to 250ºC. Although it may be possible to shift the position of this 'step' to higher temperatures by increasing the Si content in the film it was thought that this could lead to additional problems with dc sputtering of Si as discussed earlier. It was therefore decided to abandon this composition and concentrate on the more promising results achieved with the Mo doping.

Of the three CuAlMo film samples, those containing ≈35 and 58at.% Al give the most useful TCR results, passing the zero line at 300-400ºC and 400-500ºC respectively. The more Cu rich films containing ≈15at.% Al have a positive as-grown TCR, which subsequently increases to beyond +200ppm/ºC following treatment at 400ºC.

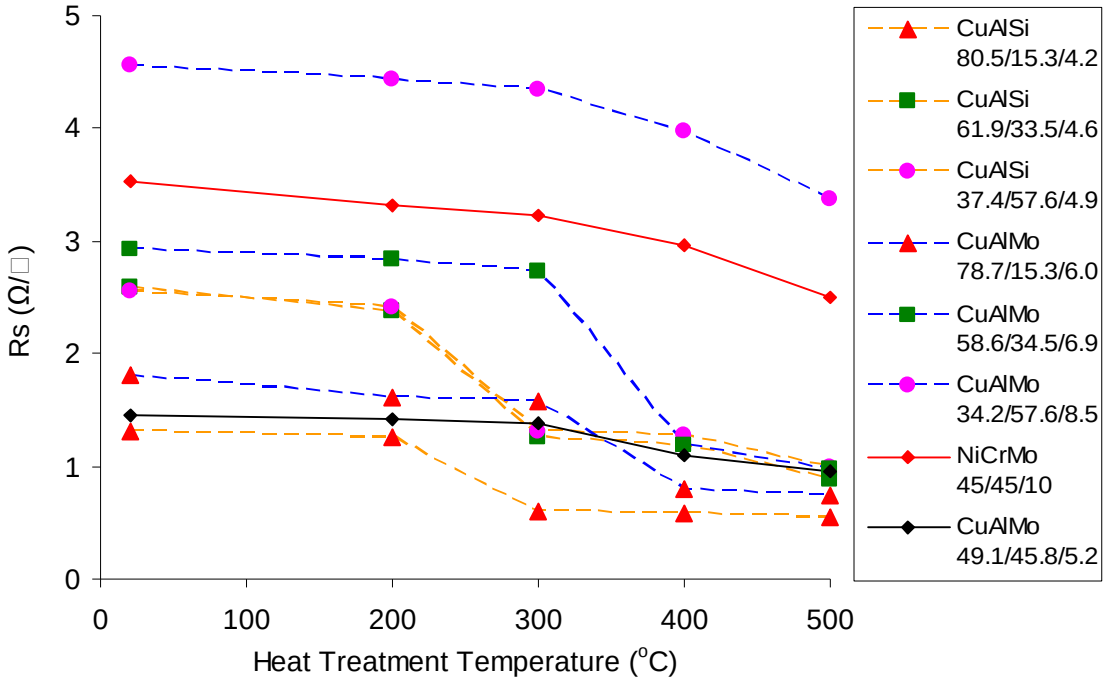

Fig. 3.2 - Sheet resistance following heat treatment in air for 5hrs at varying temperatures.

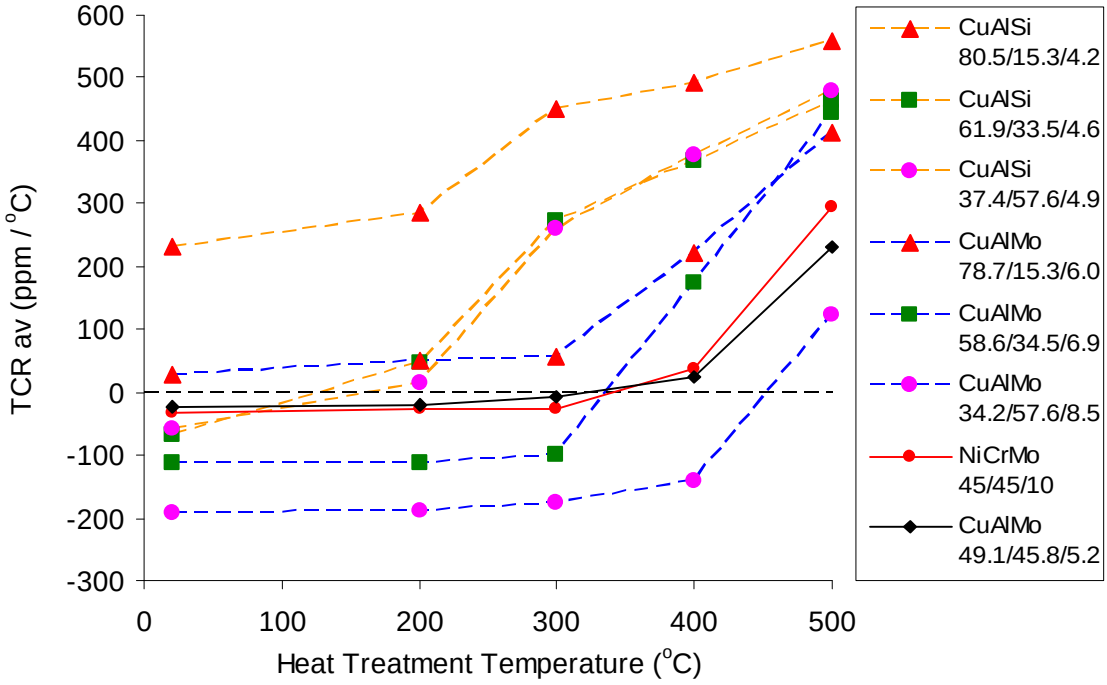

Fig. 3.3 - TCR following heat treatment in air for 5hrs at varying temperatures.

There is also a marked difference in the shape of the plots for the CuAlMo films. As previously mentioned the 15 and 35at.% Al films have this step decrease in sheet resistance occurring between 300 and 400ºC, whereas the 58at.% Al film has a more controlled gradual decline. This difference could be attributed to the increased Al content or possibly the unusually high content of 8.5at.% Mo present in the 58at.% Al film. For comparison the sheet resistance and TCR results for the NiCrMo control film have been plotted alongside the CuAlMo results in Figures 3.2 and 3.3. As can be seen the shape of both the curves for the 58at.% Al film and the NiCrMo film are very similar and although the base binary alloys are completely different the result does suggest that the Mo content plays a significant role in stabilising both film types.

Although the error bars have been excluded from Figures 3.2 and 3.3 for clarity, the distributions of measurements improved with increasing heat treatment temperature and in all instances were well within the target distribution of 50ppm/ºC.

At this stage only the 35 and 58at.% Al films are capable of yielding a TCR near the target specification of ±25ppmºC following heat treatment. However the sheet resistance of the 58at.% Al film is ≈4Ω/□ which is higher than the NiCrMo control and obviously unacceptable.

It was therefore decided to try modifying the composition of the 58at% Al film slightly to increase TCR to nearer zero and hence reduce Rs. To achieve this, the Cu content was increased and the Al and Mo contents were reduced to produce a film with a composition of 49.1/45.8/5.2at.% CuAlMo. Again samples were manufactured and tested under identical conditions.

Sheet resistance and TCR curves for the modified film composition are plotted in solid black lines in Figures 3.2 and 3.3. The increase in copper and reduction in molybdenum content has given the desired effect of reducing the as-grown sheet resistance value. Indeed the figure of 1.45Ω/□ is lower than all the other three CuAlMo compositions including the film containing ≈79at.% Cu. Moreover, when compared to the result of 3.5Ω/□ obtained for the NiCrMo film (solid red curve) the ratio is approximately 1:2.5 and remains around this value throughout the heat treatment temperature range, as evidenced by the close similarity in curve shapes. These results suggest that it is the molybdenum content rather than the copper or aluminium content which has the most significant effect on sheet resistance value. The more gradual controlled shape of the curves appears to be a function of both molybdenum incorporation and the higher aluminium content in the 46 and 58at.% Al films.

The TCR result for the modified film is also very encouraging. It bears close similarity to that of the NiCrMo control plot in both shape and value and having an as-grown value of -25ppm/ºC and crossing the zero TCR line between 300 and 400ºC it is ideally suited for use in thin film resistor applications.

In order to test the resistance stability of the CuAlMo films, samples containing 35, 46 and 58at.% Al were subjected to a 1000hr dry heat test at 155ºC following TCR heat treatment at 300 and 400ºC. Results of these tests are presented in Figure 3.4. Results are based on the measurement of 6 films for each chemical composition.

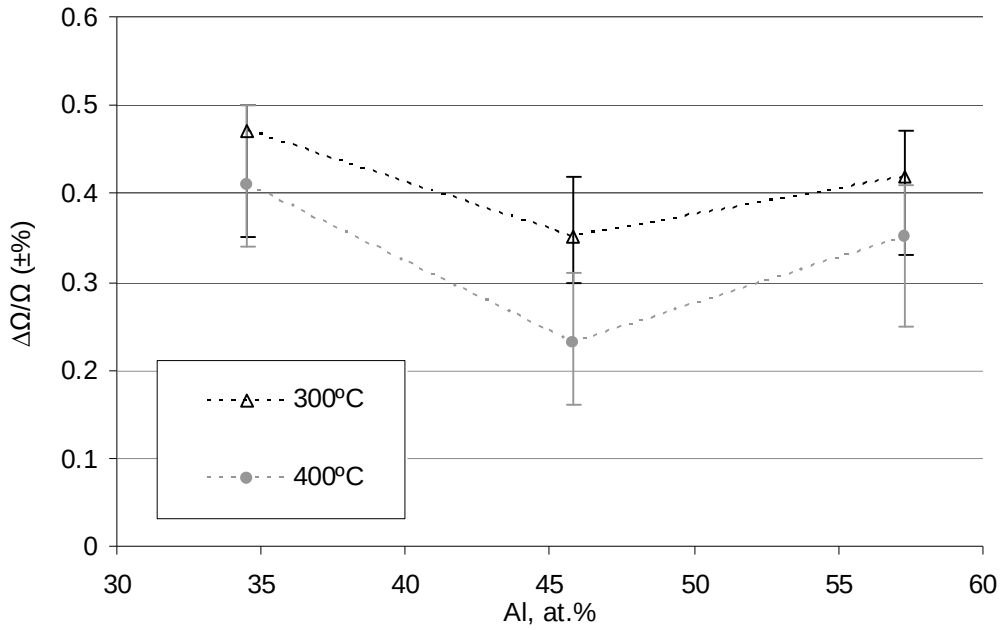

Fig. 3.4 - Mean resistance stability of CuAlMo samples following 1000hrs at 155ºC in air

The stability of all three films is within the target specification of 0.5% and as expected the change in resistance of the films pre-treated at the higher temperature of 400ºC is lower when subsequently subjected to the test temperature of 155ºC. Overall the results are very similar to those obtained for the CuAl binary films and neither an improvement nor deterioration in performance is evident. This result supports the aforementioned theory that the aluminium has more effect on the stability of the film whereas the main role of the molybdenum is to reduce the TCR to a workable level.

3.4 FINE TUNING OF MOLYBDENUM DOPING

A summary of the main electrical results obtained for the CuAlMo films are presented in Table 3.4 along with those obtained for the NiCrMo control.

Film composition CuAlMo (at.%)	Rs (Ω/□)		TCR (ppm/°C)		ΔΩ/Ω (%)	
	300ºC	400ºC	300ºC	400ºC	300ºC	400ºC
58.6/34.5/6.9	2.75	1.20	-100	+175	0.47	0.41
49.1/45.8/5.2	1.40	1.15	-10	+25	0.35	0.23
34.2/57.6/8.5	4.30	3.95	-175	-140	0.42	0.35
NiCrMo control	3.25	2.95	-25	+35	0.23	0.15

Table 3.4 – Summary of the main electrical properties for the CuAlMo films

As can be seen the modified CuAlMo film with an approximate composition of 49/46/5at.% gives the best results for all three parameters and satisfies the main specification objectives laid out in chapter 1.

- The sheet resistance is ≈2.5 times lower than that obtain for the NiCrMo control.
- The TCR_{av} is better than !25ppm/ºC and has a similar controlled slope to the NiCrMo control, passing the zero TCR line between 300 and 400ºC.
- The dry heat resistance stability, 1000hrs at 155ºC, is slightly inferior to that of the NiCrMo control but is well within the limit of 0.5%

To further investigate the effects of varying the Mo content on the electrical performance of the films, it was decided to fine tune the composition. However due to the aforementioned sputtering target to film composition errors and the central location of the Mo doping section, sample manufacture was transferred from flat substrates to cylindrical substrates, as the sputtering method employed for axial product involves tumbling a large batch of rods in a deposition barrel, thus providing better film uniformity.

3.4.1 Experimental

Preparation of resistive films

The sputtering was carried out in a Teer Coatings MSBP deposition plant and as with the planar sample manufacture, again a dc magnetron technique was employed, see Figure 3.5.

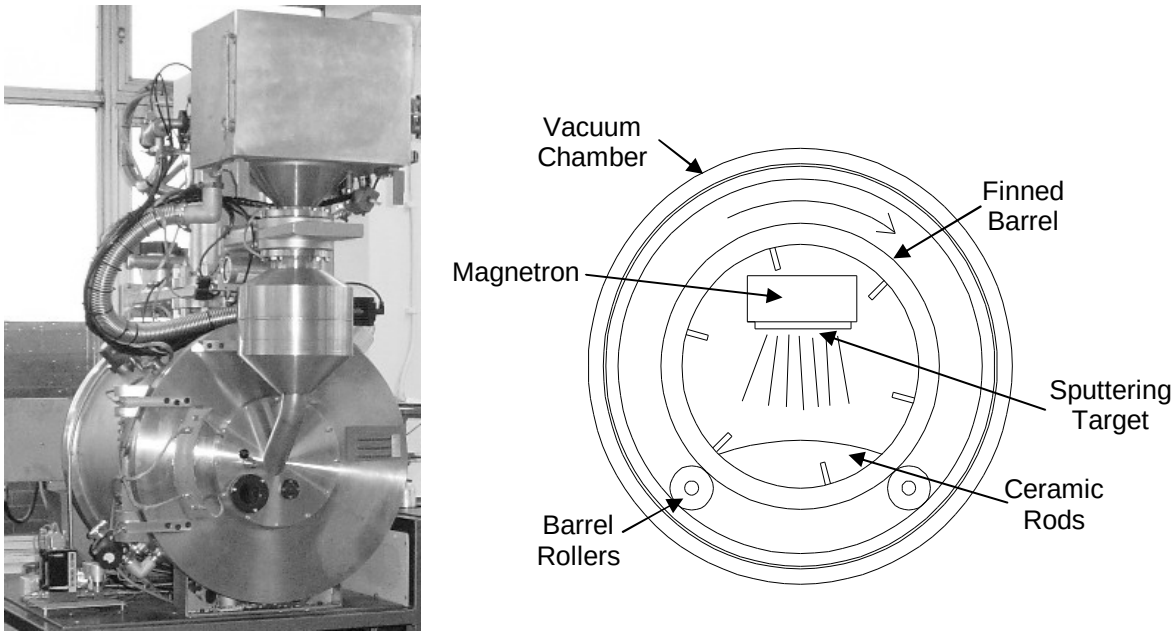

Fig. 3.5 – Barrel sputtering process

The barrel sputtering process involves mixing the ceramic rods in a finned barrel or drum whilst the cathode material is deposited onto them. The mixing of the rods produces a uniform film thickness throughout the batch but results in increased deposition times as the rods tumble against each other constantly removing a percentage of the deposited film. The film thickness is controlled by varying the deposition time, power level and drum rotation speed whilst keeping the sputtering pressure constant.

The eighteen piece sputtering target used to deposit the planar substrates was machined down to fit the smaller barrel sputtering magnetron. In order to further investigate the electrical properties of CuAlMo thin films, the following four batches, each containing 50,000, 1.7mm diameter x 5mm long 85% Al_2O_3 cylindrical substrates, were sputtered and subsequently investigated. Again films were also deposited from the standard 45/45/10wt.% NiCrMo target to be used as a control.

Trial No.	15	16	17	18	19
Al	65	66	67	68	
Cu	30.5	30.5	30.5	30.5	NiCrMo
Mo	4.5	3.5	2.5	1.5	

Table 3.5 – CuAlMo film compositions %area

All batches were sputtered under identical conditions as shown in Table 3.6. The vacuum plant was evacuated to a base pressure of $5x10^{-5}$ Torr using a combination of a mechanical roughing pump and then a cryo pump. Pure Ar was introduced at a constant flow rate of $35cm^3$/sec to achieve the desired sputtering pressure of $3x10^{-3}$ Torr. The sample batches of 50kpcs were then sputtered with the various CuAlMo film compositions at a target power of 2kW dc for 8 hours. This deposition time, target power and barrel rotation speed was set to give a low sheet resistance of around 1Ω/□.

Process parameter	Setting
Base pressure	$5x10^{-5}$ Torr
Sputter pressure	$3x10^{-3}$ Torr
Ar flow rate	35 cm^3/sec
Barrel rotation speed	3 rpm
Deposition time	8 hrs
Deposition power	2 kW
Target to substrate distance	250 mm

Table 3.6 – Barrel sputtering process parameter settings

Following deposition, samples of 1000 parts from each batch were annealed at temperatures of 200, 300, 400 and 500^{o}C in air for a period of 5 hours. Nickel-plated steel termination caps were then fitted and subsequently resistance welded with 0.6mm diameter tin plated copper termination wire to permit good electrical contact.

Characterisation of Films

The resistance values of a sample of 50 parts from each trial were measured at 20^{o}C and 70^{o}C in a thermostatically controlled oil bath (Grant LTD20G) using a conventional four wire technique in conjunction with a digital multimeter (Agilent 3458A). TCR was then calculated using Equation 1.3.

Film resistivity was calculated from the measured resistance and film dimensions of a sample of 5 parts. Film thickness was measured at several points on the cross section of the sputtered rods using a SEM. Stability of resistance of a sample of 50 parts from each trial was measured after subjection to 1000 hours at 155^{o}C ambient in air.

Film composition was calculated from sputtering target weight loss (Salter type 424) and analysed using EDX. For EDX the composition was measured at 5 separate locations on the cross section of 5 films per trial.

Environmental Testing

Following initial classification, films containing 2.3 and 4.1at.% Mo were subjected to a series of environmental tests to check their suitability as thin film resistors. At this stage films of NiCrMo were also tested as a control. The tests performed included:- voltage load, voltage overload, dry heat, damp heat steady state, temperature rapid change, resistance to solder heat, vibration and bump, and climatic cycle. The sample size for each test was 20 parts.

3.4.2 Results and Discussion

Chemical Composition

EDX analysis of the mean chemical compositions of the films resulted in a significant shift in comparison to the nominal target compositions, see Figure 3.6. This discrepancy can be largely explained by the variation in sputter yields of the individual target segments, which were confirmed by measuring the weight loss during sputtering. The sputter ratio of Cu:Al:Mo was found to be approximately 2:1:0.8, which corresponds well with previous data [167]. This result also shows that the problem with excess Mo being sputtered from the centre of the target has been eradicated through use of the barrel sputtering technique.

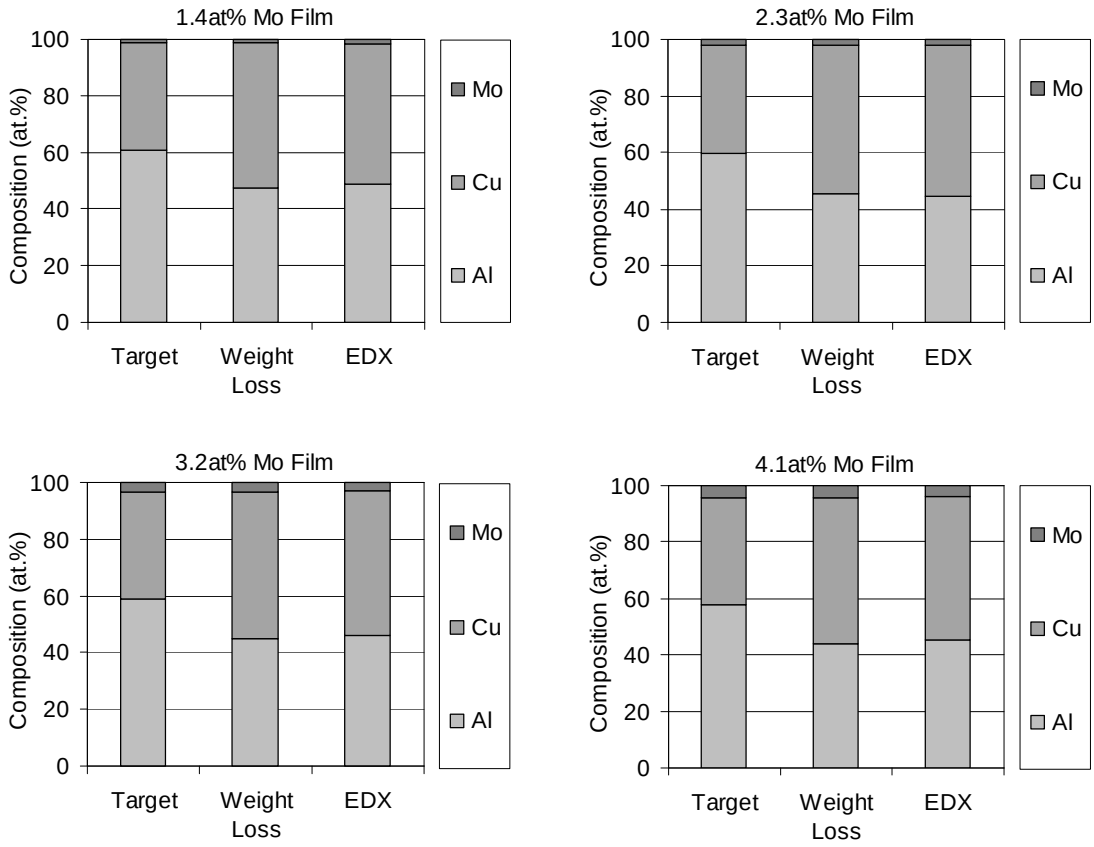

Fig. 3.6 - Sputtering target and mean film composition, for the CuAlMo films

Electrical and Structural Properties

For all compositions the film thickness was determined to be 1100 ± 100nm. Thus with a deposition time of 8 hours the sputter rate was calculated to be ≈2.3nm/min. This slow deposition rate was related to the large test batch size of 50,000 substrates and also the need to run the sectioned and clamped target arrangement at a reduced power level for cooling purposes. This result suggests that the small changes in Mo content between the four target compositions are not sufficient to affect the overall sputter rate of the alloys.

The effect of Mo content on the resistivity and TCR value of the sputter deposited CuAlMo films is shown in Figure 3.7. Each result is based on measurement of a sample of 50 parts.

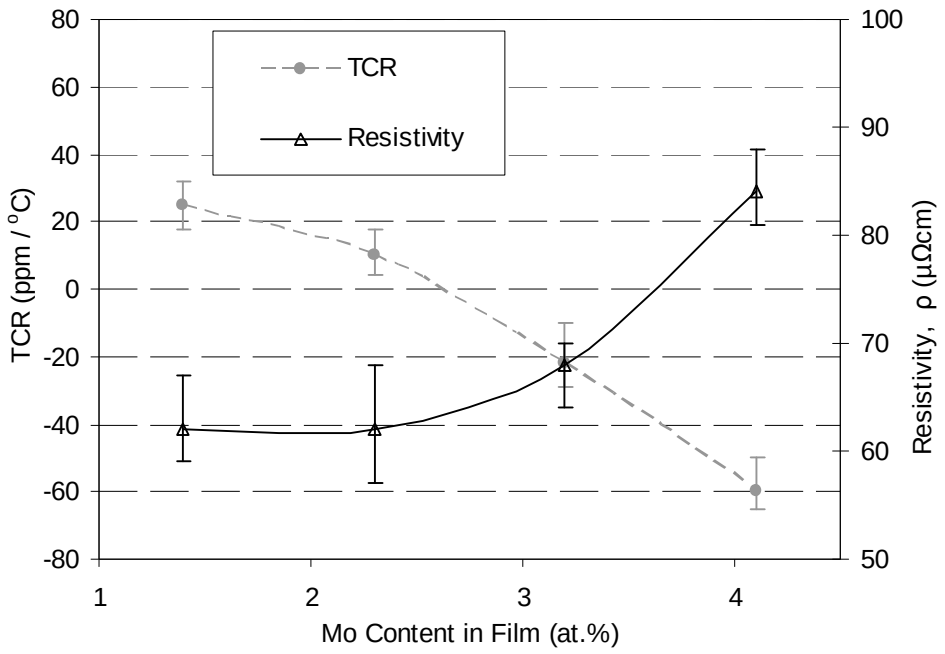

Fig. 3.7 – Effect of Mo concentration on the as grown sheet resistance and TCR of the CuAlMo films

In general, increase in Mo content has the effect of decreasing TCR and in turn increasing resistivity from a mean values of 25ppm/^{o}C and 60µΩcm at 1.4at.% Mo, to -60ppm/^{o}C and 85µΩcm at 4.1at.% Mo. However the influence of the Mo doping appears to diminish at levels ≤ 2.3at.%, where both TCR and resistivity curves begin to flatten off. This suggests that the most useful region is between approximately 2 and 4at.% Mo. where a practical TCR can be achieved whilst maintaining a lower resistivity. Again this result is in agreement with the well documented theory that the introduction of small quantities of doping impurities either in the sputtering gas or target itself can result in more amorphous structures with decreasing conductivity and TCR [20].

The effect of annealing temperature on the TCR and resistivity of the films is shown in Figure 3.8. Each result is based on measurement of a sample of 50 parts.

TCR remains relatively unchanged and only increases gradually at temperatures below 300^{o}C, beyond this temperature it rises significantly and after treatment at 500^{o}C the TCR of all four films is in excess of 200ppm/^{o}C and hence no longer suitable for use as a thin film resistor. The resistivity values of the films demonstrate a similar but inverse trend to that of TCR and decrease with increasing annealing temperature.

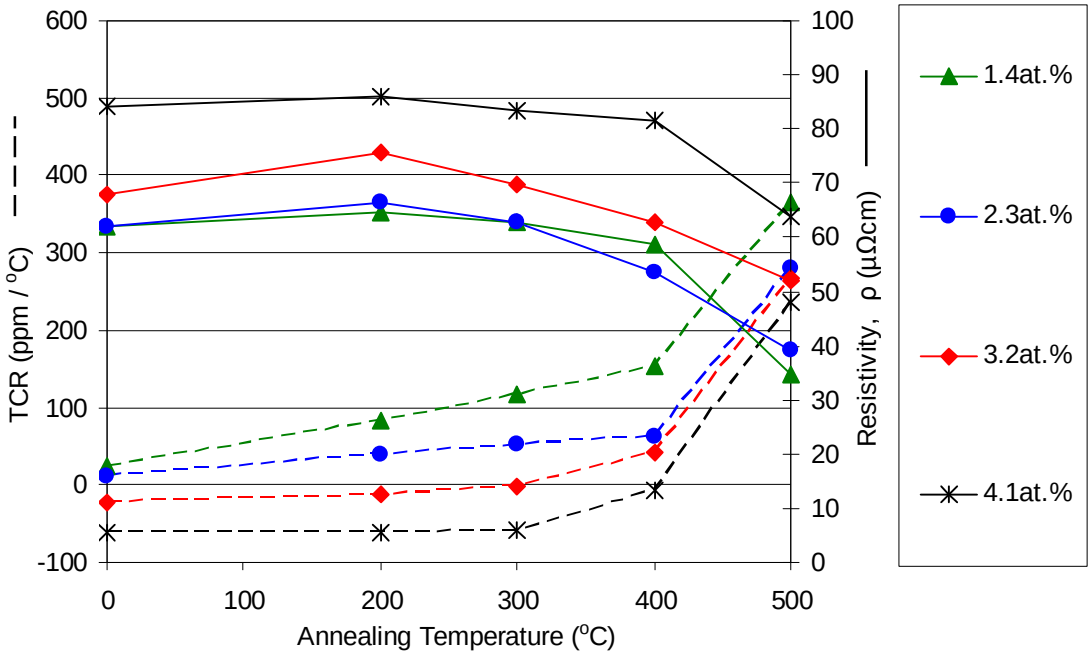

Fig. 3.8 – Effect of annealing temperature on the TCR and resistivity of the CuAlMo films

On average, mean resistivity falls by about one third of its original value after treatment at 500°C. Again, the largest value shifts appear to take place at temperatures in excess of 300°C. The most useful temperature region is that between 300°C and 400°C, where TCR is controllable to ±50ppm/°C for all except the 1.4at.% Mo film. The best results come from the two films with the highest Mo content, which can both be controlled around the zero TCR line. Of additional benefit is that this region lies beyond the maximum thin film resistor assembly processing temperature, which is generally accepted to be around 300°C [5], so TCR will be unaffected by subsequent operations.

Although the error bars have been excluded from Figure 3.8 for clarity, the distributions of measurements improved with increasing heat treatment temperature and in all instances were inside those reported for the as-grown films in Figure 3.7.

These results are in good agreement with previous work, where annealing of films sputtered from mixed composition targets at temperatures in excess of 300°C leads to a positive shift in TCR and indeed follows the general theory of annealing out micro-imperfection and impurities inside grains and recrystallisation of the film leading to a reduction in resistivity [176]. In this investigation the structural transformation can be distinguished by three annealing states, as illustrated in Figure 3.8. At first the sputtered film is in an amorphous state with a negative TCR. At annealing temperatures below approximately 400°C crystals with positive TCR are formed and the films are in a metastable state. Here zero TCR can be achieved through careful

adjustment of Mo concentration and annealing temperature. At temperatures in excess of 400^{o}C further crystallisation and grain growth takes place leading to a positive shift in TCR and reduction in resistivity towards that of the individual bulk elements [68, 120]. These theories are discussed further in chapter 5.

Results for resistance stability of the various film compositions after storage for 1000 hours at 155^{o}C in air, following stabilisation at 400^{o}C for 5 hours in air, are given in Figure 3.9. Results are based on the measurement of 50 parts per experimental trial

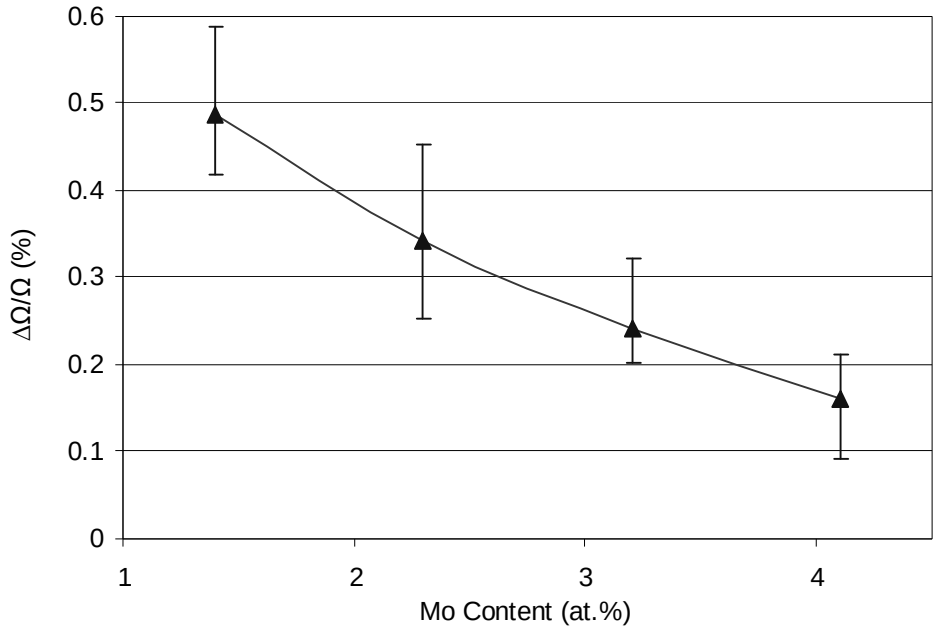

Fig. 3.9 - 1000 hour Resistance Stability at 155ºC vs Mo Content in the CuAlMo films

Resistance stability improves quite linearly with increasing Mo content. At 1.4at.% Mo, the mean change in resistance is around 0.5% and reduces to around 0.15% for the 4.1at.%. Mo film. This improvement can be related to the rectory nature of the Mo which has a small mobility of defects at normal operating temperatures, thus stability improves as its content in the film increases [20].

As illustrated in Fig 3.10, the vast majority of resistance change takes place in the first 48 hours of the stability test. This result can be explained by initial oxidation and degradation of the films, followed by stabilisation as the protective oxide layer is formed, retarding the rate of any subsequent changes.

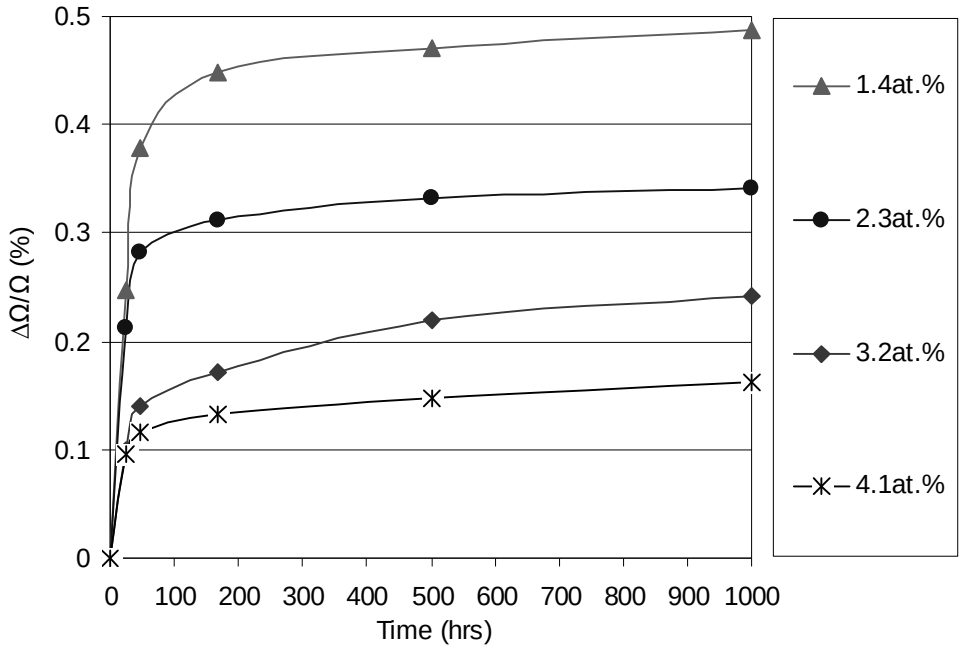

Fig. 3.10 - Resistance Stability at 155°C, measurements taken after 24, 48, 168, 500 and 1000hrs.

Environmental Testing

CuAlMo films containing 2.3 and 4.1at.% Mo were laser adjusted to target value using a Nd:YAG laser (Nohau LSS600) before being encapsulated in a modified epoxy coating. These samples were then subjected to a series of environmental tests in accordance with BS EN 60115-1 [12] together with the NiCrMo control standards. Maximum and typical results of these tests for a sample of 20 parts are presented in Table 3.7.

Test specification		**Performance**					
		CuAlMo 52.7/45/2.3		CuAlMo 51.3/44.6/4.1		NiCrMo	
		Max	Typ	Max	Typ	Max	Typ
Load: 1000hrs @ 70°C	ΔΩ%	0.25	0.2	0.15	0.08	0.3	0.1
Short term overload	ΔΩ%	0.01	0.01	0.01	0.01	0.1	0.02
Dry Heat: 1000hrs @ 155°C	ΔΩ%	0.6	0.4	0.25	0.2	1	0.15
DHSS: 56 days @ 40°C/93%RH	ΔΩ%	0.20	0.15	0.12	0.09	0.5	0.1
Temperature rapid change	ΔΩ%	0.33	0.27	0.14	0.05	0.2	0.05
Resistance to solder heat	ΔΩ%	0.03	0.02	0.03	0.01	0.06	0.03
Vibration and bump	ΔΩ%	0.39	0.31	0.1	0.08	0.06	0.02
Climatic cycle	ΔΩ%	0.67	0.35	0.33	0.13	0.3	0.1

Table 3.7 – Environmental test results for CuAlMo and NiCrMo films

Again it is clearly evident that an increase in Mo content gives a step improvement in the electrical performance of the CuAlMo films regardless of the test environment and conditions. Results of maximum resistance change ($\Delta\Omega$%) for the 4.1at.% Mo film outperform that of the 2.3at.% Mo film for all tests undertaken. Moreover, comparison against the results for the NiCrMo control film shows a similar performance level. Any minor differences between the results of the two film types appear to be attributable to the test conditions. For example the CuAlMo film gives better results for the lower temperature and load tests, whilst the NiCrMo performs the best at higher temperatures such as the dry heat test and also the climatic cycle, which contains a 40 hour dry heat soak at 155^{o}C. Again this result can be attributed to initial oxidation of the film as highlighted in Figure 3.10 and can be further supported by the similarity of the dry heat and climatic cycle results, which suggests that the majority of resistance change is taking place in the first 40 to 48 hours.

3.5 SUMMARY

Work conducted in this chapter has shown that the addition of varying amounts of Mo to the CuAl films discussed in chapter 2 can be used to develop thin film resistors with lower resistivity and equal electrical performance to that of NiCrMo. The TCR of the films increases and resistivity decreases with reduction in Mo concentration form 4.1 to 1.4at.% and these changes are further augmented through annealing of the films at temperatures above 300^{o}C.

The CuAlMo films are characterised by metastable behaviour, which with correct adjustment of Mo concentration and annealing temperature can be utilised to obtain films with near zero TCR, possessing defined electrical properties such as a resistivity of 60 to 80$\mu\Omega$cm and a long term stability of less than 0.2%.

Chapter 4

Composite Sputtering Target

4.1 INTRODUCTION

In the preceding chapters it has been established that a ternary thin film of CuAlMo shows much promise in the application of low value thin film resistors.

However all investigations thus far have been conducted using an experimental sputtering target consisting of individual sections of Cu, Al and Mo. Although this approach was deemed acceptable to gain an initial impression of varying the film composition on electrical performance of the resistors, it would certainly not be practical in a production environment due to high cost of target manufacture and also the possibility of target to film compositional errors [1,120].

It was therefore decided to employ a production type composite target of CuAlMo for all further experimentation.

This chapter therefore deals with firstly the chemical analysis of the CuAlMo films sputtered from the sectioned target, in order to specify and subsequently have manufactured a composite target, and secondly to conduct experimentation to verify the performance and suitability of this target.

In addition to chemical analysis, the film dimensions of a number of samples were also measured in order to accurately determine the resistivity of the CuAlMo films.

4.2 FILM CHARACTERISATION

4.2.1 Film Thickness and Resistivity

In order to compare the CuAlMo films to other published work and against the NiCrMo films, the resistivity was calculated by measuring the resistance and dimensions of the films. The length and width were measured using a digital measurescope for the planar samples and a micrometer and vernier for the cylindrical samples. The thickness was measured using the following four techniques:

1. SEM - FEI Quanta 200
2. Ball Cratering - Eifeler Nord Caloprep coupled with SiS Analysis software
3. Profilemeter - Taylor-Hobson Talystep
4. XRF – Fischerscope XDAL

Cylindrical substrates were used for the SEM and XRF tests. However planar substrates were required for the profilemeter and ball cratering methods. Hence films of similar sheet resistances were sputtered onto polished Al_2O_3 and glass substrates in the barrel sputtering plant. For SEM measurements the substrates were cross

sectioned. Details of the measurement sample sizes and an estimate of the uncertainty for each method are given in Table 4.1. Where possible the same samples were used for each measurement technique.

Measurement method	Substrate type	Estimated uncertainty (nm)	No. of samples	No. of measurements
SEM	Cylinder	< ±100	5	5
	Flat	< ±50	2	5
XRF	Cylinder	< ±100	2	2
	Flat		2	2
Ball cratering	Flat	< ±100	1	1
Profile meter	Flat	< ±30	2	2

Table 4.1 – Film thickness measurement uncertainties and sample sizes

Results of film thickness and resistivity for all four methods are presented in Table 4.2. As can be seen the resistivity of the CuAlMo films is two to three times lower than that of the NiCrMo control film, with values of 56 to 98μΩcm and 192 to 215μΩcm respectively for all test methods used, except that of ball cratering. Moreover the results correspond well with previous data for ternary NiCr films reported in chapter 1.

Target composition		Film thickness (nm) / film resistivity (μΩcm)					
		SEM		XRF		Ball crater	Profile meter
		Cylinder	Flat	Cylinder	Flat	Flat	Flat
CuAlMo	1.4at.% Mo	1080-1160 / 58-61	1210-1280 / 57-58	1100-1300 / 61-65	1300-1400 / 62-63	N / A	1225-1250 / 56-58
	2.3at.% Mo	1060-1150 / 59-62	1270-1340 / 60-63	1200-1300 / 67-70	1400-1500 / 68-70	N / A	1250-1300 / 59-62
	3.2at.% Mo	1050-1200 / 67-70	1160-1230 / 68-69	1200-1300 / 76-77	1200-1400 / 71-77	N / A	1175-1225 / 68-70
	4.1at.% Mo	1050-1190 / 82-83	1200-1270 / 82-83	1200-1400 / 94-98	1300-1400 / 88-90	2800 / 184	1225-1250 / 81-83
NiCrMo		830-1000 / 192-196	910-1040 195-198	900-1100 / 209-215	1000-1100 / 209-214	2600 / 281	925-1025 / 195-198

Table 4.2 – Film thickness and resistivity results for CuAlMo and NiCrMo films

In addition to the advantage of lower resistivity, a comparison of film thicknesses for the two film types reveals that the CuAlMo also sputters at a faster rate than the NiCrMo with thicknesses in the range 1050 to 1500nm and 830 1100nm respectively under identical process conditions. Again this result was to be expected, taking into account the sputter rates of the individual elements [168].

Of the test methods utilised, the films sputtered onto flat glass or polished Al_2O_3 and measured by profile meter or SEM gave the most consistently accurate results. This was due to their superior surface finish which made visual examination (SEM) and profile measurement much easier, see Figure 4.1a. Although the SEM analysis of the cylindrical rods also produced results within ±3μΩcm to that obtained with the flat samples, there was considerable measurement uncertainty due to the rough surface finish of the substrates, see Figure 4.1b.

The thickness measurements taken using XRF were less consistent than the SEM and profile meter methods and on average produced slightly higher resistivity results. This discrepancy was thought to be attributed to the inaccuracy when measuring the lighter elements such as Al. The ball cratering method was deemed incapable of measuring the film thickness due to poor adhesion on the glass samples and poor surface finish on the Al_2O_3 samples as shown in Figures 4.1c and 4.1d respectively. This method was abandoned after trying the NiCrMo film and one of the CuAlMo films.

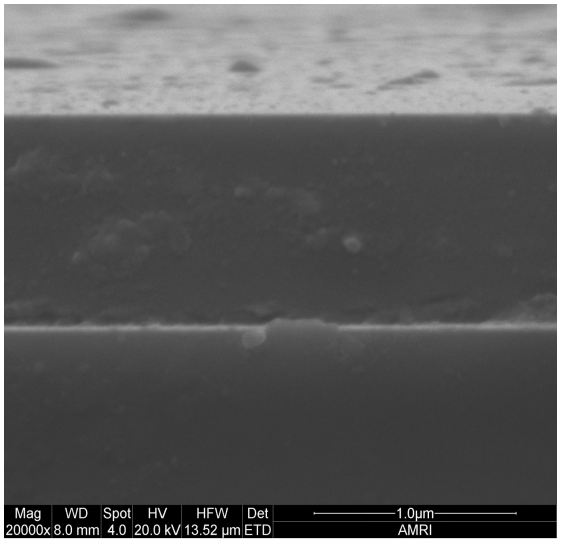

Fig. 4.1a – SEM image of CuAlMo film on glass slide

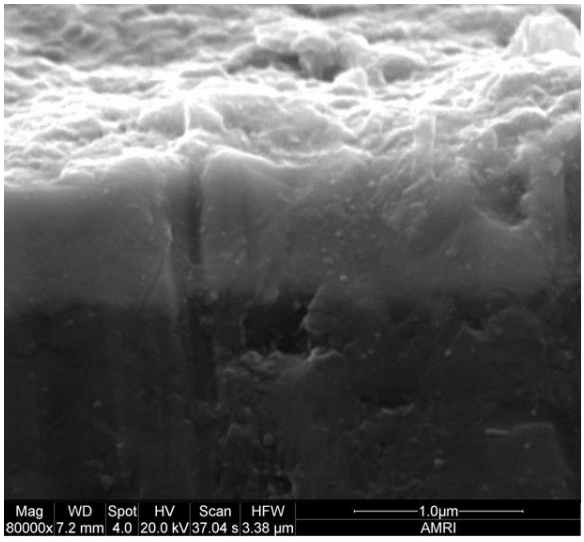

Fig. 4.1b – SEM image of CuAlMo film on Al_2O_3 rod

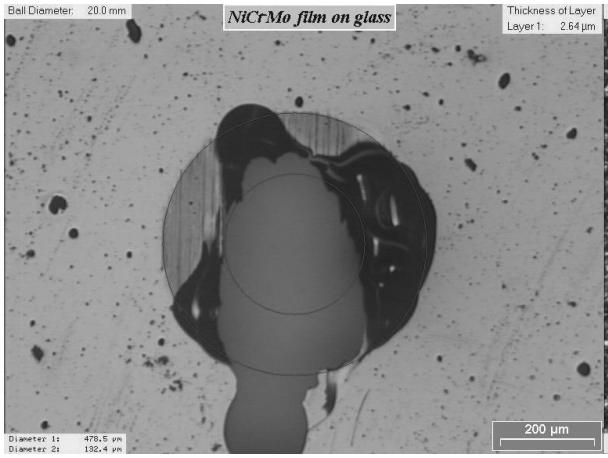

Fig. 4.1c – Ball cratering of NiCrMo film on glass

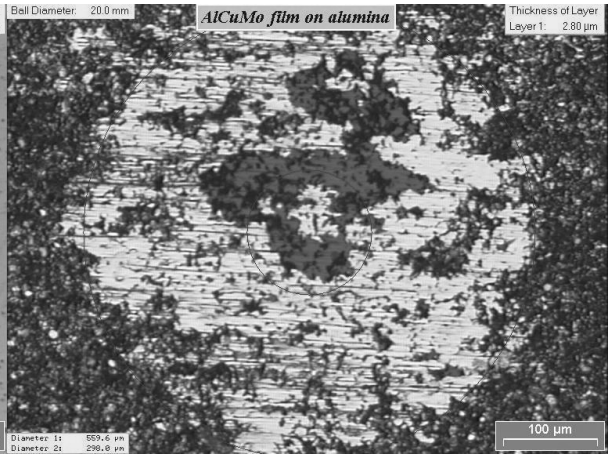

Fig. 4.1d – Ball cratering of CuAlMo film on Al_2O_3

4.2.2 Film Composition

To allow specification of a composite sputtering target, the chemical compositions of the CuAlMo films were analysed. Four different techniques were used:

1. Target weight loss calculation - Salter type 424
2. SEM:EDX - FEI Quanta 200 coupled with EDX analysis
3. XRF – Spectra-Analytical X-Lab 2000
4. ICP-MS - Agilent 7500ce

The target weight loss method entailed accurately weighing the individual target pieces before and after deposition, then calculating the composition ratio from the losses. For SEM:EDX the cylindrical substrates were cross sectioned and a line scan was conducted on the film to try and avoid the influence of the Al in the substrate which has been previously encountered when analysing perpendicular to the film surface [178]. For ICP-MS analysis the films were dissolved off the substrates in nitric acid and then made into solutions. A sample of blank substrates were also analysed to allow deduction from the film results.

Details of the measurement sample sizes and an estimate of the uncertainty for each method are given in Table 4.3.

Measurement method	Measurement uncertainty (%)	No. of samples	No. of measurements
Weight loss	< ±1.00	N/A	3
EDX	< ±0.10	5	5
XRF	< ±0.18	50	3
ICP-MS	< ±0.08	50	1

Table 4.3 – Film composition measurement uncertainties and sample sizes

Table 4.4 shows the mean film composition analysis results for the CuAlMo and NiCrMo films. All results are expressed in weight percent (wt.%), the standard unit used when specifying a target for manufacture.

Composition (wt.%)		Cu/Al/Mo	Cu/Al/Mo	Cu/Al/Mo	Cu/Al/Mo	Ni/Cr/Mo
Target		58 / 39 / 3	57 / 38 / 5	56 / 37 / 7	55 / 36 / 9	45 / 45 / 10
Film	wt. loss	70.5 / 26.5 / 3	69.5 / 26 / 4.5	68.5 / 25 / 6.5	68 / 24 / 8	N / A
	EDX	67 / 29.5 / 3.5	70.5 / 25 / 4.5	68 / 26 / 6	64.5 / 27.5 / 8	44 / 45 / 11
	XRF	N / A	71 / 27 / 2	N / A	69.5 / 27 / 3.5	46 / 44.5 / 9.5
	ICP	N / A	71.5 / 24.5 / 4	N / A	69 / 24 / 7	45.5 / 44.5 / 10

Table 4.4 – Mean film composition results for CuAlMo and NiCrMo films

There is a considerable shift in composition between the target and film weights of the CuAlMo films. As discussed in chapter 2, this error can largely be explained by the sputter rates of the individual element sections of the target. It can also be observed that this discrepancy does not appear to occur with the NiCrMo composite target. These results suggest that the films sputtered from the multi section development target vary from the target itself according to the sputter rates of the elements involved, whilst films sputtered from a composite target match closely to the target composition. This result is in good agreement with previous work in this area and is largely due to the homogenous mixing of the elements when in composite form [1,10].

The variation in chemical composition across the samples was found to be no worse than ±2 wt.% for each of the individual measurement methods. The weight loss, EDX and ICP techniques gave the most consistent results, whilst those for XRF were ≈50% lower in Mo content for the CuAlMo films. This result could be attributed to additional signals from the Al in the underlying substrate, as the X-ray is directed to a sample of 50 rods rather than at the cross section of the film as is the case with the EDX method. It was therefore decided to exclude the results obtained using this method when deciding upon the final target composition.

Of the three remaining methods, there is still significant variation in the compositional results, with deviations as large as 5 wt.% for the Cu and Al elements. Hence it was foreseen that it would not be possible to accurately specify the composition of the composite CuAlMo target first time and that further targets might be required to fine tune the film properties. The above results were therefore used as a guideline on which to select the target composition.

4.3 SPUTTERING TARGET SELECTION

From the electrical performance results presented in chapter 3 and also the film compositional results above, the final composition specified for target manufacture was Cu-Al-Mo 69-24-7wt.%.

The target was manufactured by Testbourne Ltd [179]. Due to the large differences in the melting points of the individual elements the powder sintering technique was used. Because of difficulties in machining the brittle material, the target was eventually assembled from 5 equal 3” x 4.75” x 0.25” (76.2mm x 120.65mm x 6.35mm) sections with total target dimensions of 15” x 4.75” x 0.25” (381mm x 120.65mm x 6.35mm) and was bonded to an MRC copper backing plate.

Once received, a sample of material was removed from each of the five sections for chemical analysis using EDX (see Figure 4.2), the mean results of which are presented in Table 4.5. Each sample was measured 3 times in 3 different areas and the composition across all five target sections was found to be homogeneous to within ± 2 wt.%.

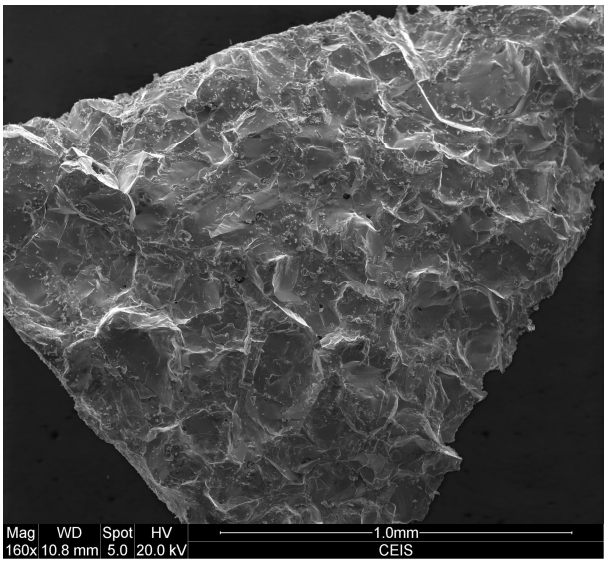

Fig. 4.2 – Sample taken from CuAlMo composite sputtering target section

Element	Mean target composition (wt.%)			
	Specified ratio	Supplier analysis	EDX Analysis	
			Target No.1	Target No.2
Cu	69	68.95	58.27	65.46
Al	24	24.05	23.33	23.52
Mo	7	6.92	18.40	11.02
S		0.04		
Zn		0.02		
Fe		0.01		
Pb		0.004		
Ti		0.004		
Total		100	100	100

Table 4.5 – Chemical analysis of the CuAlMo sputtering targets

As can be seen there was a large discrepancy between the target supplier's analysis and the EDX analysis of the target. On average the target composition was rich in Mo and deficient in Cu, the mean Mo content being 18.4 wt.% instead of 7 wt.%.

The supplier was informed of the problem and advised that this was the first time they had attempted to manufacture this material combination and had experienced problems with fractionation of the elements leading to a rise in the Mo content. They agreed to supply a second target, in which they tried to improve the composition by offsetting the starting material quantities. The EDX analysis of this material is also given in Table 4.5

Although the composition of target number 2 was much closer to the specified ratio the Mo content was still high at 11 wt.%. However because of the long timescale involved in manufacturing a third target, a decision was taken to sputter samples from target number 2 to check their electrical performance.

4.4 EXPERIMENTAL AND CHARACTERISATION

All film samples were prepared and characterised under the same conditions as the binary CuAl films described in chapter 2. Planar substrates were used, 96% Al_2O_3 for electrical measurement and borosilicate glass for chemical and structural analysis.

4.5 RESULTS AND DISCUSSION

Results of mean chemical analysis for the composite target and films sputtered from it are presented in Figure 4.3. The two results are of close similarity with the largest error between target and film being no more than 2 at.%. Again this small error is due to the films being slightly rich in Cu. However the discrepancy is much improved from the result attained with the sectioned target, which is also plotted in Figure 4.3. In this case the error is greater than 13 at.%. This result confirms the theory that sputtering from a homogeneously mixed composite target can give good chemical correlation between target and film, regardless of the sputter yields of the individual elements.

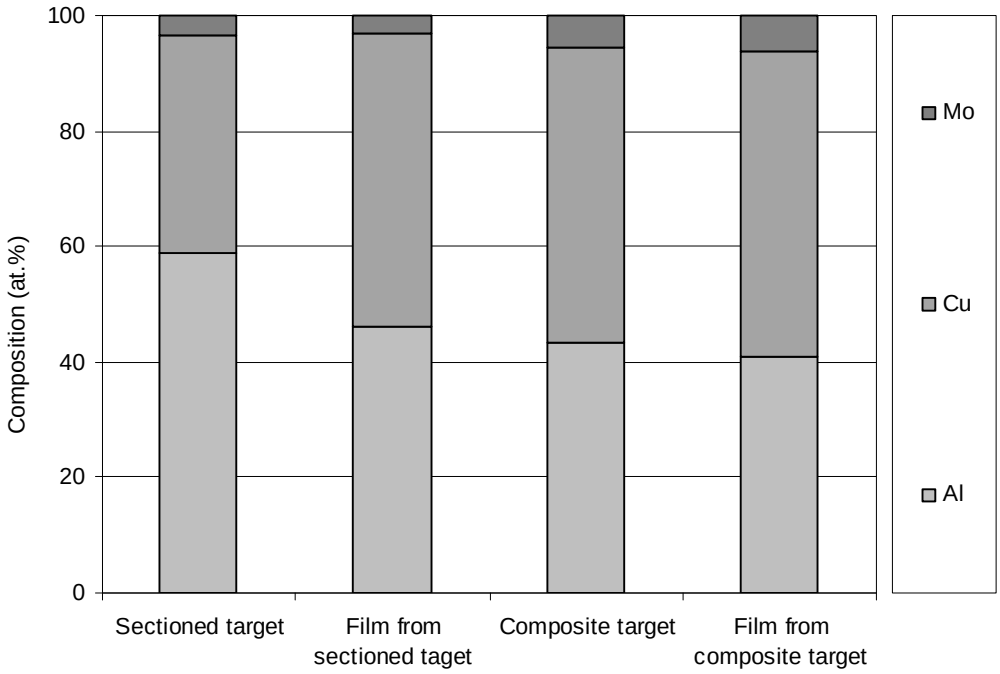

Fig. 4.3 – Chemical composition of CuAlMo sectioned and composite sputtering targets and films sputtered from them

Results of resistivity and TCR_{av} with increasing annealing temperature in air are presented in Figure 4.4 for films sputtered from both the sectioned and composite targets under identical conditions. Results at each temperature are based on the measurements of a sample of 6 films taken from across the sputtering pallet.

The as-grown resistivity of the film from the composite target is higher than that from the sectioned target at 94 and 68$\mu\Omega$cm respectively. Although every effort was made to ensure that sputtering conditions were identical, this could not be guaranteed. However the most likely cause of this increase in resistivity is the larger fraction of Mo present in the composite target film. As already shown in chapter 3, increasing the Mo content in

the film effectively increases the doping or impurity concentration thus increasing resistivity and reducing TCR.

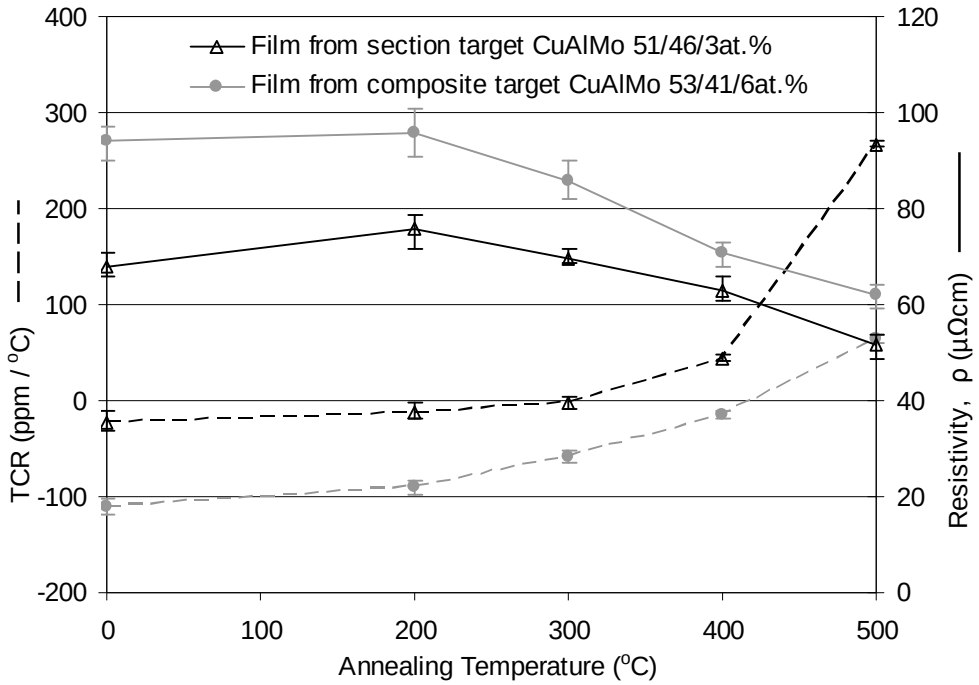

Fig. 4.4 – Comparison of electrical properties of films sputtered from sectioned and composite CuAlMo targets

In the present case the excess Mo content resulted in an increase in the mean resistivity value to 94μΩcm for the as grown films. This in turn produced a subsequent decrease in TCR_{av} to -110ppm/ºC.

Although it can be postulated that this undesirable result could be eradicated through further reducing the Mo content of the target, it can also be perceived from Figure 4.4 that resistivity and TCR properties in line with those produced from the sectioned target are achievable through use of a higher heat treatment temperature. As shown in Figure 4.4 a near zero TCR and resistivity of ≈60-70μΩcm are achieved at annealing temperatures of ≈300ºC for films from the sectioned target and ≈420ºC for the composite target.

Furthermore, the sudden increase in TCR at ≈400ºC observed for the films from the sectioned target does not appear to take place with those from the composite target and the curve is more controlled. Again this result is most likely due to the increased Mo content and is good agreement with the results presented in chapter 3 for the higher Mo content CuAlMo films and also the NiCrMo films. The increase in annealing temperature required to achieve a near zero TCR should not raise any manufacturing

concerns and if anything should give a further improvement in resistance stability, especially when combined with the increased Mo content in the film.

Results of resistance stability for films sputtered from both the sectioned and composite targets following storage for 1000 hours at 155^{o}C in air following stabilisation for 5 hours in air at the temperature required to give a near zero TCR are given in Figure 4.5. Results are based on the measurements of a sample of 6 films taken from across the sputtering pallet.

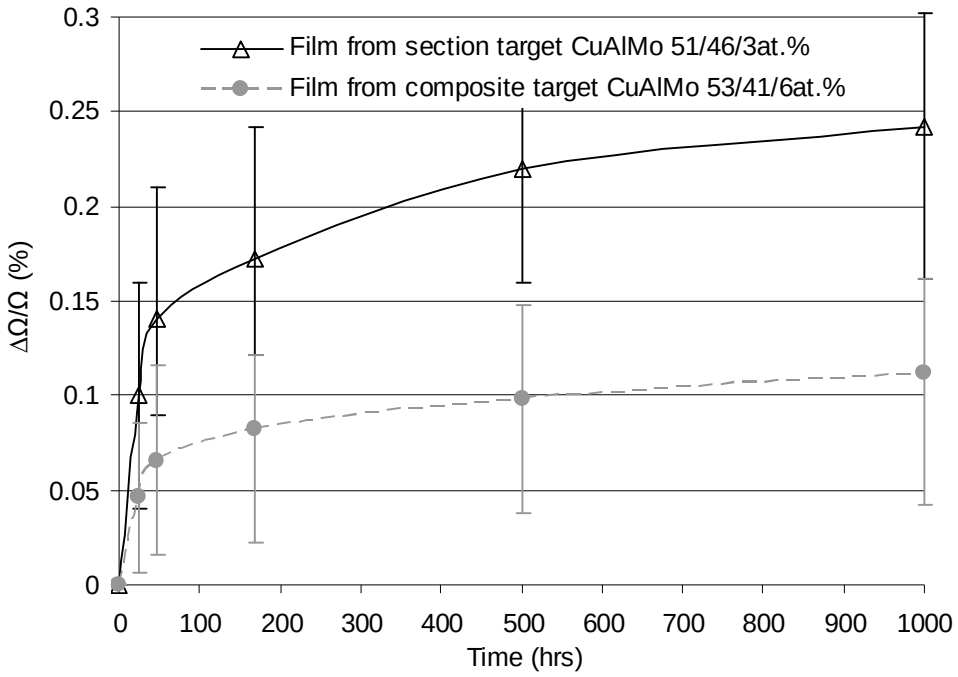

Fig. 4.5 - Comparison of mean resistance stability at 155^{o}C of films sputtered from sectioned and composite CuAlMo targets, measurements taken after 24, 48, 168, 500 and 1000hrs

The mean resistance change for the films sputtered from the composite target is half that of those from the sectioned target at values of 0.12 and 0.24% respectively, following 1000hrs subjection to dry heat. Again this result is most likely a function of the increased Mo doping and gives good correlation with the stability results presented in chapter 3 for various Mo concentrations.

4.6 SUMMARY

Work conducted in this chapter has shown that thin films of CuAlMo have two distinct advantages over the standard NiCrMo film in achieving low value resistors; firstly the resistivity of the CuAlMo film following heat treatment is around three times lower than that of NiCrMo at ≈70 and 210μΩcm respectively, and secondly it also sputters at ≈1.2 times the rate of NiCrMo.

Of the methods used to measure film thickness for the resistivity calculations, the SEM and profilemeter gave the most reliable results, whilst those recorded using the XRF and ball cratering methods were inconsistent and were deemed unsuitable in this application.

The chemical compositions of the CuAlMo films sputtered from the sectioned development target have also been analysed in order to specify a composite sputtering target for use in production. Target weight loss, EDX and ICP methods gave consistent results, whilst XRF gave incoherent results when measuring the films grown on Al_2O_3 substrates.

Chemical analysis of the composite CuAlMo target revealed that it was rich in Mo, and films sputtered from it matched this composition with good accuracy. Although the excess Mo was undesirable when trying to achieve low resistivity films, by heat treating the films at higher temperatures in the range 400 to 450ºC it was possible to overcome the effect of the increased Mo doping and produce films with near zero TCR and resistivites in the 70μΩcm region. Furthermore the increase in Mo also gave the desirable effect of improving 1000 hour dry heat resistance stability from 0.24% to 0.12%, when compared with films sputtered from the section target, which contained a lower Mo concentration.

Chapter 5

Deposition and Annealing Process Optimisation

5.1 INTRODUCTION

It has been shown in the preceding chapters that thin films of CuAlMo show much promise in the application of low value thin film resistors. However all resistor samples investigated thus far have been manufactured under 'typical' process conditions that were previously established for the production of NiCr type films.

The work described in this chapter is concerned with studying the effect of varying sputtering and heat treatment process parameters on the key electrical properties of the films, with the aim of specifying a set of optimum conditions under which the CuAlMo films can be manufactured to specification.

Due to the wide range of process variables involved in the sputtering and subsequent heat treatment processes, a large number of experiments would be required to study their effects efficiently. Accordingly, it was decided to utilise the design of experiments (DOE) and analysis of variance (ANOVA) methods in order to decrease the number of experiments required for determining the optimum process conditions.

DOE and ANOVA are powerful statistical techniques which use the variances of data to study the effect of several process variables affecting the response or output of a process. They were first developed in the 1920's by Sir Ronald Fisher, his approach to experimentation was a direct replacement of traditional one factor at a time methods [179].

Although DOE methodologies have been practiced for several decades, it is only over the last 20 years or so that they have gained wider acceptance as an essential tool for improving process effectiveness and product quality [180-188]. This recognition is largely due to the work of Genichi Taguchi, a Japanese engineer who promoted the importance of making robust products and processes through the application of DOE [189].

Following this wider acceptance, DOE has found application in many scientific areas such as biometry, agronomy, psychology, analytical chemistry and process engineering [190-194]. However it is not until more recently that these methods have been applied in the field of thin films for the efficient optimisation of sputtering conditions [190, 195-204].

The effects of varying sputtering conditions on the preferred *c*-axis orientation of aluminium nitride thin films, for use in acousto-optic applications, have been studied by Akiyama, M et al [1990, 202] and more recently by Adamczyk, J et al [195]. Akiyama found that the process factors having the most statistically significant effect on the orientation of the films were sputtering power, sputtering pressure, substrate temperature and

target to substrate distance. Adamczyk on the other hand found the interaction between pressure and N_2 concentration to be the most influential factor.

DOE has also found application in the optimisation of hard coatings such as CN_x, TiN and ZrN. Akiyama, M et al [201] found that sputtering pressure, substrate temperature and target to substrate distance were the most significant factors effecting the hardness of CN_x thin films prepared by dc magnetron sputtering. Whilst Chou, W et al [199] determined substrate bias and N_2 partial pressure to be the most sensitive parameters effecting film hardness of magnetron sputtered coatings of TiN and ZrN.

Other areas of thin film processing in which DOE has found application include, Al-based films for liquid diplays [203], Cr doped YAG films for fluorescent devices [196] and SiO_2 for thin film transistor applications [198]. Again factors having statistically significant effects on the properties of these films included sputtering pressure, sputtering power and also substrate bias.

Although DOE has begun to find application in the area on thin films over the last decade, in the more specific field of thin film resistors, there appears to have been little or no published research in this area to date.

5.2 EXPERIMENTAL

5.2.1 Design Selection

To gain an initial impression of the effects of varying the sputtering and heat treatment parameters on the electrical properties of the films, a 2-level factorial design was utilised. This type of design can look at 'k' parameters or "factors" in 'n' observations or "treatment combinations" (tc's), with each factor having two levels. The observations are then analysed together as an experimental unit to provide mathematically independent or "orthogonal" assessments of the effects of each of the factors under study. The number of tc's required is determined as follows [181]:

$$tc = 2^k \qquad \textit{Equation 5.1}$$

Where there are '2' levels and 'k' factors. Initially the following five factors and levels were selected for investigation, see Table 5.1:

Factor	Low level (-)	High level (+)
Sputter power (W)	250	1000
Sputter time (min)	6	24
Sputter pressure (mTorr)	1	6.5
Anneal temperature (ºC)	250	450
Anneal time (hrs)	1	5

Table 5.1 – DOE experimental factors and levels

Generally the factor level settings were based on a combination of the working ranges of the process and also previous results for the CuAlMo films. The high level sputtering power was restricted to 1000W to avoid eroding the target material too quickly and the low level power and sputtering times were selected to allow comparison of films grown for similar kilowatt hours at different power levels i.e. 250 x 24 = 1000 x 6 = 3kWhrs.

As the vacuum plant employed was already being used in production it was not feasible to adjust the position of the cryo pump throttle valve and hence the sputter pressure could only be varied using the argon flow rate. The low level setting of 1mTorr was selected to be just above the pressure at which a plasma could be maintained and the high level setting of 6.5mTorr was the highest pressure achievable at the maximum gas flow of 100sccm. Prior to sputtering the experimental samples, it was confirmed that the plant could operate consistently under these conditions without loss of plasma or unacceptable heating of the cryo pump.

The low level annealing temperature of 250ºC was selected to be above the maximum device processing and operating temperatures of 220 and 155ºC respectively. The high

level setting was selected to be near the zero TCR annealing temperature determined in chapter 4. In addition to the annealing time of 5hrs used in all experimentation thus far, a reduced time of 1 hour was selected for the low level to see if suitable film properties could be attained more rapidly.

From equation 5.1 it can be seen that for a 5-factor experiment, 2^5 or 32 treatment combinations were required as shown in Table 5.2. To allow orthogonal analysis of the experiment, the levels were coded into design units i.e. '+' and '-', as defined in Table 5.1. The standard order of experiments shown in Table 5.2 follows the conventional alternation of -'s and +'s or Yates order, which is useful during analysis, however when the factorial experiment is run, it is done so in a randomised order as shown in column 2. This ensures that any unwanted or unknown sources of variation will appear randomly rather than systematically and thus will not 'cloud' the results. In addition, to further improve accuracy, the experiment was also duplicated.

Std order	Run order	Sputter power	Sputter time	Sputter pressure	Anneal temperature	Anneal time
1	5	250	6	1	250	1
2	24	1000	6	1	250	1
3	1	250	24	1	250	1
4	4	1000	24	1	250	1
5	28	250	6	6.5	250	1
6	3	1000	6	6.5	250	1
7	30	250	24	6.5	250	1
8	17	1000	24	6.5	250	1
9	11	250	6	1	450	1
10	27	1000	6	1	450	1
11	9	250	24	1	450	1
12	19	1000	24	1	450	1
13	8	250	6	6.5	450	1
14	10	1000	6	6.5	450	1
15	25	250	24	6.5	450	1
16	18	1000	24	6.5	450	1
17	22	250	6	1	250	5
18	23	1000	6	1	250	5
19	12	250	24	1	250	5
20	26	1000	24	1	250	5
21	32	250	6	6.5	250	5
22	14	1000	6	6.5	250	5
23	7	250	24	6.5	250	5
24	13	1000	24	6.5	250	5
25	16	250	6	1	450	5
26	20	1000	6	1	450	5
27	2	250	24	1	450	5
28	15	1000	24	1	450	5
29	6	250	6	6.5	450	5
30	31	1000	6	6.5	450	5
31	29	250	24	6.5	450	5
32	21	1000	24	6.5	450	5

Table 5.2 – 2-level factorial design for sputtering and heat treatment processes

Again the following three main electrical properties of the films were selected as experimental outputs:

1. Room temperature sheet resistance, Rs, (Ω/□)
2. TCR_{av} 20/70^{o}C, (ppm/^{o}C)
3. Resistance Stability, ΔΩ/Ω, (%)

5.2.2 Process Conditioning

All sample films were deposited in the CPA 900 planar substrate sputtering plant as described in chapter 2. Prior to each experimental run the plant was conditioned in order to make the comparison of results as accurate as possible.

This process involved firstly evacuating the plant to a base pressure of $1x10^{-7}$ Torr, followed by a footprint analysis of the gases present in the chamber using a residual gas analyser (RGA) type MKS e-vision Mass Spectrometer coupled with RGA Data Recall software. An example of the RGA analysis is given in Figure 5.1 and for each run this was compared to a control footprint for the plant, to check for any potential problems such as gas or water leaks.

Once the base pressure was satisfactory, the CuAlMo target was pre-sputtered for 30 minutes under the required conditions for that experimental run, in order to remove contaminations from the target surface and stabilise the magnetron discharge parameters.

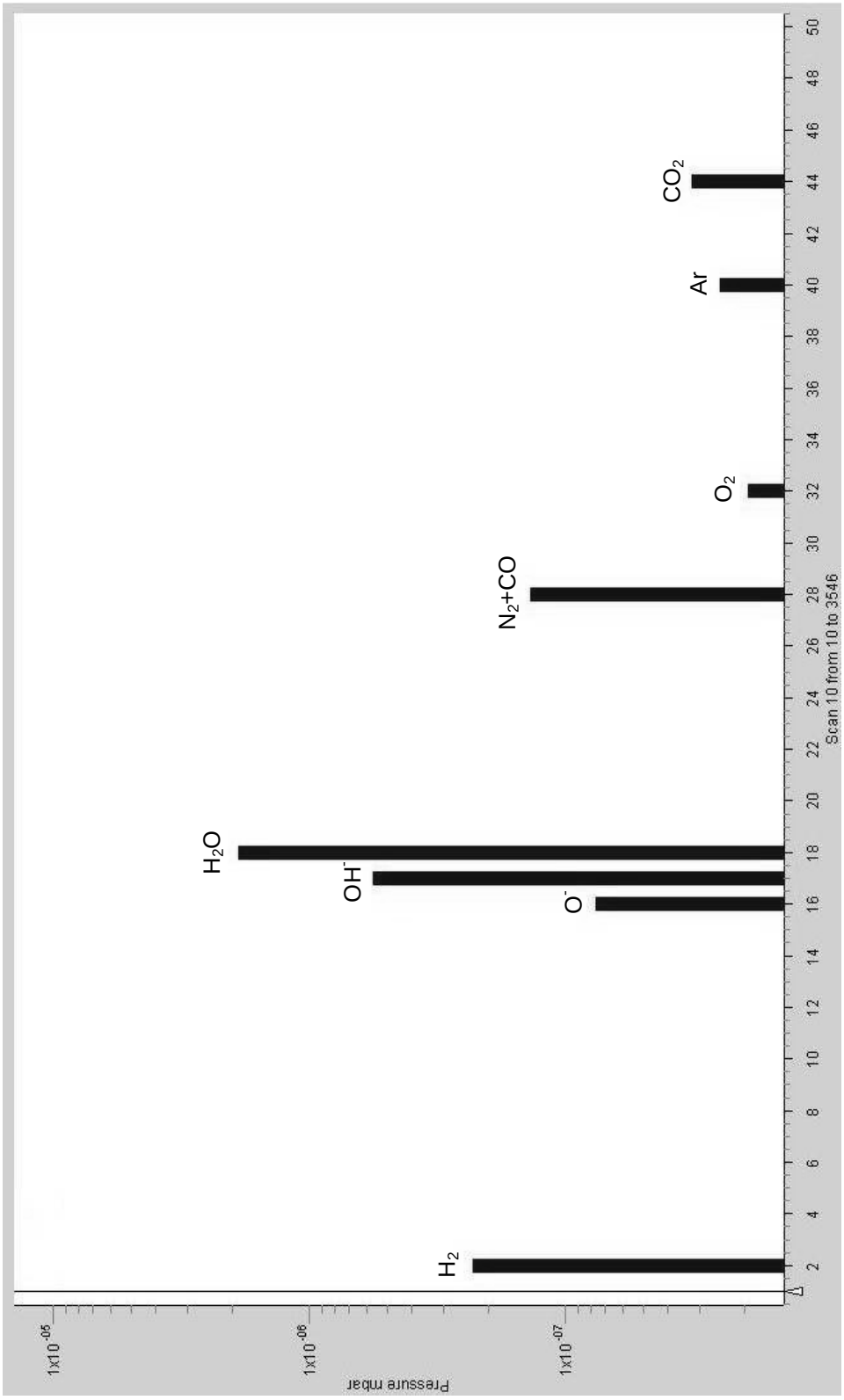

Fig. 5.1 – Typical RGA footprint taken for the CPA sputtering plant at a base pressure of $1x10^{-7}$ Torr.

5.3 RESULTS AND DISCUSSION

5.3.1 2-Level Factorial Experiment

To help with the analysis of the experiment, Minitab 15 [205] statistical software package was used. Firstly a hypothesis test was carried out to determine which of the factors and their interactions or terms had the greatest effect on the electrical properties of the films.

The null hypothesis, H_0, is that the effect of the term is not significant and the alternative hypothesis, H_a, is that the effect of the term is significant. The alpha (α) risk value is used to set a maximum level of risk at which to reject H_0 and therefore assume H_a, and is most commonly set at 0.05. Therefore at this level the probability (P) of finding an effect which is not really significant is 5% [206], hence:

For $P > \alpha$, accept H_0 - the term is not statistically significant

$P \leq \alpha$, reject H_0 and accept H_a – the term is statistically significant

Figures 5.2a to 5.2c show the terms which have P-values less than the α-level of 0.05 (following reduction of the experimental model by removal of insignificant terms) and therefore a statistically significant effect on the electrical properties of the films. The results are all based on the measurements of 20 samples from each experimental trial.

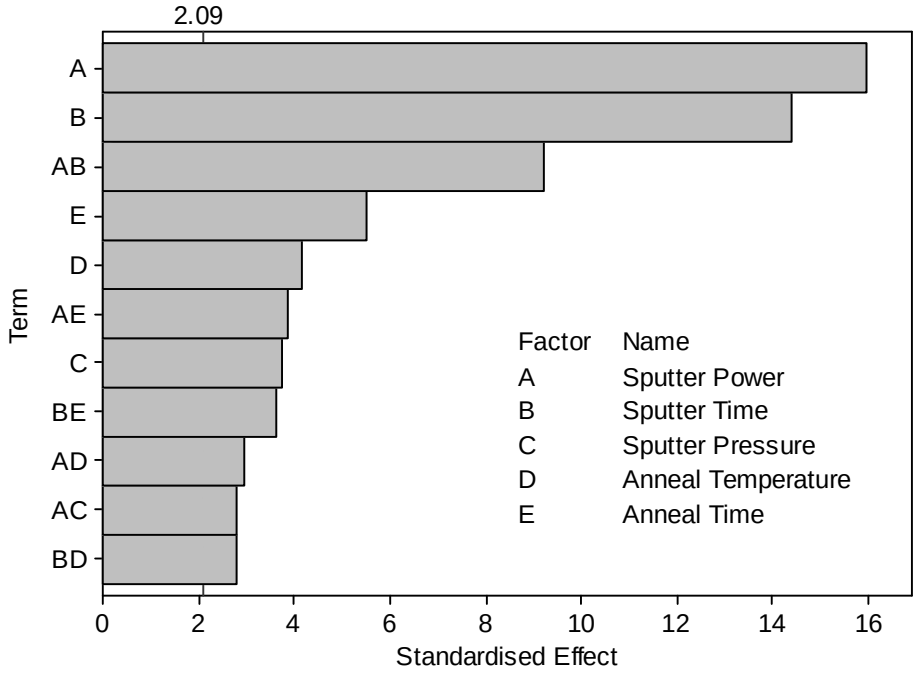

Fig. 5.2a – Pareto chart of the standardised effects of sputtering and heat treatment factors and their interactions on the sheet resistance of the CuAlMo films.

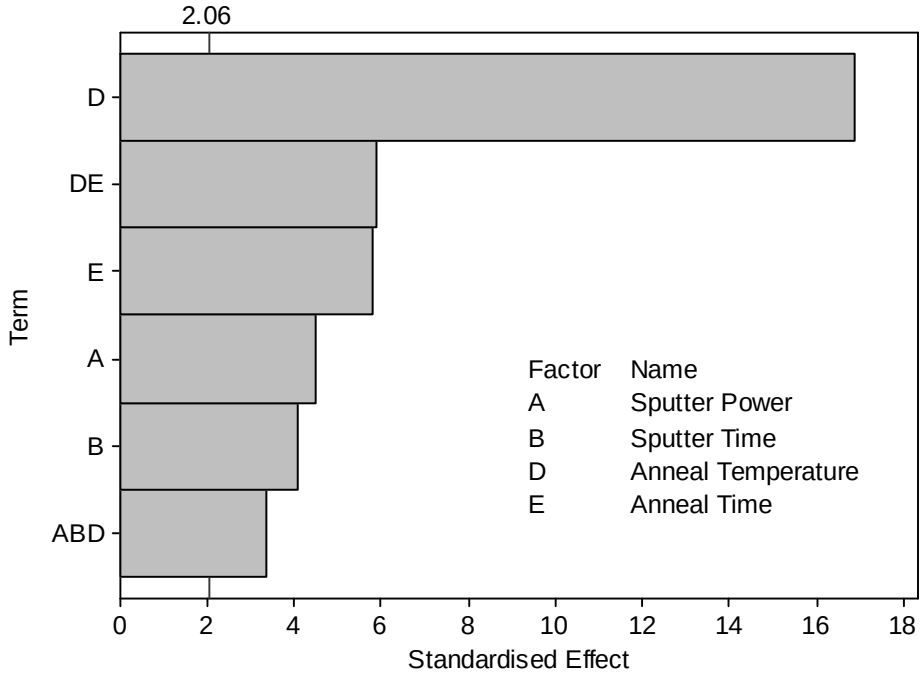

Fig. 5.2b – Pareto chart of the standardised effects of sputtering and heat treatment factors and their interactions on the TCR_{av} of the CuAlMo films.

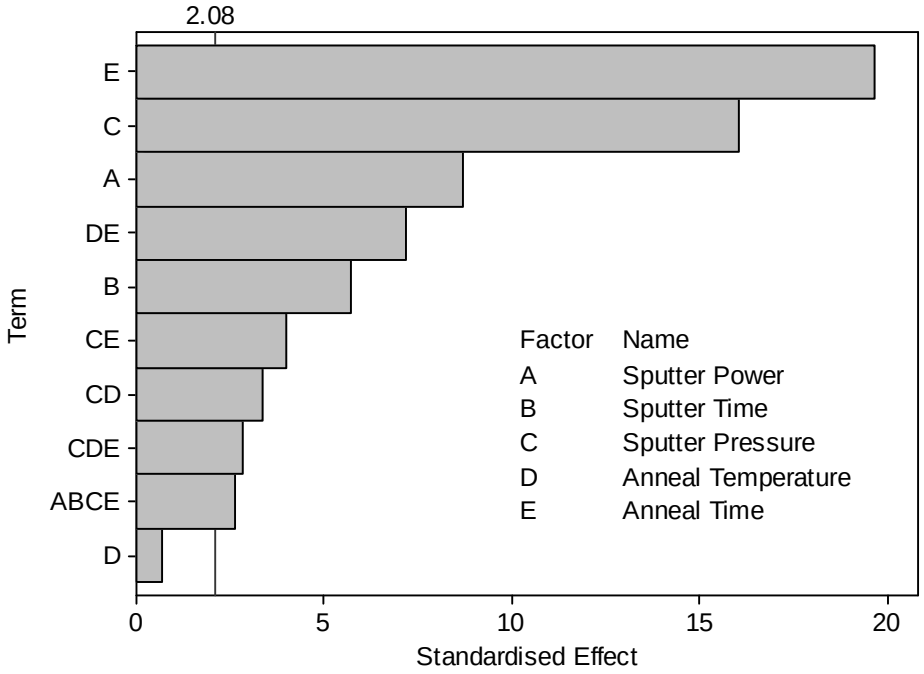

Fig. 5.2c – Pareto chart of the standardised effects of sputtering and heat treatment factors and their interactions on the resistance stability of the CuAlMo films.

Figure 5.2a shows that all the individual factors have a significant effect on the sheet resistance of the films, along with a number of two factor interactions, the most significant of which is that between sputtering power and sputtering time. Main effect plots for each of the factors and the interaction between sputtering power and time are shown in Figures 5.3 and 5.4 respectively.

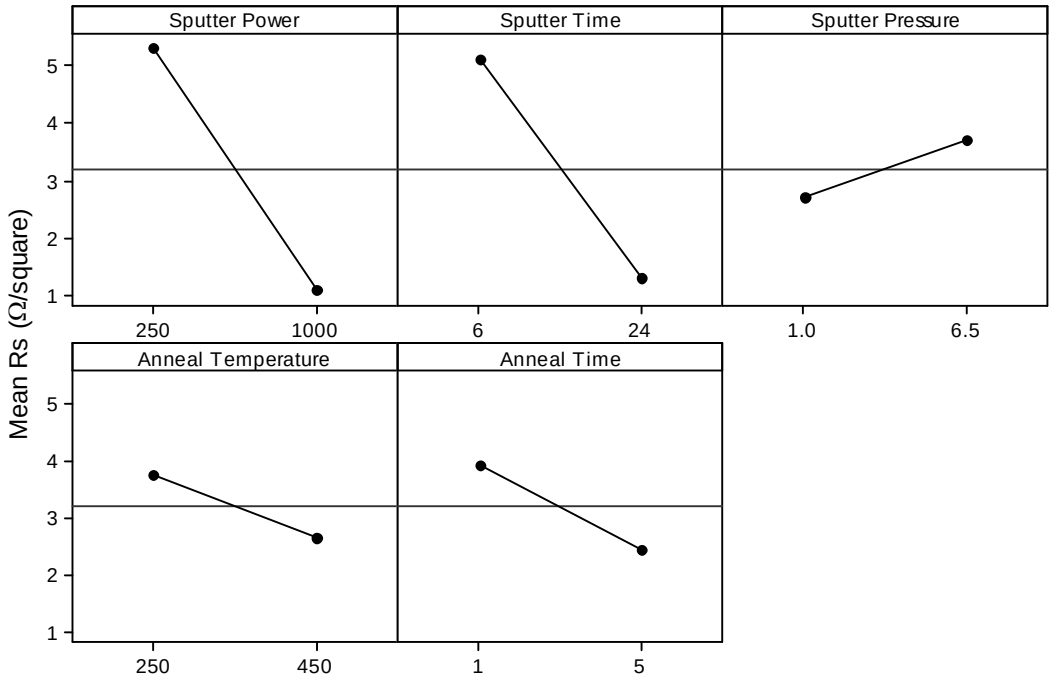

Fig. 5.3 – Main effects plot of sputtering and heat treatment factors on the sheet resistance of the CuAlMo films

On average, the variation of sputtering power and sputtering time factors have the greatest effect on the sheet resistance and this is indicated by the sharpness in the gradient of their slopes in Figure 5.3. The higher power setting of 1000W and the longer sputtering time of 24 minutes gave the lowest values of ≈1Ω/□. The effect of sputtering pressure, annealing temperature and annealing time were less, but still statistically significant. The lowest values of sheet resistance were achieved at a sputtering pressure of 1mTorr and an annealing profile of 5 hours at 450ºC.

The strong interaction between the sputtering power and sputtering time is signified by the two lines with sharply differing slopes in Figure 5.4. This result indicates that the lowest sheet resistance is achieved with a high sputtering power and long sputtering time.

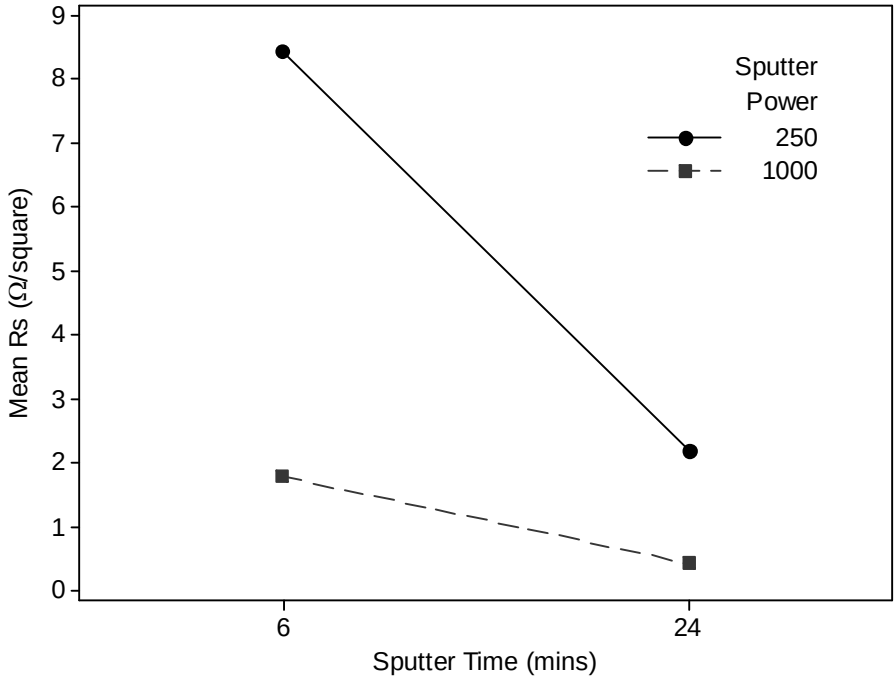

Fig. 5.4 – Interaction plot of sputtering power and time factors on the sheet resistance of the CuAlMo films

Figure 5.2b shows that the factor having the most significant effect on the TCR value of the films is annealing temperature. The extent of this result is highlighted in Figure 5.5 along with the other main effects plots for TCR.

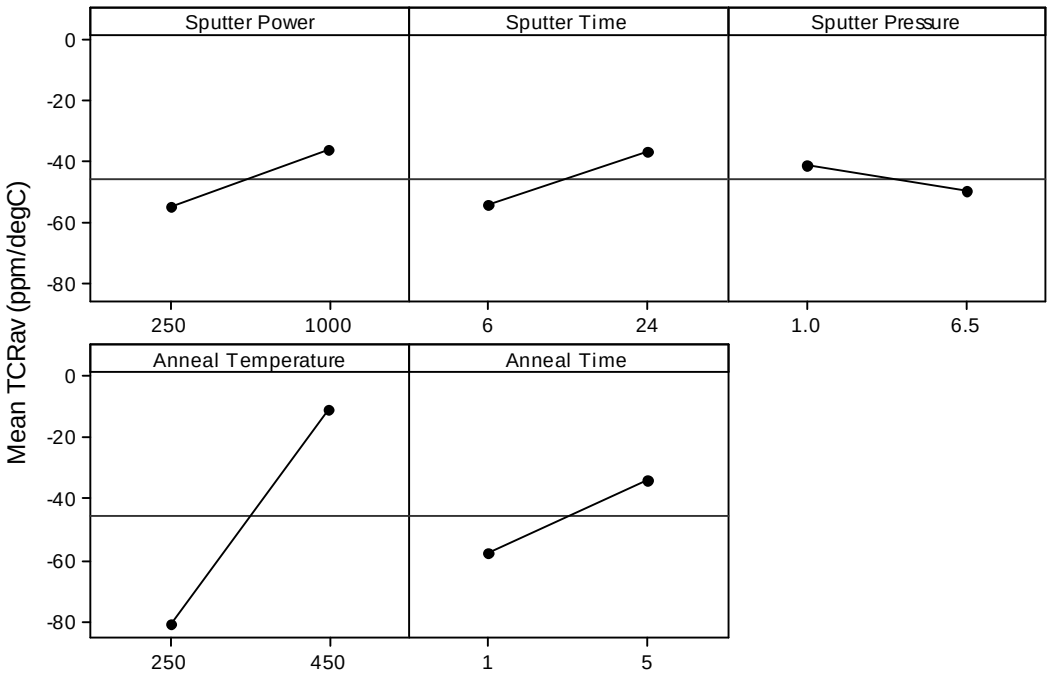

Fig. 5.5 – Main effects plot of sputtering and heat treatment factors on the TCR_{av} of the CuAlMo films

In addition to an annealing temperature of 450ºC, as with the main effects plots for sheet resistance, the parameters having the largest effect on the TCR properties of the films are a high sputtering power and time, low sputtering pressure and a long annealing time.

Moreover as shown in Figure 5.6 there is a strong interaction between annealing time and temperature and by treating the films at 450ºC for 5 hours the mean value of the films can be shifted positive through the zero TCR line. Also of interest in this plot is that the annealing time appears to have little effect on the TCR of films treated at the lower temperature of 250ºC, indicated by the flatness of the plot.

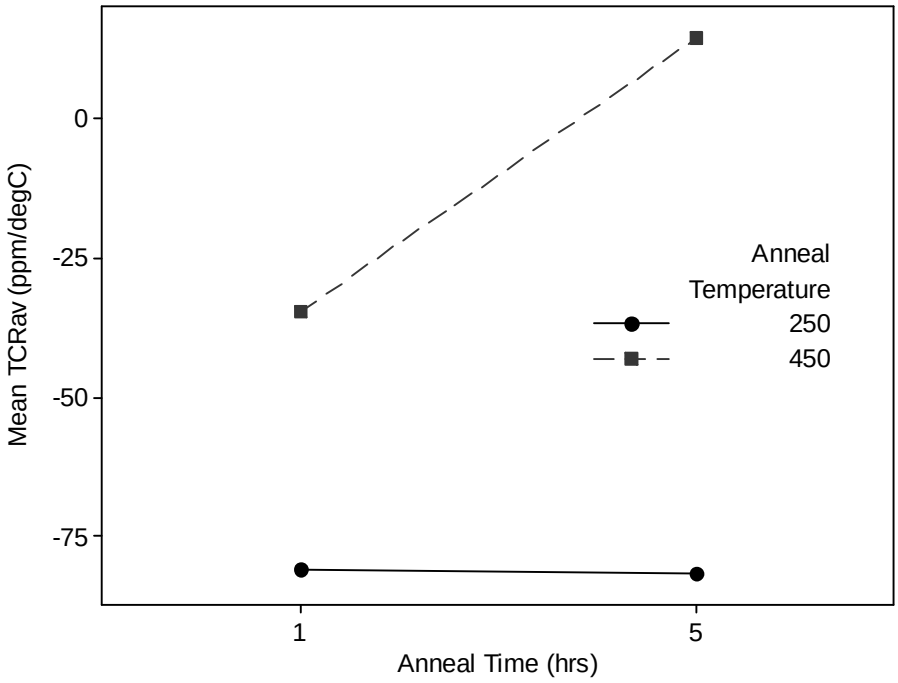

Fig. 5.6 – Interaction plot of annealing temperature and time factors on the TCR_{av} of the CuAlMo films

From Figure 5.2c it can be seen that two factors having very significant yet opposing effects on the resistance stability of the films are sputter pressure and annealing time. Low sputtering pressure and long annealing times appear to be desirable if good long term stability is to be achieved as shown in Figure 5.7. In addition, high sputtering power and longer sputtering time also play a role in reducing the resistance drift, whilst in this case annealing temperature does not appear to be as significant.

However there is evidence of an interaction between annealing time and temperature as plotted in Figure 5.8 and following treatment for 5 hours, the stability of the films annealed at 250ºC is better than those at 450ºC.

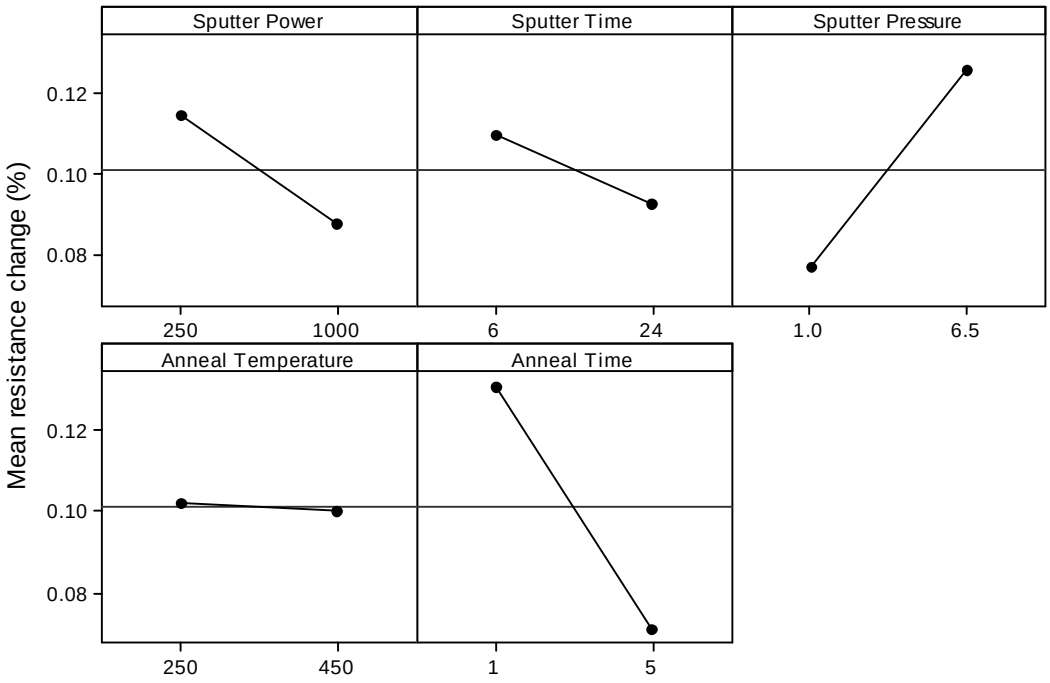

Fig. 5.7 – Main effects plot of sputtering and heat treatment factors on the resistance stability of the CuAlMo films

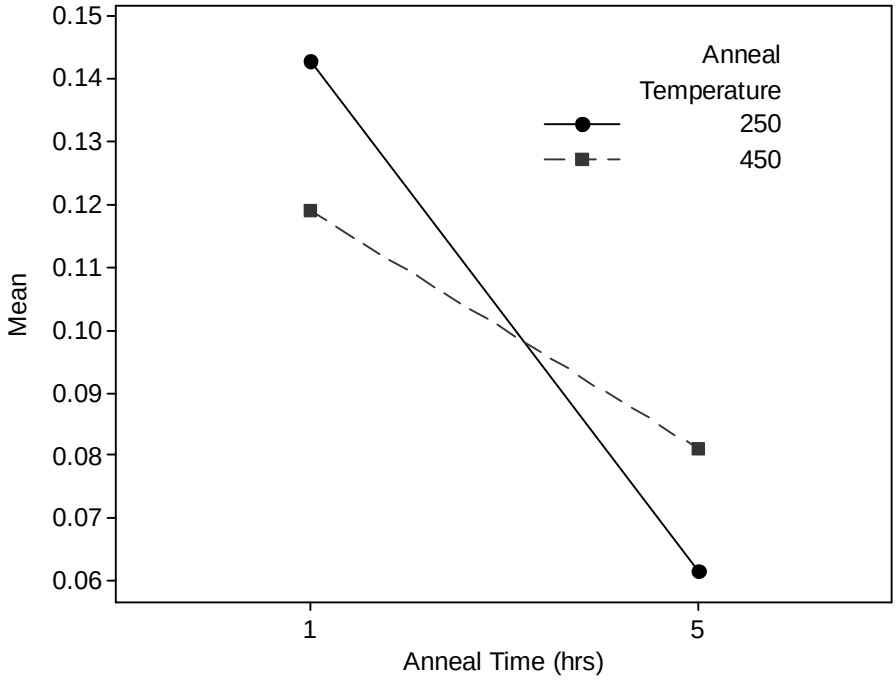

Fig. 5.8 – Interaction plot of annealing temperature and time factors on the resistance stability of the CuAlMo films

Table 5.3 gives a summary of the main effect results presented in the previous figures.

Factor	Mean effect of increasing factor on:		
	Rs	TCR	ΔΩ/Ω
sputter power	↓	↑	↓
sputter time	↓	↑	↓
sputter pressure	↑	↓	↑
anneal temperature	↓	↑	-
Anneal time	↓	↑	↓

Table 5.3 – Summary of mean effect of increasing factors on the sheet resistance, TCR_{av} and resistance stability of the CuAlMo films

In order to understand the influence of the sputtering and heat treatment process parameters in more detail, the structural transformations taking place inside the films during the growth process must be considered. There have been numerous studies undertaken previously in this area [207-221].

Obviously the reduction in sheet resistance and increase in TCR with sputtering time are largely attributable to increasing film thickness. Furthermore increasing sputtering power will also produce a thicker film due to the higher deposition rate.

In addition to film thickness, the deposition rate influences the grain size and the number of residual gas molecules or impurities captured in the growing film. Increasing the deposition rate generally leads to the formation of fine grained structures with a low concentration of impurities [20].

However, increasing the sputtering rate through the energy of the bombarding Ar ions can in turn lead to an increase in the energy of the ejected atoms from the target. On reaching the substrate these atoms will have a higher surface mobility, thus raising the temperature of the substrate and resulting in a larger grained film structure [1].

Moreover it has also been shown that exceeding a critical deposition rate can lead to the burial of these mobile surface atoms, thus impeding grain growth [222]. This situation can also result in an increase in the density of vacancies captured in the film, since they have less time to escape.

In addition to deposition rate, sputtering pressure and substrate temperature are also known to play a significant role in determining the structure of the growing film [167]. The combined influences of substrate temperature and sputtering pressure have been considered in a now classical article by Thornton [223].

A schematic representation of Thornton's model is depicted in Figure 5.9. An Increase in sputtering gas pressure allows more Ar atoms to be adsorbed at the substrate surface. This limits the mobility and hence surface diffusion of arriving adatoms. Conversely an increase in substrate temperature enhances surface mobility and conventional bulk diffusion.

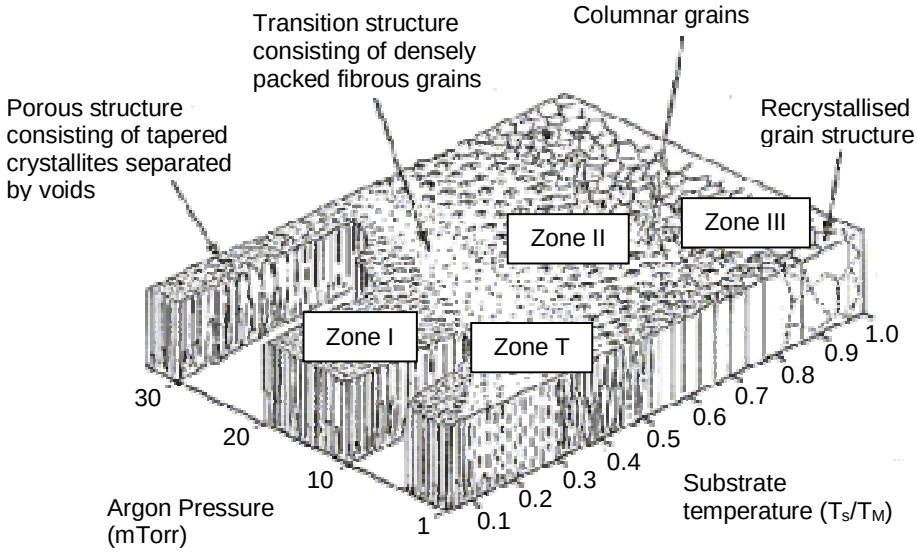

Fig. 5.9 – Influence of substrate temperature and argon pressure on microstructure of thin films [223].

Film growth in Zone I of the model tends to produce porous grain boundaries due to the preferential collection of incident atoms at protuberances on the substrate surface, which due to the low substrate temperature do not have sufficient thermal energy to diffuse into a continuous structure.

In Zone T the substrate temperature is still too low to permit significant diffusion but there is sufficient energy to overcome the main surface irregularities and produce a continuous film having a dense fibrous structure similar to that in the open grains of Zone I.

In Zone II the effects of inert gas adsorption no longer play any significant role due to the increased substrate temperature, and surface diffusion processes are now dominant, producing a film structure consisting of columnar grains with fully dense boundaries.

Finally in Zone III the high temperature produces substantial bulk diffusion, resulting in grain growth and re-crystallisation in the film structure.

To allow comparison of the above theory with the experimental findings it was necessary to establish the temperature of the substrate during deposition. To achieve this, two 0.2mm diameter fibreglass braided, type-K thermocouples were attached to the top and bottom surfaces of alumina substrates positioned under the centre and to the two extremes of the sputtering target as illustrated in Figure 5.10 [220 & 227].

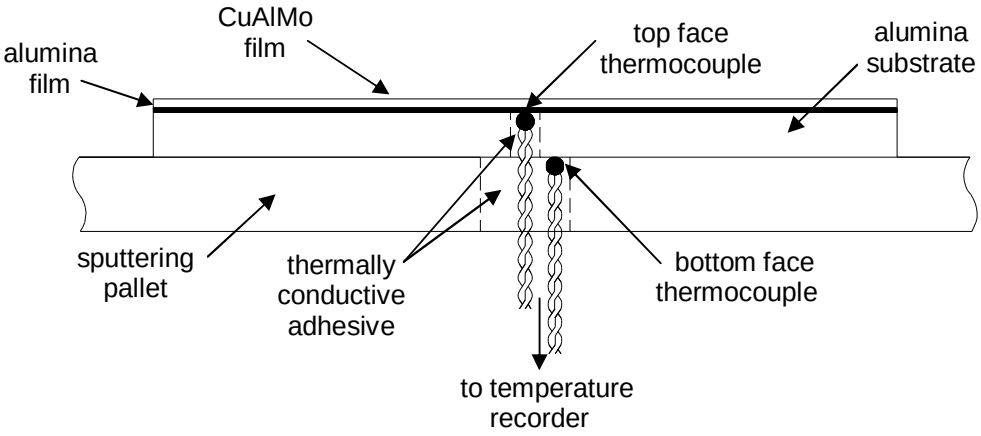

Fig. 5.10 – Schematic of film and substrate temperature measurement setup

Both thermocouples were fed through a pre-drilled hole in the sputtering pallet. The bottom face thermocouple was positioned on the rear of the substrate and the top face thermocouple was mounted in a laser drilled hole in the substrate. Both thermocouples were then secured in place using thermally conductive adhesive. The top face was then polished flat before being sputtered with a thin layer (approx 200nm) of Al_2O_3 to shield the thermocouple from the plasma [227].

Electrical connection was achieved via a multi pin feed through connector in the base of the chamber and temperature measurements were recorded using a PicoLog USB temperature recorder and software [228].

Plots of film and substrate temperature with increasing sputtering time and power are presented in Figures 5.11a and 5.11b respectively. The variation in temperature was found to be < ±5ºC once it had stabilised at each cathode power setting.

The temperature increase of the film (top surface of the substrate) is reasonably linear, rising from 60ºC at a sputtering power of 100W to 320ºC at 1000W. The peak temperature plot obtained for the bottom face of the substrate is lower than that of the film and becomes increasingly more so as the target power is ramped.

For example the temperature recordings at the DOE upper and lower power levels of 250 and 1000W were 110ºC and 320ºC for the upper surface versus 95ºC and 220ºC

for the lower surface of the substrate. Moreover the response of temperature to power increase was instantaneous at the film surface whereas a distinct lag was observed at the rear face of the substrate. These differences in results are largely attributable to the vast heat sink effect of the stainless steel sputtering pallet onto which the substrate is mounted [220 & 227].

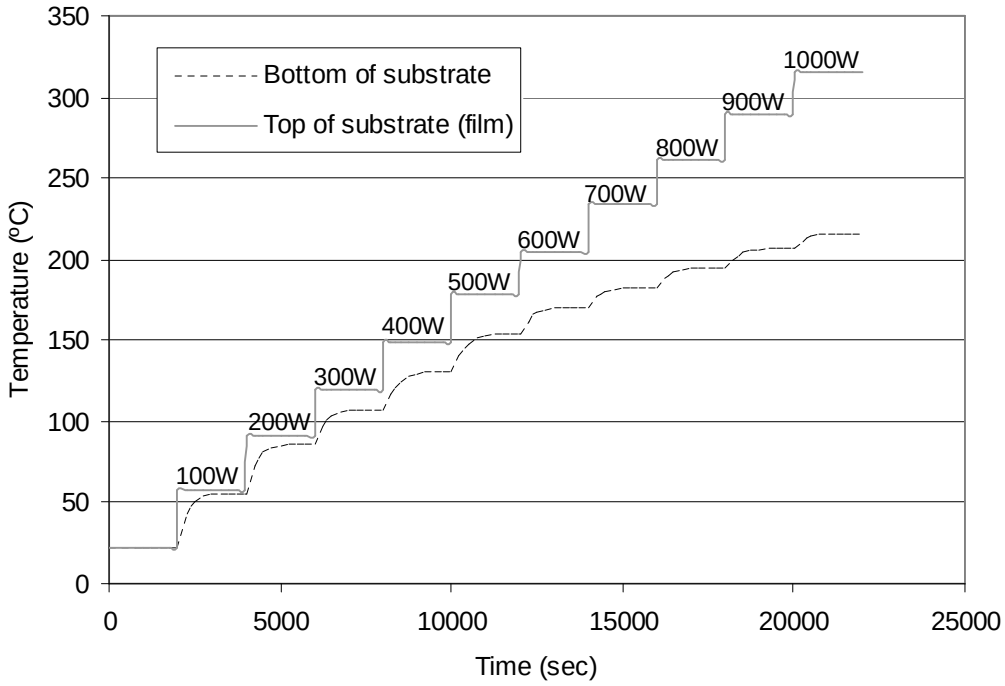

Fig. 5.11a – Variation in CuAlMo film and substrate temperature as a function of increasing cathode power with time.

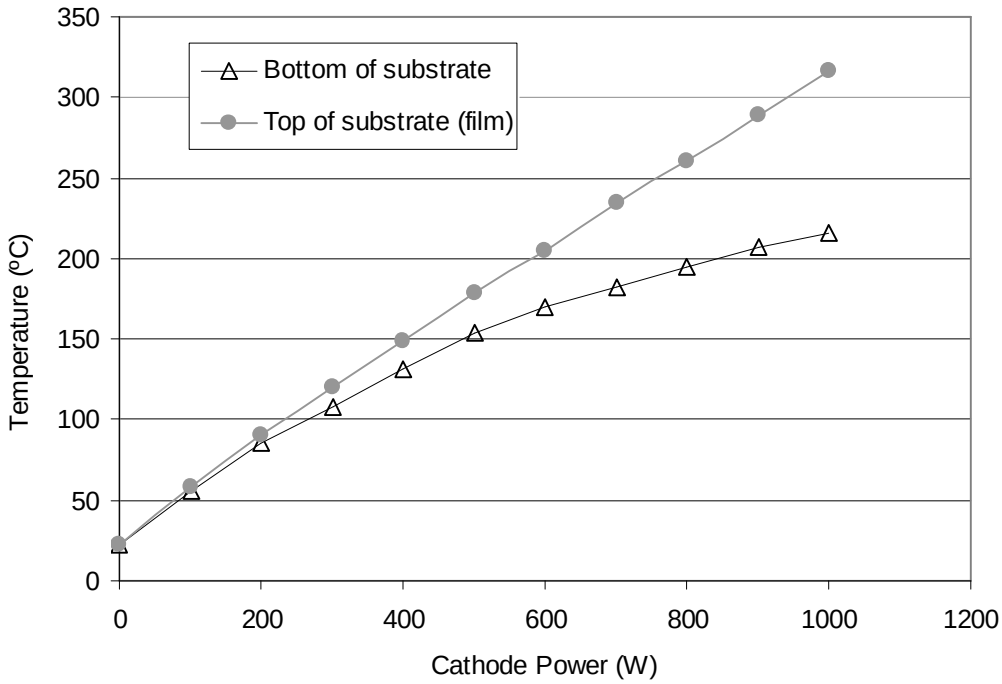

Fig. 5.11b – Variation in CuAlMo film and substrate peak temperature as a function of increasing cathode power.

To help understand the combined effect of increasing sputtering power, and hence film temperature, and sputtering pressure on the structural properties of the films, samples were investigated using SEM and X-Ray diffraction (XRD). All XRD patterns were collected using a Siemens D5000 X30 diffractometer with Cu Kα radiation at 40kV and 40mA, with a scanning speed of 0.01° per second. Details of the SEM have been discussed previously in chapter 2.

Initially films sputtered onto Al_2O_3 substrates were analysed, see Figure 5.12. However due to problems with the substrate morphology dominating over that of the film and also the crystalline nature of the alumina clouding the XRD result, it was decided to use borosilicate glass substrates for the analysis. Prior to investigation the electrical properties of the films on glass were confirmed to be in line with those on Al_2O_3.

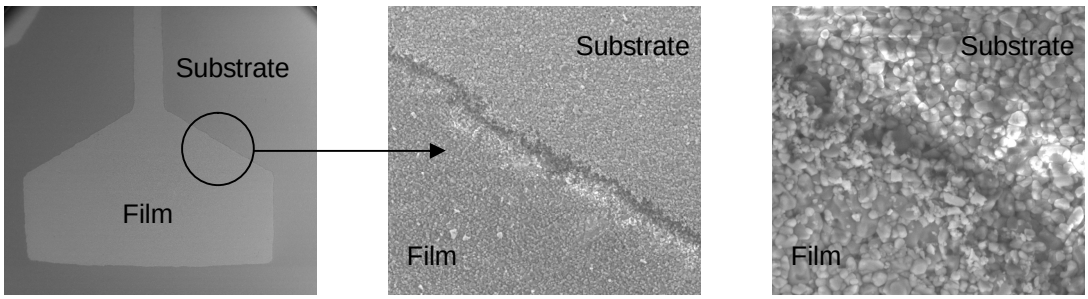

(a) x40 mag *(b) x750 mag* *(c) x3000 mag*

Fig. 5.12 – CuAlMo film grown on Al_2O_3 showing rough surface morphology of the substrate dominating over that of the film.

SEM micrographs of surface morphology for films sputtered on glass at 250W and 1000W at pressures of 1mTorr and 6.5mTorr are presented in Figures 5.13a to d.

The images show that the structure is very fine grained and is typical of an amorphous material. Even at a magnification of x240K it was difficult to detect any significant structure. The production of fined grained materials is frequently encountered when sputtering multi component materials due to the reduction in grain boundary mobility [256-257] and is regularly reported for thin resistive films such as NiCr [23, 35, 44-45].

There also appears to be very little difference between the morphology of the films grown at different temperatures or pressures. It could be considered that for the low sputtering power of 250W the film grown at 1mTorr has a more dense structure and that grown at 6.5mTorr is slightly more porous. Moreover perhaps a slight increase in grain size is observable with sputtering power, but again these features are much too small to be measured with any degree of confidence using the SEM.

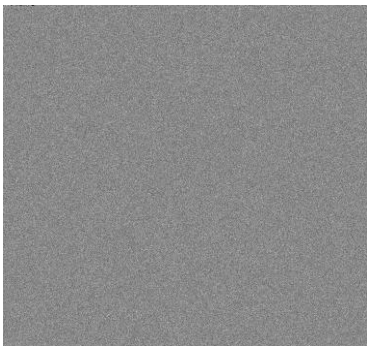

(a) 250W and 1mTorr (x240K)

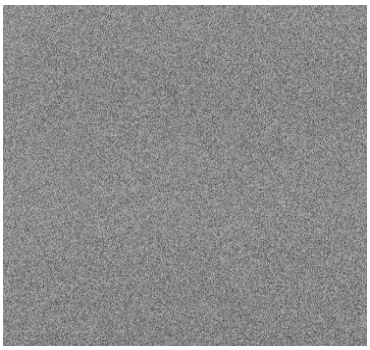

(b) 1000W and 1mTorr (x240K)

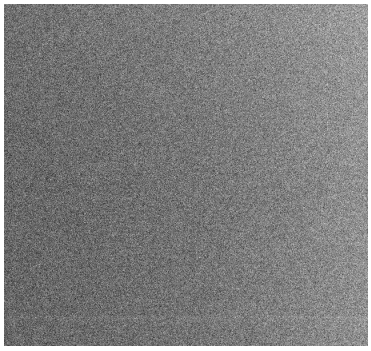

(c) 250W and 6.5mTorr (x240K)

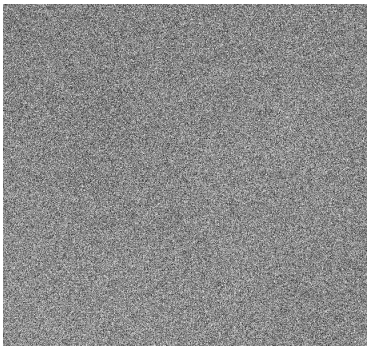

(d) 1000W and 6.5mTorr (x240K)

Fig. 5.13 – SEM images of CuAlMo films grown on glass substrates at pressures of 1mTorr and 6.5mTorr and power levels of 250W and 1000W.

XRD plots for the film samples are presented in Figure 5.14. Although there was no significant difference in the visual appearance of the films using SEM, the XRD patterns clearly show an increase in crystallisation with sputtering power.

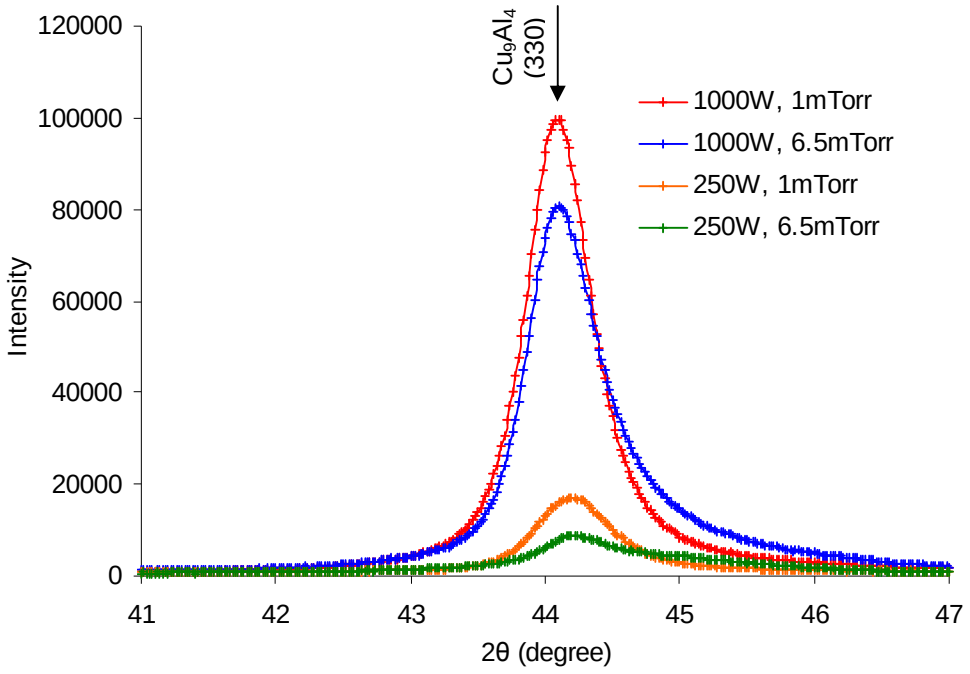

Fig. 5.14 – XRD patterns for CuAlMo films grown at pressures of 1mTorr and 6.5mTorr and power levels of 250W and 1000W.

The effect of sputtering pressure is less significant and results are more comparable for films grown at 1mTorr and 6.5mTorr at both power levels. This result is in line with the main effects plot for sheet resistance in Figure 5.3, where the slope of the sputtering power is much steeper than pressure.

This result is perhaps not too surprising when it is considered that only a small region of the Ar pressure range depicted in Thornton's model is being considered in the current investigation. Nevertheless the DOE main effect plots show an increase in sheet resistance with pressure, suggesting that the above discussed processes are indeed taking place to some degree.

Only one pattern was detected on the XRD plot and this was identified as the γ_2 (Cu_9Al_4) phase as discussed in chapter 2, with orientation along the (330) direction. The γ_2 phase is known to have a stability range of around 31-37at.% Al for bulk samples [173] and has been shown to be stable over a much wider range of approximately 28-62at.% Al for thin films [121]. This composition corresponds well with the current work where the Al content was measured to be 36-38at.%. Furthermore the temperatures involved in the phase formation are also consistent with those characterised by the CuAl phase diagram and discussed in chapter 2.

Using the XRD results, the average particle size of the films can be related to the variation in the full width half maximum (FWHM) for the (330) peak and is calculated using the Scherrer formula [229]:

$$L = \frac{K l}{b \cos q} \qquad \textit{Equation 5.1}$$

Where L is the crystallite size, K is the Scherrer constant (=0.90), l is the wavelength of the x-ray, b is the real width of the peak ($b^2 = B^2 - b^2$, where B = experimental width, b = instrumental resolution) and q is the Bragg angle.

The variation of the FWHM and corresponding calculated mean grain size as a function of high and low sputtering powers and pressures are reported in Table 5.4.

The calculated grains sizes for the as grown films are extremely small in the range of <15nm. This result corresponds well with the lack of observable structure shown in the SEM micrographs in Figure 5.14.

Power (W)	Pressure (mTorr)	FWHM (º)	Mean grain size (nm)
1000	1	0.6	14.28
	6.5	0.66	12.98
250	1	0.7	12.25
	6.5	1.1	7.79

Table 5.4 – Variation in FWHM and corresponding calculated mean grain size for CuAlMo films grown at pressures of 1mTorr and 6.5mTorr and power levels of 250W and 1000W.

There is a decrease in FWHM with both increasing sputtering power and decreasing pressure, which results in a slight coarsening of the particle size. This evolution of grain size can be related to the evolution of conductivity, reported in Figure 5.3; however it should be noted that the grain size alone does not solely determine the electrical properties of the films. The number of voids and impurities in the film and also the grain growth mechanisms require consideration.

One final point worthy of mention is that there is no detection of a Mo containing crystal structure in the film by XRD, either as a pure element or as a binary or ternary compound. Two possible explanations for this outcome are, firstly, the small content of Mo present in the film (≈6at.%) and, secondly, the higher energy and temperature levels required for the formation of Mo containing phases.

In the binary Cu-Mo phase diagram there is no solid solubility of Cu in Mo and the liquidus temperature rises quickly as Mo is dissolved in molten copper. The only stable crystal structures known in the CuMo system are those of the pure elements themselves [230].

On the other hand the AlMo phase diagram is far more complex and contains a number of intermediate phases [231-233]. In addition to the solid solution, the Al rich end of the diagram contains a number of low temperature forming phases, most notably that of $MoAl_6$ which occurs at temperatures below approximately 700ºC and has a similar compositional ratio to that detected in the current film of Mo:Al 6:36 at.%.

These binary Al-Mo phases along with those discussed for the Cu-Al system in chapter 2 are also shown on the ternary CuAlMo [226] phase diagram in Figure 5.15.

Following preliminary studies by Shubert[234] and Raman[235], Prevarskiy[226] investigated the ternary CuAlMo system in terms of an isothermal section by means of XRD and metallographic analysis of alloys arc melted and annealed at 600ºC for 400 hours.

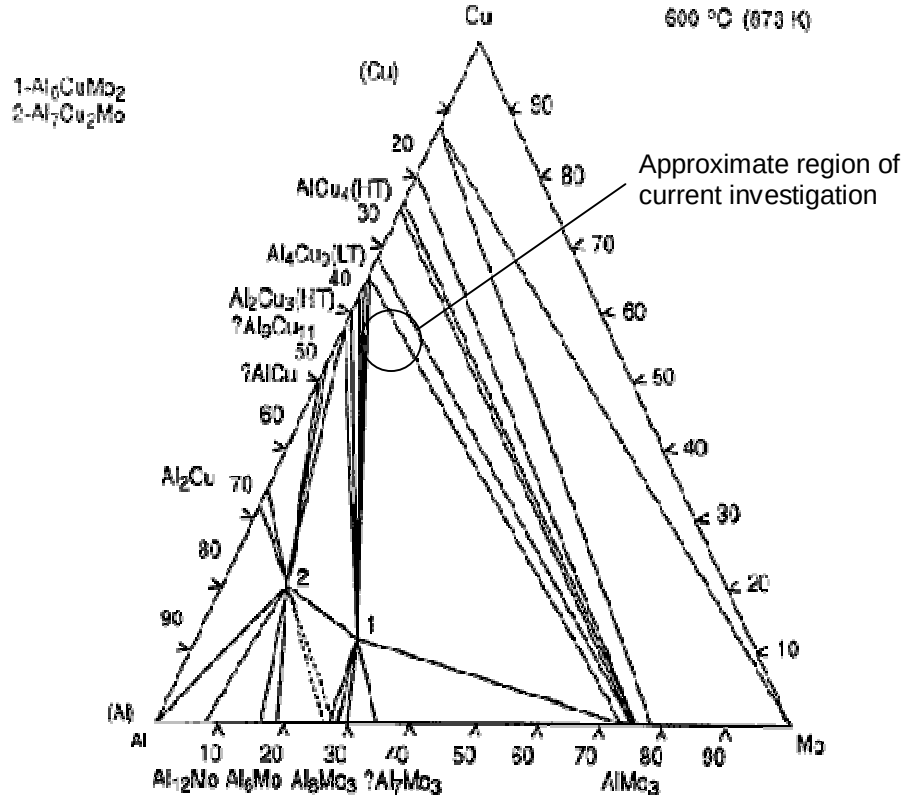

Fig. 5.15 – Copper-Aluminium-Molybdenum phase diagram at 600ºC [226].

Phase analysis data was taken from 83 specimens covering the full compositional range. Only two ternary compound phases were discovered; τ_1 ($CuAl_6Mo_2$) and τ_2 (Cu_2Al_7Mo) with practically no homogeneous ranges indicated. Mutual solid solubilities of the binary phases were insignificant. As shown in Figure 5.15 the compositions of the τ_1 and τ_2 ternary CuAlMo phases are far from the area of investigation in the current study and their formation is highly unlikely.

As there is no evidence of any Mo containing structure from the XRD results, it can be postulated that the small quantity of Mo incorporated in the film must reside at the grain boundaries between the Cu and Al, resulting in the formation of a heterogeneous structure [224]. Its role is firstly to react with residual oxygen in the chamber to form semiconducting phases having negative TCR properties, and secondly to stabilise the film through its refractory nature as reported in chapter 3 [20].

5.3.2 Summary for 2-Level Factorial Experiment

At this stage in the optimisation process the following initial observations can be made:

- High sputtering power and long sputtering time are desirable to produce films with low sheet resistance

- High sputtering power and low sputtering pressure increase the thermal energy during deposition producing films with larger grain size and lower impurity incorporation, resulting in lower sheet resistance, a less negative TCR, which can be shifted to 0ppm/ºC during heat treatment, and higher stability.

- Low sputtering power and high sputtering pressure result in a more porous structure with a smaller grain size and higher impurity incorporation. This results in a more unstable film with a negative TCR, which cannot be annealed to 0ppm/ºC regardless of heat treatment regime.

- Heat treatment time and temperature are critical parameters in determining the TCR and stability of the film. For films sputtered at high power and low pressure, heat treatment at high temperature for 5 hours results in a near zero TCR and good long term stability. An annealing time of 1hr is not sufficient to realise a zero TCR or stabilise the film sufficiently.

5.3.3 Multi Level Experiments

As the initial DOE design could only consider two levels, a high and low setting, to permit analysis of interactions, it did not allow for the possibility of non linear relationships, see Figure 5.16 [181]. To account for this possibility and to further optimise the sputtering and heat treatment process it was decided to study the effects of sputtering pressure, heat treatment temperature and heat treatment time in more detail. The sputtering power and sputtering time were not investigated as they would be set at their upper levels of 1000W and 24mins with a view to achieving films of low sheet resistance and zero TCR, which are of course two of the major objectives of this work.

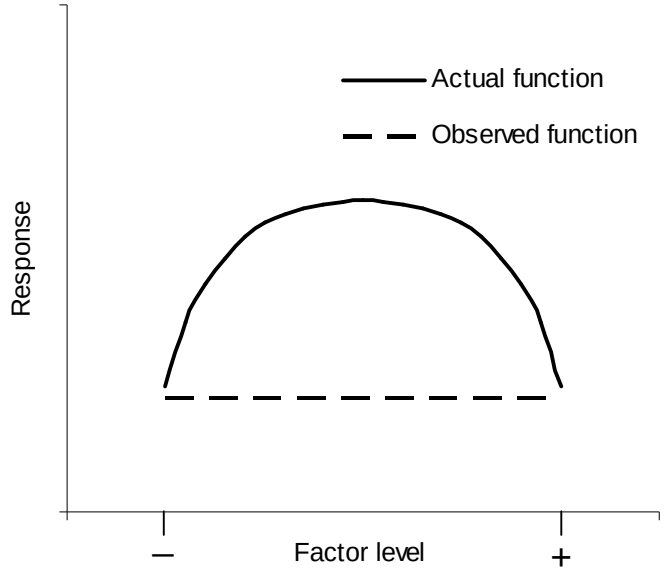

Fig. 5.16 – Non linear relationship between experimental factor and response [181]

The as-grown electrical properties of the films with variation in sputtering pressure are shown in Figure 5.17. All results are based on the measurement of a sample of 20 films.

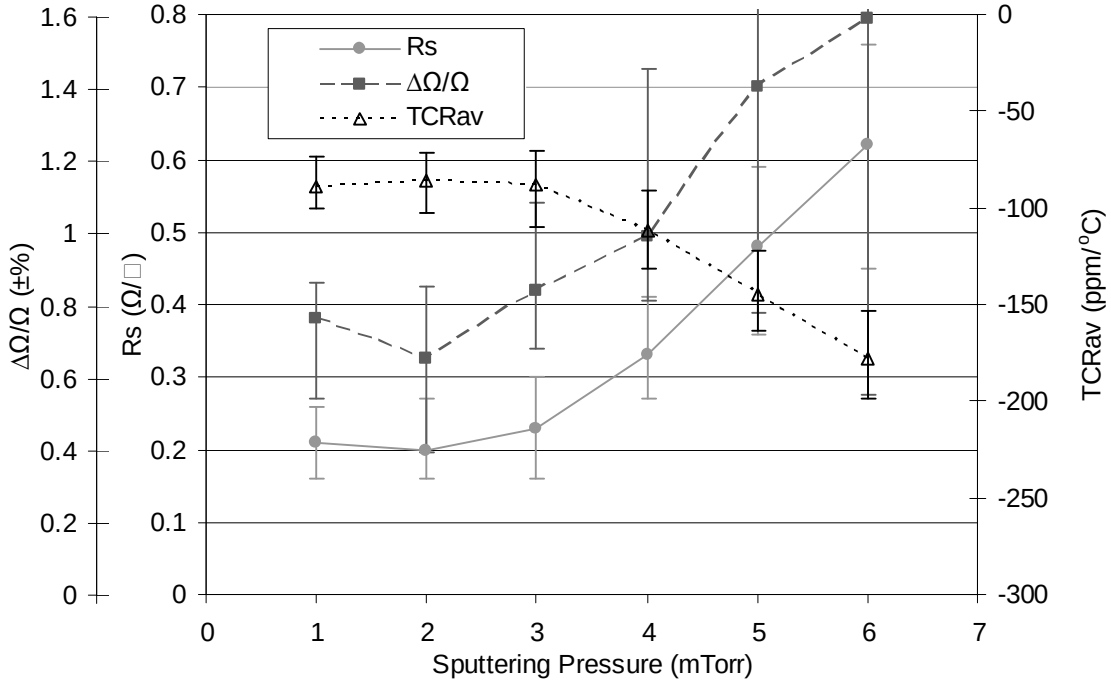

Fig. 5.17 – As grown electrical properties of CuAlMo films grown at different sputtering pressures

It can be clearly seen that the changes in film structure with increasing sputtering pressure cause an increase in sheet resistance coupled with a decrease in the magnitude of TCR. This change is quite linear in the higher pressure range of 3 to 6mTorr, however at the low pressure range of 1 to 3mTorr the electrical properties appear to be relatively unaffected by changing pressure. This phenomenon has been encountered by other workers and can be related to a plateau in deposition rate as the sputtering pressure approaches the minimum region in which a plasma can be sustained [208, 215]. This apparently stable pressure range of 1 to 3mTorr forms a useful region for process optimisation as variability in as grown properties will be significantly reduced.

The effect of increasing sputtering pressure on resistance stability is also significant. Again films in the 1 to 3mTorr pressure range are the most consistently stable, whilst those sputtered at higher pressures are considerably more unstable. This result can be related to the formation of a more porous structure with higher defect concentration at higher pressures. However, even the films sputtered at lower pressures exhibit significant resistance changes of around 1%, thus suggesting that post deposition annealing is essential to stabilise the films.

The combined effect of sputtering pressure and heat treatment temperature on the sheet resistance, TCR and resistance stability of the films is illustrated in Figures 5.18a to 5.18c. All results are based on the measurement of a sample of 20 films.

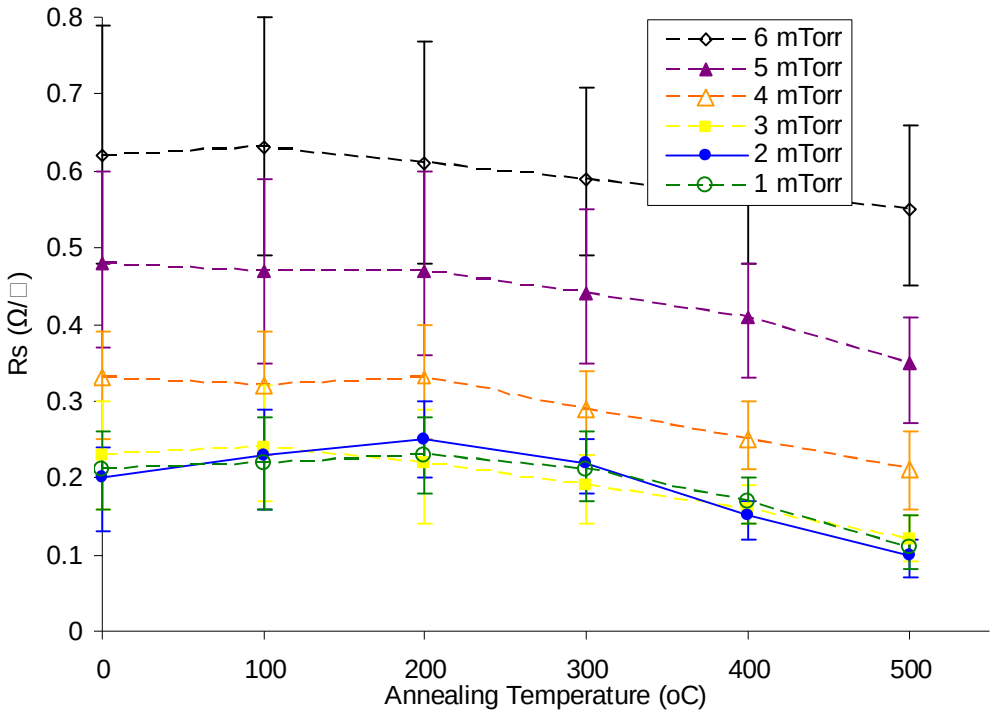

Fig. 5.18a – Combined effect of sputtering pressure and heat treatment temperature on the sheet resistance of the CuAlMo films.

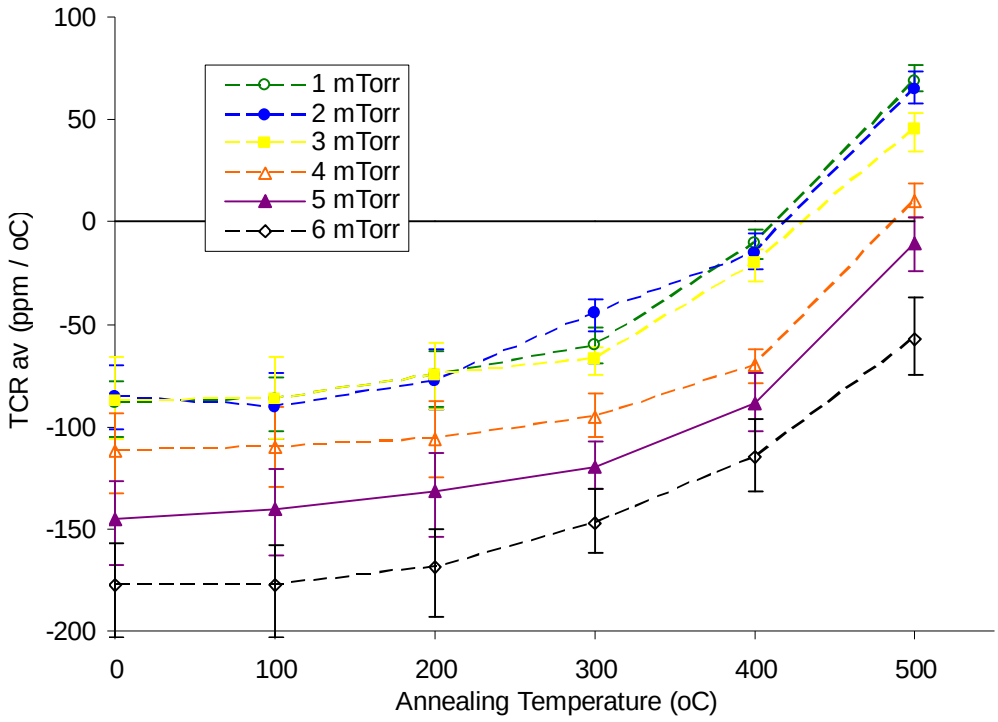

Fig. 5.18b - Combined effect of sputtering pressure and heat treatment temperature on the TCR_{av} of the CuAlMo films.

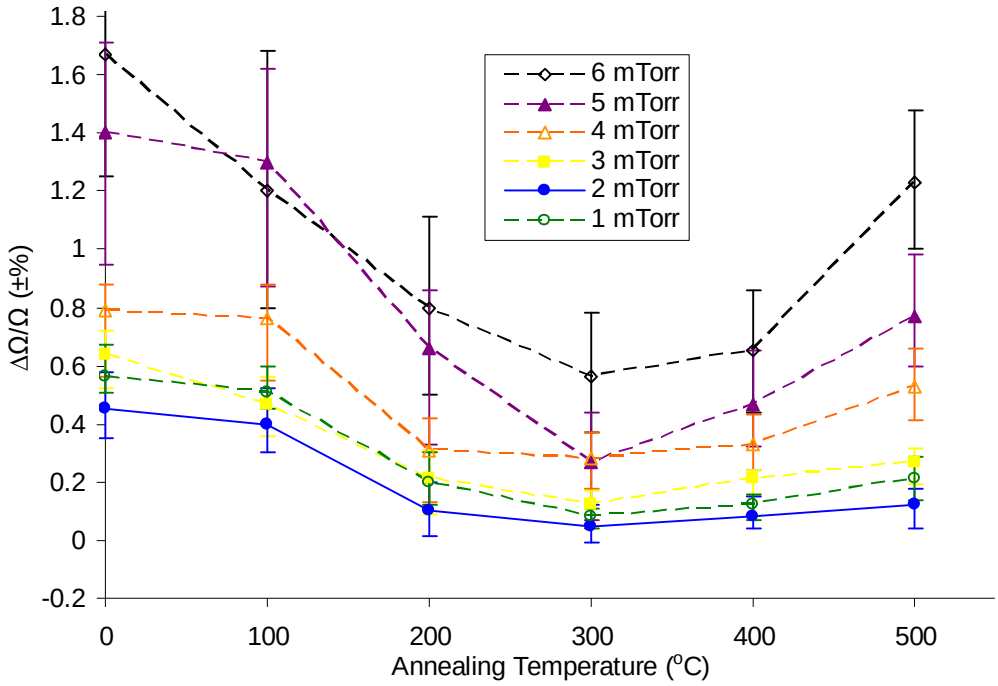

Fig. 5.18c - Combined effect of sputtering pressure and heat treatment temperature on the resistance stability of the CuAlMo films.

The reduction in sheet resistance with increasing heat treatment temperature follows a similar curvature for films grown at different sputtering pressures, see Figure 5.18a. The results for films sputtered in the 1 to 3mTorr range are very consistent in the range 0.1 to 0.2Ω/□, whilst those sputtered at higher pressures have increased sheet resistances with a maximum value of around 0.6Ω/□ at 6mTorr.

The results for TCR_{av} follow a similar but inverse trend to the sheet resistance plots, their values increasing with heat treatment temperature, see Figure 5.18b. Again results obtained for the films grown in the 1 to 3mTorr pressure range are comparable and all pass through the zero TCR line at 400-430ºC. For films grown at higher pressures the TCR becomes increasingly negative and for those sputtered above 4mTorr, a zero TCR is not attainable at the maximum annealing temperature of 500ºC.

Films grown in the 1 to 3mTorr range are also the most stable, see Figure 5.18c. The plot of stability versus annealing temperature follows a similar trend for all films, the greatest improvement being made for films treated at 200ºC, which is of course above the dry heat stability test temperature of 155ºC. This stability improvement with increasing heat treatment temperature continues up to 300ºC at which point the films are at their most stable. Beyond this temperature the resistance stability of the films begins to decline, the level of deterioration appearing to be a function of initial sputtering pressure. For the films grown in the 1 to 3mTorr range and subsequently annealed at temperatures of 300 and 500ºC this increase is <0.10%, compared to 0.25 to 0.70% for films sputtered at higher pressures of 4 to 6mTorr.

The reason for this decrease in resistance stability for films grown at higher sputtering pressures, especially when treated at higher annealing temperatures is thought to be due to the more open porous structure which lends itself to higher levels of impurity incorporation during deposition and also makes it more susceptible to attack in high temperature oxidising environments.

To investigate this theory further the level of oxygen present in films before and after heat treatment was measured using SEM-EDX. Results of surface analysis for films sputtered on glass at pressures of 1, 3 and 5mTorr and subsequently annealed at 300 and 450ºC are presented in Figures 5.19a to 5.19c. All results are based on the mean of 3 measurements at different areas of the film surface. The films were found to be homogeneous with variation in results of less than ±2at.%.

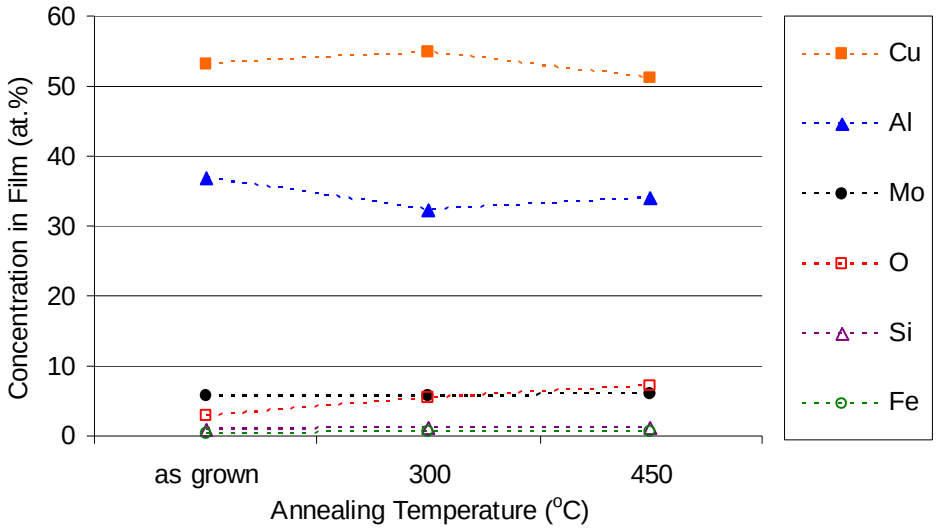

Fig. 5.19a – Mean chemical composition with increasing heat treatment temperature for CuAlMo films grown at 1mTorr.

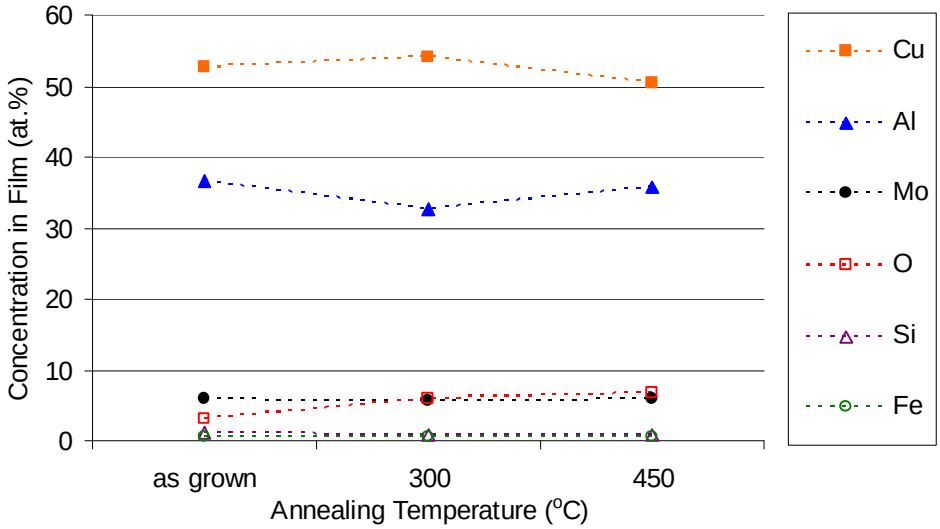

Fig. 5.19b - Mean chemical composition with increasing heat treatment temperature for CuAlMo films grown at 3mTorr.

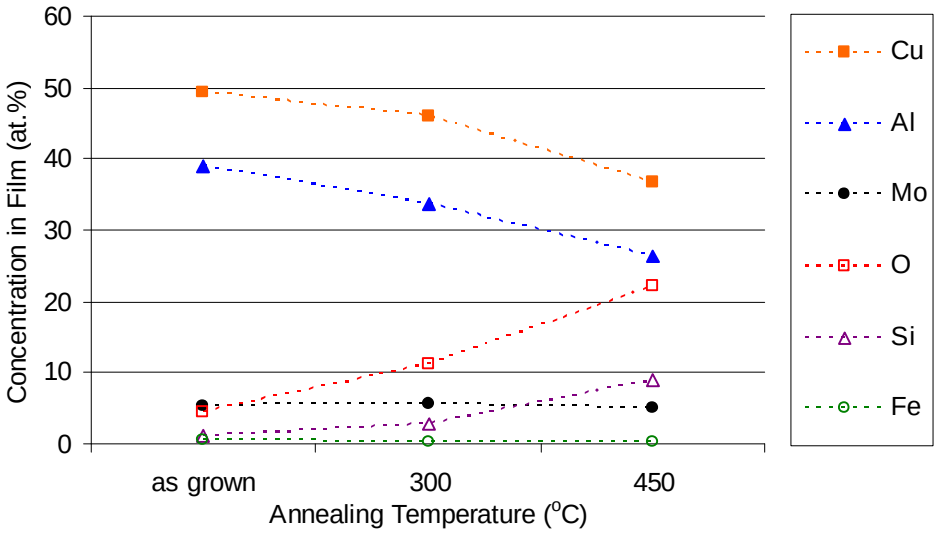

Fig. 5.19c - Mean chemical composition with increasing heat treatment temperature for CuAlMo films grown at 5mTorr.

For the films deposited at 1 and 3mTorr the as-grown compositions are almost identical with the concentration of oxygen being <3at.%. There are also small levels of both Si and Fe present in the films which are believed to originate from the borosilicate substrate beneath. Following heat treatment at 300ºC for 5 hours, the oxygen level increases to ≈6at.% and that of the aluminium decreases, thus suggesting the formation of a stable aluminium oxide layer. After treatment at 450ºC there are further increases in the oxygen content of both films to ≈7at.% and also a slight decrease in the Cu concentrations, suggesting the formation of a less stable copper oxide. There is no noticeable change in the levels of Si and Fe with increasing heat treatment temperature.

For the films deposited at 5mTorr there is a noticeable change in the as-grown composition. The film is deficient in Cu and slightly rich in both Al and Mo when compared with those films grown at lower pressures. There is also a slight increase in the oxygen content to 4.5at.%, whilst that of the Si and Fe remained at below 1at.%. It is thought that this shift in composition is due to the increased oxidation of the copper during the lower rate deposition. These discrepancies are further augmented during heat treatment, and following annealing for 5 hours at 300ºC there are noticeable decreases in the levels of both Cu and Al, whilst the level of oxygen has increased rapidly to above 11at.%.

This result suggests that higher levels of aluminium and copper oxide are formed in the films sputtered at higher pressures. The reaction is even further accelerated at an annealing temperature of 450ºC, where the oxygen content has increased to over 22at.%, reducing the levels of Cu and Al to 37 and 26at.% respectively. These results can be attributed to the more open porous structure of the film which makes it more susceptible to attack from the oxygen containing environment, a reaction which is known to increase rapidly with temperature. There is also an uncharacteristic increase in the Si content of the films with temperature. Again this result is thought to relate to porous structure allowing access to the underlying glass substrate.

The above chemical analysis results correlate well with the stability measurements reported in Figure 5.18c and are further supported by visual analysis of the film surface before and after heat treatment. Figure 5.20 shows typical examples of CuAlMo films grown at pressures of 3 and 5mTorr in both the freshly deposited and annealed state.

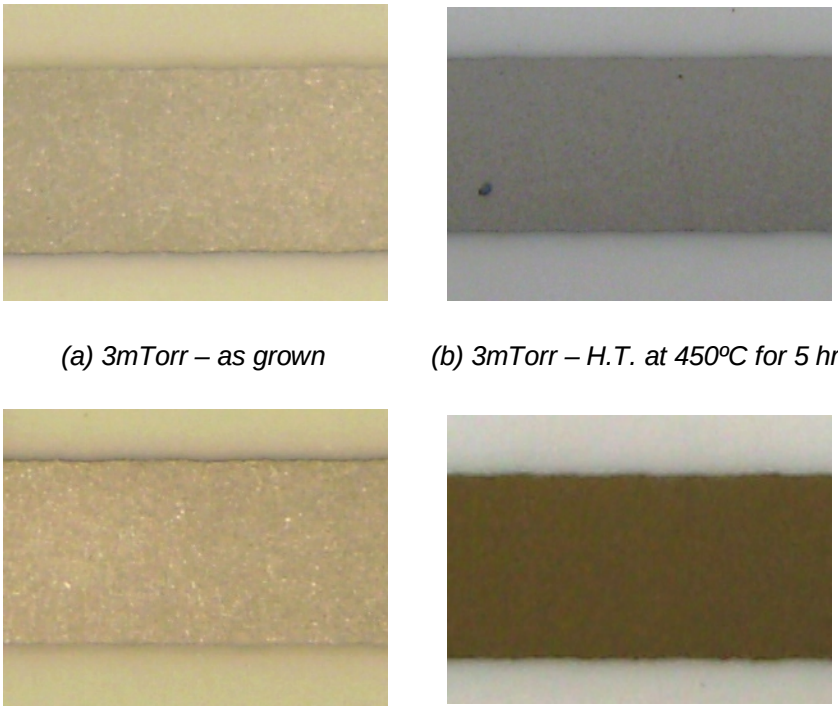

(a) 3mTorr – as grown *(b) 3mTorr – H.T. at 450ºC for 5 hrs*

(c) 5mTorr – as grown *(d) 5mTorr – H.T. at 450ºC for 5 hrs*

Fig. 5.20 – Photos of CuAlMo films on Al_2O_3 showing changes in film colour with sputtering pressure and heat treatment

For the as grown samples there is very little difference in the visual appearance of the films deposited at different pressures and both are silver in colour. Following annealing at 450ºC for 5 hours there are noticeable changes for both films. There is a slight darkening in colour of the film grown at 3mTorr. However the film grown at 5mTorr has changed in colour to a golden brown, again suggesting the formation of copper oxide.

To confirm that the formation of an aluminium oxide layer was responsible for the superior stability properties of the films grown at lower pressures, the chemical composition with film depth was analysed using the MiniSIMS technique. The equipment used was a manufactured by Millbrook instruments Ltd with 6 keV gallium ions (Ga^+) used as the primary ion beam. Figure 5.21 shows results for a CuAlMo film grown at 3mTorr and annealed at 450ºC for 5 hours in air.

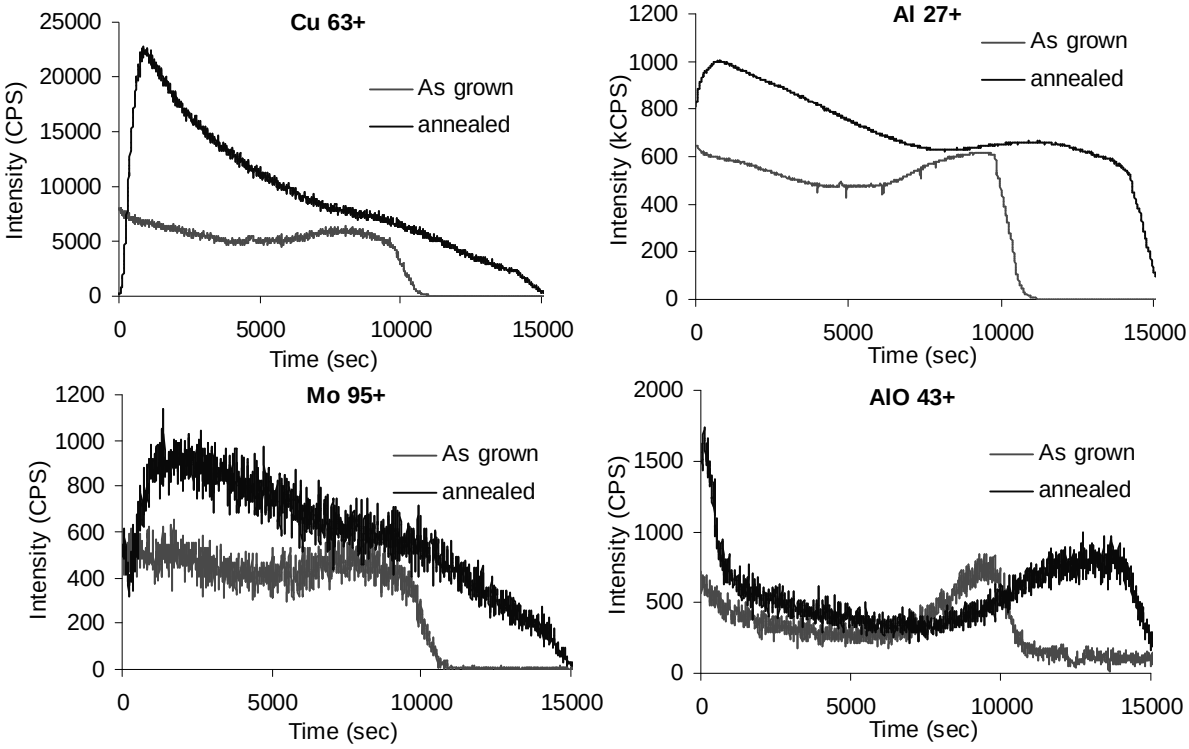

Fig. 5.21 – MiniSIMS analysis of a CuAlMo film grown on Al_2O_3 at 3mTorr and annealed in air for 5hrs at 450ºC.

For the freshly deposited film the concentrations of Mo and Cu are relatively uniform with film depth, whilst the intensity of the aluminium is already increased at the surface, suggesting the formation of an aluminium oxide layer. This result is confirmed by the increase in the AlO level at the film surface. The intensity of Al and AlO is also increased at the bottom of the film due to the Al_2O_3 substrate and at this point the Cu and Mo results fall to zero.

Following heat treatment all three elements have diffused towards the film surface due to their chemical affinity with oxygen. However once near the surface their intensities fall sharply and at this point the intensity of the protective AlO layer is observed to increase rapidly from its as grown level.

Figure 5.22 shows XRD results for films sputtered at 1000W and 3mTorr and annealed at various temperatures for 5hrs.

It can be clearly seen that there is an increase in the crystalinity of the films with annealing temperature. The relatively small difference in intensity between the as grown film and the film annealed at 300ºC is most likely related to the similarity in substrate temperature during deposition, which was reported to be 325ºC for a cathode power of 1000W (see Figure 5.11).

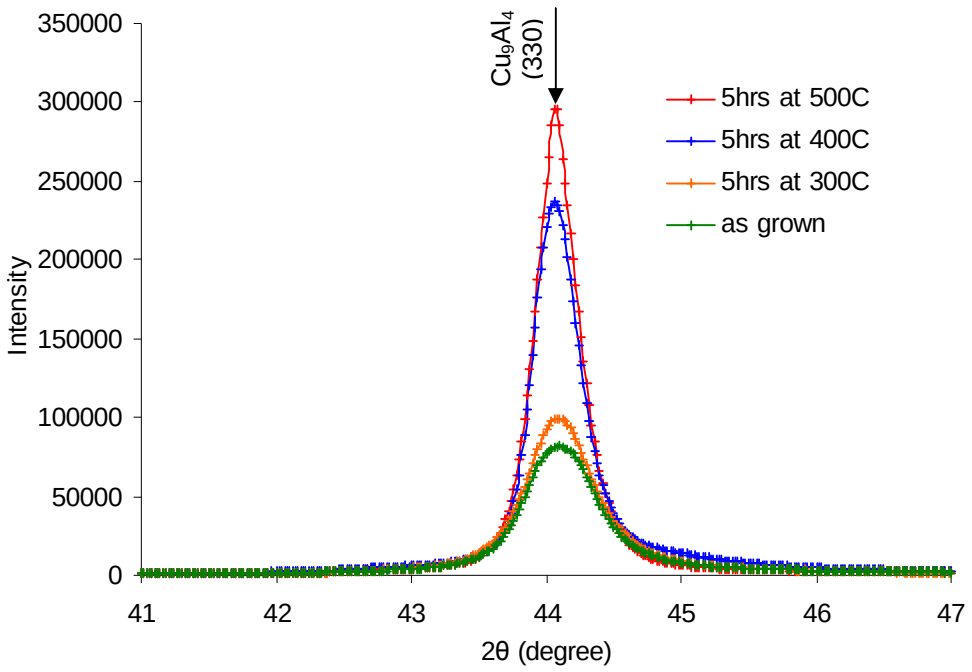

Fig. 5.22 – XRD patterns for CuAlMo films grown at 1000W and 3mTorr and heat treated for 5hrs in air at various temperatures.

The variation in FWHM and mean crystalite size, calculated using the Scherrer formula, as a function of annealing temperature are plotted in Figure 5.23.

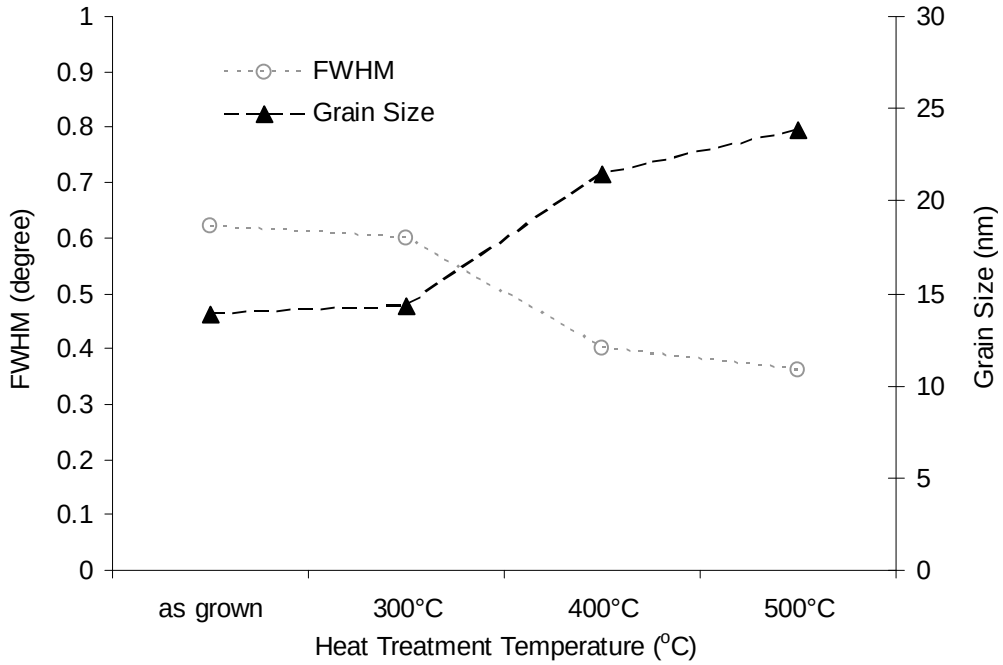

Fig. 5.23 – Variation in FWHM and corresponding calculated mean grain size for CuAlMo films grown at 1000W and 3mTorr and heat treated for 5hrs in air at various temperatures.

The average grain size increases from 14nm to 24nm with increasing heat treatment temperature. The above results correspond well with change in the electrical properties of the films reported in Figure 5.18. Increase in grain size and consequent decrease in grain boundaries lead to an increase in the conductivity of the films due to the reduction in charge-carrier scattering by grain boundaries [35].

The electrical properties of films grown at 1 and 3mTorr as a function of annealing time at 425ºC (the approximate temperature required to achieve near zero TCR) are presented in Figures 5.24a to 5.24c. All results are based on the measurement of a sample of 20 films.

It appears that a minimum heat treatment time of 3 to 4 hours is required to give stable electrical properties. For films sputtered at both 1 and 3mTorr it takes 3hrs at 425ºC for the TCR_{av} to increase from an as-grown value of -90 to a final value of 0 ± 10ppm/ºC. Further heat treatment time has negligible effect on TCR and it remains better than 0 ± 20ppm/ºC across the range 3 to 7 hours.

The films are also at their most stable in this time range and typical resistance shifts of less than 0.2% following storage in air for 168hrs at 155ºC are achieved for films sputtered at both 1 and 3mTorr.

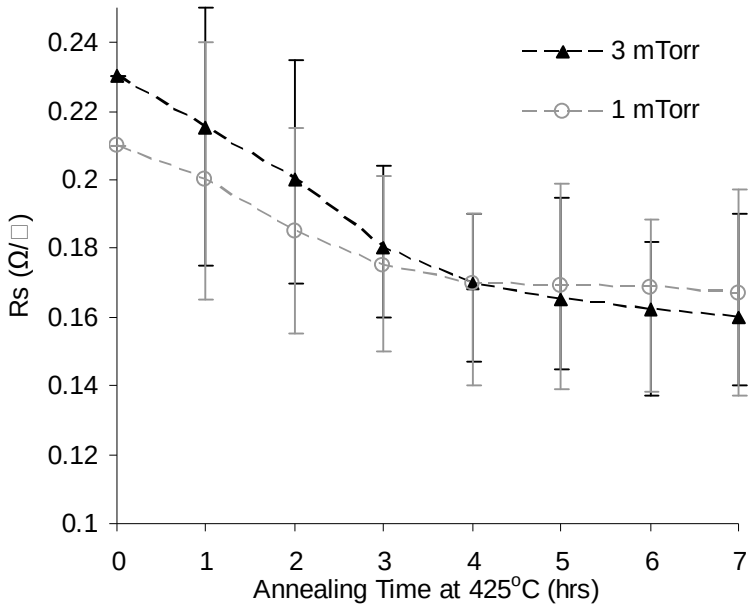

Fig. 5.24a – Effect of heat treatment duration at 425ºC on the sheet resistance of CuAlMo films grown at sputtering pressures of 1 and 3mTorr

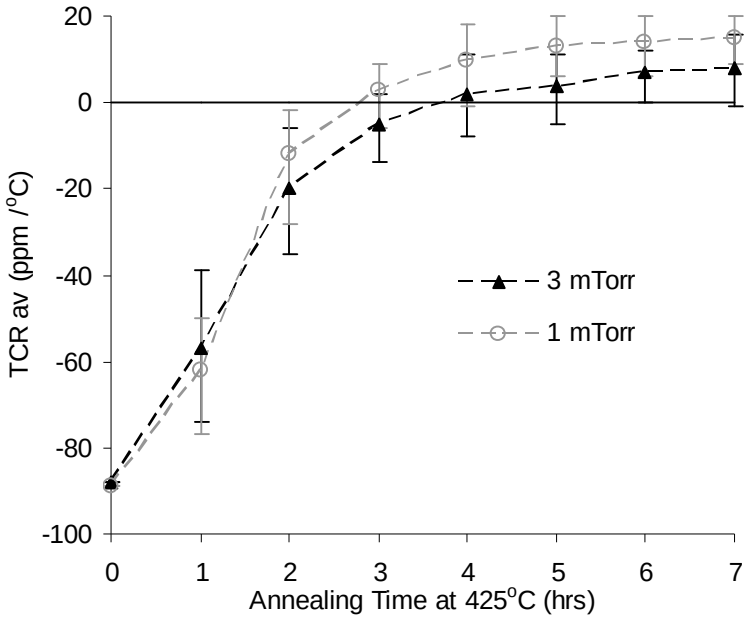

Fig. 5.24b - Effect of heat treatment duration at 425ºC on the TCR_{av} of CuAlMo films grown at sputtering pressures of 1 and 3mTorr

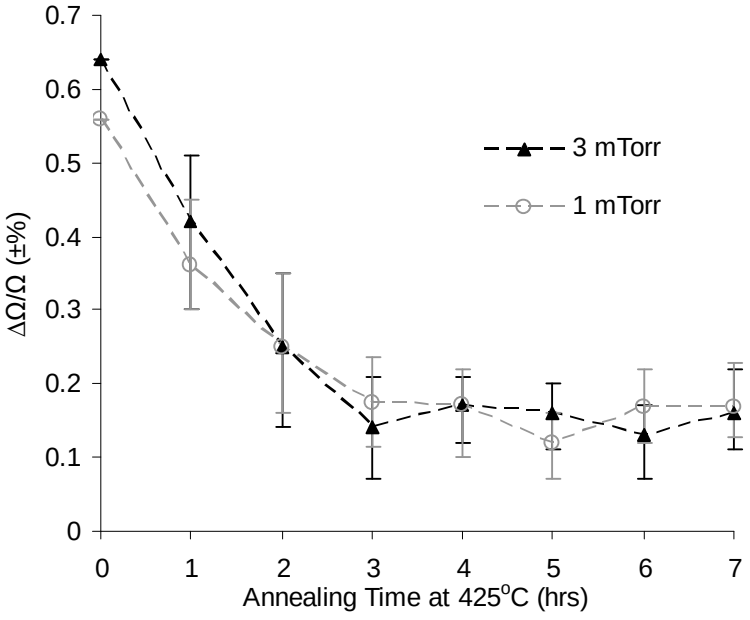

Fig. 5.24c - Effect of heat treatment duration at 425ºC on the resistance stability of CuAlMo films grown at sputtering pressures of 1 and 3mTorr

5.4 SUMMARY

Work conducted in this chapter has shown that the electrical properties of the CuAlMo thin films are not only a function of their chemical compositional ratio but also strongly depend on the sputtering and heat treatment process settings.

To obtain films of low sheet resistance with near zero TCR and good long term stability a high deposition rate and low sputtering pressure in the range 1 to 3 mTorr are required.

The development of the film structure during sputtering appears to follow the classical Thornton's model. For films sputtered at high power and low pressure, a more dense structure with lower impurity incorporation is produced. Moreover, the increase in substrate temperature with sputtering power also results in an increase in the crystallinity of the films and hence an improvement in conductivity. However for films grown at lower powers or higher pressures the resulting structure is more amorphous with a higher content of impurities being incorporated during deposition.

Subsequent annealing of the films in air results in further crystallisation with grain growth and stress relief which gives increases in conductivity and TCR. For films grown at pressures of 1 to 3mTorr the TCR can be controlled around the zero TCR line following heat treatment at ≈425ºC. For films grown at higher sputtering pressures the TCR is much more negative and cannot be heat treated to zero within the temperature range of investigation.

The evolution of mean grain size in the film, calculated from the FWHM of the Cu_9Al_4 (330) XRD peak, was 8 to 15nm in the as-grown state, depending on sputtering power and pressure and grew to ≈25nm following annealing at 400 to 500ºC.

In addition to the deposition parameters, the stability of the films was also shown to improve with heat treatment temperature due to the formation of a protective aluminium oxide layer. The optimum results were achieved for films annealed at 300ºC. At higher temperatures the stability was inferior, especially for those films which were grown at higher sputtering pressures. This phenomenon was thought to be due to the porous grain structure being more susceptible to attack from the hot, oxidising environment.

The effect of heat treatment dwell time at the optimum annealing temperature was also studied. It appears that a minimum of 3 hours is required for the structural transformations to take place and to set the electrical properties. Beyond this time the changes are insignificant and the films are stable.

From this work the following set of optimum sputtering and heat treatment process parameters have been concluded, see Table 5.5. As will be discussed in chapter 8, these settings have been used to manufacture production size batches of chip resistors for long term reliability testing.

Process parameter	Setting
Sputtering power	1000W
Sputtering pressure	2mTorr
Sputtering time	varies depending on required Rs
Annealing temperature	≈ 425ºC (fine tuned to attain zero TCR)
Annealing time	4 hours

Table 5.5 – Sputtering and heat treatment process conditions to give optimum electrical properties of CuAlMo films.

Chapter 6

ELECTRICAL CONDUCTION MECHANISMS

6.1 INTRODUCTION

As discussed in chapter 1, it is often convenient to categorise thin films used in the manufacture of resistors by the electrical conduction mechanisms present. For thin films of conducting materials, such as metals, alloys and semiconductors, the main differences in their physical properties when compared with their bulk counterpart are due to the thinness of the film and also the preparation conditions.

The influence on the physical properties of varying process conditions during preparation were discussed in chapter 5 and related to fundamental theories regarding the condensation mechanism of thin films onto the substrate. Work in this current chapter will deal with the effect of the film thickness on its physical properties, with particular attention being given to electrical resistivity.

The type of electrical conduction mechanism dominant is strongly dependant on the degree of thinness of the film, which is usually categorized by two distinct stages of growth; discontinuous and continuous.

During the early stages of growth the film consists of small islands separated from each other by small distances of 0.1 to 10nm. This type of film is called a discontinuous or island film. The electrical properties of such a film are very different to the properties of a bulk metal and are closer to that of a semiconductor, the resistivity often being many orders of magnitude higher.

The conduction in a discontinuous film is basically a function of the spaces between the islands, through which electrons must jump to enable an electric current to flow, the resistance of the islands themselves being insignificant in comparison.

As the deposition process continues, these islands increase in size and eventually become so large that they join to form a continuous film, showing metallic type conductivity. The thickness at which this phenomenon occurs is deemed the critical thickness, h_{cr}.

For film thicknesses beyond h_{cr} the metal film is continuous and the main contribution to the total resistance is from the resistance of the grains themselves. The resistance of the film decreases by an order of magnitude in this transition from an island structure to a continuous film. A typical example of the dependence of resistivity on film thickness is shown in Figure 6.1 for aluminium films grown on glass substrates at various condensation temperatures [236].

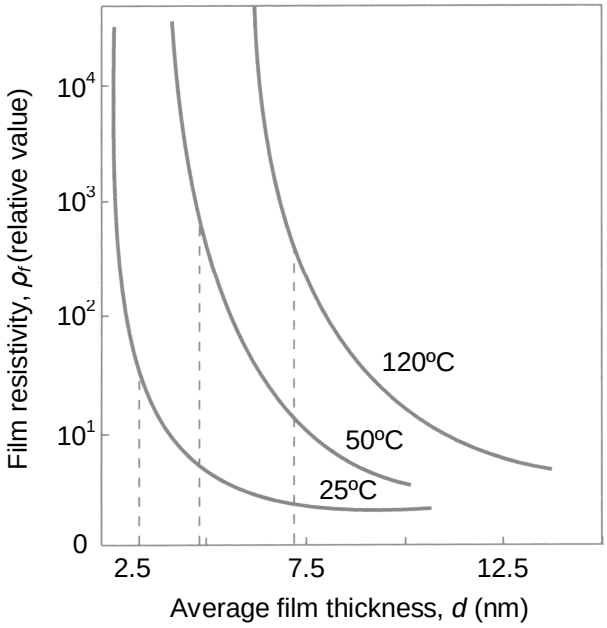

Fig. 6.1 – Dependence on thickness of the resistivity for aluminium films deposited on glass substrates at various condensation temperatures [236]

The critical thickness increases from approximately 3 to 7nm with increase in condensation temperature from 25 to 120ºC. This can be explained by the increase in mobility of the adsorbed atoms with temperature, which form fewer but larger nucleation sites or islands. Therefore the film will be thicker at the point at which these lislands join together, the critical thickness. This process is illustrated schematically in Figure 6.2 for different condensation temperatures, where $T_{c1} > T_{c2}$ [20].

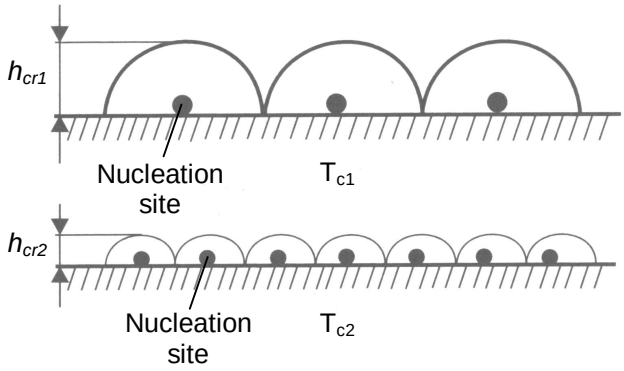

Fig. 6.2 – Decrease in the critical thickness with decrease in nucleation site size at different condensation temperatures [20]

If the thickness of a film is comparable with the mean free path (MFP) of the bulk material, the boundaries of the film impose a geometric restriction on the movement of the conduction electrons and therefore on the real MFP of the carriers, resulting in a decrease in conductivity of the metal film compared with that of the bulk material.

This scattering of conduction electrons at the film surfaces is the so called size effect and it was first predicated in a famous theoretical paper by K. Fuchs [237] in 1938 that the electrical resistivity of thin metal films increases with decreasing thickness. Due to good agreement with experimental data, Fuchs' theory was not called into question for a long period. However it later became obvious that in addition to surface scattering, grain boundary scattering [239] and surface roughness contributions [240] also have a significant effect on the resistivity behaviour of polycrystalline films.

The following section considers some aspects of the scattering hypothesis in thin films and describes experimental results for both previous investigations and also for the current work on CuAlMo films.

6.2 THE SCATTERING HYPOTHISIS

The scattering hypothesis assumes that Mathiessen's rule can be applied so that all contributions to the film resistivity, ρ_f, can be added together as follows:

$$r_f = r_0 + r_{ss} + r_{gr} + r_{sr} \qquad \textit{Equation 6.1}$$

Where ρ_0 is the resistivity of a film of infinite thickness (the bulk material) manufactured under the same conditions and having the same density of defects, and ρ_{ss}, ρ_{gr} and ρ_{sr} are additional contributions to the resistivity from surface scattering, grain boundary scattering and surface roughness scattering respectively.

If the film thickness is approaching the value of the electron MFP, then film surface and film to substrate interface scattering must be considered. In the Fuchs-Sondheimer (FS) model [237-238] for a continuous single crystalline film, the specularity co-efficient p is used to describe the fraction of incident electrons that are specularly scattered at both the film surface and the film to substrate interface and is independent of incident angle, electron energy and surface roughness. Values of p range from 0 to 1, with a low p corresponding to a high resistivity. According to this theory the increase in resistivity of the film due to surface and interface scattering can be calculated to good approximation by:

$$r_f = r_0\left[1 + \frac{3l}{8d}(1-p)\right] \qquad \textit{Equation 6.2}$$

Where ρ_0 is the resistivity of a very thick film with the same structure as the film under discussion, l is the corresponding MFP of the of the conduction electrons, d is the film thickness and p is the Fuchs scattering parameter.

There have been numerous studies considering the effects of surface scattering on the electrical resistivity of thin films [241-252]. A typical plot of resistivity against thickness for thin films of Cu is shown in Figure 6.3, together with fits of the FS model (Equation 6.2) for various values of p [249].

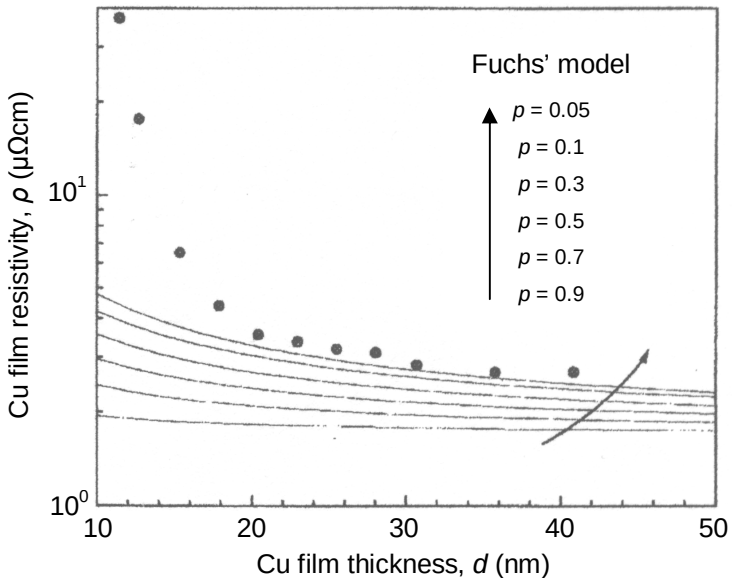

Fig. 6.3 – The Fuchs-Sonheimer model fits with various surface scattering specularity coefficient p in the range 0<p<1 [249].

The model fits the calculated resistivity data well for d>40nm with p=0.05. This low value of p indicates that diffuse scattering of the electrons at the film interfaces is the predominant conduction mechanism responsible for the resistance increase in this thickness range and is consistent with a discontinuous film morphology. For films with d<40nm the data does not fit the model with any degree of accuracy and additional scattering contributions must be considered.

As the FS model is for a single crystal it does not account for grain boundary scattering in polycrystalline films. The quantum effects of grain diameter and grain boundary reflection coefficient were studied by Mayadas et al [239].

The Mayadas-Shatzkes (MS) model describes a film that represents the grain boundaries as parallel partially reflecting planes, perpendicular to both the electric field and the plane of the sample and placed an average distance D apart:

$$r_f = \frac{r_0}{3}\left[\frac{1}{3} - \frac{1}{2}a + a^2 - a^3 \ln\left(1 + \frac{1}{a}\right)\right]^{-1} \qquad \textit{Equation 6.3}$$

$$a = \frac{l}{D}\frac{R}{1-R}$$

Where *D* is the average in-plane grain size and *R* is the grain boundary reflection coefficient. If *R*=1, electrons are confined to individual grains as they are reflected back at all surfaces. Mayadas et al found values of *R* to be 0.17 and 0.24 for Al and Cu respectively and grain size *D* was proportional to film thickness *d*, $l/D \propto l/d$ and therefore form Equation 6.3, a is also a function of film thickness.

Again there have been many reviews concerning the additional effects of grain boundary scattering on the electrical resistivity of thin films [243-251, 253-254]. Figure 6.4 shows the result for the copper film from Figure 6.3 with curves calculated from the MS model fitted for *p*=0.05 and *R*=0.24.

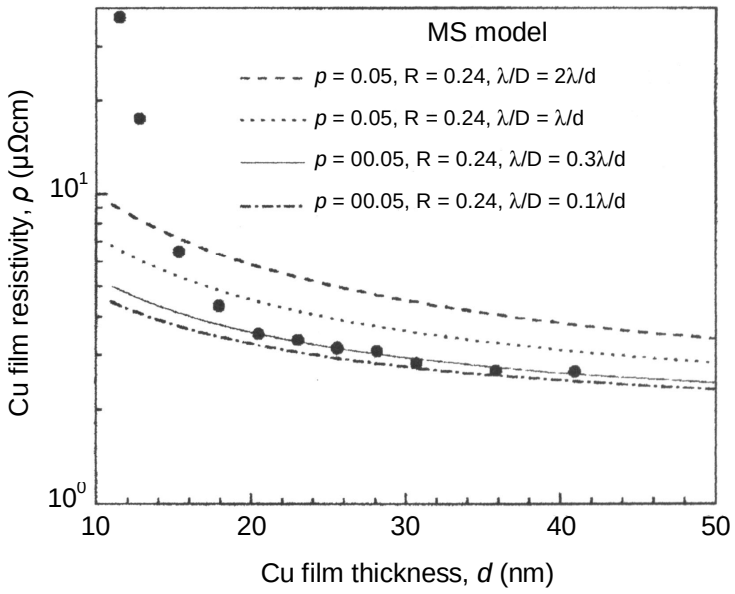

Fig. 6.4 – The Mayadas-Shatzkes model fits with p=0.05 and R=0.24 and a grain size assumed to be proportional to thickness, with different proportionality constants [249].

A good match between the experimental data and calculated resistivity is achieved for *d* ~ 20-40nm when $l/D = 0.3 l/d$. However for d<20nm experimental values still lie above the values predicted by the model. This phenomenon is due the surface roughness effect which must be taken into account for very thin films. The film can no longer be regarded as a homogeneous layer of constant thickness and must be considered to have a thickness which varies around a mean value i.e surface roughness. Hence areas of the film which are thinner than others will contribute to an increase in resistivity with increased weighting.

A model that includes the effect of surface roughness in addition to surface and interface scattering on the resistivity of thin metal films was proposed by Namba [240]. This model is widely referred to as the Fuchs-Namba model [249-252] and considers the

film surface to consist of sinusoidal undulations with irregular indentations. A simplified version of the model can be written as:

$$r_f = r_0\left[1-\left(\frac{h}{d}\right)^2\right]^{-\frac{1}{2}} + r_0\frac{3l}{8d}(1-r)\left[1-\left(\frac{h}{d}\right)^2\right]^{-\frac{3}{2}} \qquad \textit{Equation 6.4}$$

Where *h* is the peak to valley height of the sinusoidal roughness.

The best fit of Namba's model for the copper film discussed in Figure 6.3 is shown in Figure 6.5, where *p*=0.05 and *h*=10.3nm. By including the effects of surface roughness, the model now fits the calculated resistivity across the full thickness range. However when the value of h is decreased to 3.5nm as measured by AFM, the model fits the resistivity in the high thickness regime but is lower by a factor of approximately four for the lower thickness films. As expected this result indicates that the effect of surface roughness of the copper films decreases with increasing thickness.

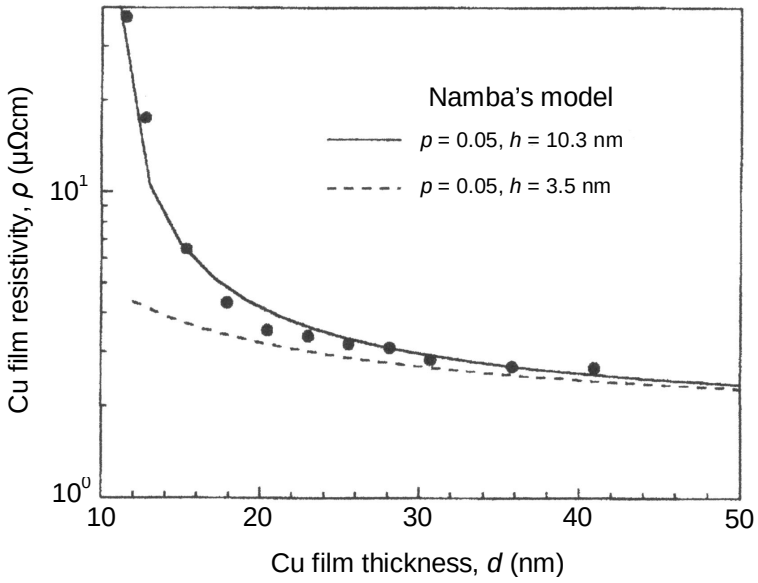

Fig. 6.5 – The Namba model fits with p=0.05 for h=10.3 and 3.5nm

6.3 EXPERIMENTAL

All film samples used for conduction studies were prepared on glass slides under the optimised sputtering conditions proposed in chapter 5. The slides were ultrasonically cleaned in acetone prior to insertion into the plant.

The deposition rate of the CuAlMo film was determined by sputtering samples for a range of times and then measuring the film thickness using SEM. A typical plot of sputtering time vs. film thickness *d* is shown in Figure 6.6. As expected the deposition rate was quite linear and was determined to have an average value of approximately 190nm/min.

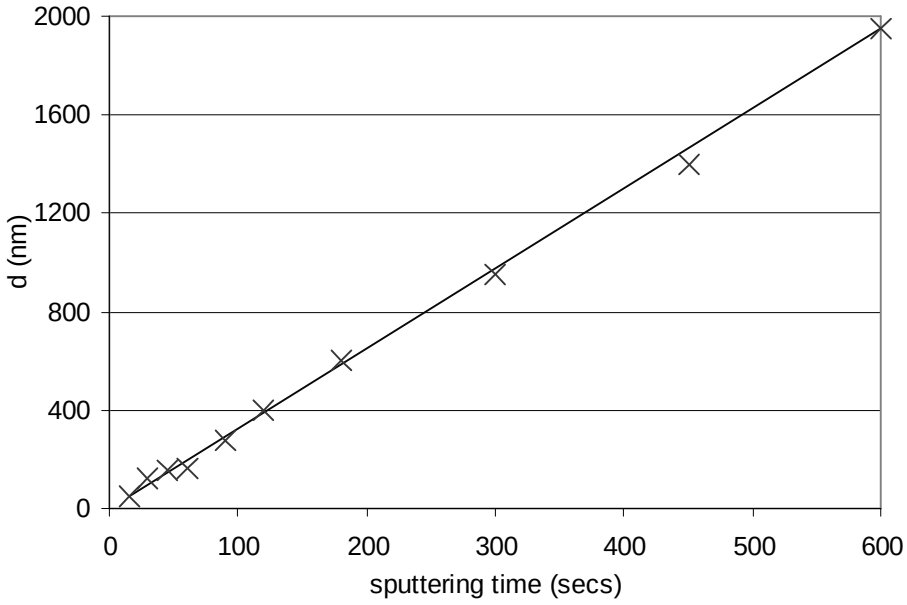

Fig. 6.6 – Film thickness vs. sputtering time for the CuAlMo films

The resistance of the growing film was measured during deposition using a simplified version of the setup described by Barnet et al [255], suitable for measurements without a substrate bias. The setup is illustrated in Figure 6.7 and consists of a four terminal resistance measurement, where the voltage over the film is measured directly and the current is measured indirectly by measuring the voltage across the 50Ω resistor in series with the film, thus eliminating the effects of contact resistance.

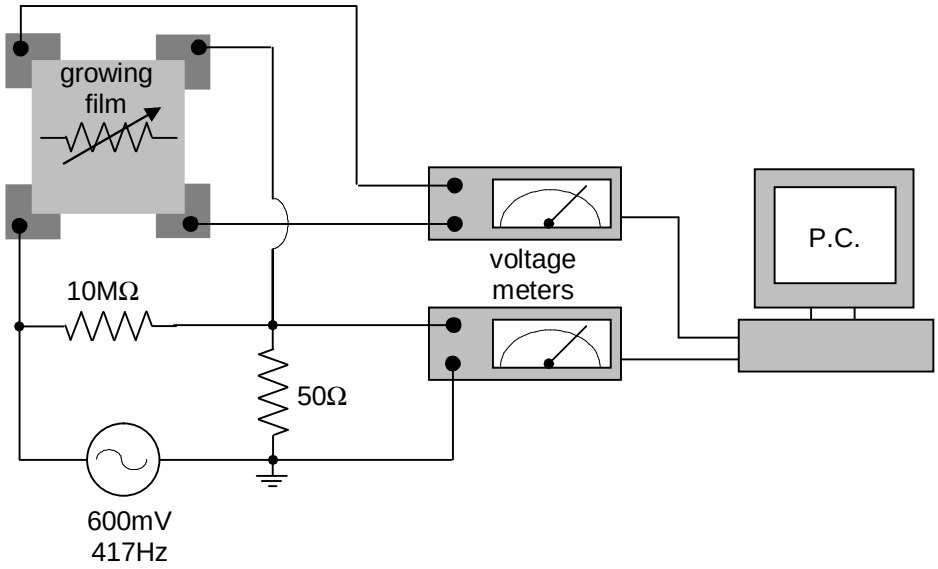

Fig. 6.7 – Schematic drawing of the in-situ measurement setup.

To permit good electrical connection to the film, four thick termination pads were sputtered from Ti/Pd prior to measurement, leaving a square of uncoated substrate onto which the CuAlMo film was deposited. The measured sheet resistance of the termination pads was found to be less than 0.01Ω/□ which was more than one order of magnitude less than the lowest value measured for the CuAlMo films. Therefore the resistance contribution of the terminations could be ignored and the pads assumed to be equipotential surfaces.

The resistance data from the growing film was collected at a rate of 5 times per second by a PC which was interfaced with the measuring equipment. During deposition the termination pads and connecting wires were shielded from the flux of the plasma by a thin mask of alumina, thus restricting film growth to the exposed square of substrate beneath.

Following deposition, the dimensions of the film square were accurately determined using a measurescope and the thickness of the film was confirmed to be in good

agreement with that reported in Figure 6.6. The resistivity of the film p_f throughout its growth, as calculated using Equation 1.2 is plotted in Figure 6.8

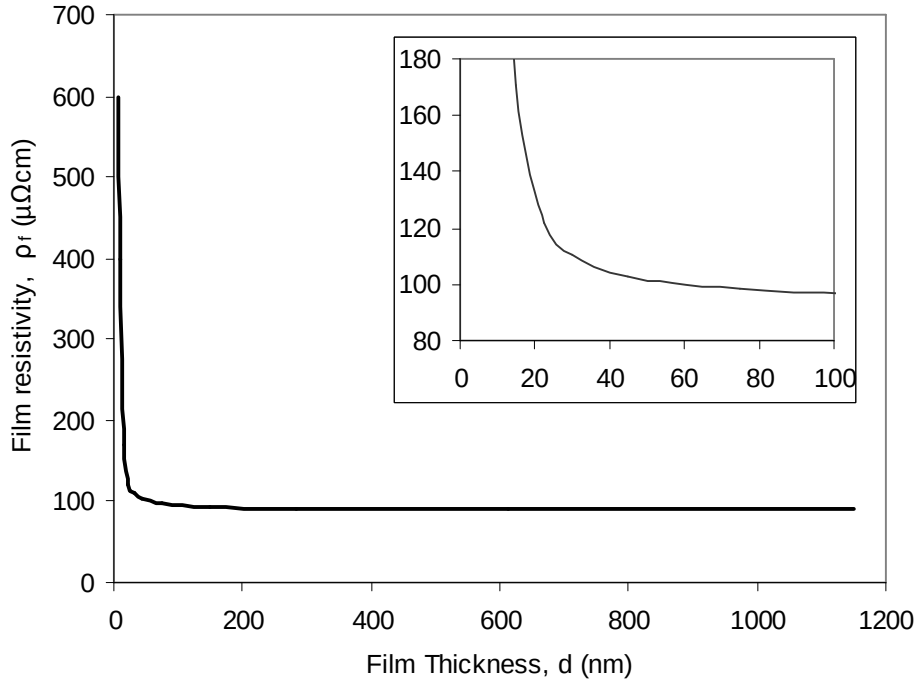

Fig. 6.8 – Film resistivity as a function of thickness for the CuAlMo films.

The resistivity of the film decreases rapidly in the first 20nm of growth, from approximately 600μΩcm at 7nm to 125μΩcm at 20nm, marking the transition from an island to a continuous film. After this point the reduction is more gradual and by approximately 200nm the curve flattens off to a value of around 90μΩcm, indicating the bulk resistivity, p_0. This figure is in good agreement with the as grown resistivity value of 94μΩcm reported for the CuAlMo films in chapter 4.

For comparison of the experimental results with the theoretical models discussed in section 6.2 it is convenient to rearrange the Fuchs' equation 6.2 as follows:

$$r_f d = r_0 \left[d + \frac{3l}{8}(1-p) \right] \qquad \textit{Equation 6.5}$$

It then follows that the graph of dependence $\rho f(d)$ plotted in the coordinates $\rho_f d$, d will be given by a straight line of slope ρ_0 and intercept $\rho_0(3/8)l(1-p)$. As the specularity co-efficient p is not very sensitive to range of values $d/l \pi 1$ used to generate the straight line, no conclusion concerning its magnitude can be drawn from the graph of equation 6.5 and its value can be taken as zero. Thus it is possible to determine the values of ρ_0 and l from the experimental data.

Figure 6.9 shows the resistivity data obtained for the CuAlMo films plotted in *d* vs *ρf(d)* coordinates.

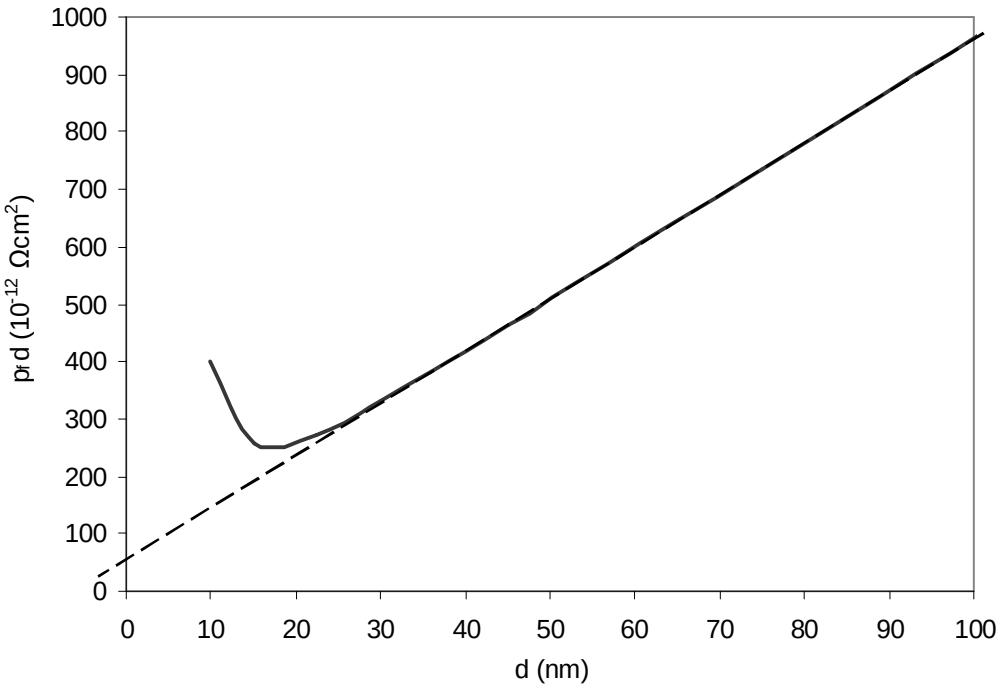

Fig. 6.9 – Size dependence of the magnitude of pfd on the thickness d for the CuAlMo films

The values of the bulk resistivity, ρ_0 and MFP, l were determined from the graph to be as follows:

$$\rho_0 = 91.16\mu\Omega cm \qquad l = 15.7nm$$

This theoretical value of ρ_0 is in good agreement with the experimental result for films in the high thickness regime presented in Figure 6.8. As there has been no previous study undertaken on the CuAlMo system it is difficult to assess the accuracy of the calculated value of l, however it is interesting to note that previous conduction studies on thin films of Cu and Al have yielded typical values of 39nm and 18nm respectively [243]. However when the Cu film was alloyed with 0.5at.% Al the value of l was suggested to be <10nm [241].

To model the increase in ρ_f over ρ_0 with decreasing film thickness it is convenient to plot the ratio of $\rho f/\rho_0$ vs d. Figure 6.10 shows the experimental resistivity data plotted in these co-ordinates for d<100nm with lines fitted for the FS model given in equation 6.2 for different values of the specularity parameter p.

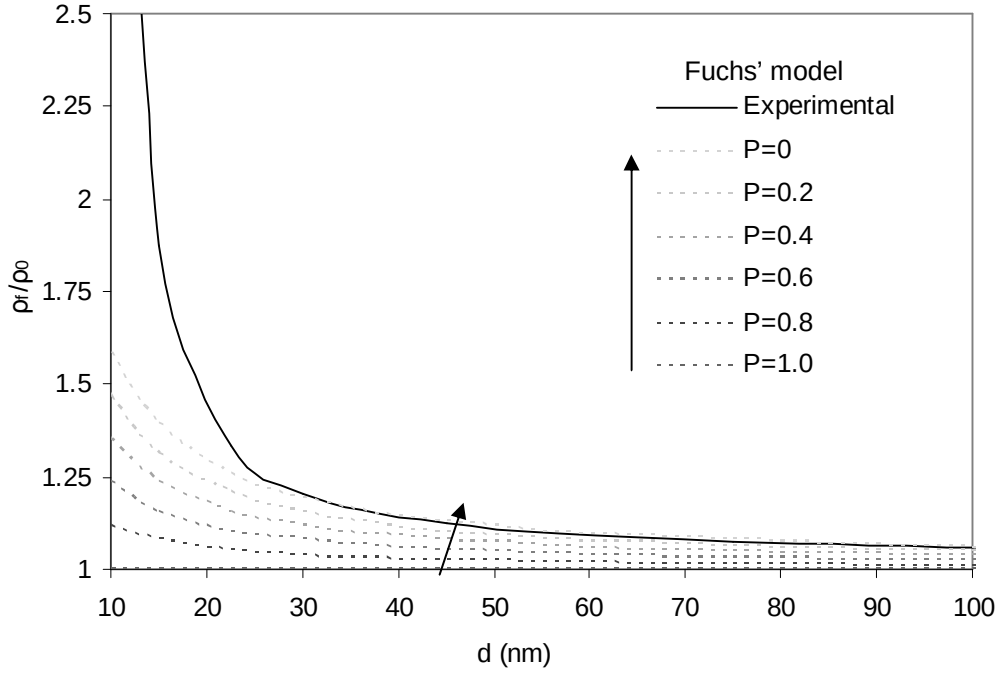

Fig. 6.10 - The Fuchs-Sonheimer model fits to the CuAlMo film resistivity data with various surface scattering specularity coefficient p.

For values of d>40nm the best match between the experimental data and theoretical model is achieved when p<0.05. This result suggests that diffuse scattering of the conduction electrons at the two surfaces is the predominant mechanism for the increase in ρ_f in this thickness range. The calculated resistivity does not match the data for d<35nm and other mechanisms must be considered.

Figure 6.11 shows the curves calculated from the MS model given in equation 6.3 with p=0.05. When R=0.22 and $l/D=0.85\,l/d$ a good fit was found with the experimental results for d ~ 25-40nm. However for d <20nm the calculated values are low compared to experimental results.

The results of the Fuchs Namba model are also plotted in Figure 6.11. By incorporating the effects of surface roughness in addition to surface and interface scattering, excellent correlation between the model and the experimental result is achieved. The best fit was attained with values of p=0.05 and h=9nm. Although it was not possible to confirm the magnitude of the film roughness experimentally, the result of 9nm is in good agreement with other results reported using the Namba model [249].

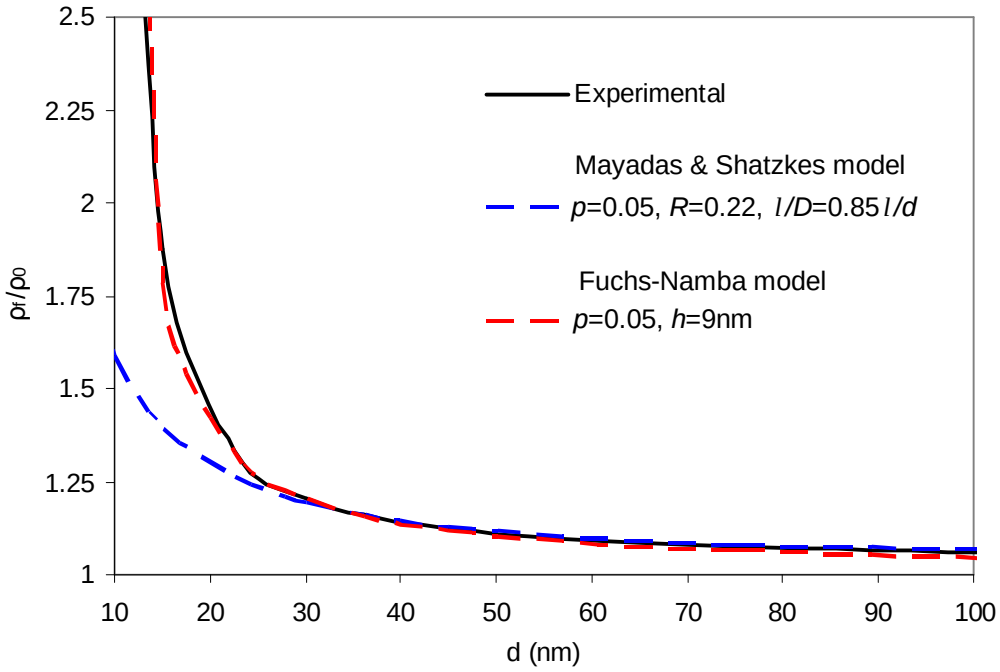

Fig. 6.11 – The Mayadas & Shatzkes and Fuchs-Namba model fits to the CuAlMo film resistivity data with p=0.05, R=0.22, l/D=0.85 l/d and h=9nm.

6.4 SUMMARY

Although work in this chapter constitutes only a very preliminary study into the dominating conduction mechanisms, many useful results have been considered.

By theoretically modelling the evolution of resistivity during the growth of the CuAlMo films under optimised sputtering conditions it has been possible to gain an insight into the types of electrical conduction involved with increasing film thickness, see Figure 6.12.

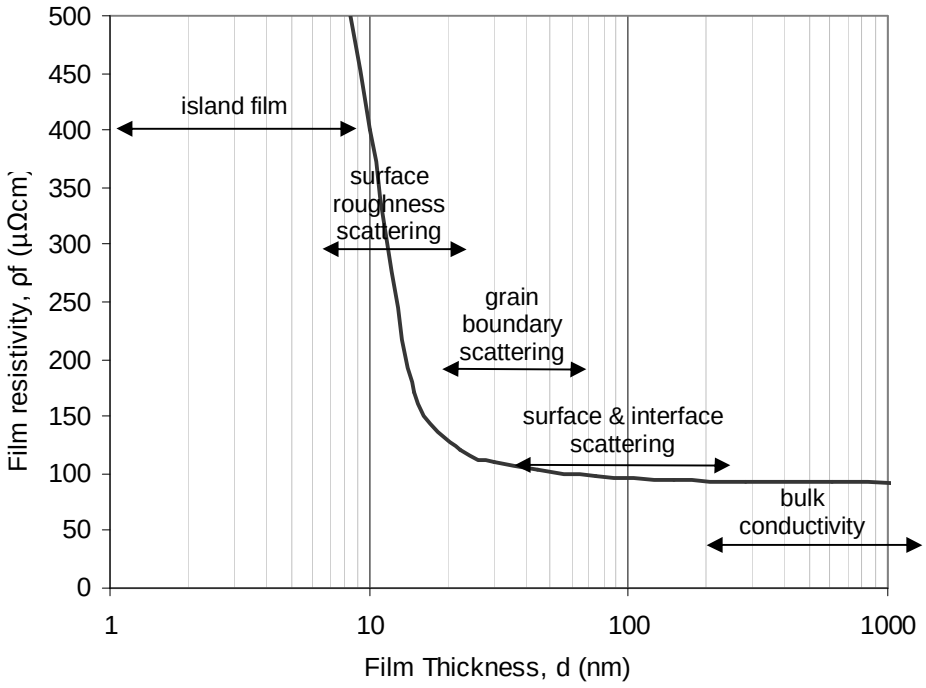

Fig. 6.12 – Dominant conduction mechanisms with increasing thickness of CuAlMo films

For d ~ <10nm the film is in a discontinuous state and consists of a network of isolated islands with infinite resistivity. As these islands start to grow and coalesce, a continuous film is formed, which is marked by the rapid increase in conductivity for d=10-25nm. Electrical resistivity in this thickness range was assumed to be a function of the film surface roughness and was suitably described using Namba's model which assumes the sample surface to consist of sinusoidal undulations with irregular indentations.

As the film grows further the resistivity begins to level off towards the bulk resistivity and the effects of surface roughness are decreased. In this thickness range the effects of grain boundary and surface scattering of electrons become the dominant mechanisms.

For d=25-40nm the experimental data was most accurately fitted using the Mayadas and Shatkes model which accounts for grain boundary scattering of the conduction electrons.

For d>40nm, the thickness of the film was found to be controlling factor and the Fuchs-Sonheimer model was used to fit the experimental data, with diffuse scattering of the conduction electrons at the two film surfaces.

By combining the Fuchs and Namba models a suitable correlation between theoretical and experimental resistivity can be achieved across the full film thickness range of 10-1000nm.

For d ~ >200nm the resistivity curve flattens off completely and bulk conductivity is assumed. The calculated bulk resistivity of 91.16μΩcm is in good agreement with earlier experimentation for as-grown CuAlMo films.

As one of the primary objectives of this work is to attain films of low sheet resistance, the vast majority of CuAlMo films under investigation will be in the thickness range dπ200nm. Hence, from the work in this chapter it can be concluded that bulk conductivity will be the dominating conduction mechanism in these films.

However it should be re-emphasised that bulk resistivity is not only a result of the originating CuAlMo composition but is also a function of the film structure which is in turn strongly dependant on deposition conditions and film treatment as discussed in chapter 5.

Chapter 7

Laser Trimming Process Optimisation

7.1 INTRODUCTION

For thin film resistors it is generally impossible to deposit batches of product with resistance tolerances better than about ±10% [4]. This is partly due to problems in attaining uniform sheet resistance, but mainly due to dimensional variation of the individual resistor elements in the batch, a problem which is amplified as the resistor size decreases [21].

Therefore when a precision of <10% is required, it is normal practice to fabricate the resistor film to a lower resistance value than required and then adjust it by removing or 'trimming' away sections of the film material to increase the resistance to its target value [261].

There are a number of different trimming methods which can be used to adjust the value of the resistor, including anodisation, heat trimming, electrical trimming, mechanical trimming, chemical trimming and laser trimming [4, 21, 258-260]. However, of these techniques laser trimming is by far the most effective and popular method and is still a subject of continuing theoretical and experimental analysis and optimisation [261-281].

The laser uses a light beam of a few μm in diameter to remove the resistive film from the ceramic substrate in a very short time period of less than 1ms. On impacting the resistor film the high intensity coherent light pulse is absorbed by the material causing it to heat and vaporise. The process is dependant on several variables such as the intensity of the laser pulse, or the power level, the focus of the pulse and also the properties of the material being ablated [4].

The laser beam is scanned across the resistor to produce a continuous kerf, changing the resistance value of the film as it progresses. In addition to the properties of the beam itself, the accuracy to which the resistance value can be adjusted is strongly dependent on both the shape of the cut and also the speed at which the measurement system can switch the laser beam off between pulses once the target resistance value is reached [4].

There are two main types of laser used for the adjustment of resistive films; the pulsed carbon dioxide (CO_2) laser has a long pulse width with high energy per pulse, which causes vaporisation of the film. However the long pulse width can also cause damage to the substrate and the resistive material at the edge of the kerf, the heat affected zone (HAZ). The neodymium:yttrium-aluminium-garnet (Nd:YAG) laser uses an acousto-optic Q-switch to give two way optical switching of the laser beam. This

system is able to produce short pulses of high peak power at a wavelength of 1064nm, to rapidly vaporise the film, whilst minimizing heat flow and damage to the material surrounding the kerf [4]. In addition to the use of shorter pulses, more recently it has also been suggested that lasers operating in the green region of the visible spectrum can provide additional reductions in the HAZ due to the decrease in laser spot size resulting from the shorter wavelength of 532nm. [286].

As highlighted in Figure 7.1, there are various different laser trim patterns which can be used for the adjustment of surface mount bar shape resistors.

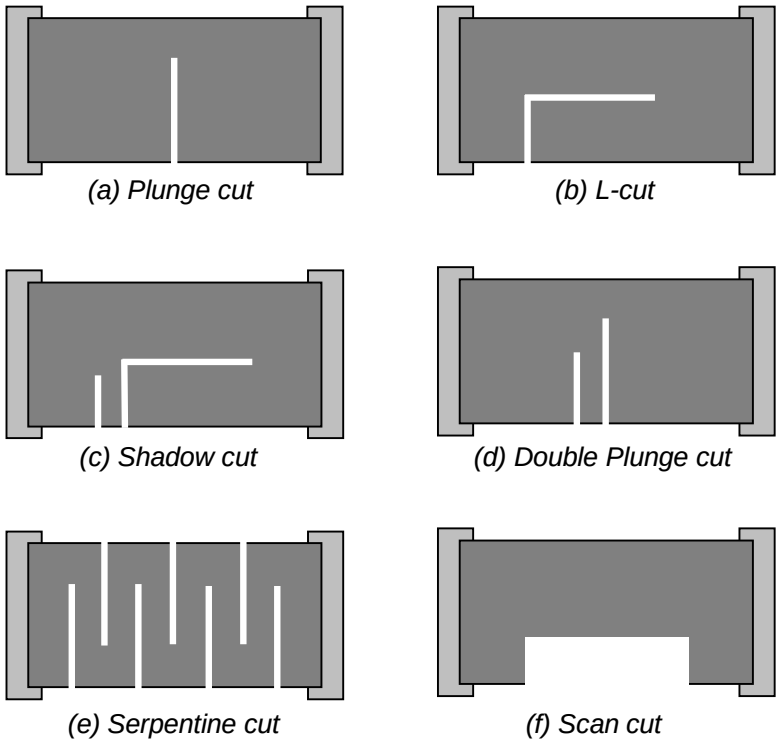

Fig. 7.1 – Commonly used laser trim kerf shapes [282]

The plunge cut is the most simplistic and economical cut consisting of a single kerf orthogonal to the current flow through the resistive element. Overall the tolerance accuracy of this cut can be less than other methods.

The 'L' cut is perhaps the most frequently employed method due to its superior stability and tolerance accuracy. With this type of cut the resistance increases rapidly as the kerf is cut perpendicular to the current flow (y direction) and then more gradually when it turns through 90º and cuts parallel to the current flow (x direction) until target value is reached i.e. in an area of equal current density, see Figure 7.2.

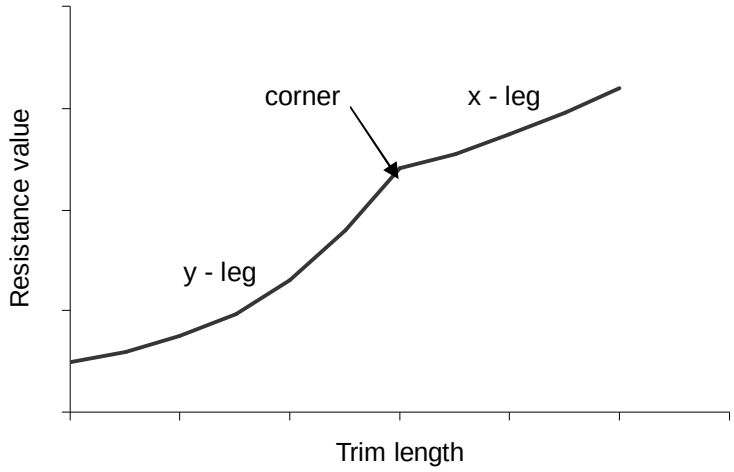

Fig. 7.2 – Typical plot of resistance increase with kerf length for the 'L' cut [261].

By varying the ratio of the x and y cut lengths the stability of the resistor can be maximised. The optimum performance is usually attained when the y leg is a short as possible leaving maximum resistor line width remaining. However, this is normally at the cost of increased trim time and also has the risk of trimming into the resistor termination with the extended x leg. It is therefore normal practice with the 'L' cut to find a balance between trim speed and tolerance and stability accuracy [279]. Because of the additional time required to perform this cut, it is slightly more expensive than the plunge cut.

A shadow cut adds an additional plunge to the side of an 'L' cut or plunge cut (double plunge). This allows even tighter resistance tolerances to be achieved as the kerf is cut in an area of low current density in the 'shadow' of the first cut. Again this type of cut is more expensive adding additional trimming time.

When the pre-value resistance is much lower than the target value a serpentine cut is usually employed. Multiple cuts are made in areas of high current density which effectively increase the geometric length of the resistor and thus its resistance value. As discussed in chapter 1 a long trim cut such as the serpentine can be used to give a large resistance gain which results in improved tolerance accuracy. However the disadvantage of a long trim length is the increased amount of HAZ surrounding it, which can lead to stability problems and in some cases where the resistance gain is very large, increases in TCR can also occur due to the amount of material which has been raised to temperatures in excess of the zero TCR heat treatment temperature without being vaporised. To overcome this problem it is common practice to employ a two stage serpentine trim when precision thin film resistors are required. The vast majority of the trimming is performed in the first stage and the resistor is adjusted to

around -1% from its target value. The device is then stabilised, typically overnight at around 200ºC to relieve stresses built up in the HAZ. As it is not possible to accurately predict the resistance change that occurs during this stabilisation operation, the second stage of the adjustment process, the fine trim, is required to accurately adjust the resistor to target value and usually consists of one or two plunges in the shadow of the first serpentine. As can be imagined this type of cut can be very time consuming and expensive, although the increasing availability of auto substrate handling equipment can help to alleviate the majority of the labour cost involved.

The scan cut is the most commonly used when the device is required for high frequency applications to minimise creation of capacitive reactance components of an RC circuit. It also finds use in high voltage situations as the likelihood of voltage breakdown across the trim kerf is greatly reduced. This type of cut is very time consuming to perform and is therefore not cost effective for general use.

From discussions thus far it is apparent that a major cause of post-trim drift in laser trimmed resistors is due to the HAZ bordering the kerf. It would therefore seem beneficial to consider this area in more detail.

A Q-switched YAG laser is typically adjusted to operate in single traverse electromagnetic (TEM_{00}) mode, with the energy profile of the beam having a Gaussian distribution. This profile is then translated into a Gaussian temperature profile in the thin film as shown in Figure 7.3

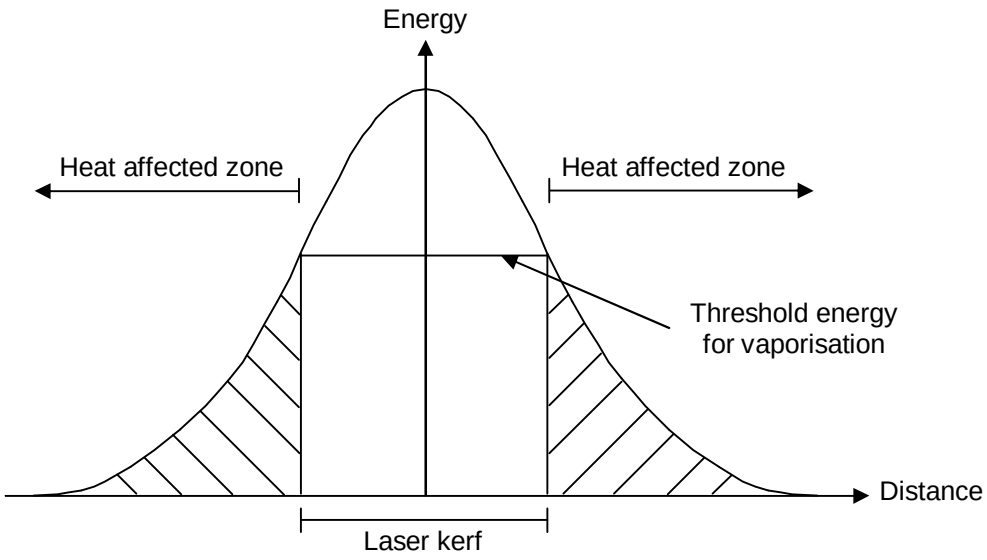

Fig. 7.3 – The fundamental mode laser beam profile as a Gaussian distribution [279].

Only the central part of the profile is of sufficient intensity to cause vaporisation of the thin film. For the areas of film adjacent to the kerf the energy absorbed from the laser beam is less than the threshold required for vaporisation. Thus this region of the film becomes a heat affected zone and is known to exhibit considerably more change in resistance with time than areas of film not irradiated by the laser beam [274].

This ageing effect is partly due to the fact that the film which was stabilised and or passivated prior to the adjustment process has now been re-exposed along the edges of the laser kerf. The remainder of the resistance changes are related to changes in the structural properties of the film material because of the rapid heating and cooling during the trimming process.

In addition to the length of the kerf and hence the amount of HAZ, the extent to which the HAZ protrudes into the current carrying path of the trimmed resistor is an important parameter in determining the overall stability of the resistor [279]. As discussed above, these parameters can usually be suitably optimised through variation in the shape of the continuous trim and also the properties of the laser beam itself.

However a more direct solution to this problem is to trim by link cutting. This process involves sequentially opening up shorting bars in loop and ladder type patterns to increase the resistance in discrete steps. Once the trimming bars are opened the current is redirected around the new longer path thus eliminating any current crowding in the trimmed area or HAZ. Although this method can eliminate aging effects, substantially greater chip area is required compared to the conventional bar design. Moreover as the resistance is adjusted in discrete steps a very large number of links may be required to give resolution comparable with the continuous trim approach [272].

There have however been methods reported to make the benefits of the link cutting approach applicable to bar resistors. Perhaps the most notable of these involves cutting a Swiss cheese pattern in the resistor which forces current crowding only in non heat affected areas [283].

More recent studies have focussed on both the effect of replacing the two contact bar resistor with a three contact distributed structure, trimmed by narrow cuts around the additional contact of various shapes [266] and also a random trim approach whereby a single plunge cut is proceeded by multiple holes cut in a random pattern across the resistor film [261].

Although some encouraging results were concluded for both of these methods, the additional trimming time and materials required did not appear to justify the improvements in resistor performance reported.

Work conducted in this chapter deals with firstly developing and specifying the optimum laser settings for the efficient resistance trimming of CuAlMo films resulting in minimum post laser drift and maximum tolerance accuracy. Secondly these optimised laser parameters are used in assessing the effects of varying trim shape and length on the electrical performance of the films.

7.2 EXPERIMENTAL

7.2.1 Sample Preparation

All CuAlMo films used in this investigation were prepared under the optimum sputtering and heat treatment conditions described in chapter 5. The films were grown on 60 x 70mm, 96% alumina substrates, each scribed into 798 standard 1206 size (3mm x 1.5mm) chips. The resistor shape was patterned in a bar configuration via a screen printable mask, which was applied prior to deposition and subsequently removed with a light solvent wash. To permit accurate resistance measurement of the films once deposited, 15µm thick palladium silver (1:3) terminations were screen printed onto the substrates prior to deposition.

The mean resistance value of the films in the as-grown state was ≈1.25Ω, which translated into a sheet resistance of ≈0.75Ω/□ taking the aspect ratio of the bar pattern into account. This relatively high value was a function of the minimum pallet drive speed setting of the sputtering plant and also the cathode power restriction of 1000W which was being enforced for the purpose of reducing target wear rate. Although much lower sheet resistance values were reported in previous experiments these were achieved with the pallet being stationary, positioned directly beneath the sputtering target. However this setup was not suitable for the current investigation as improved film uniformity was required across a larger area of 12 substrates to provide sufficient samples to the laser trimming process.

It is envisaged that much lower sheet resistance values will be achievable when the CuAlMo film is manufactured in full production by modifying the deposition plant drive system to achieve slower pallet speeds and also through increasing the target power level. In addition to this, the measured value of the resistors will be further reduced by modifying the aspect ratio of the film pattern using methods such as angled termination pads.

Once deposited, the films were annealed for 4 hours at 428ºC in an air atmosphere. This process resulted in TCR_{av} of +5 ± 3ppm/ºC and a decrease in resistance from the as grown value of 1.25Ω to a final value range of 0.93 to 1.07Ω for a sample of 200 chips taken across the pallet of 12 substrates.

7.2.2 Laser Trimming System

The equipment used in this investigation was a GSI Lumonics W778-2000 trim system incorporating a High Power Spectra Physics X30 Green, Diode Pumped Laser (DPL) which has been specifically designed to trim thin film resistors. The DPL supplies a cutting beam of 532nm wavelength having an average Q-switched output power of 3W in fundamental TEM_{00} mode. The main components of the system are illustrated schematically in Figure 7.4.

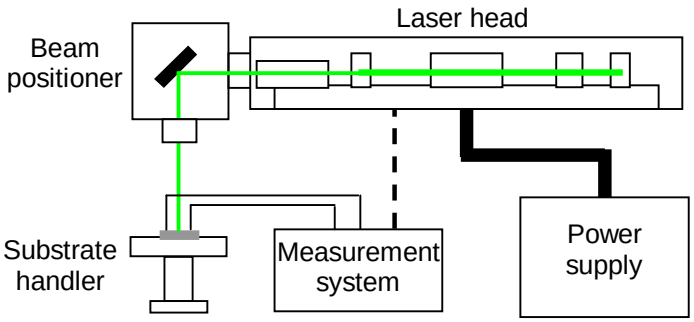

Fig. 7.4 – Schematic representation of the GSI W778 laser trimming system.

The diode module in the power supply generates an optically pumped power output which is routed through a metal-encased fibre optic bundle to an optical port mid way along the laser head, producing an infrared (1064nm) output power. A frequency-doubling (harmonic) module is attached to the laser head to produce the green (532nm) output power.

On entering the laser head the light energy is focused onto and absorbed by the lasing medium (YAG rod) which is housed inside a reflective cavity. When more atoms are excited than not excited in the YAG rod, a population inversion occurs and it is at this point that the lasing action begins.

The laser head also contains a pair of mirrors, which with the help of the reflective cavity, force the laser beam to flow through the cavity to one of the mirrors and then reflect back to the other mirror. When the beam passes back through the cavity further stimulation of the YAG rod occurs.

On striking the front mirror, a small amount of the beam is transmitted through the mirror and the rest of the beam is reflected into the cavity. It is this small amount of the beam which is then focussed and used to trim the resistor material.

The previous paragraphs describe a continuous wave (CW) laser with a steady state energy output which is never interrupted. As discussed in section 7.1, this type of output is not ideal for trimming as the resistor material adjacent to that being trimmed may become overheated and the trim may be uneven, or the power may be too low to trim.

To overcome this problem the laser head also contains a Q-switch which interrupts the optical cavity for a short period of time by blocking the flow of light from the internal cavity to the mirror to produce a high peak power output. The continuous pumping during this interruption causes an increase in the population inversion inside the YAG rod. Hence once the optical cavity is restored the pulse is much shorter in duration and much more powerful. Thus the resistive material can be easily removed whilst minimising heat flow into the surrounding area.

On exiting the laser head the beam then enters the beam positioner. This part of the system is used to firstly attenuate the beam by reflecting a portion of it onto an absorption block, or beam dump, and the rest is then transmitted to the beam expander which uses a zoom telescope to expand the beam into the galvo block so that it ultimately produces the required spot size at the work surface. The high speed galvo block consists of two closed-loop galvanometers (X and Y), two galvo mirrors that position the laser beam on the work surface and an objective cutting lens that focuses the beam onto the work area. The positioning of the X and Y galvanometers is precisely controlled by the trim controller computer.

The substrate handler is also fully automatically controlled via the trim controller computer allowing several different trim pattern programmes too be run in sequence with capability to continuously trim up to 4,200 standard 60 x 70mm substrates.

Finally the measurement system consists of a high-speed V900 bridge with a capability of 0.1Ω to 1000MΩ and full Kelvin connection to one row of resistors on the substrate via a tungsten tipped probe card. A voltage source provides a programmed voltage to the part being trimmed and a voltage of opposite polarity to an internal standard resistor. When the current, measured by the ammeter circuitry, through the part being trimmed is equal but opposite to the current through the standard resistor, the bridge is balanced and the resistor is in value. At this point the bridge outputs a signal to the laser and trimming stops. Once the first full row of resistors has been trimmed, the

substrate handler indexes the next row into the measurement position and trimming re-commences. This process continues until all rows on the substrates have been trimmed and then the handler loads the next untrimmed substrate.

7.2.3 Design Selection

The first stage of the investigation involved optimising the laser conditions to give minimum post trim resistance drift and maximum tolerance accuracy. To achieve this, a Central Composite Design (CCD) consisting of a three factor face centered cube was utilised, see Figure 7.5. This type of design allows for the investigation of interactions, plus the centre points in the middle of the cube and also on all six faces allow for the investigation of non-linear relationships and generally increase the scope of the experiment when compared with factorial designs [181].

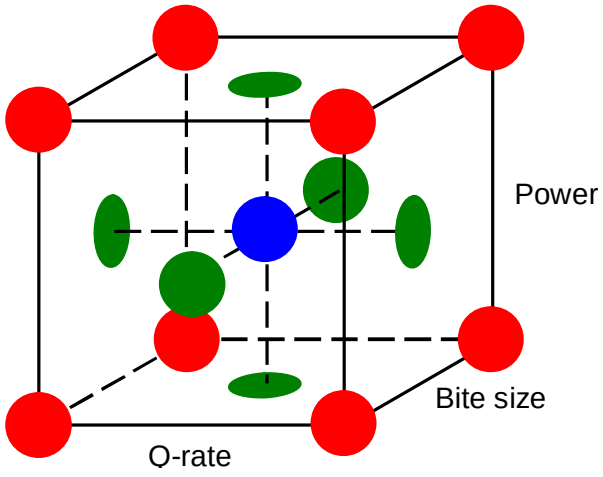

Fig. 7.5 – Three factor face centered cube design

The three parameters selected for investigation were as follows:

Power	the measured power of the laser beam used to trim the resistor material.
Q-rate	the frequency at which the Q-switch interrupts the laser beam and hence its peak power and pulse duration.
Bite size	the distance that the laser beam is moved across the resistor surface between pulses and hence the amount each pulse overlaps.

Thus the cube model shown in Figure 7.5 can be used to represent these three parameters with the x, y and z axis being Q-rate, power and bite size respectively.

To determine the boundary limits for the laser power, firstly some initial reflectance measurements were taken for the CuAlMo films and compared directly with those obtained for NiCrMo films, see Figure 7.6. The measurements were taken using a Hitachi U-3000 Spectrophotometer.

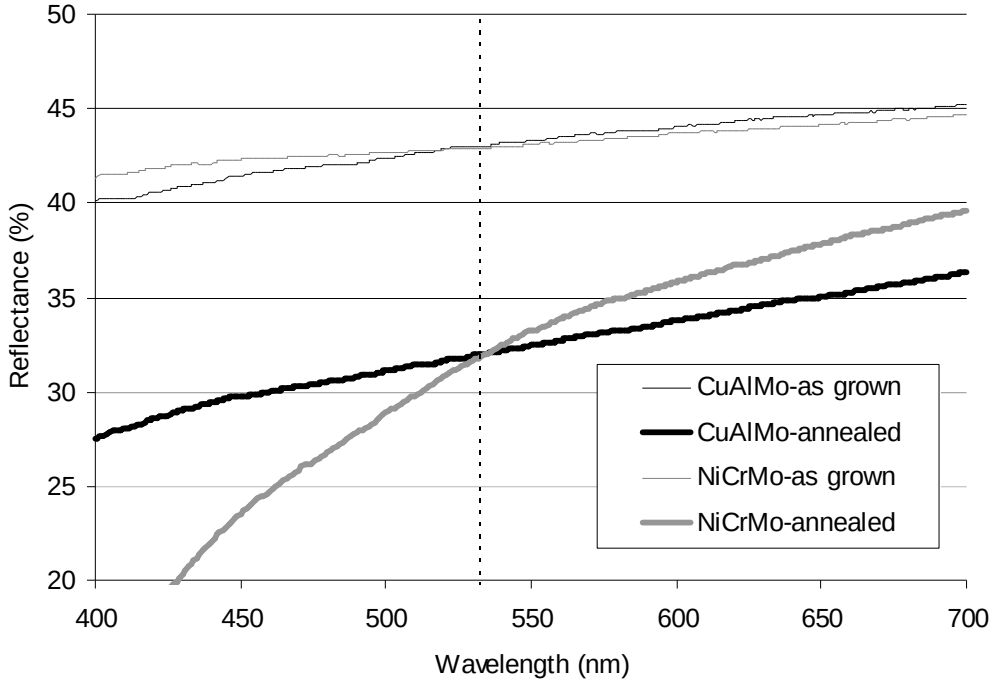

Fig. 7.6 – Reflectance results for CuAlMo and NiCrMo films, both as grown and following heat treatment

As can be seen the reflectance results for both as grown and heat treated films of both chemical compositions are almost identical at a wavelength of 532nm (the wavelength of the laser). As the optimum power required to vaporise the NiCrMo was already well established, this could be used to estimate that required to vaporise an equal amount of CuAlMo film.

Using this power estimate as a starting point, some initial samples were trimmed to determine the upper and lower parameter levels which could be used to produce a laser kerf of consistent visual quality. The final levels chosen for the three factors are given in Table7.1.

Factor	Lower Level	Mid level	Upper level
Power (mW)	500	750	1000
Q-rate (kHz)	8	12	16
Bite size (µm)	5	7.5	10

Table 7.1- Experimental design factor levels

The design matrix for the Face Centered Cube design is given in Table 7.2. In total 20 trials or were required, consisting of 15 distinct combinations of parameters and an additional 5 replicates at the midrange levels, which were used to provide a better model and allow an estimate of the experimental error.

Std order	Run order	Power	Q-Rate	Bite Size
1	19	500	8	5
2	8	1000	8	5
3	4	500	16	5
4	13	1000	16	5
5	10	500	8	10
6	12	1000	8	10
7	17	500	16	10
8	3	1000	16	10
9	20	500	12	7.5
10	6	1000	12	7.5
11	15	750	8	7.5
12	9	750	16	7.5
13	7	750	12	5
14	11	750	12	10
15	2	750	12	7.5
16	5	750	12	7.5
17	18	750	12	7.5
18	16	750	12	7.5
19	1	750	12	7.5
20	14	750	12	7.5

Table 7.2 – Face centred cube design matrix for laser trimming process

Table 7.2 displays the trials in standard order; however the experiment was run in the randomised order given in the ‘Run Order’ column. In addition the experiment was replicated twice, given a total of three runs per trial. This gave a higher degree of confidence in the model by eliminating any potential pattern or trend in the trimming or film properties. A total of 190 resistors (5 rows of 38parts) were trimmed per trial giving a total of 570 parts per data set across the 3 experiments.

The following two electrical properties of the films were selected as experimental outputs:

1. Post trim resistance drift (72hrs at room temperature), $\Delta\Omega/\Omega$, (%)
2. Trim tolerance accuracy (standard deviation of batch), Ω, (%)

7.2.4 Process Considerations

The following factors were taken into consideration prior to commencing the experiment:

Acceleration of galvanometers

From the design matrix in Table 7.2 it can be seen that a maximum trimming speed of 160mm/second was required, occurring when the Q-rate=16kHz and the bite size=10µm/pulse. It was therefore necessary to calculate how far the beam would travel before the galvanometers would reach this speed. The distance required was calculated to be less than 0.05mm. As the resistor films are spaced approximately 0.25mm apart on the substrate there was sufficient room, and it was decided to initiate the trimming 0.075mm from the edge of the resistor film to allow the galvanometers to reach full speed and ensure that the laser beam is travelling at a constant velocity before reaching the edge of resistor film.

Measurement variation

As discussed earlier a full Kelvin probe card, with two probes per conductor pad, was used for all measurements. Firstly the probes were planarised and repeated probing of the 1Ω pre value resistor material indicated that the resistance variation was better than 0.01%. As all trimmed parts would have higher resistance values, it was expected that the measurement variation would be no worse than 0.01%. This was confirmed during the experiment by taking each resistance measurement at least three times and eliminating any measurements with non typical variation.

Power stability

Before commencing the experiment it was confirmed that the laser could operate in fundamental TEM_{00} mode across the full power range under investigation by examination of the spot shape. The spot size had a diameter of approximately 15µm, this being a function of the laser optics design. The resulting kerf width was slightly larger and is discussed in more detail in section 7.3.

Prior to starting each experimental run the laser power output was measured using a Molectron P5100 10W power meter to confirm that it was set exactly as specified in the

design matrix. The Q-rate vs peak power, and pulse width for the W778 laser are specified in Figure 7.7

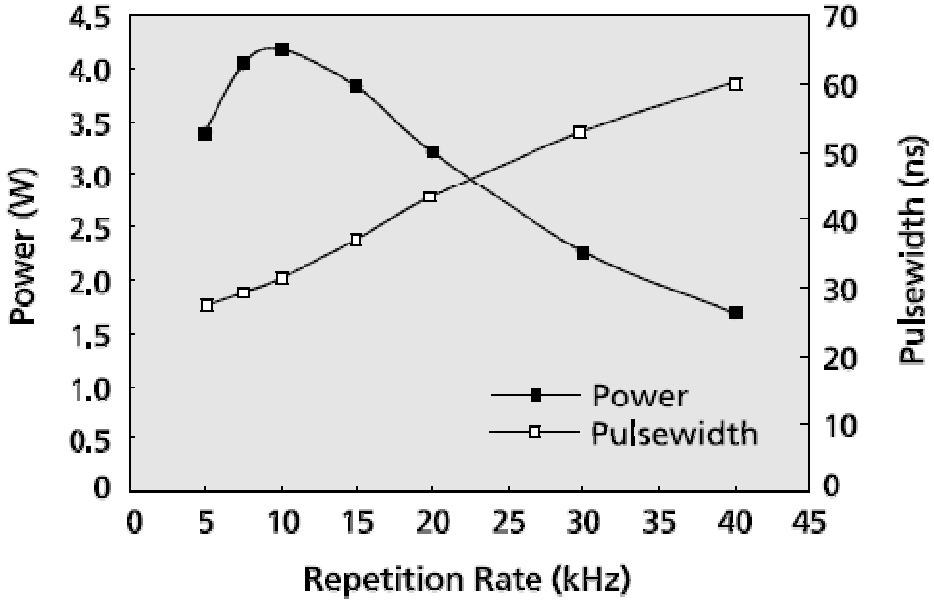

Fig. 7.7 – Relationship between Q-rate vs peak power, average power and pulse width for the W778 laser [284].

7.2.5 Trimming and Measurement Process

Once the initial checks had been made on the laser, the cut shape parameters were loaded. A standard L cut was selected with a first leg plunge depth of 50% of the width of the film, starting 20% of the film length from one conductor pad. The kerf then turned through 90º and the second leg was cut down the centre line of the resistor, with maximum length at 10% of the film length from the second conductor pad. The trim pattern is shown in Figure 7.8.

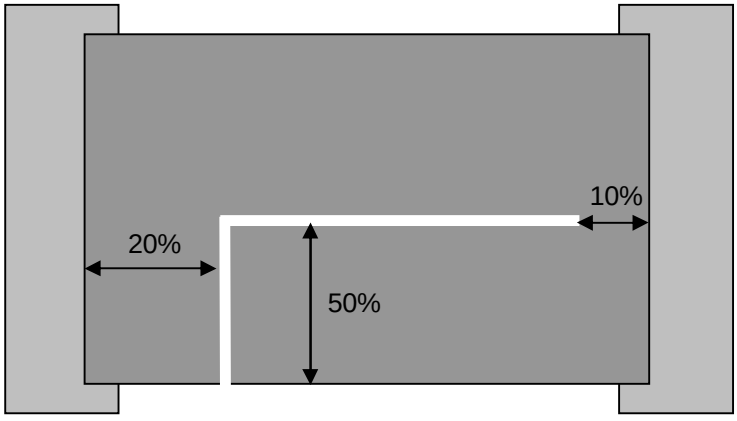

Fig. 7.8 – L cut trim pattern used in determining the optimum laser beam settings

The actual point at which the second leg finished was when the target value was reached and this was in turn dependent upon the exact pre value resistance and also the laser conditions for that run.

Five rows of resistors were trimmed for each experimental run. Once all 20 runs were complete the parts were allowed to cool and stabilise before the trimmed resistance value of each part was automatically measured and stored by the laser system. To determine the post trim resistance drift, the parts were stored in air at room temperature for 72 hours before the resistance value was measured and stored again.

7.3 RESULTS AND DISCUSSION

7.3.1 Optimisation of Laser Beam Parameters

To help with the analysis of the experiment, Minitab 15 [205] statistical software package was used. Table 7.3 shows the P-values for the effects of the three main factors and their interactions on the standard deviation of resistance and 72 hour post trim resistance drift of the CuAlMo films. The results are all based on the mean of 570 measurements with an alpha (α) risk value of 0.05 selected. Again those effects which have P-values (probability) less than the α-level of 0.05 are considered to be significant and are highlighted in bold.

Term	P-value	
	Std dev	**72hr drift**
Power	0.494	0.258
Q-Rate	0.09	**0.006**
Bite Size	**0**	0.274
Power*Q-Rate	0.725	0.408
Power*Bite Size	0.735	0.926
Q-Rate*Bite Size	0.283	0.153

Table 7.3 – P-values for the effect of laser trim factors and their interactions on the standard deviation and 72hr post trim resistance drift of the CuAlMo films

The factor having the largest effect on the standard deviation of resistance of the batch is bite size, having a p-value of 0. This result is highlighted graphically in the main effects plot in Figure 7.9. The result for Q-rate is less significant with a p-value of 0.09, whilst those for power and the interactions of the factors appear to be relatively insignificant.

Figure 7.9 shows that the mean value of standard deviation of resistance decreases quite linearly with decreasing bite size from a value of 0.16% at 10µm to less than 0.10% at 5µm. The results for power and Q-rate are much flatter with the best results being achieved at maximum settings for both.

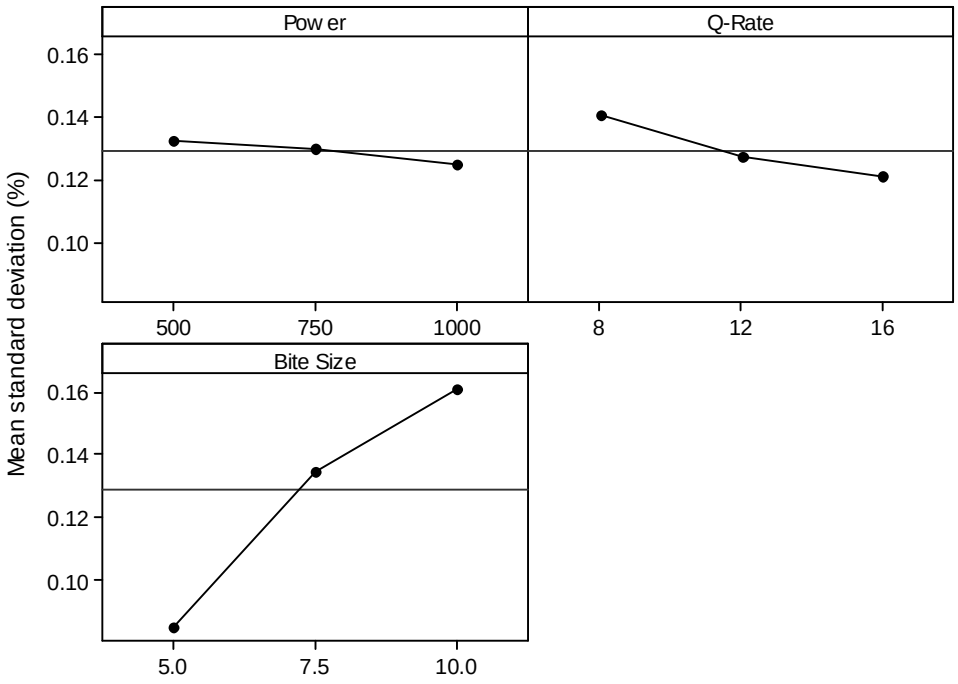

Fig. 7.9 – Main effects plot of laser trim factors on the standard deviation of resistance of the CuAlMo films

The improved result with decreasing bite size can be easily explained by the degree of pulse overlap. With a short bite size the laser pulse centres will be closer together and will therefore overlap by a greater amount, for a fixed pulse diameter. With more overlap, the amount of material removed per pulse will be less and therefore the resistance change per pulse will be less. As discussed in chapter 1 the laser must complete its last pulse once it receives a signal that the resistor has reached target value, it therefore follows that parts trimmed with a smaller bite size will produce a batch with a tighter resistance distribution.

The pulse overlap for the minimum and maximum bite size settings of 5 and 10µm are illustrated diagrammatically in Figure 7.10. For comparison the figure also shows SEM micrographs of laser kerfs trimmed under these two settings with the power and Q-rate set at their median values.

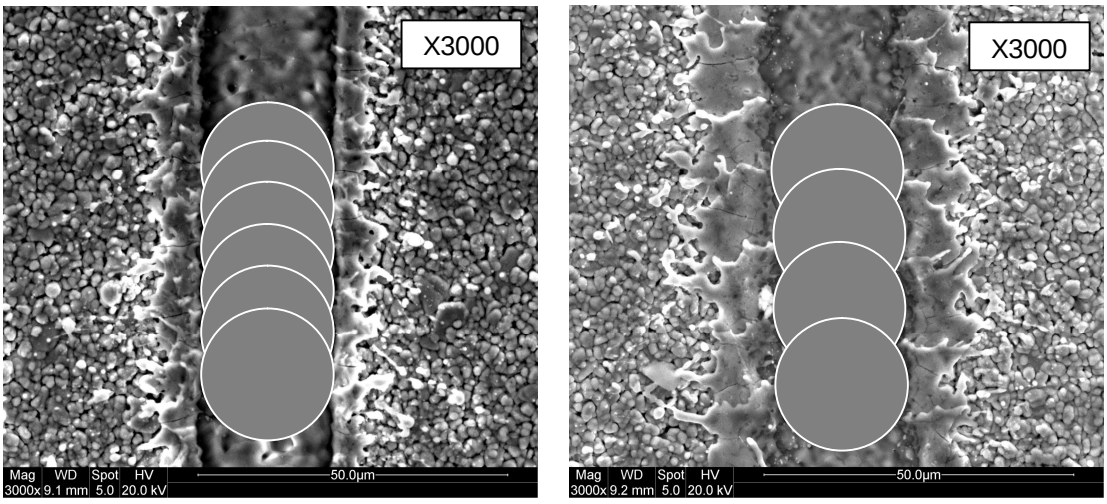

(a) Bite size = 5µm *(b) Bite size = 10µm*

Fig. 7.10 – Model of laser kerfs with variation in bite size and SEM micrographs of experimental results

Although the variation in standard deviation of resistance with changing Q-rate is much less significant than that of bite size, there is a noticeable improvement between the minimum and maximum settings as shown in Figure 7.9. This result could perhaps be explained by the decrease in peak power with increasing Q-rate as highlighted in Figure 7.7. SEM micrographs of laser kerfs trimmed at the minimum and maximum Q-rate settings with power and bite size at their median values are shown in Figure 7.11.

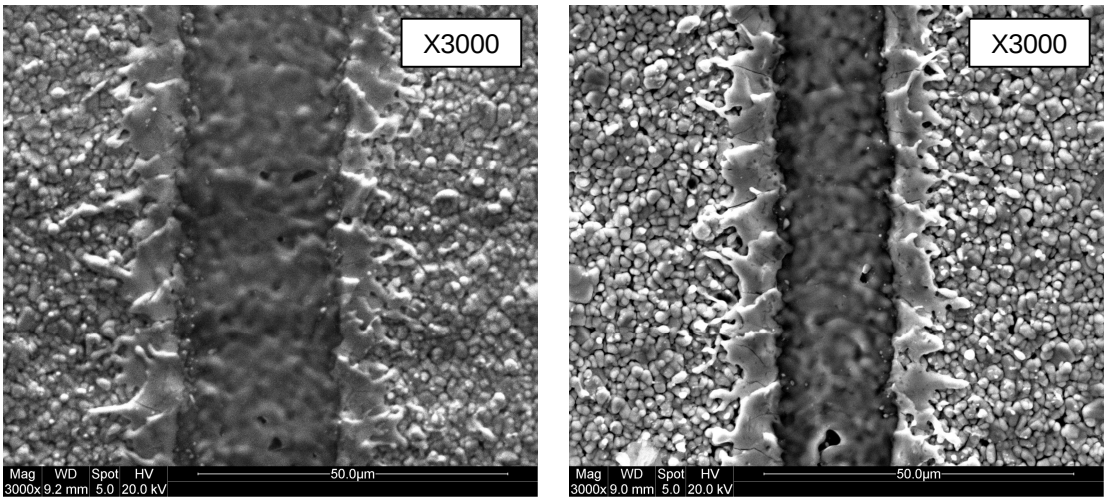

(a) Q-rate = 8kHz *(b) Q-rate = 16kHz*

Fig. 7.11 – SEM micrographs of laser kerfs trimmed at minimum and maximum Q-rate settings with power and bite size set at their median values

The kerf width is noticeably wider at the minimum Q-rate setting of 8kHz than at the maximum of 16kHz, having values of 26μm and 18μm respectively. This is due to the increase in peak power as the laser has more time to build up energy when the Q-switch is switching at a lower frequency. This increase in kerf width with a lower Q-rate setting means that again more material will be removed per pulse and hence the resistance distribution of the batch will be wider.

Another look at the results in Table 7.3 shows that the factor having the most significant effect on post-trim resistance drift is Q-rate, having a p-value of 0.006. The other main factors and interactions are insignificant in comparison with p-values in the range ≈0.15 to 0.93.

The main effects plots for 72 hour post trim resistance drift are presented in Figure 7.12.

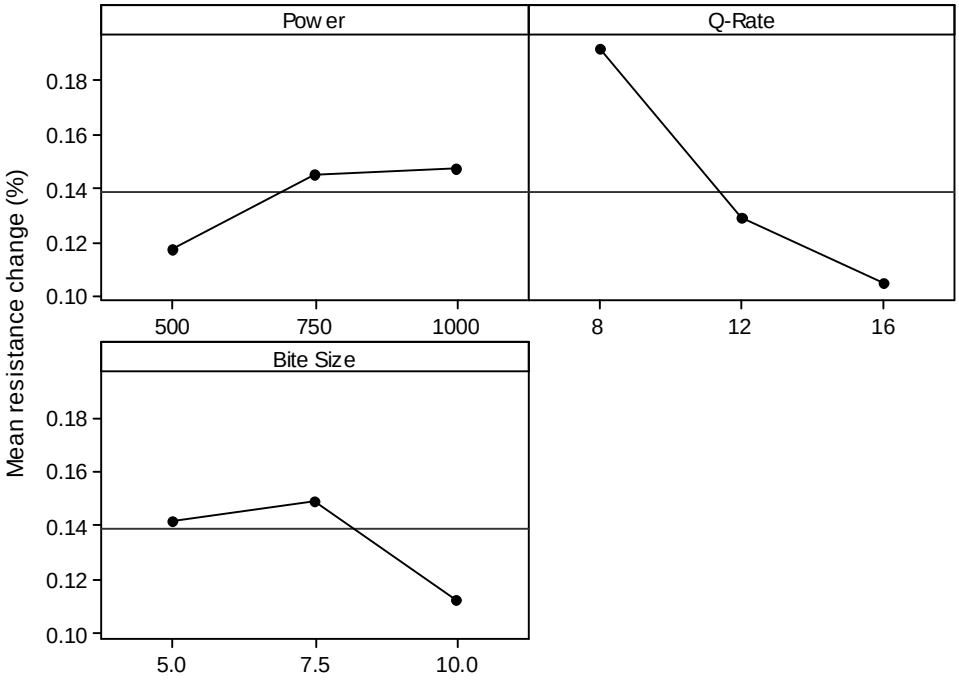

Fig. 7.12 – Main effects plot of laser trim factors on the 72hour post trim drift of resistance of the CuAlMo films

The mean value of post trim resistance drift decreases quite steeply from a maximum of 0.19% at a Q-rate of 8kHz to 0.13% at 12kHz and then more gradually to a minimum of 0.11% at 16kHz. The main effects of power and bite size have less influence on the degree of post trim drift, however the best results of around 0.12% are achieved with minimum power (500mW) and maximum bite size (10μm). It is interesting to note that the effects of power and bite size appear to level off between values of 750 to 1000mW and 5.0 to 7.5μm respectively.

One other point worthy of note is that there were no negative resistance drift results, indicating that the laser kerf was clean and of adequate depth under all trial combinations. The power of the laser beam needs to be controlled to penetrate the alumina substrate by sufficient depth to ensure removal of all the resistive material. If this situation is not satisfied, instability and negative resistance drift can result due to shallow trimming and dirty kerfs [285]. Conversely if the power is too intense, excessive positive drift can occur due to very deep kerfs and thermal damage to the surrounding resistor material, the HAZ.

It is therefore possible to relate the positive resistance drift results in this investigation to the intensity of the laser beam under each set of experimental conditions and therefore the amount of HAZ surrounding the kerf. For example the reduction in post trim drift with increasing Q-rate can be explained by the reduction in peak power as illustrated in Figure 7.7. Similarly a reduction is also apparent with decreasing laser power level. Moreover a reduction in bite size will give more pulse overlap and therefore more energy will be concentrated in the same area of film.

To support these hypotheses, SEM micrographs of trim kerfs produced at maximum power with minimum Q-rate and bite size and also minimum power with maximum Q-Rate and bite size are presented in Figure 7.13.

It is clearly seen that the thermal damage to material surrounding the laser kerf, the HAZ, is much greater with higher power and lower Q-rate and bite size and is thus the main reason for the increase in post trim resistance drift of the CuAlMo films.

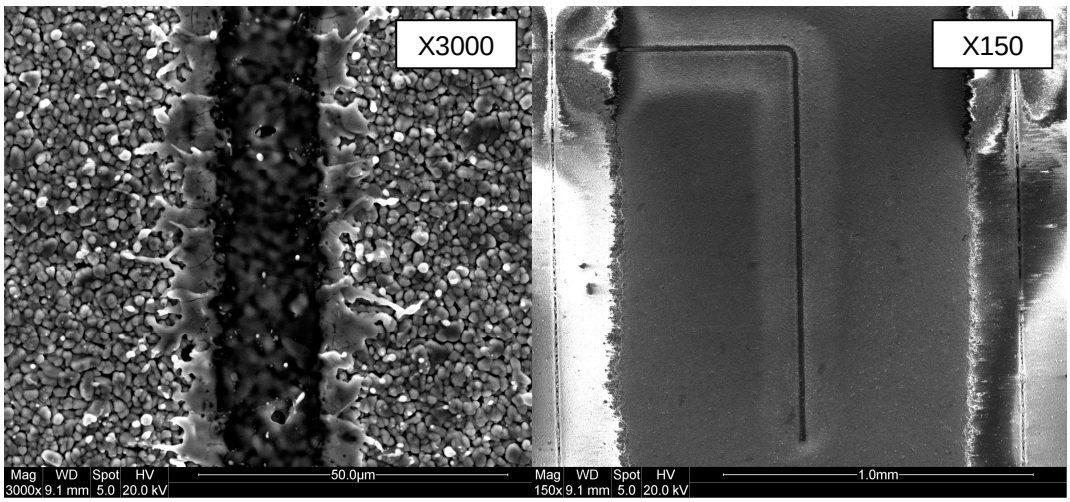

(a) Power = 500mW, Q-rate = 16kHz, Bite size = 10µm

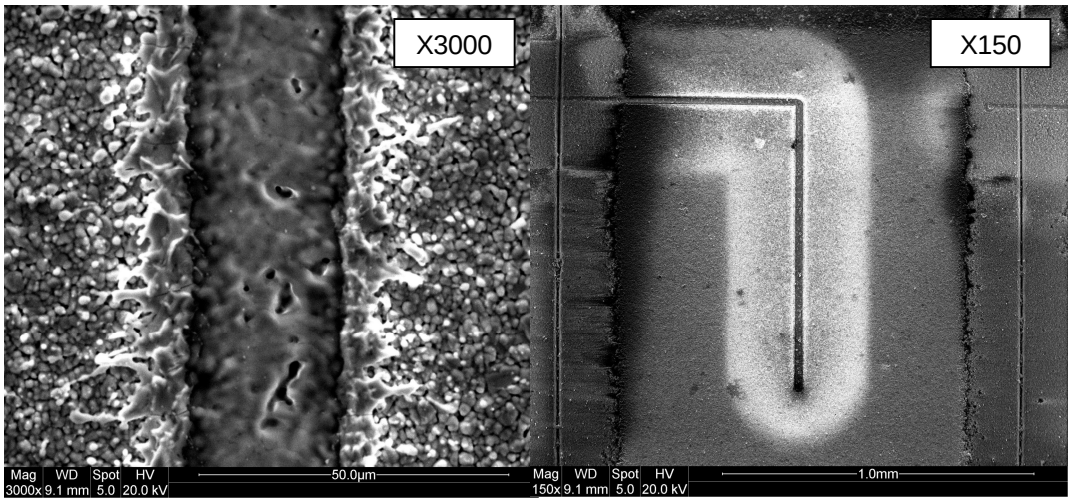

(b) Power = 1000mW, Q-rate = 8kHz, Bite size = 5µm

Fig. 7.13 – SEM micrographs of laser kerfs trimmed at minimum and maximum parameter settings.

7.3.2 Selection of Optimum Laser Beam Parameters

To help with the selection of the optimum laser beam parameters, contour plots were generated from the standard deviation and post trim drift data using the statistical software, see Figures 7.14 and 7.15. The contour plots are essentially slices taken through the experimental cube given in Figure 7.5, on a plane parallel to one of the sides. Therefore for each plot that is generated, one of the three parameters is held constant at its median value, whilst the results vary based on the level of the other two parameters.

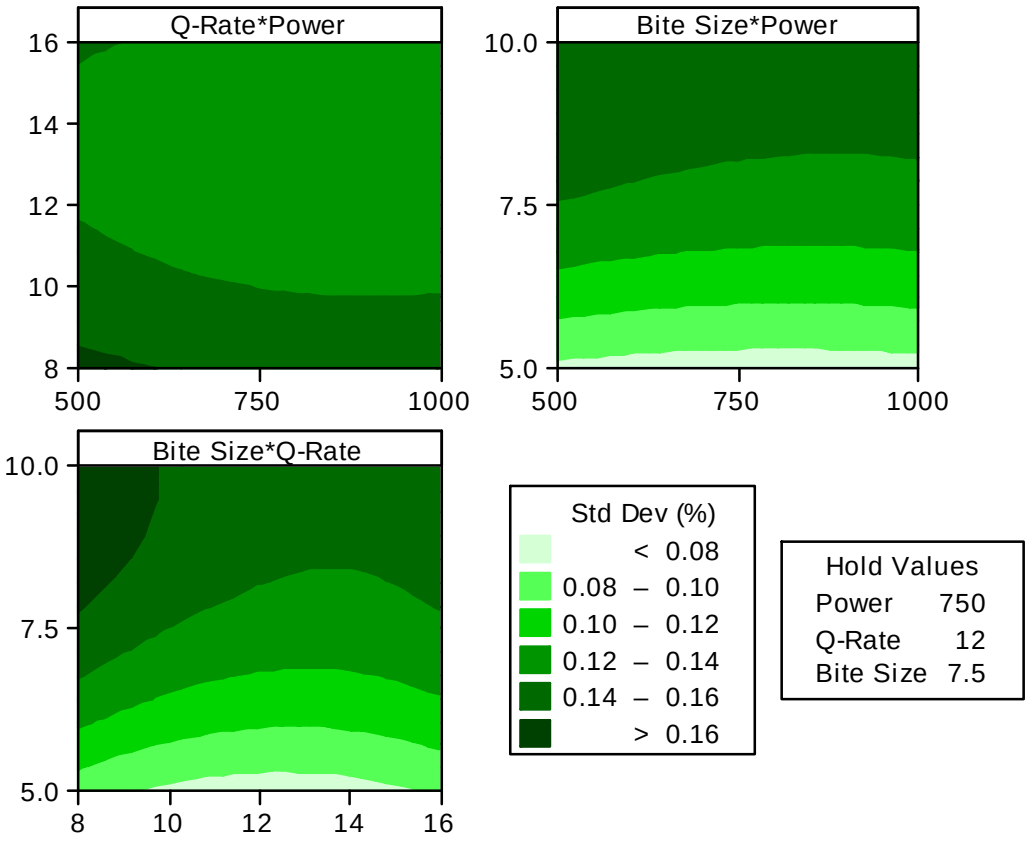

Fig. 7.14 – Contour plots for standard deviation of resistance with varying laser beam parameter settings

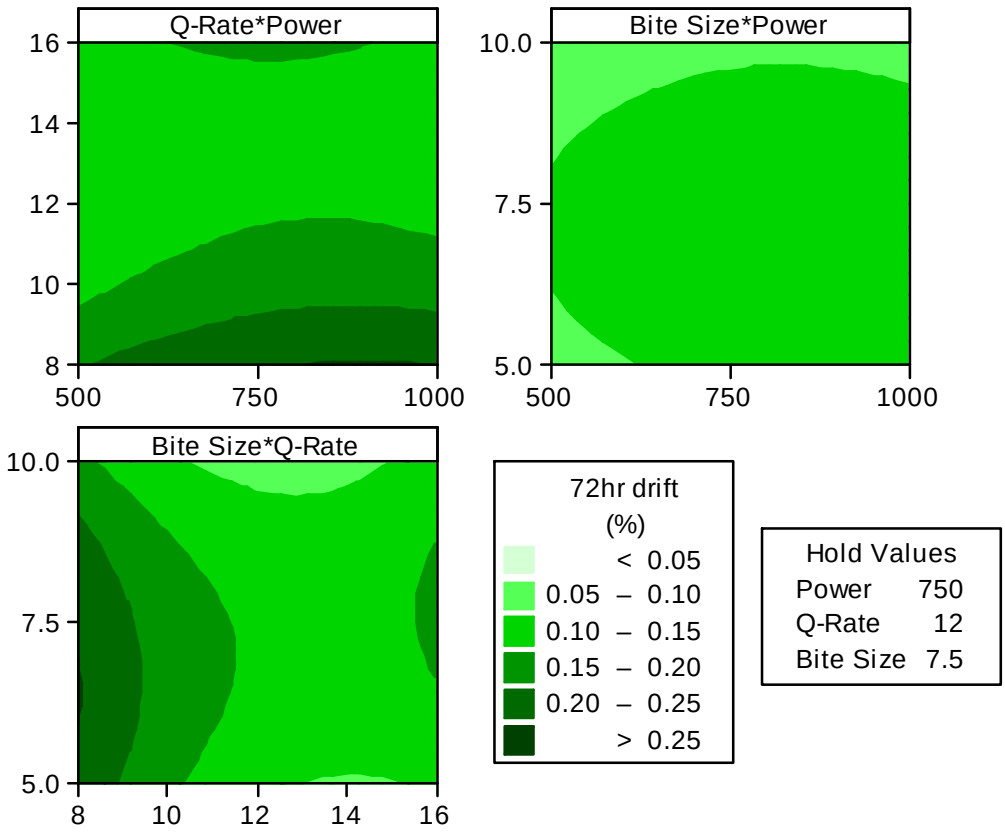

Fig. 7.15 – Contour plots for 72hr post trim resistance drift with varying laser beam parameter settings

From the contour plots it can be seen that minimum standard deviation and post trim stability of resistance are achieved when the laser power and bite size are set at their minimum values of 500W and 5.0µm and with a Q-rate of approximately 14kHz.

To confirm these results, the statistical software was used to automatically predict the optimum settings for each parameter the results of which are presented in Figure 7.16. and summarised in Table 7.4.

Laser parameter	Optimised setting
Power	500mW
Q-rate	13.6kHz
Bite size	5µm

Table 7.4 – Summary of optimum laser parameter settings predicted by Minitab software

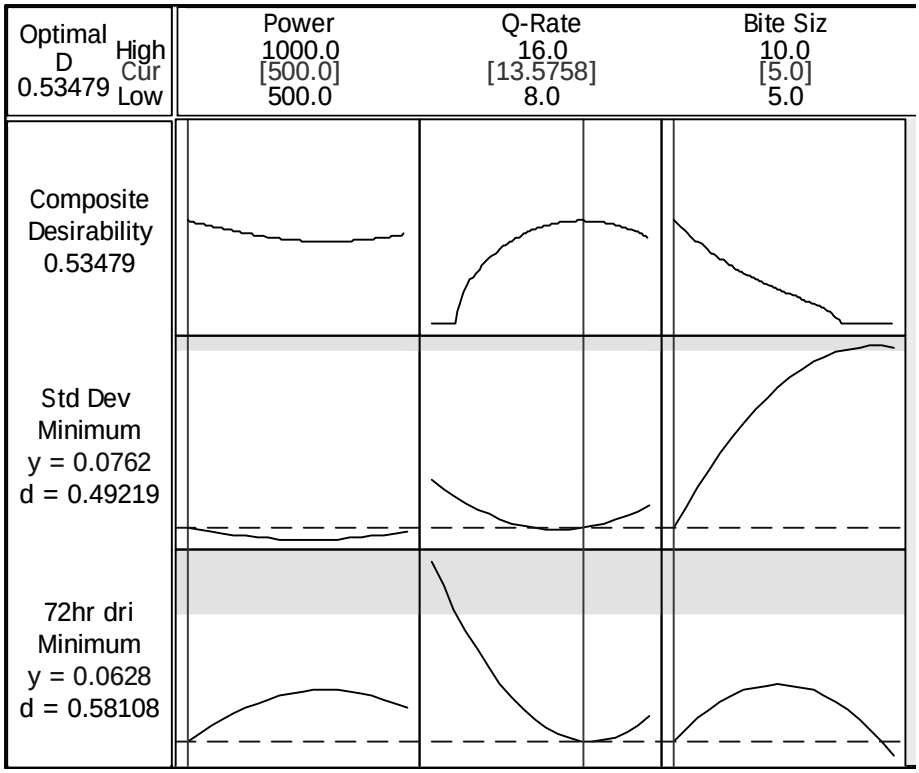

Fig. 7.16 – Optimum laser parameter settings predicted by Minitab software

7.3.3 Trim Pattern Selection

Single Stage Adjustment

Once the optimum laser settings had been established, they were then used to adjust films using various trim patterns to determine to the most appropriate cut type depending on the required resistance gain.

Resistor films from the same batch, having a pre-value resistance of ≈1Ω were adjusted with the following trim gains, see Table 7.5.

For trim gains of 1.5 to 5 both the L cut and serpentine cut were used. As the maximum gain that could be achieved with the L cut was around 6, only the serpentine cut was used for trim gains above 5. The basic layouts of the two trim patterns are shown in Figure 7.17.

Trim gain	Target value (Ω)	Cut Type	No. of plunges	Plunge depth (%)
1.5	1.5	L cut	1	45
2	2		1	55
3	3		1	75
5	5		1	85
1.5	1.5	Serpentine	1	75
2	2		1	
3	3		1.5	
5	5		1.5	
10	10		2.5	
20	20		4	
40	40		6.5	
60	60		9	
80	80		12	
100	100		15	

Table 7.5 – Trim parameters used for single stage adjustment of the CuAlMo films

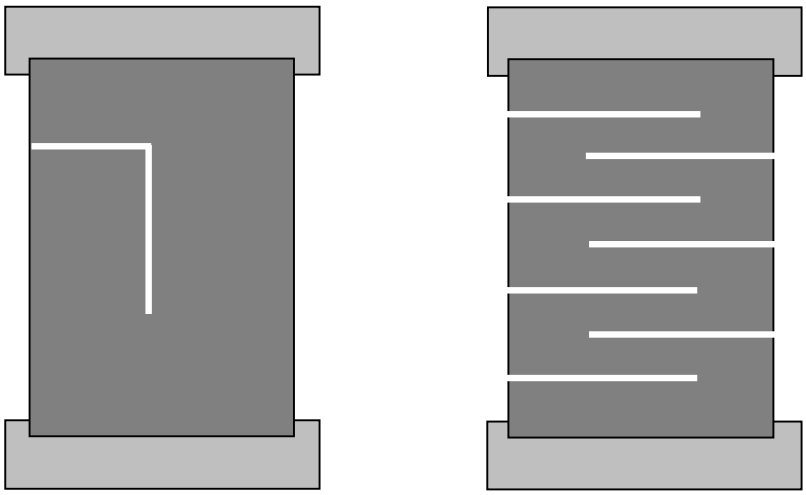

Fig. 7.17 – Layout of L cut and serpentine cut used to trim CuAlMo films

The plunge depth of leg 1 of the L cut was set to minimum length to give maximum length on leg 2 for accuracy and also to leave maximum resistor width remaining for reliability. The plunge depth of the serpentine cuts were set to 75% of the resistor width, as this was determined to be an appropriate length that would allow a suitable trim gain to be achieved in a reasonable number of plunges without the risk of trimming too close to, or through the other side of the film should there be variation in the sputtered pattern dimensions. In all cases the serpentine cuts were as evenly spaced as possible across the film to reduce the effects of current crowding.

Post trim distribution

The post trim distribution is often used as an initial indication of good laser trimming. A tight distribution allows maximum process yields to be achieved, whilst a wide distribution may mean that some of the parts fail to meet the specified tolerance limits. The actual offset of the distribution from the target value is usually not important as this can be compensated for using the laser measuring system. Typically a standard deviation of resistance of less than half of the specified tolerance is acceptable. This allows for errors in target value offset and also any subsequent process changes. Therefore to produce a batch with a resistance tolerance of ±0.5% a standard deviation of ≤0.25% is desired

The standard deviation of resistance of the batch with increasing trim gain for both cut types is presented in Figure 7.18. Again the results are based on the mean of three measurements of 570 chips per experimental trial.

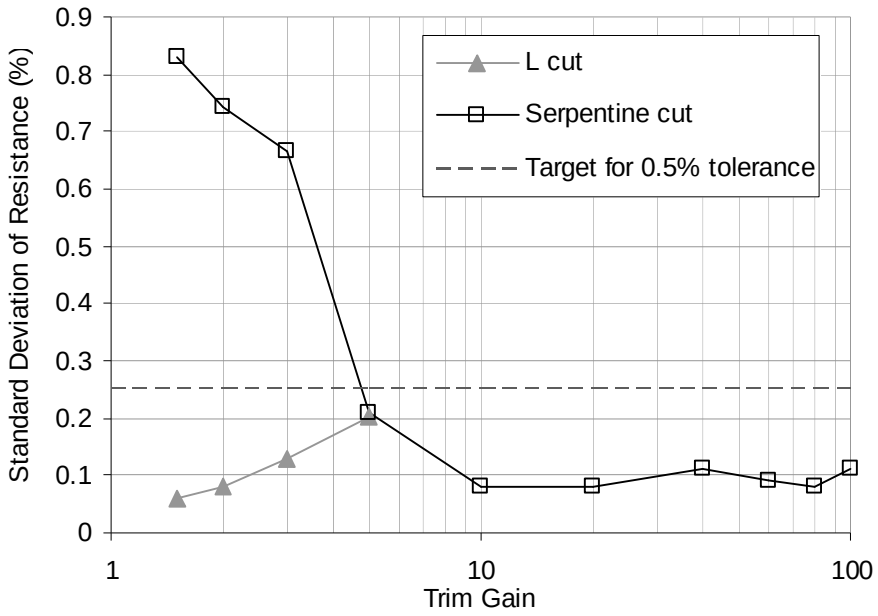

Fig. 7.18 – Variation in standard deviation of resistance with increasing trim gain for both L cut and serpentine cut

For trim gains of ≤5 the L cut gives the smallest standard deviation of resistance of 0.06% for a gain of 1.5 to 0.2% for a gain of 5. This increase in standard deviation with increasing trim gain can be related to the plunge depth of leg one of the cut, see table 7.5. In order to increase trim gain, the plunge depth of leg one must increase to leave a narrower resistor as the cut turns into leg two. However this also means that the rate of change of resistance with the increasing length of leg two is higher. Thus the resistance distribution of the batch is wider.

On the other hand, the standard deviation of resistance for the serpentine cut is much worse for trim gains of ≤5, having a value of 0.83% for a gain of 1.5 and falling to 0.20% for a gain of 5, which is more in line with that of the L cut and inside the target of 0.25%. However once the trim gain has increased to 10 the standard deviation falls to a value of 0.08% and remains around this figure for all further increases up to the maximum trim gain of 100.

As discussed in chapter 1, this decrease in standard deviation with increasing trim gain can be explained by the number of plunges and hence the overall length of the trim kerf, see table 7.5. Unlike the L cut, the serpentine cut only makes cuts in the film perpendicular to the current flow. Hence the rate of change of resistance per plunge will be almost linear. However as the trim gain and hence the number of plunge cuts increase the percentage of target value trimmed per plunge will decrease and the accuracy to which the laser can switch off at target value will improve.

Post trim stability

Following laser adjust the films were stored for 168hrs at 125ºC in air to check their resistance stability. Results of mean resistance change for both cut types and also for untrimmed films are presented in Figure 7.19

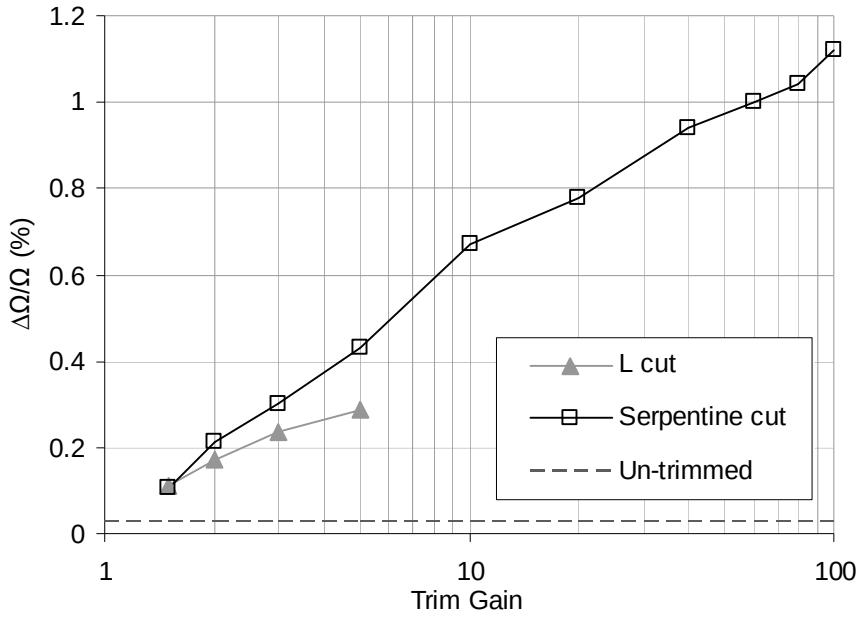

Fig. 7.19 – Variation in post trim resistance stability following storage at 125ºC for 168hrs for both L cut and serpentine cut with increasing trim gain

The first thing to notice is that the stability of the untrimmed resistor is far superior to that of the trimmed resistor having mean resistance shift of 0.03%. This result indicates that the laser trimming is responsible for the inferior performance of the trimmed films

and this is further supported by the increase in mean resistance shift with increasing trim length.

For films trimmed with the serpentine cut the mean stability result increases quite linearly from a value of 0.11% for a trim gain of 1.5 to a figure of 1.12% for a gain of 100. The result for films trimmed with the L cut is slightly less severe, but still increases with trim length from an initial value of 0.11% for a trim gain of 1.5 to a maximum value 0.29% for a trim gain of 5. Thus, as the trim gain increases so does the trim length and hence the amount of HAZ, which causes the film to become increasingly unstable.

The target specification for the dry heat stability test for chip resistors is a shift of ≤0.5% following 1000hrs storage at 125ºC, see Appendix 1. Therefore the results reported in Figure 7.19 following 168hrs exposure, are clearly unacceptable, particularly for the higher trim gain parts.

Two Stage Adjustment – Fine Trim

To try and overcome this stability problem a two stage adjustment process was employed. As described in section 7.1, this is common practice for thin film resistors, especially when high trim gains are required. The majority of the trimming takes place in the first stage and the device is adjusted to around -1% of its target value. After which it is stored at high temperature before a second or final trim is utilised to adjust the device to target value.

This method of trimming has two main advantages over the single trim techniques. Firstly the fine trim is usually designed so that it cuts the film in an area of relatively low current density in the shadow of the first trim, therefore having a much lower rate of change of resistance and allowing a tighter resistance distribution to be achieved. This trim position in an area of low current density also means that any HAZ effects will be significantly reduced.

A model of current density for the L cut with a shadow fine trim is shown in Figure 7.20 along with the corresponding calculated rate of resistance change plot for a CuAlMo film trimmed from a pre-value of 1Ω to a target value of 2Ω.

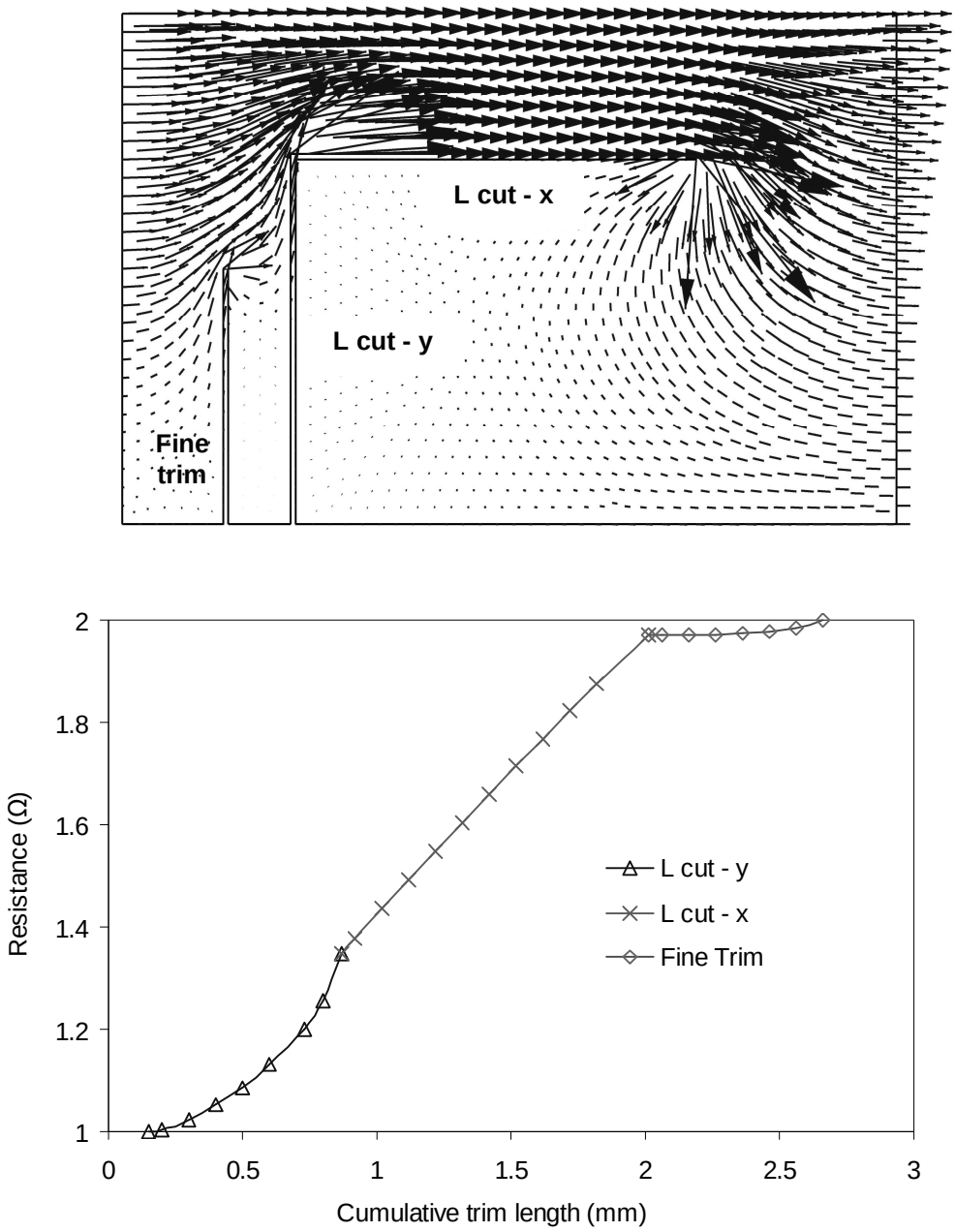

Fig. 7.20 – Model of current density and corresponding rate of resistance change for a CuAlMo film trimmed from a pre-value of 1Ω to a target value of 2Ω, using the two stage L cut and shadow fine trim.

For the initial L cut, the resistance increases rapidly as the kerf is cut perpendicular to the current flow (y direction) towards the opposite edge of the resistor film. For the second leg of the L cut, the rate of resistance change is more linear as the kerf is cut parallel to the current flow (x direction). Finally for the fine trim, the kerf is cut in the shadow of the L cut in an area of low current density and the rate of change of resistance is very slow. Therefore provided that the length of the fine trim is controlled so that it does not plunge into areas of high current density surrounding the corner of the L cut (through correct first trim resistance offset), good accuracy of resistance value should be achieved.

The second advantage of the two stage adjustment is that the high temperature storage is used to relieve stresses built up in the HAZ surrounding the first trim, producing a much more stable device. The choice of storage temperature used between the two trim stages is usually selected to be above the upper category operating temperature of the device and also above any temperature seen at subsequent process stages, but must not be so high that it could spoil the TCR of the film. Thus in effect the dry heat stability performance is being improved by storing the device at a temperature higher than that at which it will ultimately be tested.

The duration of the storage is also important. It must be of sufficient time to remove the majority of the resistance shift from the films, but must not be so long as to affect the manufacturing timescale. Typically the process will take place overnight, allowing the first and second trims to be carried out on successive days.

The required storage duration can be estimated from a plot of resistance change with time for the single stage adjusted films, see Figure 7.21.

As can be seen the vast majority of post trim resistance change takes place in the first 24 hours of testing, regardless of trim gain, after which the change begins to slow down and level off. It therefore seems feasible that an overnight stove of 16hrs (5pm day one to 9am day two) at a higher temperature of ≈250ºC would be sufficient to remove the majority of the post trim resistance shift.

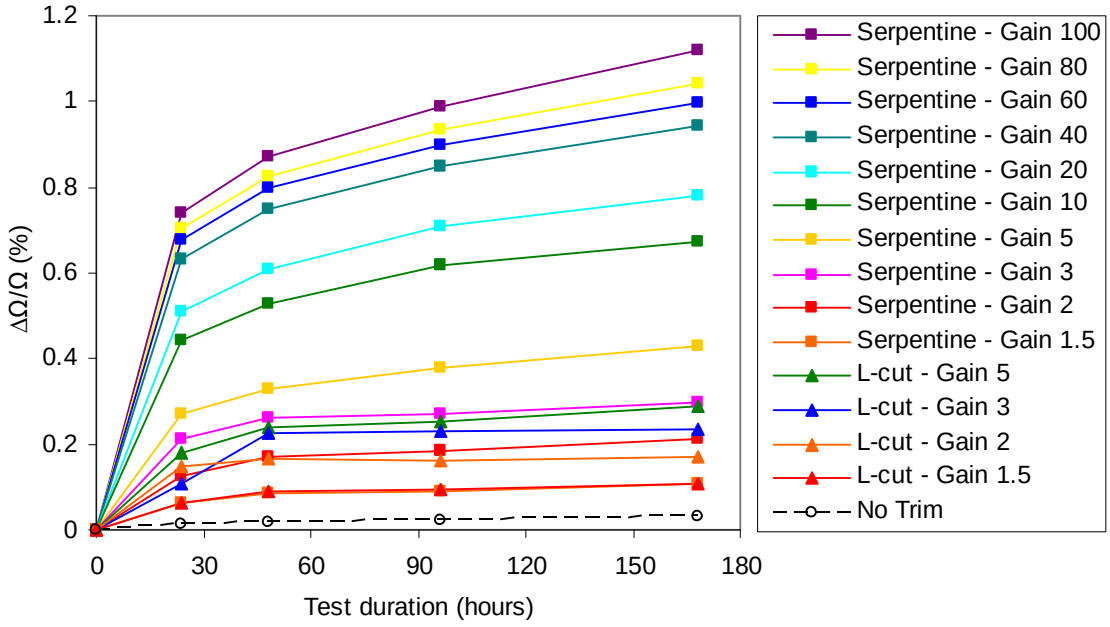

Fig. 7.21 - Variation in post trim resistance stability with storage time at 125ºC, for both L cut and serpentine cut with various trim gains

To investigate this theory, films of CuAlMo from the same batch of 1Ω pre-values were again adjusted to the following trim gains, see Table 7.6. Due to the superior resistance distribution results achieved with the L cut it was decided to use this cut type for trim gains in the range 1.5 to 5 and the serpentine cut for gains greater than 5. The basic layouts of the two fine trim patterns are shown in Figure 7.22 and details of the other trimming and stabilisation parameters are presented in Table 7.6.

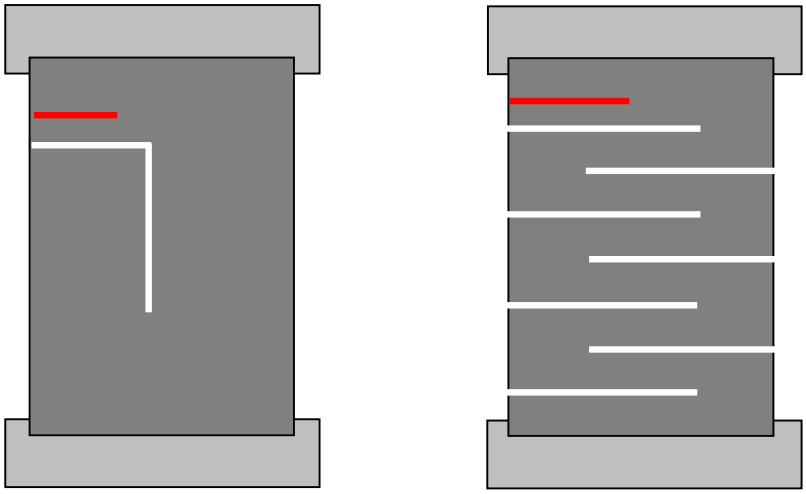

Fig. 7.22 – Two stage adjustment trim patterns for both L cut and serpentine cut.

Trim gain	Target value (Ω)	1st trim parameters				Stabilisation parameters		Fine trim parameters		
		Target value offset (%)	Cut Type	No. of plunges	Plunge depth (%)	Temp (ºC)	Time (hrs)	Target value offset (%)	Cut Type	Max plunge depth (%)
1.5	1.5	-0.5	L cut	1	45	250	16	-0.10	Shadow plunge	35
2	2	-0.5		1	55			-0.10		45
3	3	-0.75		1	75			-0.15		65
5	5	-1.00		1	85			-0.15		75
5	5	-1.00	Serpentine	1.5	75	250	16	-0.15	Shadow plunge	65
10	10	-1.25		2.5				-0.20		
20	20	-1.50		4				-0.20		
40	40	-1.75		6.5				-0.25		
60	60	-2.00		9				-0.25		
80	80	-2.25		12				-0.30		
100	100	-2.50		15				-0.30		

Table 7.6 – Trim parameters used for two stage adjustment of the CuAlMo films

The values for the trim target offsets were estimated from the stability results reported for the single stage adjusted films, i.e. how much the resistance would change during storage. The shadow plunge depth was restricted to a maximum length of 10% less

than that of the first trim plunge to prevent it from entering areas of high current density as shown in Figure 7.20.

The resistance distributions of the batches after first trim were measured to be in line with that reported for the single stage adjusted films. The resistance shift following stabilisation in air at 250ºC for 16hrs is shown in Figure 7.23.

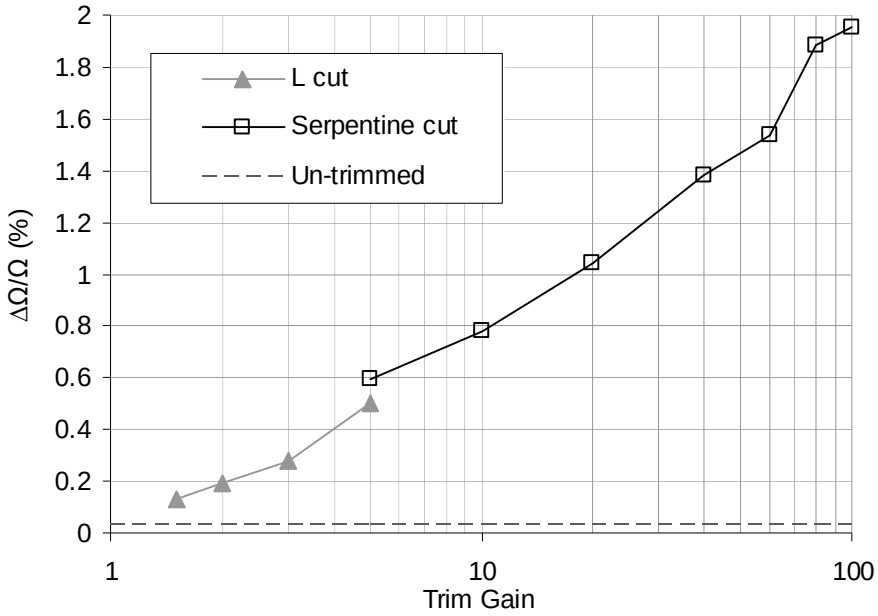

Fig. 7.23 - Variation in resistance shift following stabilisation at 250ºC for 16hrs for both L cut and serpentine cut with increasing trim gain

The stability of the films decreases with increasing trim gain and the shape of plot is very similar to that reported for the single stage adjusted films after storage at 125ºC for 168hrs. However the value of the resistance shift is on average 40% higher following storage at 250ºC. This is an encouraging result as it suggests that the resistance shift resulting from 168hrs storage at a 125ºC can be removed in less than 16hrs at a higher temperature of 250ºC. Thus the films should be much more stable when subsequently tested at the dry heat stability test temperature of 125ºC.

The standard deviations of resistance of the batches with increasing trim gain following fine trim are plotted in Figure 7.24 along with those obtained for the single stage adjusted batches both after trim and following the 16 hour stabilisation.

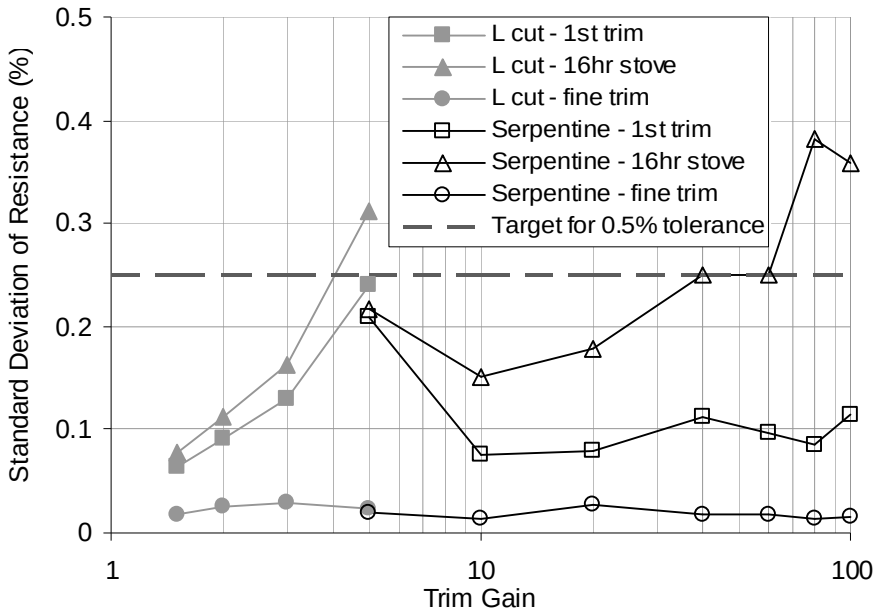

Fig. 7.24 - Variation in standard deviation of resistance with increasing trim gain for both L cut and serpentine cut following first trim, stabilisation and fine trim

By positioning the fine trim in an area of low current density the standard distribution of the two stage adjusted films is far superior to that of the single stage and is better than 0.05% for all trim gains. This would allow for a final resistance tolerance of ±0.1% to be feasible with the correct trim offset selection (assuming that the distribution does not widen significantly during the remaining process stages).

Following final trim, the films were stored at 125ºC for 168hrs to check resistance stability. Results of maximum resistance shift of the batches with increasing trim gain are plotted in Figure 7.25 together with the mean results obtained for the single stage adjusted batches and the maximum result for untrimmed parts.

Using the two stage adjustment technique has greatly improved the dry heat stability performance over that obtained for the single stage method. The vast majority of instability associated with the HAZ surrounding the laser kerf has been removed during the 16 hour stove at 250ºC. Again the positioning of the fine trim and also its relatively short length in comparison with the first trim appear to have minimal affect on the stability of the film. Thus the maximum resistance shift has reduced to less than 0.08% following the two stage adjustment and is much closer to the result of 0.013% obtained for the untrimmed films stabilised under identical conditions.

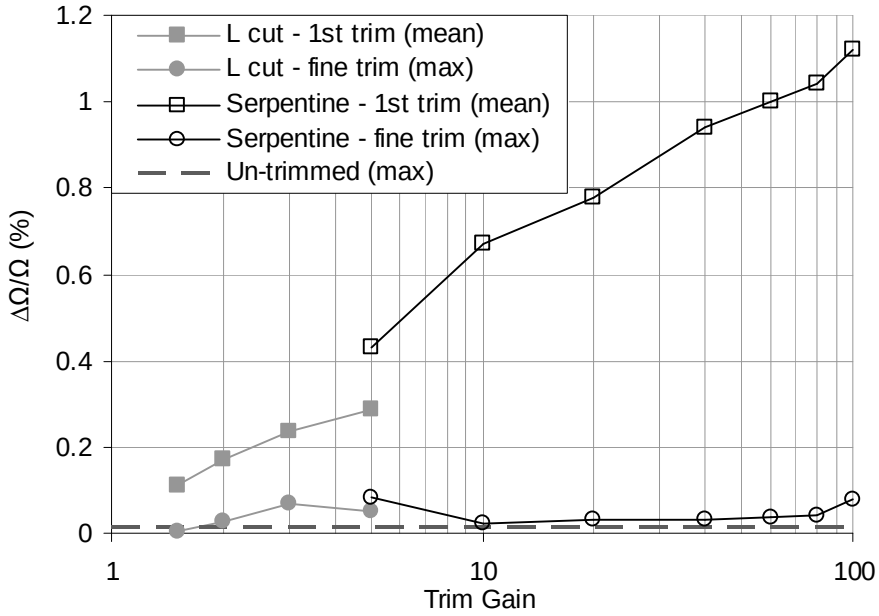

Fig. 7.25 - Variation in post trim resistance stability following storage at 125ºC for 168hrs with increasing trim gain for both L cut and serpentine cut following first trim, stabilisation and fine trim

Finally the TCR_{av} of a random sample of 20 parts from each batch was tested to ensure that the laser trimming and or stabilisation parameters had not had any effect causing it to move out of specification. Figure 7.26 shows the results of TCR_{av} for the samples with increasing trim gain and also for untrimmed films, which are plotted at a trim gain value of one.

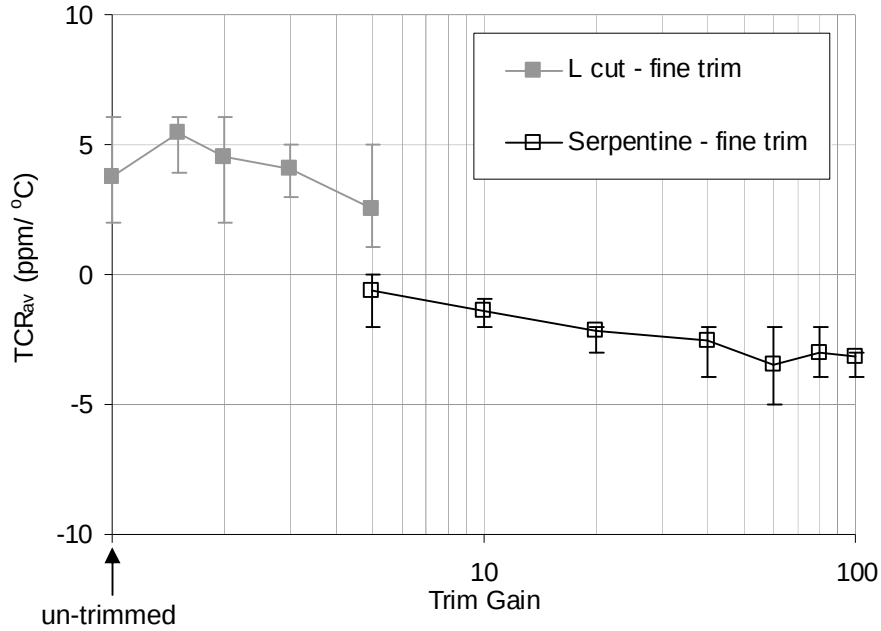

Fig. 7.26 - Variation in post trim TCR_{av} with increasing trim gain for both L cut and serpentine cut

The results for the untrimmed films and those trimmed using the L cut are very similar to that measured for the pre-value films prior to commencing the trimming process, which had a value of +5 ± 3ppm/ºC. There is a slight decrease in the mean TCR result for the films adjusted using the serpentine cut, which decreases further with increasing trim gain. As the results for the untrimmed films are similar to that of the pre-value films then this decrease in TCR when using the serpentine cut must be related to the cut type or trim gain rather than the stabilisation process during trimming. One possible explanation could be the highly positive TCR of the silver termination pads, causing a series TCR effect with the resistor film, a phenomenon which is known to have an increasing effect with decreasing resistance value or in this case trim gain [16, 178].

Nevertheless, the overall the effect of the laser trimming process on the TCR of the films is minimal and the results for all of the batches are still well within the target specification of ±15ppm/ºC.

7.4 SUMMARY

From the work carried out in this chapter it can be concluded that the laser trimming process plays a critical role in adjusting the resistance of the CuAlMo films to the desired target value and tolerance and also has a significant influence on their long term resistance stability.

Through systematic investigation of key process parameters such as laser power, Q-rate and bite size, it was possible to improve the resistance distribution of the batch of CuAlMo films from pre-value range of around 10% to attain trimmed tolerances of < ±0.5%. This was achieved across a wide trim gain range of 1.5 to 100 through use of two basic trim cut patterns; the L cut for gains < 5 and the serpentine cut for gains > 5.

These optimised results were achieved with low laser power and bite size and mid-range Q-rate settings, which enabled material to be vaporised whilst minimising heat flow into the remaining film and allowing accurate control over trim length and hence resistance value.

Although optimisation of the laser beam parameters produced suitable results for resistance distribution, there was still an unacceptable level of resistance instability being introduced into the film via the heat affected zone surrounding the laser kerf. This was determined through dry heat stability testing at 125ºC and the level of instability was proportional to the trim length, increasing from a value of 0.11% for a trim gain of 1.5 to 1.12% for a trim gain of 100, following 168 hours exposure.

To overcome this problem it was necessary to utilise a two stage adjustment process, which incorporated a post first trim stabilisation at 250ºC followed by a fine plunge trim to target value. This procedure was successful in reducing the dry heat stability figure to less than 0.1% across the full range of trim gain and also allowed for the possibility of attaining much tighter resistance tolerances of < ±0.1%.

The laser trimming process was also found to have limited affect on the TCR distribution of the batch and all samples remained well within the target specification of ±15ppm/ºC.

As will be discussed in the following chapter, the optimised laser trim settings have been used to manufacture production batches of chip resistors for long term reliability testing.

Chapter 8

Process Verification

8.1 INTRODUCTION

Work conducted in chapters 1 to 7 has focused on the research and development of a new thin film material of copper, aluminium and molybdenum to be used for the production of low resistance thin film resistors and also on the experimental determination of a set of optimised process conditions using DOE, under which these resistors can be successfully manufactured.

This current chapter deals with, firstly, manufacturing a production size batch of CuAlMo thin film surface mount resistors under the optimised process conditions, and secondly, verifying their performance against criteria such as manufacturability to specification, and long term reliability.

In order to establish the performance of the CuAlMo resistors, a target product specification has been generated, see Appendix 1. This specification is based on a combination of historical performance requirements of thin film chip resistors, which are controlled by both CECC [12] and MIL [313] standards, and also recent market demands for lower resistance value devices.

The PCF series is currently the main thin film chip resistor range manufactured and sold by Welwyn Components Ltd. The present resistance value range offered by this series is restricted to 10Ω to 1MΩ, with NiCr films being used for values 10Ω to 20KΩ and CrSiO films being used for values >20KΩ.

The objective is therefore to extend this resistance range by using CuAlMo films for values 0.1Ω to 10Ω, thus enabling an overall resistance range of 0.1Ω to 1MΩ to be offered. However, due to the current capabilities of the sputtering plant, discussed in chapter 7, a more restricted value range of 1Ω to 10Ω has been assessed during this investigation.

8.1.1 Introduction to Reliability Testing of Thin Film Resistors

If a component is ‘reliable’ it could take many years to fail under normal operating conditions, or in fact it might never fail. It is therefore not practical to establish the performance of a device under ‘typical’ conditions. For this purpose various accelerated tests have been established, allowing the long term reliability of resistors to be predicted in a realistic timescale.

There have been numerous studies undertaken on the reliability of thin film resistors [287-309] and again most of these deal with the performance of the well established film systems of NiCr, TaN and CrSiO. Although there are a number of other criteria which

must be satisfied including mechanical strength, solderability, insulation resistance etc, the tests which appear to present the highest level of severity to thin film resistors fall into three broad categories of temperature, endurance, and humidity.

Temperature test

As discussed in chapter 1, the temperature, or dry heat, test is the most straightforward test to implement and is therefore the most widely used. Commonly accepted criteria for surface mount chips are a resistance change of <1% following storage for 1000 hours at 125ºC. The thermal ageing that takes place during this test is usually a measure of the level of oxidation at the film surface and also internal changes such as annealing and precipitation that may occur. However these processes also serve to stabilise the resistor making it appear to improve as the tests proceeds. As shown in chapter 7 it is therefore possible to improve the performance of the device by increasing the amount of heat treatment it receives during the manufacturing process. For this reason it is not adequate to judge the long term reliability of the resistor based on the temperature test alone, and its performance under other test conditions must be evaluated.

Endurance test

The resistance change resulting from the endurance, or load, test should be very similar to that from the dry heat test performed at the same temperature that is being generated by the load. There are however a few exceptions to this similarity, making it necessary to perform both tests:

- Electrolytic corrosion can result if any moisture is allowed to condense on the resistor surface and penetrate the protection. This process is more likely to occur if the load on the resistor is insufficient to drive off the moisture.

- Electrolysis of ions in the substrate can occur and increases rapidly with increasing temperature.

- Under conditions of very high d.c. current densities, metal migration can take place causing a redistribution of material with metal migrating away from the cathode.

- Hot spots are potentially the most likely cause of failure during load testing but are sometimes difficult to identify due to their random occurrence.

Another important consideration which must be taken into account is the geometry of the resistor. Wherever possible it is good practice to use straight line resistors instead of meandering or serpentine patterns to give the most uniform distribution of the electric field.

Typical load test conditions for both axial and surface mount devices are 1000 hours at 70ºC with full power rating being applied, with maximum allowable resistance change being <0.5%.

Humidity test

The humidity test is usually a test of how impervious to moisture the coating used to protect the resistor is. However if the protection happens to become penetrated, then the moisture resistance of the resistor film itself becomes important.

Typical test conditions are 1000 hours or 56 days storage at 90-95% relative humidity at a temperature of 40ºC. It is also common practice to split the test sample and apply a light electrical load to one half of the parts. In this case, as discussed above, the main source of drift results from electrical corrosion. However unlike the endurance test the applied load must be mild enough to allow moisture to condense on the resistor surface. If the load is increased further the test will become less severe as the heat generated by the resistor will drive off the moisture. Again typical maximum allowable resistance changes for this test are <1%.

8.2 EXPERIMENTAL / MANUFACTURE

All resistor samples manufactured were standard 1206 surface mount size. The basic construction of the device is shown in Figure 8.1.

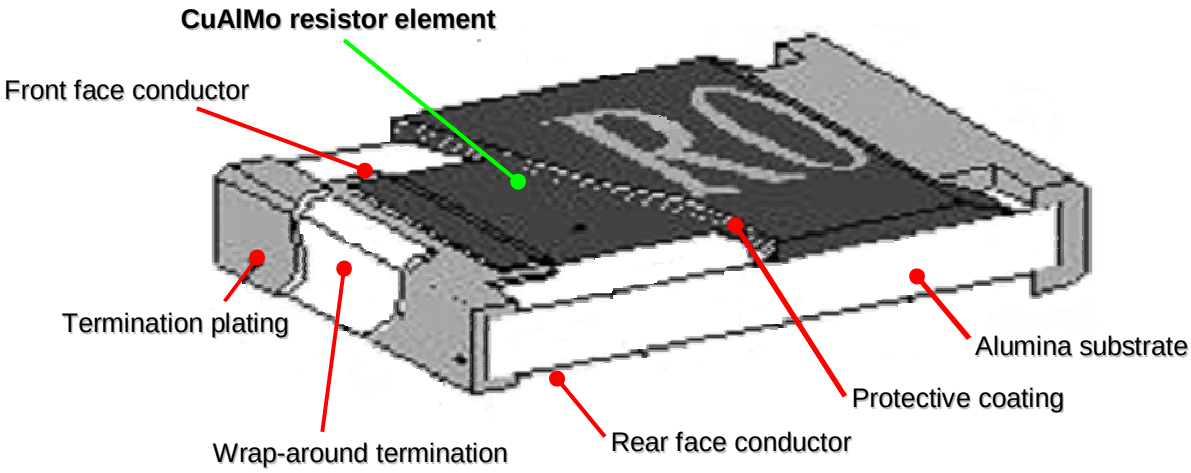

Fig. 8.1 - Basic construction of the 1206 size surface mount resistor

The process flow for the manufacture of experimental samples is given in Table 8.1.

Operation Number	Process description	Materials
1	Screen print and fire rear face conductor pads (40mins at 850ºC peak)	As fired 96% Al_2O_3 60x70mm 1206 type substrates and 100wt.%Ag ink, 23-28µm dried thickness
2	Screen print and fire front face conductor pads (40mins at 850ºC peak)	Ag/Pd 97/3wt.% ink, 10-15µm dried thickness
3	Screen print and dry resistor mask (20mins at 120ºC)	Overglaze, 20-25µm dried thickness
4	Sputter resistor under optimised conditions (320ºC peak at 1000W)	CuAlMo 69/24/7 wt.% target, ≈1.3µm thickness
5	Ultrasonically clean off resistor mask (2mins at 60ºC)	Stage 1 = de-ionised water and detergent 5:1 ratio Stages 2 - 4 = de-ionised water
6	Heat treat and TCR test (4hrs at ≈430ºC)	
7	Laser adjust - 1st trim	
8	Stabilise (16hrs at 250ºC)	
9	Laser adjust - fine trim	
10	Screen print and dry 1st protection layer (20mins at 200ºC)	Epoxy protection, 20-25µm dried thickness
11	Screen print and cure 2nd protection layer (1hr at 200ºC)	Epoxy protection, 20-25µm dried thickness
12	Snap substrates into strips	
13	Apply wraparound terminations and cure (1.5hr at 200ºC)	Ag 65wt.% epoxy ink, 25-40µm dried thickness
14	Snap substrate strips into single chips	
15	Plate outer terminations and dry (1hr at 70ºC)	Ni, 7-15µm thickness Sn, 5-15µm thickness
16	100% automatic visual inspection	
17	100% final resistance measure and tape pack	Anti static 1206 size carrier tape and cover tape. 7” taping reel.

Table 8.1 – Process flow for sample manufacture.

Once the front and rear face conductor pads and the resistor mask had been applied to the substrates, the batch was split into three smaller batches, A, B and C, prior to sputtering. Each batch contained 12 substrates, which were laser scribed into 798 chips, giving a total of 9,576 chips per batch.

To analyse process repeatability, the three batches were sputtered under the optimised conditions on three separate days. They were then heat treated for 4 hours in air at various temperatures around 430ºC until a near zero TCR_{av} was achieved.

Following heat treatment, substrates from each batch were laser trimmed to target values of 1.5Ω and 4Ω using the two stage L-cut and 5Ω and 10Ω using the two stage serpentine cut, both under the optimised laser beam settings. The films were then protected by applying a screen printed epoxy protection to the substrates.

During the next stage the substrates were snapped into strips and an epoxy silver wraparound termination was applied to both edges of the strip to form an electrical connection between the front and rear face conductor pads. The strips were then further sub divided into individual chips before the wraparound termination was plated with Ni and Sn to give good solderability.

The manufacture of the resistor was now complete and the final 100% testing of the batch was carried out. This included automatic visual inspection, to check for any poor quality terminations or protection, and also final resistance measure and tape packing. The parts were now complete and ready for environmental testing.

8.3 ENVIRONMENTAL TEST PROCEDURES

In terms of testing the performance of fixed resistors, the generic CECC [313] standard referred to is BS EN 60115-1:2001 “Fixed Resistors for use in Electronic Equipment” [12]. This specification details the general test procedures and requirements. The more specific performance requirements are laid down in a series of additional standards and depend on the technology i.e. thin film, thick film, wirewound etc, and also the power rating of the device under test. The most applicable of these standards for thin film technology are shown in Table 8.2.

Specification BS CECC	Technology	Resistance range (W)	Resistance tolerance (%)	Rated dissipation @ 70°C (W)	TCR (ppm/°C)
40101-019 40101-803	Axial metal film	1-1M	0.5, 1, 2	0.125, 0.25, 0.50	50, 100, 250
40101-004 40101-804	Precision axial metal film	1-1M	0.05, 0.1, 0.25, 0.5, 1	0.0625, 0.125, 0.25, 0.50	15, 25, 50, 100
40401-801 40401-804	Precision SMT metal film	1-3M	0.1, 0.25, 0.5, 1	0.05, 0.075, 0.1, 0.125, 0.25	10, 15, 25, 50

Table 8.2 – CECC specific standards for axial leaded and surface mount metal film resistors

BS EN 60115-1 is applicable to fixed resistors for use in electronic equipment. It establishes standard terms, inspection procedures and methods of test for use in sectional and detail specifications of electronic components for quality assessment or any other purpose. An outline of the main electrical test procedures and sequences required to qualify fixed resistors to CECC specification is given in Appendix 2, full details of all tests can be found within the specification itself.

As discussed in section 8.2, production batches were manufactured to target values of 1.5Ω, 4Ω, 5Ω and 10Ω. A summary of the environmental tests undertaken for all four batches are presented in Table 8.3.

Test Parameter	Conditions	Sample size		Limits of resistance change (ΔΩ%+0.05Ω)	
		CECC 40401-801 requirement	No. tested	CECC 40401-801 requirement	Target
Endurance at 70ºC	1000hrs cyclic load at 70°C	20	40	0.50	0.25
Damp heat steady state (DHSS)	1000hrs at 40ºC, 90-95%RH	20	40	1.00	0.30
Short term overload	6.25 x rated power for 5sec	20	40	0.25	0.25
Endurance at 125ºC	1000hrs at 125ºC	20	40	1.00	0.25
Rapid change of temperature (TRC)	5 cycles -55 to +125ºC	20	40	0.25	0.10
Resistance to soldering heat	270ºC for 10sec	20	40	0.25	0.20
Termination solderability	235ºC for 2sec	40	40	95% minimum coverage	

Table 8.3 – Environmental test parameters with sample sizes and limits

8.4 RESULTS AND DISCUSSION

8.4.1 Production Batch Manufacture

Sputter Deposition

A summary of the electrical properties of Batches A to C in both the as-grown state and following heat treatment at the optimum temperature for four hours, are presented in Table 8.4. The resistance measurement results are percentage deviation from the target pre-value of 1Ω and are based on all 9,576 chips in the batch, the TCR_{av} results are based on a sample of 10 chips per substrate, i.e 120 chips per batch.

Batch No.	Resistance deviation from 1Ω (%)		TCR_{av} (ppm/ºC)		Final heat treatment temperature (ºC)
	as grown	heat treated	as grown	heat treated	
A	+11 to +53	-9 to +5	-144 to -100	-2 to +10	425
B	+7 to +67	-6 to +8	-143 to -100	-7 to +8	425
C	0 to +46	-12 to +4	-130 to -85	-8 to +9	425

Table 8.4 – Summary of the as grown and heat treated electrical properties of production batches A, B and C.

The resistance deviations of batches A and B in the as-grown state are similar at +11 to +53% and +7 to +67%, whilst that for Batch C is slightly lower at 0 to +46%. The reason for this decrease could be due to a reduction in impurity levels in the deposition chamber during the sputtering of Batch C, since this was the last batch to be processed. However there were no obvious differences between the background gas analysis plots taken before each run.

Nevertheless this theory is further supported by the results for as-deposited TCR_{av}, which also shows that Batches A and B had similar results of -144 to -100ppm/ºC and -143 to -100ppm/ºC, whilst that for Batch C was more positive at -130 to -85. As discussed in chapter 5, other possible explanations for this result could be an increase in the substrate temperature or a decrease in the sputtering pressure, both of which could result in lower resistivity films.

Whatever the true underlying cause of this discrepancy, it is of greatly reduced significance following heat treatment, as both the resistance and TCR distributions of all three batches are much narrower and of similar mean values.

On average the resistance value decreases by 25 to 30% following annealing for four hours at 425ºC and the overall distribution of all three batches is 20%. This decrease in resistance can be related to processes such as grain growth and annealing of impurities, both of which have been discussed in detail in previous chapters. In addition, the reduction in resistance distribution of the batches following heat treatment is perhaps related to a variation in impurity levels captured in the films during deposition which are subsequently annealed out and also improvements in the orientation of the film structure following heat treatment.

Although this pre value resistance distribution of 20% would be considered acceptable for laser trimming it could lead to large variations in trim length within a batch. It was

therefore considered worthwhile to try and understand the reasons for the relatively large as-grown resistance distributions in more detail, to see if this could be improved for future batches.

To help with this analysis a contour plot showing uniformity of resistance value across the sputtering pallet for Batch B in the as-grown state is shown in Figure 8.2.

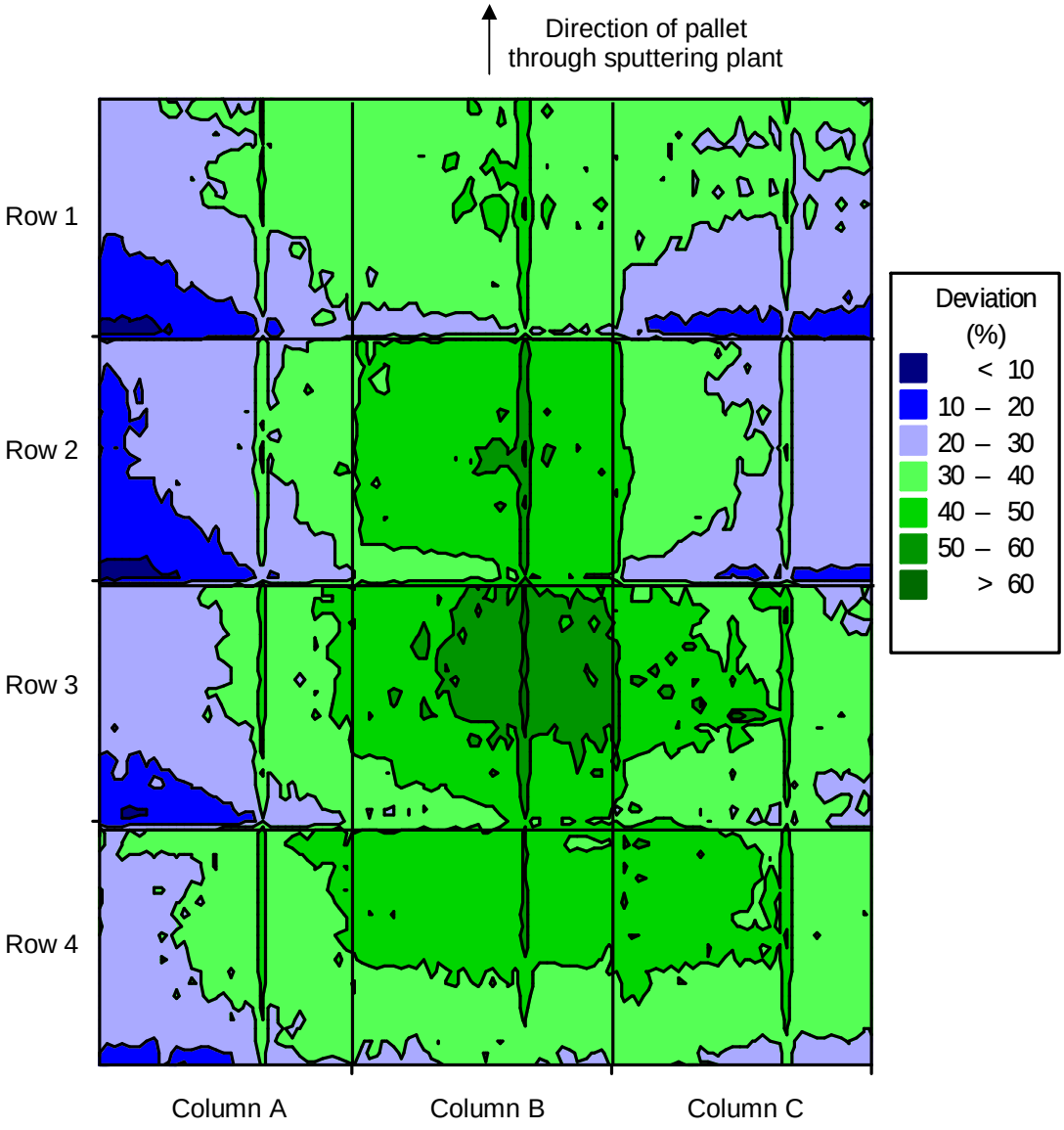

Fig. 8.2 – Contour plot showing as-grown resistance distribution across sputtering pallet for Batch B

From the uniformity plot three observations can be made:

1. On average the resistance values are higher down the centre column of substrates on the pallet and lower on the outside columns.
2. There is a line of higher resistance running through the right centre of all three columns of substrates.
3. There is a slight resistance value gradient across each individual substrate, with values being higher at the front of the substrate and lower at the back

Of these three observations, number 1 is the most difficult to explain and could be related to the homogeneity of the sputter target or possibly the uniformity of the sputtering plasma. It should therefore perhaps be noted that on several occasions during sputtering, the plasma was observed to consist of two distinct clouds, each covering approximately half of the target and therefore producing an area of apparently lower intensity in the centre. This phenomenon was particularly noticeable when sputtering at lower powers in the range 200 to 600W.

The cause of observation number 2 was found to be due to the sectioned construction of the sputtering target. Once all depositions were complete the target was removed from the plant and aligned with the sputtering pallet. This revealed that three of the joints between the five sections that made up the sputtering target lined up with the position of the lines of higher resistance observed on the sputtering pallet uniformity plot.

There are two possible explanations for the occurrence of observation number 3. Firstly it could be related to the application of the resistor mask through which the film pattern is generated. For example if an unequal amount of pressure is applied to the squeegy blade during printing of the mask, then the print lines will be of different thicknesses and thus the resistor patterns will vary in size.

Secondly, this apparent gradient of resistance value across the individual substrates could be directly related to a temperature gradient set up across the substrate during sputtering. As the substrate enters the plasma the temperature across it will increase, reaching its highest point at the back, where the lowest resistance values have been recorded.

To try and confirm if either of these two theories was applicable, a fourth batch was sputtered. However in this case the substrates were rotated through 180º prior to sputtering.

The contour plot of as-grown resistance for this batch was very similar to that for Batch B and the gradient had not rotated. This result suggested that the poor uniformity of resistance was related to variation in film temperature across the substrate and therefore in the structural properties of the films rather than variation in the resistor dimensions, which are in turn a function of the accuracy of the screen printed resistor mask.

As summarised in table 8.4, the TCR_{av} distributions of the batches were also observed to decrease following heat treatment. The variations in TCR of all three batches with increasing heat treatment temperature are plotted in Figure 8.3.

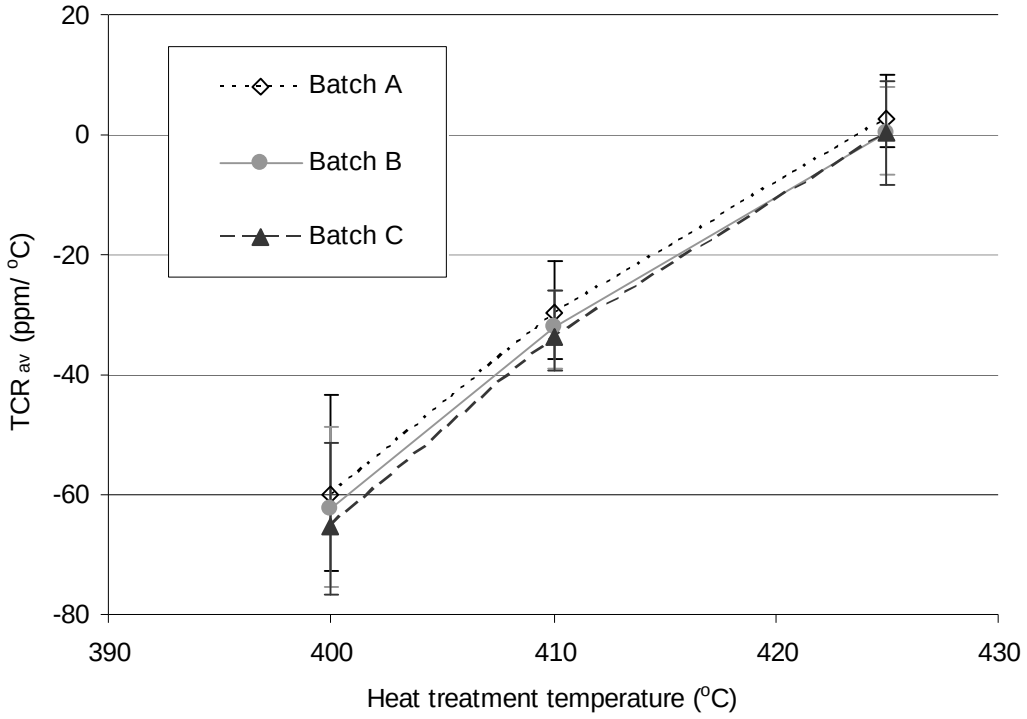

Fig. 8.3 – TCR_{av} results for batches A, B and C following heat treatment for 4 hours at various temperatures

Both the mean TCR and distribution of TCR steadily improve with increasing temperature from an as-grown value for all three batches of -144 to -85ppm/ºC to 0±10ppm/ºC following heat treatment for 4 hours at 425ºC. Again these improvements can be related to the structural and chemical changes taking place inside the film.

Although the TCR distributions of all three batches are within the target specification of 0±15ppm/ºC following heat treatment, the as-grown distribution is much larger at around 50ppm/ºC. As with the variation in as-grown resistance distribution, it was also possible to relate the variation in TCR to differences in the structural properties of the film due to the temperature gradient across the substrate during deposition.

Laser Trim

One substrate was taken from each of the three pre-value batches and laser adjusted to the target value. This meant that each of the four target values; 1.5, 4, 5 and 10Ω contained three substrates (one from each pre value batch) giving a total of 2,394 resistors per job.

Plots of resistance distribution before and after each stage of the laser trim process for all four target values are presented in Figures 8.4a to 8.4d.

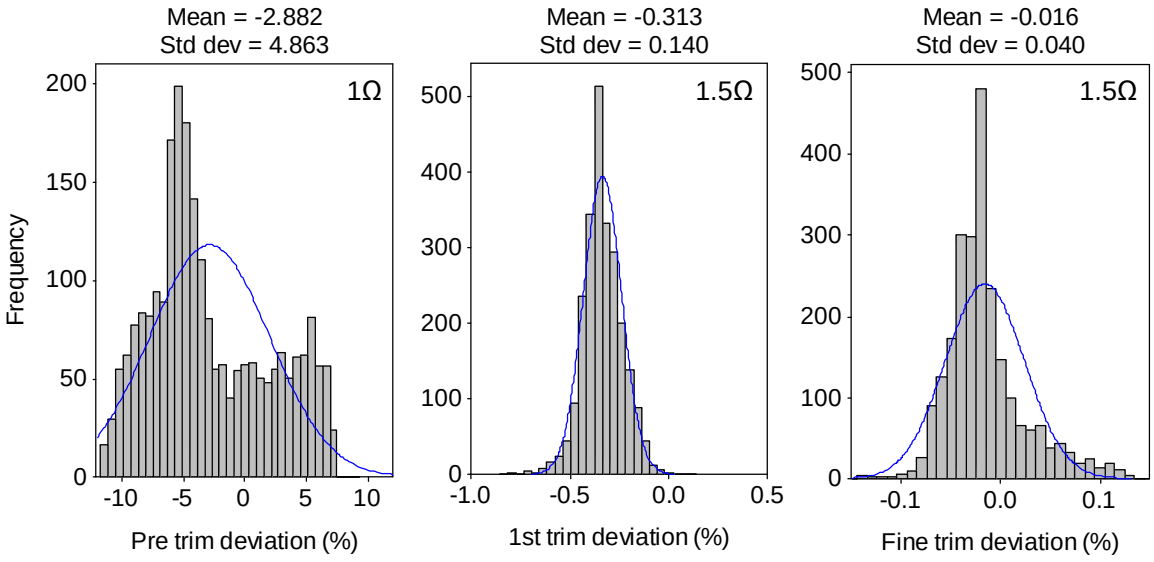

Fig. 8.4a – Resistance deviation from pre trim value of 1Ω and target trim value of 1.5Ω. L-cut used for first trim and shadow plunge used for fine trim.

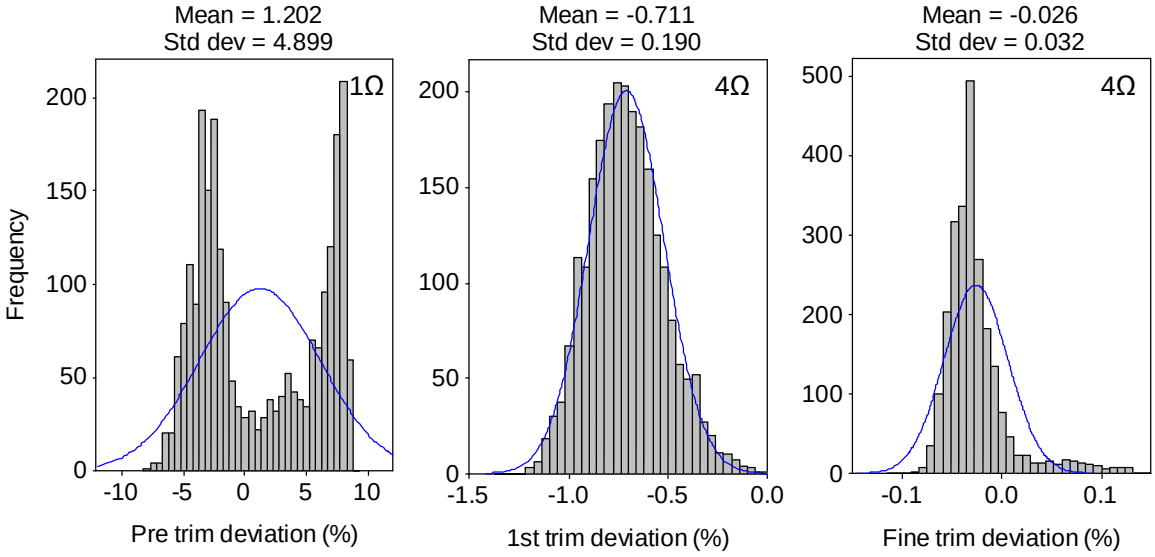

Fig. 8.4b – Resistance deviation from pre trim value of 1Ω and target trim value of 4Ω. L-cut used for first trim and shadow plunge used for fine trim.

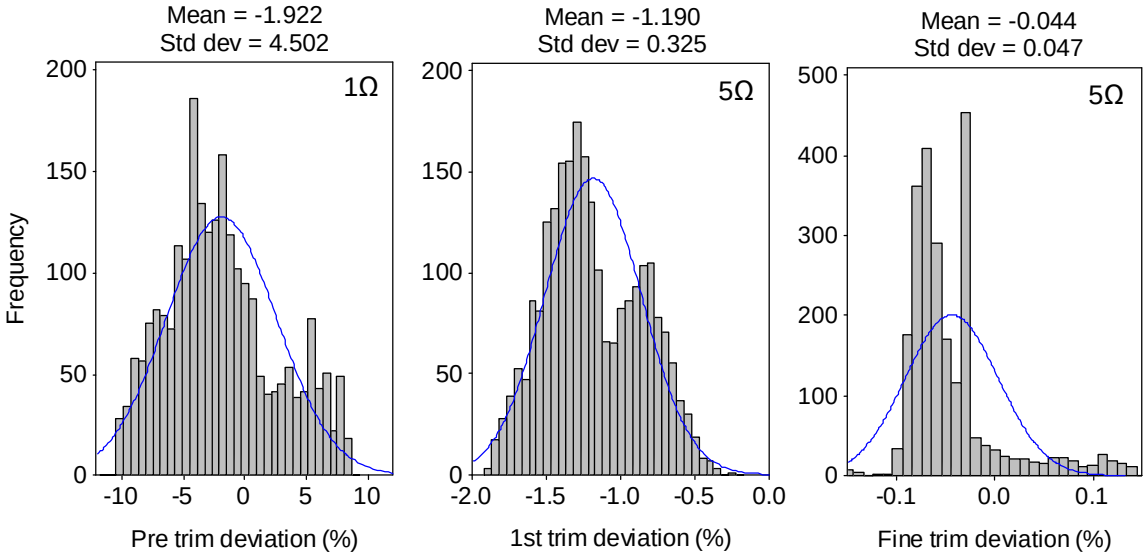

Fig. 8.4c – Resistance deviation from pre trim value of 1Ω and target trim value of 5Ω. Serpentine used for first trim and shadow plunge used for fine trim.

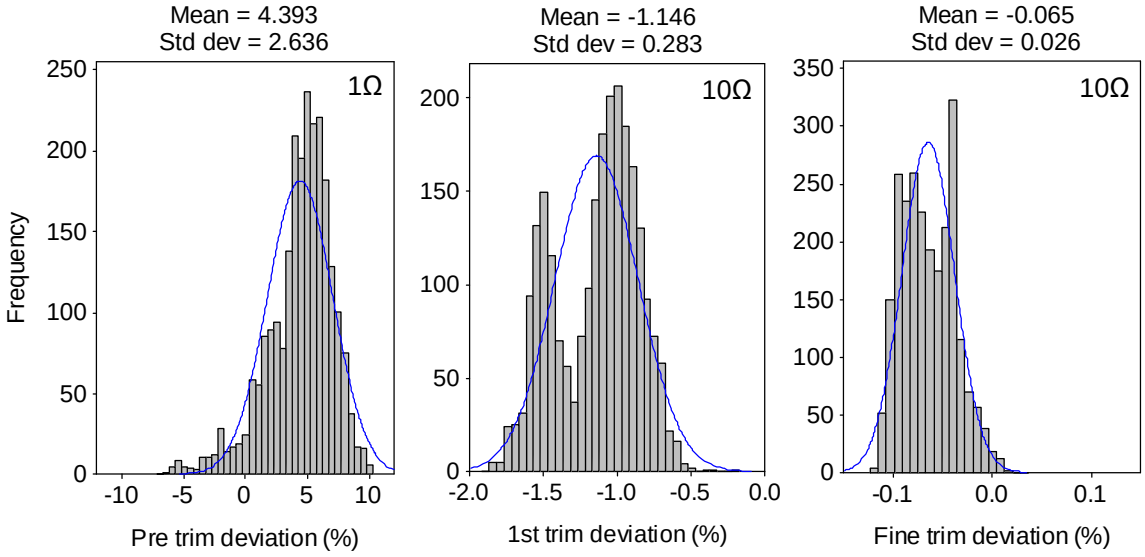

Fig. 8.4d – Resistance deviation from pre trim value of 1Ω and target trim value of 10Ω. Serpentine used for first trim and shadow plunge used for fine trim.

The standard deviation improves with each stage of the trimming process for all target values, from an average pre trim value of 4.23% to a first trim value of 0.23% and finally to a fine trim value of 0.036%.

Following fine trim the distribution is around ±0.1% for all four batches and at this stage the target tolerance limit of ±0.25% looks achievable. However during the fine trim stage it was observed that a number of chips were not being trimmed. The cause of this problem was found to be due to the resistance value shifting too positive during the

16 hour stabilisation stage between first trim and fine trim. This result is characterised by the extended 'tail' on the positive side of the fine trim distributions for the target values of 1.5Ω, 4Ω and 5Ω.

To understand if a lower first trim target offset would overcome this problem a decision was taken to fine trim the 10Ω batch to a slightly higher target value of 10.1Ω i.e. 1% higher. As shown the 'tail' has been eliminated from the fine trim distribution of the 10Ω batch and the standard deviation has been reduced to 0.026%. This result shows that lower first trim offsets are required to ensure that all chips in the batch remain low enough through the stabilisation process to allow them to be fine trimmed.

Final measure and TCR sample check

Once the four jobs were completed the resistance value of every chip was automatically measured on the tape packing machine. The resistance distribution data for a sample of 200 parts from each job is shown in Figure 8.5. The resistance tolerance limits were set in line with the tightest available for that value range in the target specification, see Appendix 1.

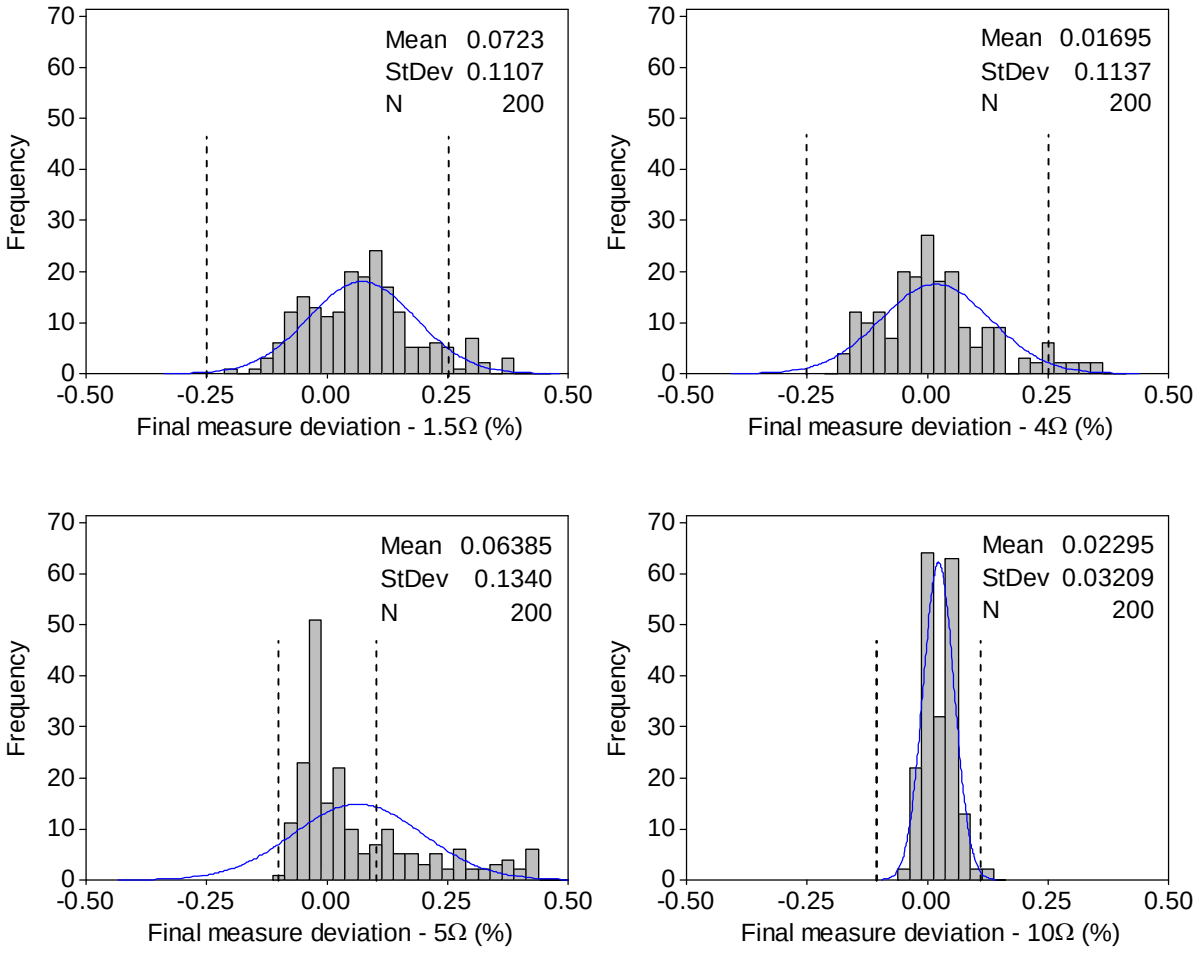

Fig. 8.5 – Final measure resistance deviations from target values of 1, 4, 5 and 10Ω, showing upper and lower tolerance limits

A summary of the end of line process yield achieved for each job is given in Table 8.5., together with results of TCR_{av} based on a random sample of 100pcs from each job.

Job value	Tolerance (±%)	Start qty	Good qty	Reject qty	Process yield (%)	TCR_{av} (±ppm/°C)	
						target	actual
1.5Ω - L cut	0.25	2394	2097	297	87.6	25	-7 to +9
4Ω - L cut			2140	254	89.4		-5 to +8
5Ω - Serpentine	0.10		1688	706	70.5	15	-8 to +4
10Ω - Serpentine			2238	156	93.5		-11 to +2

Table 8.5 – Summary of process yield data and TCR_{av} results for 1, 4, 5 and 10Ω jobs.

The process yields for the 1.5Ω and 4Ω batches are similar at 87.6 and 89.4% respectively, when measured to a final resistance tolerance of ±0.25%. Figure 8.5 shows that the mean value of the final measure distribution from the 4Ω batch is positioned very close to zero at 0.017%. Thus the fine trim offset of -0.025% used for this batch was reasonably accurate with the mean value moving ≈0.04% between laser and final measure. However the final measure data also shows that there is still a 'tail' of results on the positive side of the distribution caused by the first trim offset being too high. It appears that if this offset had been more accurate a greater proportion of the batch would have been within the final measure tolerance limits of ±0.25%.

The same can be said for the final measure distribution of the 1.5Ω batch, which also has a 'tail' of results outside the positive control limit. However in this case the mean of the data is also too positive at 0.07% and further improvements in yield could be achieved through a reduction in the final trim offset as well as that of the first trim.

This problem is amplified further for the 5Ω batch where a tighter final measure tolerance of ±0.1% was applied. Again a positive 'tail' of results has been left over from the inaccurate first trim offset, and, due to the tightened tolerance limits, has resulted in a further reduction in yield to 70.5%. However in this case, if the 'tail' of results is ignored, it can be seen that the distribution of the remaining data is adequately tight to achieve a much improved yield at the applied tolerance limit of ±0.1%.

Indeed, this assumption is confirmed by the result of the 10Ω batch, which was deliberately fine trimmed to a higher target value of 10.1Ω to overcome the effects of the inaccurate first trim offset. The standard deviation of this batch is 0.03% which is approximately three times lower than that of the other batches and results in a process yield of 93.5% when finally measured to the tighter tolerance of ±0.1%.

The results of TCR_{av} for all four batches are also presented in Table 8.5. Again the results for the 1.5Ω and 4Ω batches are comparable at -7 to +9 and -5 to +8ppm/ºC respectively. These figures are very similar to those reported in Table 8.4 for batches A to C following heat treatment, where the overall range of results was -8 to +10ppm/ºC.

The results for the 5Ω and 10Ω batches are slightly lower at -8 to +4 and -11 to +2ppm/ºC respectively. As discussed in chapter 7 this phenomenon is thought to be related to the decrease in the series TCR effect of the Ag terminations with increasing resistor element value.

Overall the results for TCR_{av} are within the target specifications of ±25ppm/ºC for values ≤4.7Ω and ±15ppm/ºC for values >4.7Ω (see Appendix 1). Furthermore the similarity between results at the heat treatment stage and for the completed parts demonstrates that the manufacturing process stages following heat treatment have negligible effect on the TCR_{av} of the batches. Indeed this result could possibly have been predicted from the fact that any temperature exposure that the films are subjected to during the process stages after heat treatment are much lower than the heat treatment temperature itself, as illustrated in Table 8.1.

8.4.2 Environmental Test Results

Environmental test results for all four jobs are presented in Tables 8.6a to 8.6d.

	Resistance change (ΔΩ%)				**Limits of resistance change (ΔΩ%+0.05Ω)**	
Test Description	**Min**	**Mean**	**Max**	**Std Dev**	**CECC 40401-801**	**Target**
Endurance at 70ºC	0.028	0.088	0.170	0.035	0.50	0.25
Damp heat steady state (DHSS)	0.017	0.072	0.129	0.024	1.00	0.30
Short term overload	0.010	0.033	0.088	0.024	0.25	0.25
Endurance at 125ºC	0.001	0.033	0.091	0.023	1.00	0.25
Rapid change of temperature (TRC)	0.005	0.053	0.19	0.051	0.25	0.10
Resistance to soldering heat	-0.075	0.042	0.124	0.055	0.25	0.20
Termination solderability	Pass				95% minimum coverage	

Table 8.6a – Environmental test performance data for 1.5Ω CuAlMo film resistors

	Resistance change (ΔΩ%)				Limits of resistance change (ΔΩ%+0.05Ω)	
Test Description	**Min**	**Mean**	**Max**	**Std Dev**	**CECC 40401-801**	**Target**
Endurance at 70ºC	0.010	0.054	0.093	0.023	0.50	0.25
Damp heat steady state (DHSS)	0.040	0.068	0.095	0.016	1.00	0.30
Short term overload	0.002	0.020	0.105	0.023	0.25	0.25
Endurance at 125ºC	0.019	0.058	0.111	0.025	1.00	0.25
Rapid change of temperature (TRC)	0.005	0.063	0.188	0.053	0.25	0.10
Resistance to soldering heat	0.000	0.044	0.137	0.042	0.25	0.20
Termination solderability	Pass				95% minimum coverage	

Table 8.6b – Environmental test performance data for 4Ω CuAlMo film resistors

	Resistance change (ΔΩ%)				Limits of resistance change (ΔΩ%+0.05Ω)	
Test Description	**Min**	**Mean**	**Max**	**Std Dev**	**CECC 40401-801**	**Target**
Endurance at 70ºC	0.018	0.048	0.086	0.017	0.50	0.25
Damp heat steady state (DHSS)	0.064	0.083	0.118	0.014	1.00	0.30
Short term overload	-0.006	0.012	0.104	0.026	0.25	0.25
Endurance at 125ºC	0.012	0.056	0.110	0.027	1.00	0.25
Rapid change of temperature (TRC)	0.002	0.043	0.160	0.045	0.25	0.10
Resistance to soldering heat	-0.067	-0.007	0.067	0.045	0.25	0.20
Termination solderability	Pass				95% minimum coverage	

Table 8.6c – Environmental test performance data for 5Ω CuAlMo film resistors

	Resistance change (ΔΩ%)				Limits of resistance change (ΔΩ%+0.05Ω)	
Test Description	**Min**	**Mean**	**Max**	**Std Dev**	**CECC 40401-801**	**Target**
Endurance at 70ºC	0.006	0.041	0.074	0.018	0.50	0.25
Damp heat steady state (DHSS)	0.061	0.078	0.096	0.010	1.00	0.30
Short term overload	-0.002	0.000	0.003	0.001	0.25	0.25
Endurance at 125ºC	0.012	0.065	0.108	0.025	1.00	0.25
Rapid change of temperature (TRC)	0.000	0.027	0.12	0.026	0.25	0.10
Resistance to soldering heat	-0.066	-0.023	0.000	0.027	0.25	0.20
Termination solderability	Pass				95% minimum coverage	

Table 8.6d – Environmental test performance data for 10Ω CuAlMo film resistors

From Tables 8.6a to 8.6d it can be seen that the environmental test results for all four CuAlMo resistor batches meet the target specification and are well within the CECC limits.

In addition to the excellent high temperature performance, which has been well established throughout the course of this research, the CuAlMo films also appear to perform well under the other environmental conditions such as humidity, load and overload.

However it should be re-emphasised that the DHSS test is largely a test of the resistance to humidity of the films protection layer rather than that of the film itself. Moreover the d.c. voltage stresses applied during load and overload testing are also at a minimum for low resistance parts for a fixed power rating.

Although these observations should not detract too much from the excellent reliability results achieved, they do support the initial decision made in chapter 1 to use the simple dry heat test as a benchmark of stability performance.

Of the environmental tests undertaken, that of TRC gave the worst result for all four resistor values when compared with test limits. Maximum resistance changes ranged from 0.12 to 0.19% against a target specification of ±0.1%+0.05Ω and CECC limit of ±0.25%+0.05Ω .

The TRC test comprises five cycles between the upper and lower device operating temperatures of -55ºC and +125ºC, with 30 minute soaks at each extreme. As the stability of the CuAlMo films had been well established at the upper category temperature (UCT), for periods of up to 1000 hours, it was suspected that the majority of resistance change was taking place during the lower category temperature (LCT) exposure.

To test this theory, the TCR of the CuAlMo film was tested across an extended temperature range of -75 to +175ºC. Figure 8.6 shows results for both CuAlMo and also NiCrMo 1Ω/□ films. The resistance measurements were carried out in a temperature cycling chamber (Associated Testing Laboratories, Type SLHU-1-LC), using a combination of CO_2 gas and electric heaters to achieve the required test temperature. The temperature was adjusted in 5ºC increments starting at +25ºC and decreasing to -75ºC and then increasing to +175ºC before finally decreasing back to +25ºC, with a 5 minute soak at each point. Resistance measurements are all based on the average of ten components each measured three times at every temperature increment.

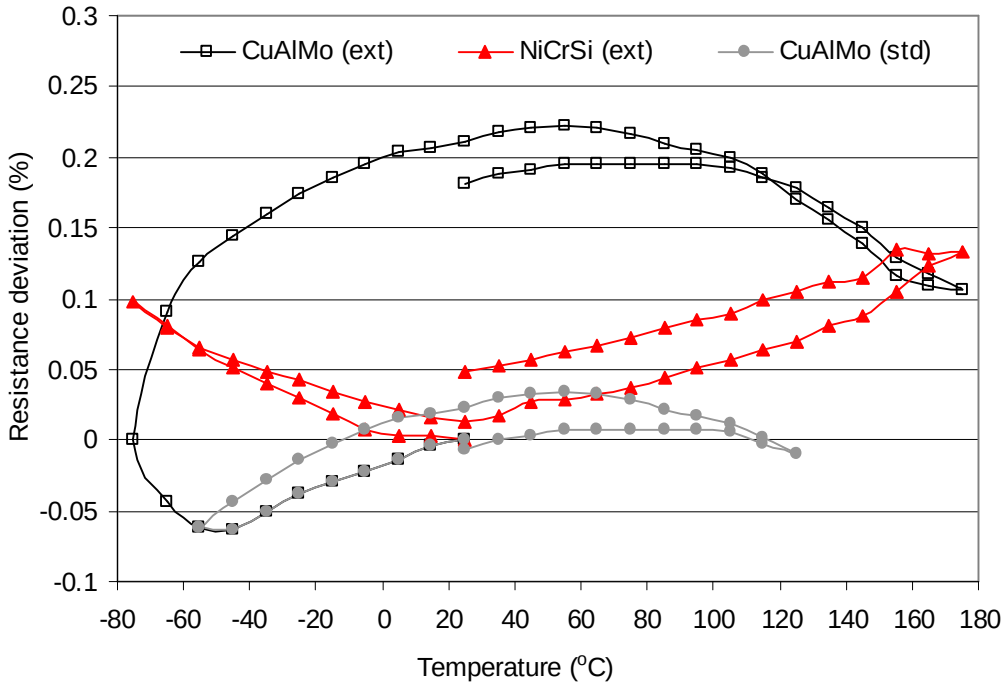

Fig. 8.6 – Resistance deviation with temperature for CuAlMo and NiCrMo 1Ω/□ films across an extended operating temperature range of -75 to +175ºC

Two important results which can be established from Figure 8.6 are the irreversibility of resistance and the extended TCR (TCR_{ex}) of the films. For both of these tests it is usual to specify an upper and lower temperature result as reported in Table 8.7.

Test	Temperature Range (ºC)	NiCrMo (ext) (-75 to +175ºC)	CuAlMo (ext) (-75 to +175ºC)	CuAlMo (std) (-55 to +125ºC)
Irreversibility of resistance (%)	+25 / LCT / +25	0.01	0.21	0.02
	+25 / UCT / +25	0.04	-0.03	-0.02
TCR_{ex} (ppm/ºC)	+25 to -55	+5 to +11	-12 to -2	-12 to -2
	+25 to +125	+1 to +11	-8 to 0	-8 to 0
TCR_{av} (ppm/ºC)	+25 to +75	0 to +9	-3 to +5	-3 to +5

Table 8.7 – Mean irreversibility of resistance and TCR results for CuAlMo and NiCrMo 1Ω/□ films

From Figure 8.6 it can be seen that the mean resistance of the CuAlMo films decreases with both negative and positive changes in temperature, whilst that of the NiCrMo films increase in both temperature directions. Indeed the plots for the two materials are virtually a mirror image of one another.

As reported in Table 8.7 the irreversibility of resistance for the NiCrMo film is better than 0.05% following subjection to both negative and positive extended temperatures of -75 and +175ºC. However the same cannot be said for the CuAlMo film where there is a mean change of >0.2% following the negative temperature cycle. Although this result would appear to be unacceptable, it can be seen from Figure 8.6 that the vast majority of this resistance change occurs in the temperature range -60 to -80ºC, which is outside the specified device operating temperature range of -55 to +125ºC.

To determine if the performance of the CuAlMo films would be acceptable across this normal operating temperature range, a second curve, CuAlMo (std), has been plotted in Figure 8.6, the results of which are also reported in Table 8.7. By restricting the test temperature range to -55 to +125ºC the resistance changes following subjection to both negative and positive temperature cycles is reduced to an acceptable figure of ±0.02%.

The results for the TCR_{ex} are also reported in Table 8.7. For both film types a figure of less than ±15ppm/ºC is achieved with the sign of the results determined by the shape of the plot in Figure 8.6., positive for NiCrMo and negative for CuAlMo. It is also interesting to note the flatness of the CuAlMo plot in the 25 to 100ºC temperature range, which is the area in which $TCR_{av,}$ the most universally accepted TCR specification, is calculated. Results for TCR_{av} are also presented in Table 8.7 and the figure of -3 to +5ppm/ºC reported for the CuAlMo film is again well within the target of ±15ppm/ºC and gives good comparison with previous results.

8.5 SUMMARY

Work carried out in this chapter has focused on the repeatable manufacture of production size batches of CuAlMo thin film resistors under the previously established optimum process conditions.

Three separate batches of standard 1206 size surface mount resistors, each containing ≈10,000 parts, were deposited with the CuAlMo film and annealed under the optimum conditions reported in chapter 5. The pre-value resistance distribution across all three batches was found to be within ±15% of the target value of 1Ω and the TCR_{av} was ≤ 0±10ppm/ºC following heat treatment for four hours at 425ºC.

Substrates from each of the three pre-value depositions were then mixed together to produce four jobs containing ≈2,400 parts each. These batches were laser adjusted to target values of 1.5, 4, 5 and 10Ω using the optimised two stage laser adjust process established in chapter 7. The laser had no difficulties in handling the mixed pre-value resistance distribution of ±15% and, with correct resistance offset selection, was able to produce final trim resistance distributions of < ±0.10% of target value.

Following laser adjustment, manufacture of the components was completed under standard process conditions. No major problems were encountered during this stage and overall process yields in the range 70.5 to 93.5% were achieved for the four target values, with the highest yield being achieved for the 10Ω batch after adjustment of the laser trim offset. The end of line TCR_{av} of all four batches was also found to still be within the target 0±15ppm/ºC, thus confirming that the manufacturing process stages following heat treatment had negligible effect on the TCR of the CuAlMo films.

Once completed the four batches were subjected to a series of environmental tests to check their reliability. In addition to their excellent dry heat performance, which has been established in earlier chapters, the CuAlMo films were also found to perform well under other environmental conditions such as humidity, load and overload, and the results of all tests were within both the target and CECC specifications.

One slight concern highlighted during environmental testing was the results achieved for the TRC test. Although these figures were within specification, they were on average, inferior to those obtained for the other tests. Further investigation of this result revealed the low temperature exposure during the TRC test to be the most likely cause, where the CuAlMo films were found to be unstable at temperatures just below the LCT of -55ºC, when compared with control samples made from NiCrMo films.

As this relative instability of the CuAlMo film appears to occur outside the normal operating temperature range of -55 to +125ºC, it is not considered a specific performance requirement, it is however suggested as a recommended area for further investigation in chapter 9.

Another important property of the CuAlMo films that has been established is that of TCR_{ex}, where figures of better than 0±15ppm/ºC were reported across both negative and positive extended temperature ranges.

Overall this chapter has given an insight into the manufacturability of CuAlMo thin film resistors in a production environment. Batches of resistors have been manufactured in the range 1 to 10Ω with excellent process yields being achieved. The reliability performance of these parts has also been verified through the successful completion of an environmental test programme to both target and CECC requirements.

Chapter 9

Conclusions

9.1 CONCLUSIONS

The research detailed in this thesis has developed a new material system of CuAlMo for use in the manufacture of low value thin film resistors.

An initial investigation into the electrical properties of binary thin films sputtered from a multi sectioned target of copper and aluminium, suggested that a composition range of approximately 30 to 60at.% Al possessed suitable electrical properties, such as low resistivity and good long term stability. However, the TCR values of these films were too positive at around +300ppm/ºC and therefore unsuitable for use as thin film resistors.

By doping the CuAl sputtering target with small amounts of molybdenum (5-10at.%) the as-grown TCR of the films was reduced, becoming negative with a value of approximately -100ppm/ºC. Following post deposition heat treatment in the temperature range 350 to 450ºC this TCR property could be raised to near zero whilst also giving a significant reduction in the sheet resistance of the films. The key mechanisms responsible for these changes were found to be annealing of impurities incorporated during the deposition process, grain growth and also the formation of a stable Cu_9Al_4 phase.

Fine tuning of the Mo concentration in the film suggested the optimum chemical composition to be ≈ 69/24/7wt.% CuAlMo. Several compositional analysis methods were employed to confirm this ratio, before it was used to specify the manufacture of a full scale composite sputtering target.

Next, the outcomes of varying the deposition parameters of this composite CuAlMo sputtering target on the properties of the films were studied. The optimum electrical performance was obtained with a high cathode power of 1000W and a sputtering pressure of 1 to 3mTorr, where the film structure was found to be more crystalline due to increases in the thermal energies involved. Following deposition, the TCR of the films could be raised to near zero by annealing at around 425ºC for 4 hours.

The electrical conduction mechanisms were then investigated by studying the variation in resistivity with increasing thickness of the CuAlMo films, sputtered under these optimised conditions. For films in the thickness range <200nm there was an increase in resistivity above the bulk value due to the combined effects of surface roughness, surface scattering and grain boundary scattering. For thicknesses beyond 200nm, bulk conductivity was assumed. For films in the as-grown state, values of the mean free path and bulk resistivity were found to be 15nm and 90μΩcm respectively.

Once optimisation of the electrical properties of the films was complete, they were then laser trimmed to target resistance value. Firstly, the effects of varying the laser beam properties on the extent of the heat affected zone (HAZ) surrounding the laser kerf were investigated. The best results were achieved using a low power, short bite size and medium Q-rate. Two cut types were then used to first trim the films to within -2% of target value; the L-cut for trim gains <5 and the serpentine cut for trim gains ≥5. The films were then stabilised for 16 hours at 250ºC to further reduce the effect of the first trim HAZ, before being fine trimmed to final tolerance. By positioning the fine trim in an area of low current density, final trim tolerances of ≤ ±0.1% were achieved.

Several production size batches were then manufactured under these optimum conditions and samples were subjected to series of environmental test procedures. Results of all tests were found to be well within both CECC specifications and also the target specifications of the investigation.

Overall, the investigation has been successful and all the required objectives have been achieved or even surpassed. Through research and systematic experimentation a new thin film resistor material of CuAlMo has been developed which has both lower resistivity and faster deposition rate properties than that of the popular NiCr system, and when manufactured using a set of optimised process parameters, thin film resistors in the value range 1 to 10Ω can be repeatedly produced to tolerances of resistance better than ±0.1% and TCR_{av} values of less than 15ppm/ºC. It has also been shown that if accurately laser adjusted to target resistance value, end of line yields in excess of 90% are achievable.

Estimated Financial Benefits

Although this study has not investigated the financial benefits of using the new CuAlMo resistor film, there are several advantages it has over the current NiCr based materials. Firstly at the duration of the deposition stage the resistivity of the CuAlMo film is around one third that of the NiCrMo film and the sputter rate is approximately 20% higher. This means that equivalent sheet resistances can be sputtered in shorter time-scales and lower sheet resistances can be achieved in an equivalent time-scale. Moreover this will also give savings in target material usage, which in addition has also been suggested to be less expensive to manufacture.

Secondly, at laser adjust, the relatively thinner CuAlMo films are also easier to laser cut through, allowing increases in trim speed to be made. Furthermore, with the potential for films with lower sheet resistances comes the opportunity to increase trim gain and in turn produce batches to tighter resistance tolerances giving increased production yields.

Although these benefits can be realised across both axial leaded and SMD technologies, it is within the axial leaded process that the greatest financial savings will be achieved, due to the long deposition cycle times. This will also give savings in equipment wear and downtime with reductions in various maintenance procedures such as target changeovers and cryo pump regeneration.

9.2 RECOMMENDATIONS

9.2.1 Recommendations Resulting From the Investigation

The following section details work required to allow the successful manufacture of both SMD and axial leaded CuAlMo resistors and also some suggestions to improve their performance.

- ***Approve full range of SMD resistor sizes***
  As the approval exercise undertaken in chapter 8 only considered one of the four standard surface mount resistor sizes, the 1206, additional work will be required to approve the other sizes detailed in the target specification i.e. 0805, 2010 and 2512.

- ***Manufacture lower sheet resistance films***
  As discussed in chapters 7 and 8, the lowest film sheet resistance sputtered for approval testing was ≈ 0.7Ω/□. This was a result of a restricted cathode power and also the lower limit of pallet drive system. Although it was shown that lower sheet resistances could be achieved with the pallet being stationary below the centre of the target, the film uniformity was inferior to the moving pallet and therefore unsuitable for use in production. To achieve lower sheet resistance films with acceptable uniformity across the sputtering pallet will require modifications to the pallet drive system and also higher cathode powers.

- ***Transfer process to axial resistor manufacture***
  Once manufacture has been fully established for the production of surface mount resistors it will then be transferred to the axial resistor process. It is within this application that the full benefits of the lower resistivity CuAlMo material will be realised. It is envisaged that films will be sputtered to lower sheet resistances than the current NiCrMo film at faster rates, giving both material and labour savings. Moreover the ‘mixing’ action of the barrel sputtering plant should produce further improvements in film uniformity, giving the possibility of achieving even tighter TCR tolerances.

- ***Optimise laser trim offsets***

  As demonstrated in chapter 8, improvements in final measure yields can be attained through accurate laser trim offset selection. This will be achieved in production by processing samples to establish the optimum trim offset before the full batch is adjusted. Once a history of offsets is built up it should be possible to use this to predict the required offset for a given target value.

- ***Improved target manufacture***

  As discussed in chapter 4, problems were encountered during the manufacture of both CuAlMo composite targets when trying to attain the required chemical composition. This is an issue which must be resolved if CuAlMo resistors with repeatable properties are to be manufactured in production. The composition of the second target was much closer to the required specification than the first and it is hoped that this situation will continue to improve as the supplier gains more experience with this material system.

9.2.2 Suggestions for Future Research

The following section highlights some potential areas worthy of further consideration.

- ***Composite TCR effect***

  As briefly discussed in chapter 7, as the sheet resistance of the CuAlMo resistor film becomes lower, the series resistance effect from the large positive TCR of the resistor terminations will have a greater impact on the overall TCR of the device. To compensate for this effect, further investigation will be required in the areas of sputter deposition and heat treatment. It is envisaged that areas such as the bulk TCR of the sputtering target and also the final heat treatment temperature may require adjustment to produce films with a lower TCR.

- ***Extended operating temperature range***

  With recent demands for resistors to operate in higher temperature applications such as automotive (under hood) and oil exploration (down hole drilling), it would be considered a useful exercise to characterise the performance of the CuAlMo resistors in the extended temperature range up to approximately 200ºC [290]. Moreover, although there is no real consumer demand for devices to operate in the extended negative temperature range beyond -55ºC, it too is also considered a beneficial area for further investigation due to the uncharacteristic stability results reported in chapter 8 in this temperature region.

- ***Effects of sputtering pressure***

  As discussed in chapter 5, due to production requirements for the sputtering plant, it was only possible to investigate the effects of sputtering pressure on the electrical properties of the CuAlMo films over a limited sputtering pressure range through adjustment of the argon flow rate. Therefore an area considered worthy of further investigation would be that of a wider sputtering pressure range through adjustment of both argon flow rate and also cryo pump throttle valve.

REFERENCES

1. L. Maissel and R. Glang, (1970), Handbook of Thin Film Technology, *McGraw-Hill Publications*, pg18-4.

2. B. Kang, S. Hur, D. Kim and S. Yoon, (2005), Thickness dependence of the electrical properties of CuNi thin film resistors grown on AlN substrates for π-type attenuator application, *Electrochemical and Solid State Letters*, 8(4) pgG92-G94.

3. R. Kennedy, (1999) Materials for thin film resistors, *Advancing Microelectronics*, 26(5) pg12-17.

4. A. Elshabini-Riad and F. Barlow, (1998), Thin Film Technology Handbook, *McGraw-Hill Publications,* pg3.1-3.19, 5.32-5.36.

5. J. Van Den Broek, J. Donkers, R. Van Der Rijt and J. Janssen, (1998), Metal film precision resistors: resistive metal films and a new resistor concept, *Philips Journal of Research,* 51(3) pg429-447.

6. A. Jankowski, (1998), Characterizing and modelling the apparent anomalous behaviour of resistivity in Cr-Si-O thin films, *Thin Solid Films,* 332 pg272-276.

7. X. Dong, J. Wu, D. Mao and L. Mao, (2000), Comparison of NiCr-O and Cr-Si thin film resistors with mid-range of electric resistance, *Shanghai Jiaotong Daxue Xuebao/Journal of Shanghai Jiaotong University*, 34(12) pg1610-1614.

8. A. Jankowski and J. Hayes, (2002), Ti-Cr-Al-O thin film resistors, *Thin Solid Films,* 420-421 pg487-491.

9. Y. Kwon, N. Kim, G. Choi, W. Lee, Y. Seo and J. Park, (2005), Structural and surface properties of NiCr thin films prepared by DC magnetron sputtering under variation of annealing conditions, *Microelectronics Engineering,* 82(3-4) pg314-320.

10. V. Seema, (2002), Development and TCR control of nichrome thin film resistors for GaAs MMICs, *Proceedings of SPIE - The International Society for Optical Engineering*, 4746(II) pg936-939.

11. G. Ventura, L. Lanzi, I. Peroni, A. Peruzzi and G. Ponti, (1998), Low temperature thermal characteristics of thin-film Ni-Cr surface mount resistors, *Cryogenics,* 38 pg453-454.

12. BS EN 60115-1, (2001), Fixed Resistors for use in electronic equipment, *CENELEC European Component Committee (CECC), where CENELEC is the European Committee for Electrotechnical Standardisation,* pg1-104.

13. F. Kruger, (1919), British Patent 157,909.

14. F. Wu, A. McLaurin, K. Henson, D. Managhan and S. Thomasson, (1998), The effects of the process parameters on the electrical and microstructure characteristics of the CrSi thin resistor films: Part 1, *Thin Solid Films,* 332 pg418-422.

15. P. Hall, (1997), Resistance calculations for thin film rectangles, *Thin Solid Films,* 300 pg256-264.

16. M. Jonas and A. Peled, (1982), The equivalent temperature coefficient of resistance of thin film resistor-conductor structures, *Thin Solid Films,* 90(4) pg385-391.

17. A. Peled, Y. Zloof, V. Baranauskas and J. Farhadyan, (1994), The midrange and high temperature dependence of vacuum deposited NiCr thin film resistors, Vacuum, 45(1) pg5-10.

18. A. Peled, (1985), Evaluating temperature coefficient of resistance values for thin film resistors, *Hybrid Circuit Technology, October 1985*, pg50-54.

19. R. Veyhl, (1991), Temperature dependence of thin film resistors, *11th Capacitor and Resistor Technology Symposium (CARTS),* pg90-94.

20. G. Zhigal'skii and B. Jones, (2003), Electrocomponent Science Monographs – The Physical Properties of Thin Metal Films, *Taylor and Francis Publications.* pg1-34.

21. L. Maissel, (1968), Thin film resistance materials and characteristics, *Solid State Technology,* 11(5) pg27-32.

22. P. Rossiter, (1987), Cambridge Solid State Science Series - The Electrical Resistivity of Metals and Alloys, *Cambridge University Press*. pg1-28, 137-271.

23. Y. Kwon, N. Kim, G. Choi, W. Lee, Y. Seo and J. Park, (2005), Structural and surface properties of NiCr thin films prepared by DC magnetron sputtering under variation of annealing conditions, *Microelectronic Engineering,* 82(3-4) pg314-320.

24. H. Degenhart and L. Pratt, (1963), Temperature and other characteristics of thin film nichrome resistors on various substrate materials, *Electronic Engineers International Convention*, 11(6) pg59-68.

25. S. Petrovic, N. Bundaleski, M. Radovic, Z. Ristic, G. Gilgoric, D. Perusko, M. Mitric, B. Pracek, A. Zalar and Z. Rakocevic, (2007), Surface composition and structure of Ni-Cr sputtered coatings exposed in air at room temperature, *Nuclear Instruments and Methods in Pysics Research B*, 256(1) pg368-372.

26. J. Swanson and D. Campbell, (1967), The structural and electrical properties of 80:20 NiCr thin films, *Thin Solid Films,* 1(3) pg183-202.

27. S. Hofmann and A. Zalar, (1976), Correlation between electrical properties and AES concentration depth profiles of NiCr thin films, *Thin Solid Films,* 39(1-2-3) pg219-225.

28. M. Birjega, N. Popescu-Pogrion, C. Sarbu and I. Teodorescu, (1978) Structural Transformations Induced During the Annealing of Thin Ni-Cr Films, *Thin Solid Films,* 57(2) pg337-341.

29. I. Kazi, P. Wild, T. Moore and M. Sayer, (2006) Characterisation of sputtered nichrome (Ni-Cr 80/20 wt. %) films for strain gauge applications, *Thin Solid Films,* 515(42) pg2602-2606.

30. J. Yan and J. Zhou, (2007), Optimising of strain sensitivity and electric characteristics of Ni-Cr thin film fabricated by magnetron sputtering, *Materials Science and Technology,* 23(2) pg195-202.

31. Z. Jicheng and Y. Jianwu, (2007), Microstructure and electrical properties of nano Ni-Cr thin-films fabricated by magnetron co-sputtering techniques, *Materials Science Forum,* 561-565(2) pg1201-1204.

32. D. Nachrodt, U. Paschen, A. Have and H. Vogt, (2008), Ti/Ni(80%)Cr(20%) thin-film resistor with a nearly zero temperature coefficient of resistance for integration in a standard CMOS process, *IEEE Electron Device Letters,* 29(3) pg212-214.

33. R. Kopf, R. Melendes, D. Jacobson, A. Tate, M. Melendes, R. Reyes, R. Hamm, Y. Yang, J. Frackoviak, N. Welmann, H. Maynard and C. Liu, (2002), Thin-film resistor fabrication for InP technology applications, *Jounal of Vacuum Science and Technology B: Microelectronics and Nanometer Structures,* 20(3) pg871-875.

34. D. Sridhara Rao, K. Muraleedharan, S. Vinayak and H. Vyas, (2002), TEM characterisation of Nichrome thin films, *Proceedings of SPIE - The International Society for Optical Engineering*, 4746(2) pg1190-1194.

35. S. Vinayak, H. Vyas, K. Muraleedharan and V. Vankar, (2006), Ni-Cr thin film resistor fabrication for GaAs monolithic microwave integrated circuits, *Thin Solid Films,* 514(1-2) pg52-57.

36. M. Birjega, C. Constantin, I. Florescu and C. Sarbu, (1982), Crystallisation of amorphous sputtered 55%Cr-45%Ni thin films, *Thin Solid Films,* 92(4) pg315-321.

37. N. Dhere, D. Vaiude and W. Losch, (1979), Composition and temperature coefficient of resistance of Ni-Cr thin films, *Thin Solid Films,* 59(1) pg33-41.

38. R. Nahar and N. Devashrayee, (1983), Electrical properties of RF sputtered NiCr thin film resistors with Cu contacts, *Electrocomponent Science and Technology,* 11 pg43-51.

39. A. Bhatt, C. Lock and D. Stevenson, (1984), DC sputtering of Ni-Cr thin film resistors, *International Society for Hybrid Microelectronics*, pg370-376.

40. H. Anklam, (1984), Influence of the substrate on the annealing behaviour of sputter-deposited Ni-Cr films, *Thin Solid Films,* 121(1) pg61-68.

41. C. Au, M. Jackson and W. Anderson, (1987), Structural and electrical properties of stable Ni/Cr thin films, *Journal of Electronic Materials,* 16(4) pg301-306.

42. W. Bruckner and S. Baunack, (1999), Electrical resistance and mechanical stress in NiCr/Cu/NiCr thin films, Journal of Applied Physics, 85(2) pg935-939.

43. B. Lee, G. Park, D. You and D. Lee, (2003), Composition control and electrical properties of Ni-Cr thin films prepared by co-sputtering method, *Conference on Electrical Insulation and Dielectric Phenomena (CEIDP), Annual Report,* pg72-74.

44. N. Phuong, D. Kim, B. Kang, C. Kim and S. Yoon, (2006), Effect of chromium concentration on the electrical properties of NiCr thin film resistors deposited at room temperature by magnetron cosputtering technique, *Journal of the Electrochemical Society,* 153(1) pgG27-G29.

45. M. Nguyen and S. Yoon, (2006), Effect of deposition temperature on the structural and electrical properties of NiCr thin-film resistors by magnetron sputtering, *Journal of the Electrochemical Society*, 153(7) pgG606-G608.

46. M. Koltai, I. Trifonov and M. Czermann, (1983), Segregation phenomena in thin NiCr layers, *Vacuum,* 33(1-2) pg49-52.

47. H. Dintner and F. Thrum, (1989), The homogeneous distribution of non-metallic bonds in as deposited NiCr-O resistive films, *Physica Status Solidi (A) Applied Research,* 111 pg551-556.

48. G. Nocerino and K. Singer, (1978), The Electrical and Compositional Structure of Thin Ni-Cr Films, *Thin Solid Films,* 57(2) pg343-348.

49. J. Griessing, (1977), Reactive sputtering of NiCr resistors with closely adjustable temperature coefficient of resistance, *Electrocomponent Science and Technology*, 4 pg133-137.

50. W. Hardy D. Murti, (1974), Electrical and structural properties of NiCr thin film resistors reactively sputtered in O2, *Thin Solid Films*, 20(2) pg345-362.

51. D. Buczek, (1978), Thin-film NiCr Resistor, *Journal of Vacuum Science and Technology,* 15(2) pg370-372.

52. G. Nocerino and K. Singer, (1979), Resistance stabilization of Ni-Cr films by surface oxide formation, *Journal of Vacuum Science and Technology,* 16(2) pg147-150.

53. J. Zelenska, V. Chudoba, J. Rehak and K. Rohacek, (1991), Thin resistive film with temperature coefficient of resistance close to zero, *Thin Solid Films,* 200(2) pg239-246.

54. E. Schippel, (1984), Properties of evaporated Ni-Cr films with an aluminum content of about 50%, *Thin Solid Films,* 123(1) pg57-62.

55. E. Schippel, (1987), Ternary alloy films of Ni-Cr-Al for thin film resistors, *Thin Solid Films,* 146(2) pg113-138.

56. A. Singh, (1986), Discharge treatment technique for fabricating Nichrome-aluminium thin film resistors, *Thin Solid Films,* 138(2) pg63-65.

57. A. Andziulis, B. Andziuliene, J. Vaupsas and M. Zadvydas, (2006), High stability nano-multilayer resistive films, *Surface and Coatings Technology,* 200 pg6212-6217.

58. W. Gawalek, (1983), Resistance, temperature coefficient of resistance and long-term stability of annealed thin NiCrSi films, *Thin Solid Films,* 116(1-3) pg205-210.

59. B. Lee, G. Park, J. Kim and D. Lee, (2002), The effect of the process parameters on the electrical properties of Ni-Cr-Si alloy thin film resistors, *Conference on Electrical Insulation and Dielectric Phenomena (CEIDP), Annual Report 2002*, pg72-74.

60. F. Chang and L. Kang, (1990), The influence of iron on properties of deposited NiCrSi resistors, *Thin Solid Films,* 185 pg341-346.

61. E. Schippel, (1986), The influence of silicon on properties of deposited Ni-Cr films, *Thin Solid Films,* 144(1) pg21-28.

62. J. Mooij and M. Jong, (1972), Structural and electrical properties of sputtered CrNi Films, *Journal of Vacuum Science and Technology,* 9(1) pg446-449.

63. R. Kaneoya, T. Matsumoto, K. Moriya and T. Jinno, (1974), Studies of high accuracy Ni/Cr/Si thin film resistor for PCM-120 system, *Review of the Electrical Communications Laboratories,* 22(1-2) pg82-91.

64. A. Satrapinski, A. Savin, S. Novikov and O. Hahtela, (2008), Experimental study of evanohm thin film resistors at subkelvin temperatures, *Measurement Science & Technology,* 19 pg1-5.

65. B. Lee and D. Lee, (2002), Electrical properties of sputtered Ni-Cr-Al-Cu thin film resistors with Ni and Cr contents, *Journal of the Korean Physical Society,* 40(2) pg339-343.

66. B. Lee, B. Lee and D. Lee, (2003), Quaternary alloy films for thin film resistors, *Japanese Journal of Applied Physics, Part 1: Regular Papers and Short Notes and Review Papers,* 42(1-3) pg1405-1409.

67. W. Isler and L. Kitchman, (1969), Influence of deposition and processing parameters on the TCR of Ni-Cr-Cu-Al alloy film resistors, *IEEE Transactions on Parts, Materials and Packaging,* 5(3) pg139-146.

68. S. Hur, D. Kim, B. Kang and S. Yoon, (2004), Effect of the deposition temperature on temperature co-efficient of resistance in CuNi thin film resistors, *Journal of Vacuum Science and Technology B: Microelectronics and Nanometer Structures,* 22(6) pg2698-2701.

69. M. Ishikawa, H. Enomoto, N. Mikamoto, T. Nakamura, M. Matsuoka and C. Iwakura, (1998), Preparation of thin film resistors with low resistivity and low TCR by heat treatment of multilayered Cu/Ni deposits, *Surface & Coatings Technology,* 110(3) pg121-127.

70. M. Ishikawa, H. Enomoto, N. Mikamoto, T. Nakamura, H. Nawafune, T. Uegaki, S. Mizumoto, M. Matsuoka and C. Iwakura, (2000), Preparation of Cu-Ni film resistors with low resistivity and low TCR, *Transactions of the Institute of Metal Finishing,* 78(2) pg86-88.

71. W. Bruckner, J. Schumann, S. Baunack, W. Pitschke and T. Knuth, (1995), Resistance behaviour and interdiffusion of layered CuNi-NiCr films, *Thin Solid Films,* 258(1) pg236-246.

72. S. Hur, D. Kim, B. Kang and S. Yoon, (2004), Characteristics of CuNi alloy deposited by magnetron sputtering for thin film resistor, *Meeting Abstracts, 2004 Joint International Meeting - 206th Meeting of the Electrochemical Society/2004 Fall Meeting of the Electrochemical Society of Japan,* pg942.

73. S. Hur, D. Kim, B. Kang and S. Yoon, (2005), The structural and electrical properties of CuNi thin-film resistors grown on AlN substrates for π-Type attenuator application, *Journal of the Electrochemical Society*, 152(6) pgG472-G476.

74. B. Kang, S. Hur, D. Kim and S. Yoon, (2005), Thicknes dependence of the electrical properties of CuNi thin film resistors grown on AlN substrates for II-type attenuator application, Electrochemical and Solid State Letters, 8(4) pgG92-G94.

75. I. Nishino, Y. Ichinose, Y. Sorimachi and I. Tsubata, (1985), Evaluation of Cu-Ni alloy as a material of thin film resistors, International Journal for Hybrid Microelectronics, 8(1) pg18-23.

76. C. Au, W. Anderson, D. Schmitz, J. Flassayer and F. Collins, (1990), Stability of tantalum nitride thin film resistors, *Journal of Materials Research*, 5(6) pg1224-1232.

77. S. Yoshida, (1982), Mass production of HCP tantalum nitride film resistors sputtered by planar magnetron, *Proceedings of the 32nd Electronic Components Conference, San Diego, CA, XII, published by IEEE*, pg530-535.

78. K. Radhakrishnan, Ng. Ing and R. Gopalakrishnan, (1999), Reactive sputter deposition and characterization of tantalum nitride thin films, *Materials Science and Engineering,* B57 pg224-227.

79. Y. Lu, R. Weng, W. Hwang and Y. Yang, (2001), Electrical properties of Ta_xN_y films by implementing OES in the sputtering system, *Materials Chemistry and Physics,* 72 pg278-280.

80. N. Cuong, D. Kim, B. Kang, C. Kim K. Yu and S. Yoon, (2006), Characterisation of tantalum nitride thin films deposited on SiO_2 Si substrates using dc magnetron sputtering for thin film resistors, *Journal of the Electrochemical Society,* 153(2) pgG164-G167.

81. A. Razborsek and F. Schwager, (1988), Thin Film Systems For Low TCR Resistors, *Vacuum,* 38(8-10) pg689-692.

82. K. Min, K. Chun and K. Kim, (1996), Comparative study of tantalum and tantalum nitrides (Ta_2N and TaN) as a diffusion barrier for Cu metalization, *Journal of Vacuum Science & Technology,* 14(5) pg3263-3269.

83. G. Chen, S. Chen, L. Yang and P. Lee, (2000), Evaluation of single and multilayered amorphous tantalum nitride thin films as diffusion barriers in copper metallization, *Journal of Vacuum Science & Technology,* 18(2) pg720-723.

84. G. Golan, A. Axelevitch, R. Margolin and E. Rabinovitch, (2001), Novel approach to sputtered tantalum film resistors with controlled pre-defined resistance, *Microelectronics Journal,* 32 pg61-67.

85. R. Pitetti, H. Keller and J. Morabito, (1982), High pressure steam stabilisation of tantalum thin film resistors, *Thin Solid Films,* 87(1) pg1-11.

86. W. Ostrander, J. Verhoef and L. Bos, (1973), Processing and performance of tantalum nitride thin film resistor networks with ±50ppm/°C TCR, *IEEE Transactions on Parts, Hybrids & Packaging,* 9 pg155.

87. R. Petrovic, T. Nenadovic, N. Kraljevic and T. Dimitrijevic, (1978), Electrical and Structural Properties of Tantalum Nitride Thin Films Deposited by Sputtering, *Thin Solid Films,* 57(2) pg333-336.

88. S. Abdin, C. Val, (1979), Production of tantalum nitride film resistors using a continuous sputtering machine, Thin Solid Films, 57(2) pg327-331.

89. N. Cuong, D. Kim, B. Kang and S. Yoon, (2006), Structural and electrical characterisation of tantalum nitride thin film resistors deposited on AlN substrates for π-type attenuator applications, *Materials Science and Engineering B: Solid State Materials for Advanced Technolgy*, 135(2) pg162-165.

90. N. Cuong, N. Phuong, D. Kim, B. Kim, C. Kim and S. Yoon, (2006), Effect of annealing temperature on structural and electrical properties of tantalum nitride thin film resistors deposited on SiO2/Si substrates by dc sputtering technique, *Journal of Vacuum Science and Technology B,* 24(2) pg682-685.

91. A. Scandurra, G. Indelli, B. Pignataro, S. DiMarco, M. Stefano, S. Ravesi and S. Pignataro, (2007), Tantalum nitride thin film resistors by low temperature reactive sputtering for plastic electronics, *Surface and Interface Analysis,* 40 pg758-762.

92. A. Das, C. Grabbe and R. Hufnagel, (2008), Complexities in the deposition of thin film resistors, *Capacitor and Resistor Technology Symposium (CARTS) 2008*, pg339-352.

93. W. Hardy, D. Mills, (1973), Effects of deposition temperatures on Ta thin film resistors reactively sputtered in oxygen, *Journal of Vacuum Science & Technology,* 10(1) pg303-306.

94. S. Kang, S. Yoon, S. Suh and D. Yoon, (2008), Control of electrical resistivity of TaN thin films by reactive sputtering for embedded passive resistors, *Thin Solid Films,* 516 pg3568-3571.

95. S. Hong R. Ravi, (2005) Fabrication of a low resistivity tantalum nitride thin film, *Microelectronic Engineering,* 83 pg206-212.

96. S. Na, I. Park, S. Park, G. Jeong, S. Suh, (2008), Electrical and structural properties of Ta-N thin film and Ta/Ta-N multilayer for embedded resistor, *Thin Solid Films,* 516 pg5465-5469.

97. C. Wang, J. Hsieh and C. Li, (2004), Electrical and piezoresistive properties of TaN-Cu nanocomposite thin films, *Thin Solid Films,* 469-470 pg455-459.

98. C. Wang, J. Hsieh, C. Li, Y. Fu and T. Chen, (2005), Effects of annealing on the microstructure and electrical properties of TaN-Cu nanocomposite thin films, *Surface & Coatings Technology,* 193 pg173-177.

99. C. Wang, J. Hsieh, Y. Fu, C. Li, T. Chen and U. Lam, (2004), Electrical Properties of TaN-Cu nanocomposite thin films, *Ceramics International,* 30 pg879-883.

100. P. Reddy, G. Bhagavat and R. Jawalekar, (1980), Ta-Al-N thin film resistors with improved electrical properties, *Thin Solid Films,* 70(1) pg27-35.

101. D. Wuu, C. Chan, R. Horng, W. Lin, S. Chiu and Y. Wu, (1999), Structural and electrical properties of Ta-Al thin films by magnetron sputtering, Applied Surface Science, 144-145 pg 315-318.

102. B. Yang and Y. Jia, (1991), Tantalum/aluminium alloy resistive film containing aluminium 50at%, *Vacuum,* 42(16) pg1073.

103. R. Duckworth, (1974), Conditions for the routine preparation of tantalum/aluminium films, Thin Solid Films, 26(1) pg77-98.

104. J. Schoen, (1974), Properties of Ta-Al films reactivity sputtered in an argon-nitrogen atmosphere, Thin Solid Films, 28(2) pg251-264.

105. O. Yukiko, S. Tajiri, T. Aozono, A. Okamoto, S. Ogawa and H. Mima, (2007), Fabrication of high TCR TaAl-N thin film by reactive sputtering method, Journal of the Vacuum Society of Japan, 50(3) pg173-174.

106. C. Backhouse, G. Este, J. Sit, S. Dew and M. Brett, (1997), Wsix thin films for resistors, *Thin Solid Films,* 311 pg299-303.

107. K. Bather, W. Hinuber, F. Lange, D. Rhede and H. Schreiber, (1984), The effect of surfaces and interfaces on the properties of thin film resistors in the Cr-Si/Al system, *Thin Solid Films,* 125(3-4) pg321-327.

108. Y. Narizuka, T. Kawahito, T. Kamei and S. Kobayashi, (1988), Properties of high-resistivity Cr-Si-O thin film resistor, *IEEE Transactions on Components Hybrids Manufacture and Technology*, 11(4) pg433-438.

109. A. Heinrich, C, Gladun, H. Schreiber, J. Schumann and H. Vinzelberg, (1990), Eelctrical properties of hetrogeneous CrSi(O,N) thin films, *Vacuum,* 41(4-6) pg1408-1410.

110. T. Couteau, (1991), High sheet resistance thin films for precision resistor applications, *Capacitor and Resistor Technology Symposium (CARTS) 1991,* pg152-156.

111. V. Fronz, B. Rosner and W. Storch, (1980), Electrical and structural properties of Cr-SiO thin films, *Thin Solid Films,* 65(1) pg33-43.

112. E. Schabowska, T. Pisarkiewicz and Z. Porada, (1980), Cermet thin film resistors obtained by flash evaporation, *Thin Solid Films,* 72(2) pgL7-L10.

113. H. Hoffman and E. Stephens, (1981), Cermet resistors on ceramic substratesI, *IEEE Transactions on Components, Hybrids and Manufacturing Technology,* 4(4) pg387-395.

114. E. Schabowska and R. Scigala, (1986), Electrical conduction in Cr-SiO cermet thin films, *Thin Solid Films,* 135(2) pg149-156.

115. P. Rachnev, P. Philippov and D. Parashkevov, (1986), Simultaneous preparation of Cr-SiO and NiCr thin film resistors on a single substrate, Thin Solid Films, 143(1) pg91-95.

116. R. Waits, (1973), Silicon-chromium thin-film resistor reliability, *Thin Solid Films,* 16(2) pg237-247.

117. K. Hieber, (1978), Amorphous chromium-silicon: a material for kilo-ohm sheet resistances, *Thin Solid Films,* 57(2) pg353-357.

118. R. Brynsvold and K. Manning, (2007), Constant current stressing of SiCr based thin film resistors: Initial wearout investigation, *IEEE Transactions on Device and Materials Reliability,* 7(2) pg259-269.

119. N. Cho and M. Kim, (2005), Preparation of Cr-Si multilayer structures for thin film heater applications, *Thin Solid Films,* 475 pg235-238.

120. J. Schuman, W. Bruckner and A. Heinrich, (1993), Properties and applications of vacuum-deposited Cu-Cr films, *Thin Solid Films,* 228(1-2) pg44-48.

121. V. Bashev, F. Dotsenko and I. Miroshnichenko, (1990), Electrical properties of sputtered Al-Cu films, *Physics of Metals and Metallography (English translation of Fizika Metallov i Metallovedenie),* 70(5) pg203-205.

122. M. Draissia, M. Debili, N. Boukhris, M. Zadam and S. Lollouche, (2007), Metastable ordered Cu_3Al phase sputter-deposited AlCu alloys system, *Copper - Published online 22 Oct 2007 - Wiley InterScience,* pg65-70.

123. S. Lallouche, M. Draissia and M. Debili, (2007), Phase transformation and microstrain study of nanostructured copper-aluminium thin films, *Copper - Published online 22 Oct 2007 - Wiley InterScience,* pg253-259.

124. N. Boukhris, M. Debili, P. Fournier and M. Draissia, (2007), Morphological stability of liquid-solid interface in some copper-aluminium alloys, *Copper - Published online 22 Oct 2007 - Wiley InterScience,* pg248-252.

125. M. Draissia and M. Debili, (2005), Observation of phase separation in magnetron sputter-deposited Al-Cu thin films, *Philosophical Magazine Letters,* 85(8) pg439-444.

126. M. Draissia, M. Debili and J. Millet, (2005), Comportement a la corrosion du systeme de films minces aluminium-cuivre, *Journal of New Materials for Electrochemical Systems,* 8 pg229-233.

127. M. Draissia and M. Debili, (2004), Atomic size effects on the hardness of RF sputtered Al-Cu(rich) thin films, *Journal of Crystal Growth,* 270 pg250-254.

128. M. Draissia, H. Boudemagh and M. Debili, (2004), Structure and hardness of the sputtered Al-Cu thin film system, *Physica Scripta,* 69 pg348-350.

129. M. Mozetic, A. Zalar and M. Drobnic, (1998), Self-controlled diffusion of Al in Cu thin film, Vacuum, 50(1-2) pg1-3.

130. M. Mozetic, A, Zalar, T. Bogataj, I. Arcon and R. Preseren, (1998), Comparison of AES and EXAFS analysis of a Cu_xAl_y layer on Al substrate, Vacuum, 50(3-4) pg299-304.

131. K. Mountfield and J. Rayne, (1984), Electronic specific heat of gamma phase copper-aluminium alloys, *Solid State Communications,* 49(11) pg1055-1057.

132. C. Macchioni, J. Rayne, S. Sen and C. Bauer, (1981), Low temperature resistivity of thin film and bulk samples of $CuAl_2$ and Cu_9Al_4, *Thin Solid Films,* 81(1) pg71-78.

133. J. Rayne, M. Shearer and C. Bauer, (1980), Investigation of interfacial reactions in thin film couples of aluminium and copper by measurement of low temperature contact resistance, *Thin Solid Films,* 65 pg381-391.

134. L. Doyen, X. Federspiel, D. Ney, G. Sers, V. Girault, L. Arnaud and Y. Wouters, (2006), Residual Resistivity model and its application, *Integrated Reliability Workshop Final Report, 2006 IEEE International,* pg134-135.

135. L. Gignac, C. Murray, K. Rodbell and M. Gribelyuk, (2002), A comparison of grain size measurements in Al-Cu thin films: imaging verses diffraction techniques, *Microscopy Microanalysis Microstructures,* 8 pg672-673.

136. K. Son, N. Missert, J. Barbour, J. Hren and R. Copeland, (2001), Growth and oxidation of thin film Al_2Cu, *Journal of the Electrochemical Society,* 148(7) pgB260-B263.

137. A. Lita and J. Sanchez, (1999), Microstructure and surface structure evolution in AlCu polycrystalline thin films, *Materials Research Society symposium Proceedings,* 562 pg135-140.

138. J. Musil, A. Bell, M. Cepera and J. Zeman, (1997), The structure of Cu-Al films prepared by unbalanced DC magnetron sputtering, *Surface and Coatings Technology,* 96 pg359-363.

139. P. Thomas, V. Vaidyan and J. Abraham, (1996), Surface oxidation studies of Al/Cu thin films, *Vacuum,* 47(1) pg83-85.

140. H. Jiang, J. Wang, B. Ding and Q. Song, (1993), SIMS studies of tracer diffusion of Al in thin film nanocrystalline Cu, *Journal of Materials Science and Technology,* 9 pg297-300.

141. R. van de Leest, (1989), The indoor exposure of thin sputtered copper-aluminium films, *Corrosion Science,* 29(5) pg497-506.

142. J. Vandenberg and R. Hamm, (1982), In situ x-ray study of phase formation in Cu-Al thin film couples, *Thin Solid Films,* 97(4) pg313-323.

143. J. Vandenberg, F. Den Broeder and R. Hamm, (1981), Formation of intermetallics and grain boundary diffusion in CuAl and AuAl thin film couples, Thin Solid Films, 93(3-4) pg277-280.

144. M. Shearer, C. Bauer and A. Jordan, (1979), Investigation of interdiffusion in thin-film couples of aluminium and copper by auger-electron spectroscopy, *Thin Solid Films,* 61(3) pg273-279.

145. S. Campisano, E. Costanzo, F. Scaccianoce and R. Cristofolini, (1978), Growth kinetics of the θ phase in Al-Cu thin film bilayers, *Thin Solid Films,* 52(1) pg97-101.

146. A. Gershinskii, B. Fomin, E. Cherepov and F. Edelman, (1977), Investigation of diffusion in the CuAl thin film system, *Thin Solid Films,* 42(1-3) pg269-275.

147. S. Kim, S. Yim, D. Lee, K. Kim, H. Kim, Ki. Kim and H. Sohn, (2008), Diffusion barriers between Al and Cu for the Cu interconnect of memory devices, *Electrochemical and Solid State Letters,* 11(5) pgH127-H130.

148. L. Barron, J. Neidrich and S. Kurinec, (2007), Optical, electrical, and structural properties of sputtered aluminium alloy thin films with copper, titanium and chromium additions, *Thin Solid Films,* 515 pg3363-3372.

149. C. Huang, C. Yang, E. Yang, T. Yang, K. Chen, J. Ku and C. Lu, (2007), The novel advanced process control to eliminate AlCu-PVD induced overlay shift, *Proceedings of SPIE,* 6518(3) pg651845.

150. W. Zhang, L. Yi, K. Tao, Y. Ma, P. Chang, D. Mao, J. Wu and S. Zou, (2006), A quick method for AlCu interconnect electromigration performance predicting and monitoring, *Semiconductor Science and Technology,* 21 pg633-637.

151. X. Zhou, G. Thompson, P. Skeldon, K. Shimizu, H. Habazaki and G. Wood, (2005), The valence state of copper in anodic films formed on Al-1at.% Cu alloy, *Corrosion Science,* 47 pg1299-1306.

152. H. Ohkubo, Y. Shimomura, I. Mukouda, K. Sugio and M. Kiritani, (2003), Formation of vacancy clusters in deformed thin films of Al-Mg and Al-Cu dilute alloys, Materials Science and Engineering, 350 pg30-36.

153. Y. Shusterman, N. Yakovlev and L. Schowalter, (2001), Ultra-thin epitaxial Al and Cu films on CaF_2/Si (1 1 1), *Applied Surface Science,* 175-176 pg27-32.

154. J. Lokker, A. Bottger, W. Sloof, F. Tichelaar, G. Janssen and S. Radelaar, (2001), Phase transformation in Al-Cu thin films: precipitation and copper redistribution, *Acta Materialia,* 49 pg1339-1349.

155. M. Catelani and R. Nicoletti, (2001), Reliability tests for thermal aging of thin film AlCu metallizations, *Instrumentation and Measurement Technology Conference, IMTC 2001,* 2 pg855-859.

156. K. Lee and Y. Lee, (1999), Effect of hydrogen and temperature on the resistivity of an aluminium-2 wt% copper thin film, *Journal of Materials Science,* 34 pg3427-3436.

157. X. Zhou, G. Thompson, H. Habasaki, K. Shimizu, P. Skeldon and G. Wood, (1997), Copper enrichment in Al-Cu alloys due to electropolishing and anodic oxidation, *Thin Solid Films,* 293 pg327-332.

158. W. Shih and A. Greer, (1994), A new precipitate phase in Al-4wt.% Cu thin-film interconnects, *Journal of Electronic Materials,* 23(12) pg1315-1323.

159. D. Frear, (1991), The effect of Cu at Al grain boundaries on electromigration behavior in Al thin films, *Proceedings of SPIE The International Society for Optical Engineering,* 1596 pg72-82.

160. A. Patrinos and J. Schwarz, (1991), The effect of microstructure on the resistance to electromigration of Al-Cu thin film conductors, *Thin Solid Films,* 196(1) pg47-63.

161. I. Vavra and S. Luby, (1980), Microstructure of aluminium-copper thin films and its relation to electromigration, Czechoslovak Journal of Physics Section B, 30(2) pg175-184.

162. K. Reddy, F. Beniere, D. Kostopoulos and J. Le Traon, (1979), Electromigration and diffusion of copper in aluminium thin films, *Journal of Applied Physics,* 50(4) pg2782-2786.

163. G. Walker and C. Goldsmith, (1973), Precipitation and solid solution effects in aluminium-copper thin films and their influence on electromigration, *Journal of Applied Physics,* 44(6) pg2452-2455.

164. B. Argawala, B. Patnaik and R. Schnitzel, (1972), Effect of microstructure on the electromigration life of thin film Al-Cu conductors, *Journal of Applied Physics,* 43(4) pg1487-1493.

165. W. Lanford, P. Ding, W. wang, S. Hymes and S. Muraka, (1995), Low temperature passivation of copper by doping with Al or Mg, *Thin Solid Films,* 262 pg234-241.

166. A. Gungor, K. Barnak, A. Rollett, C. Cabral and J. Harper, (2002), Texture and resistivity of dilute binary Cu(Al), Cu(In), Cu(Ti), Cu(Nb), Cu(Ir), and Cu(W) alloy thin films, *Journal of Vacuum Science and Technology B: Microelectronics and Nanometer Structures,* 20(6) pg2314-2319.

167. K. Chopra, (1969), Thin Film Phenomena, *McGraw-Hill Publications,* pg.23

168. N. Matsunami, Y. Yamamura, Y. Itikawa, N. Itoh, Y. Kazumata, S. Miyagawa, K. Morita, R. Shimizu and H. Tawara, (1984), Energy dependence of the ion-induced sputtering yields of monatomic solids, *Atomic Data Nuclear Data Tables,* 31(1) pg1-80.

169. ASM Handbooks, vol 3, Alloy Phase Diagrams, ASM International, Materials Park, Ohio, 2002. pg234.

170. H. Jones, (1960), Theory of brillouin zones and electronic states in crystals, *North Holland Publishing,* pg207.

171. Keithley Low Level Measurements Handbook, 6th Edition (2004), pg3-16

172. L. Nordheim, (1931), The electron theory of metals, *Annalen der Physik,* 9 pg607-641.

173. C. Macchioni, J. Rayne and C. Bauer, (1982), Low-temperature resistivity of bulk copper-aluminium alloys, *Physical Review B,* 25(6) pg3865-3870.

174. F. d'Heurle, C. Alliota, J. Angilello, V. Brusic, J. Dempsey and D. Irmischer, (1977), The deposition by evaporation of Cu-Al alloy films, Vacuum, 27(4) pg321-327.

175. B. Veal and J. Rayne, (1963), Heat Capacity of γ-CuZn Alloys below 4.2°K, *Physical Review,* 132(4) pg1617-1619.

176. P. Wissmann and F. Finzel, (2007), Electrical Resistivity of Thin Metal Films, *Springer Tracts in Modern Physics*, 223 pg9-34.

177. P. Lessard, (1990), Operation of cryogenic vacuum pumps in severe environments, Journal of Vacuum Science & Technology A: Vacuum, Surfaces, and Films, 8(3) pg2874-2876.

178. M. Birkett, (2004), Successful manufacture of the RC55 resistor in the 5Ω to 50Ω value range, *University of Northumbria at Newcastle, BEng(Hons) Manufacturing Systems Engineering*, *Final year dissertation, April 2004.* pg1-47.

179. D. Montgomery, (1992), The use of statistical process control and design of experiments in product and process improvement, *IIE Transactions,* 24(5) pg4-17.

180. D. Montgomery, (2005), Design and analysis of experiments, 6th Edition, *Wiley,* pg1-163.

181. T. Barker, (2005), Quality by experimental design, 3rd Edition, *Chapman & Hall,* pg3-480.

182. B. Bergquist, T. Olsson and E. Loven, (2006), The one-hour design of experiments course, *Quality Management Journal,* 13(1) pg26-32.

183. G. Howell, (2003), A systems approach to manufacturing process optimization, including design of experiments and Kaizen techniques, *18th International Conference on Computer-aided Production Engineering (CAPE 2003),* pg159-168.

184. R. Woll and C. Burkhard, (2003), Full factorial design, Taguchi design or genetic algorithms - teaching different approaches to design of experiments, *27th Annual Conference of the German-Classification-Society,* pg567-574.

185. S. Gleixner, G. young, L. Vanasupa, Y. Dessouky, E. Alen and D. Parent, (2002), Teaching design of experiments and statistical analysis of data through laboratory experiments, *Proceedings - Frontiers in Education Conference,* 1 pgT2D/1-T2D/5.

186. J. Antony, (2001), Improving the manufacturing process quality using design of experiments: a case study, *International Journal of Operations and Production Management,* 21(5-6) pg812-822.

187. M. Masudy, (2001), Industrial design using simulation and design of experiments, *13th European Simulation Symposium,* pg304-309.

188. I. Mezgar, Cs. Egresits and L. Monostori, (1997), Design and real-time reconfiguration of robust manufacturing systems by using design of experiments and artificial neural networks, *Computers in Industry,* 33 pg61-70.

189. G. Taguchi, (1993), Taguchi on robust technology development: Bringing quality upstream, *ASME Press, New York,* Pg1-109.

190. M. Akiyama, (1998), Statistical approach for optimizing sputtering conditions of highly oriented aluminium nitride thin films, *Thin Solid Films,* 315 pg62-65.

191. C. Anderson-Cook, (2006), Statistical design of experiments with engineering applications, *Journal of the American Statistical Association,* 101(473) pg396.

192. M. Uy, R. Hardesty, J. Fogle, and A. Moor, (2006), Use of design of experiments techniques to investigate resistance change of chip resistors in MESSENGER, *Proceedings of SPIE - The international Society for Optical Engineering,* 6291 pg102.1-102.11.

193. H. Rowlands and F. Antony, (2003), Application of design of experiments to spot welding process, Assembly Automation, 23(3) pg273-279.

194. M. Khan and P. Rega, (1990), Applying factorial design to improve the wave solder process for tinning LCCCs, *Surface Mount Technology,* 4(4) pg31-33.

195. J. Adamczyk, N. Horny, A. Tricoteaux, P. Jouan, M. Zadam, (2008), On the use of response surface methodology to predict and interpret the preferred c-axis orientation of sputtered AlN thin films, *Applied Surface Science,* 254 pg1744-1750.

196. Y. Deng, Y. Guan and P. Rack, (2006), Combinational synthesis and sputter parameter optimisation of chromium-doped yttrium aluminium garnet photoluminescent thin films, *Thin Solid Films,* 515 pg1721-1726.

197. P. Mach and M. Kocian, (2006), Modelling of evaporation of thin films using DOE, *29th International Spring Seminar on Electronics Technology, (ISSE'06),* pg273-277.

198. S. Jun. T. McKnight, A. Melechko, M. Simpson and P. Rack, (2005), Characterisation of reactively sputtered silicon oxide for thin-film transistor fabrication, *Electronic Letters,* 41(14) pg822-823.

199. W. Chou, C. Sun, G. Yu and J. Huang, (2003), Optimisation of the deposition process of ZrN and TiN thin films on Si(1 0 0) using design of experiment method, *Materials Chemistry and Physics,* 82 pg228-236.

200. A. Rosario and E. Pereira, (2002), Optimisation of the electrochromic properties of Nb_2O_5 thin films produced by sol-gel route using factorial design, *Solar Energy Materials & Solar Cells,* 71 pg41-50.

201. M. Akiyama, I. Alexandrou, M. Chhowalla and G. Amaratunga, (2001), Optimizing hardness of CN_x thin films by dc magnetron sputtering and a statistical approach, *Journal of Materials Science (USA),* 36 pg5397-5401.

202. M. Akiyama, T. Harada, C. Xu, K. Nonaka and T. Watanabe, (1999), Preparation of highly oriented AlN thin films on glass substrates by helicon plasma sputtering and design of experiments, *Thin Solid Films,* 350 pg85-90.

203. H. Takatsuji, T. Arai, S. Tsuji, K. Kuroda and H. Saka, (1999), Al-based sputter-deposited films for large liquid-crystal-display, *Thin Solid Films,* 337 pg235-239.

204. A. Barron, C. Kennemore III and A. Slomba, (1993), Employment of design of experiment for optimised development of thin film coatings, *Proceedings of SPIE - The International Society for Optical Engineering,* pg137-142.

205. Minitab ® 15.1.1.0. – Copyright 2007 Minitab Inc.

206. G. Adams, P. Cintas and X. Llabres, (2006), Selecting significant effects in factorial designs taking type II errors into account, *Quality and Reliability Engineering International,* 22(7) pg803-810.

207. A. Das, C. Grabbe and R. Hufnagel, (2008), Complexities in the deposition of thin film resistors, *Capacitor and Resistor Technology Symposium (CARTS) 2008,* pg339-352.

208. H. Khatri, (2008), The effect of deposition parameters on radiofrequency sputtered molybdenum thin films, *Journal of Physics: Condensed Matter,* 20 pg5055206.

209. S. Chandra, S. Uthanna, G. Rao, (2008), Effect of substrate temperature on the structural, optical and electrical properties of dc magnetron sputtered tantalum oxide films, *Applied Surface Science,* 254 pg1953-1960.

210. Y. Moon, B. Bang, S. Kim, C. Jeong and J. Park, (2008), Effects of working pressure on the electrical and optical properties of aluminium-doped zinc oxide thin films, *Journal of Materials Science: Materials in Electronics,* 19 pg528-532.

211. Z. He, X. Wang, Y. Fan, Z. Wang, X. Liu and Z. Xu, (2007), Study on sputtering characteristics of Ni80Cr20 alloy target, *Key Engineering Materials,* 353-358(3) pg1891-1894.

212. F. Martin, P. Muralt and M. Dubois, (2006), Process optimisation for the sputter deposition of molybdenum thin films as electrode for AlN thin films, *Journal of Vacuum Science and Technology A: Vacuum, Surfaces and Films,* 24(4) pg946-952.

213. S. Lee, S. Wang, J. Chen, J. Huang, (2006), Effects of deposition and post-annealing condiions on electrical properties and thermal stability of TiAlN films by ion beam sputter deposition, *Thin Solid Films,* 515(3) pg1069-1073.

214. M. Sinha, S. Mukherjee, B. Pathak, R. Paul and P. Barhai, (2006), Effect of deposition process parameters on resistivity of metal and alloy films deposited using anodic vacuum arc technique, *Thin Solid Films,* 515 pg1753-1757.

215. K. Chan and B. Teo, (2005), Sputtering power and deposition pressure effects on the electrical and structural properties of copper thin films, *Journal of Materials Science,* 40 pg5971-5981.

216. I. Goldberg, I. Klein and M. Hershkovich, (1988), The kinetics of thin film resistor stabilisation, *Microelectronics Journal,* 19(1) pg34-40.

217. W. Schlemminger and D. Stark, (1987), The influence of deposition temperature on the electrical resistance of thin Cu films, *Surface Science,* 189-190(2) pg1103-1110.

218. V. Stary K. Sefcik, (1981), Electrical resistivity and structure of thin nickel films - effect of annealing, Vacuum, 31(8-9) pg345-349.

219. E. Tochitski and A. Chaplanov, (1976), Annealing behaviour of polycrystalline metal films, *Thin Solid Films,* 32 pg213-215.

220. W. Hardy and D. Mills, (1973), Effects of deposition temperatures on Ta thin film resistors reactively sputtered in oxygen, Journal of Vacuum Science and Technology, 10(1) pg303-306.

221. P. Wissmann, (1972), The effect of gas adsorption on the conductivity of thin metal films, *Thin Solid Films,* 13(1) pg189-193.

222. R. Thun, (1963) Physics of thin films, *in: G. Hass (Ed.), Advances in Research and Development,* 1 pg187.

223. J. Thorton, (1977), High rate thick film growth, *Annual Review of Materials Science,* 7 pg239-260.

224. V. Grechanyuk and Y. Artyuh, (2005), Corrosion resistance of the composition materials system (Cu-Al)-Mo, obtained by the EB-PVD method, *Annals of "Dunarea de Jos", University Galati. Fascicle IX, Metallurgy and Materials Science,* 28(2) pg66-68.

225. D. White, R. Allor and J. Jones, (2000), Method of making and/or using copper based electrodes to spot weld aluminium, *United States Patent No. 6,144,006.*

226. A. Prevarskiy, Y. Kuzma and M. Onyshkevich, (1977), Phase diagram for the Mo-Cu-Al system, *Russ. Metall., translated from Izv. Akad. Nauk SSSR, Metally,* 4 pg162-164.

227. L. Shaginyan, J. Han, V. Shaginyan and J. Musil, (2006), Evolution of film temperature during magnetron sputtering, Journal *of Vacuum Science and Technology A; Vacuum Surfaces and Films,* 24(4) pg1083-1090.

228. PicoLog for windows release 5.12.1 (1997-2004) Pico Technology Ltd.

229. B. Cullity, (1978), Elements of x-ray diffraction, *Addison-Wesley Publishing Company,* pg102.

230. P. Subramanian and D. Laughlin, (1990), The Cu-Mo (copper-molybdenum) system, *Bulletin of Alloy Phase Diagrams,* 11(2) pg169-172.

231. J. Schuster and H. Ipser, (1990), Reinvestigation of the binary system Al-Mo up to 28 at.% Mo, *International Conference on Light Metals: Advanced Aluminium and Magnesium Alloys, Amsterdam,* Poster P.40.

232. J. Schuster and H. Ipser, (1991), The Al-Al8Mo3 section of the binary system aluminium-molybdenum, *Metallurgical and Materials Transactions A,* 22 pg1729-1736.

233. N. Saunders, (1997), The Al-Mo system (aluminium-molybdenum), *Journal of Phase Equilibria,* 18(4) pg370-378.

234. K. Schubert, A. Raman and W. Rossteutscher, (1964), Some structure data on metallic phases, *Naturwiss,* 51 pg506-507.

235. A. Raman and K. Schubert, (1965), On the constitution of some series of alloys related to TiAl3, III. Investigations in some systems T-Ni-Al and T-Cu-Al, *International Journal of Materials Research,* 56 pg99-104.

236. D. Shih and P. Ficalora, (1984), The effect of hydrogen chemisorption on the conductivity of evaporated aluminium films, *Journal of Vacuum Science and Technology A,* 2 pg225-230.

237. K. Fuchs and H. Wills, (1938), The conductivity of thin metallic films according to the electron theory of metals, *Proceedings of the Cambridge Philosophical Society,* 34 pg100-108.

238. E. Sondheimer, (1952), The Mean Free Path of Electrons in Metals, *Advances in Physics,* 1(1) pg1-42.

239. A. Mayadas and M. Shatzkes, (1970), Electrical-Resistivity Model for Polycrystalline Films: the Case of Arbitrary Reflection at External Surfaces, *Physical Review,* 1 pg1382-1389.

240. Y. Namba, (1970), Resistivity and Temperature Coefficient of Thin Metal Films with Rough Surfaces, *Japanese Journal of Applied Physics,* 9(11) pg1326-1329.

241. D. Campbell and A. Morley, (1971), Electrical conduction in thin metallic, dielectric and metallic-dielectric films, *Reports on Progress in Physics,* 34 pg283-368.

241. E. Lee, N. Truong, B. Prater and J. Kardokus, (2006) Copper alloys and alternative barriers for sub-45nm nodes, *Semiconductor International* - 7/1/2006.

242. T. Coutts, (1969), Conduction in thin cermet films, *Thin Solid Films,* 4(6) pg429-443.

243. M. Sinha, S. Mukherjee, B. Pathak, R. Paul and P. Barhai, (2006), Effect of deposition process parameters on resistivity of metal and alloy films deposited using anodic vacuum arc technique, *Thin Solid Films,* 515 pg1753-1757.

244. C. Tellier and A. Tosser, (1980), Comments on size effects in metallic films, *Electrocomponent Science and Technology,* 6 pg91-92.

245. V. Das and P. Ganesan, (1997), Electrical conduction studies on $(Bi_{0.6}Sb_{0.4})_2Te_3$ thin films, *Semiconductor Science Technology,* 12 pg195-202.

246. J. de Vries and F. den Broeder, (1988), Influence of interface scattering on the resistance of polycrystalline Au/Pd multilayered thin films, Journal *of Physics F: Metal Physics,* 18 pg2635-2647.

247. W. Zhang, S. Brongersma, O. Richard, B. Brijs, R. Palmans, L. Froyen and K. Maex, (2004), Influence of the electron mean free path on the resistivity of thin metal films, *Microelectronic Engineering,* 76 pg146-152.

248. K. Gylfason, A. Ingason, J. Augustsson, S. Olafsson, K. Johnsen and J. Gudmundsson, (2006), In situ resistivity measurements during growth of ultra-thin $Cr_{0.7}Mo_{0.3}$, *Thin Solid Films,* 515 pg583-586.

249. H. Liu, Y. Zhao, G. Ramanath, S. Murarka and G. Wang, (2001), Thickness dependant electrical resistivity of ultrathin (<40nm) Cu films, *Thin Solid Films,* 384 pg151-156.

250. U. Jacob, J. Vancea and H. Hoffmann, (1989), A new method for determining the electronic mean free path in polycrystalline metals, *Journal of Physics: Condensed Matter,* 1 pg9867-9873.

251. D. Dayal, P. Rudolf and P. Wissmann, (1981), Thickness dependence of the electrical resistivity of epitaxially grown silver films, *Thin Solid Films,* 79 pg193-199.

252. W. Prater E. Allen, (2005), Microstructural comparisons of ultrathin Cu films deposited by ion-beam and dc-magnetron sputtering, *Journal of Applied Physics,* 97 pg093301.

253. E. Barnat, D. Nagakura, P. Wang and T. Lu, (2002), Real time resistivity measurements during sputter deposition of ultrathin Cu films, *Journal of Applied Physics,* 91 pg1667-1672.

254. A. Tosser, C. Tellier and J. Launey, (1977), Thickness dependence effects of thermal ageing in thin conductive films, *Vacuum,* 27(4) pg335-338.

255. E. Barnet, D. Nagakura and T. Lu, (2003), Real time technique to measure the electrical resistivity of ultrathin films during growth in plasma environments, *Review of Scientific Instruments,* 74(7) pg3385-3389.

256. C. Thompson and R. Carel, (1996), Stress and grain growth in thin films, *Journal of Mechanics and Physics of solids,* 44(5) pg657-673.

257. C. Thompson, (1998), Grain growth in polycrystalline thin films of semiconductors, *Interface Science,* 6 pg85-93.

258. T. Tobita and H. Takasago, (1991), New trimming technology of a thick film resistor by the pulse voltage method, *IEEE Transactions on Components, Hybrids and Manufacturing Technology,* 14(3) pg613-617.

259. Z. Illyefalvi-vitez, (1977), Comparison of arc erosive and laser beam trimming of thin film resistors, *Electrocomponent Science and Technology,* 4 pg179-183.

260. T. Faith and J. Jennings, (1976), Fluid abrasive trimming of thin-film resistors, *IEEE Transactions on Parts, Hybrids and Packaging,* 12(2) pg133-138.

261. P. Sandborn and P.A. Sandborn, (2008), A random trimming approach for obtaining high-precision embedded resistors, *IEEE Transactions on Advanced Packaging,* 31(1) pg76-81.

262. M. Manolescu and A. Manolescu, (2007), Laser trimming modelling of thin film integrated resistors, *Semiconductor Conference, 2007. CAS 2007. International,* 2 pg473-476.

263. M. Meunier, Y. Gagnon, A. Lacourse, M. Ducharme, S. Rioux and Y. Savaria, (2007), Precision resistor laser trimming for analog microelectronics, *Conference on Quantum Electronics and Laser Science, 2007,* pg.4431515.

264. M. Meier, D. Bertsch, N. Onda, M. Etter, M. Gutsche, A. Dommann, V. Romano and M. Nicolet, (2006), Laser trimming of amorphous $Ta_{42}Si_{13}N_{45}$ thin films with ultrashort pulses, *Microelectronic Engineering,* 83 pg2234-2237.

265. Y. Antonov, (2006), Use of laser trimming for the development of a project for accuracy-normalisation of the resistance of resistors in hybrid integrated circuits, *Journal of Communications Technology,* 51(12) pg1351-1355.

266. S. Kaminski, E. Mis, M. Szymendera and A. Dziedzic, (2005), New trim configurations for laser trimmed thick-film resistors - experimental verification, *Journal of Microelectronics and Electronic Packaging,* 2(1) pg19-24.

267. G. Lullo, A. Castiglia, G. Carini and C. Arnone, (2004), Chalcogenide thin films for direct resistors fabrication and trimming, *Materials Science in Semiconductor Processing,* 7 pg337-341.

268. E. Gofuku, T. Ohnawa, M. Kohara and M. Nunoshita, (1993), Resistance adjustment with short-pulse Nd:YAG laser for RuO2-based thick film resistors burried in polymide film, *IEEE Transactions on Components, Hybrids and Manufacturing Technology,* 16(6) pg592-597.

269. Y. Kurihara, (1991), Laser trimming of thick film metal resistors on aluminium nitride substrates, *IEEE Transactions on Components, Hybrids and Manufacturing Technology,* 14(1) pg204-210.

270. V. Schultze and A. Fischer, (1989), Laser trimming of NiCr thin film resistors I: Thin film resistors without a protective layer, *Thin Solid Films,* 182(1-2) pg23-34.

271. H. Schmidt and B. Couch, (1989), Predicting the effect of high speed laser trimming on resistor stability, *Proceedings of the 39th Electronic Components Conference, 1989,* 39 pg585-592.

272. J. Shier, (1988), A finite-mesh technique for laser trimming of thin-film resistors, *IEEE Journal of Solid-State Circuits,* 23(4) pg1005-1008.

273. R. Neidorff, (1982), Laser-trimmed thin-film resistors hold voltage references steady, *Electronics, June 16, 1982,* pg131-134.

274. A. Kestenbaum and T. Baer, (1980), Trimming behaviour and post trim characteristics of Ta2N resistors on silicon, *IEEE Transactions on Components, Hybrids and Manufacturing Technology,* 3(4) pg637-646.

275. A. Kestenbaum and T. Baer, (1980), Photoexcitation effects during laser trimming of thin film resistors on silicon, *IEEE Transactions on Components, Hybrids and Manufacturing Technology,* 3(1) pg166-171.

276. R. Dow, M. Mauck, T. Richardson and E. Swenson, (1978), Reducing post-trim drift of thin-film resistors by optimising YAG laser output characteristics, *IEEE Transactions on Components, Hybrids and Manufacturing Technology,* 1(4) pg392-397.

277. R. Aggleton, (1977), Improved laser trimming geometry for thick film resistors - philosophy and example, *Circuit World,* 7(2) pg11-12.

278. R. Aggleton, (1977), Improved laser trimming for close tolerance resistors, *Circuit World,* 3(3) pg18-19.

279. G. Bulger, (1975), Stability analysis of laser trimmed thin-film resistors, *IEEE Transactions on Parts, Hybrids and Packaging,* 11(3) pg172-177.

280. A. Albin and E. Swenson, (1972), Laser resistance trimming from the measurment point of view, *IEEE Transactions on Parts, Hybrids and Packaging,* 8(2) pg14-19.

281. P. Fehlhaber, (1971), Laser trimming of silicon-chromium thin-film resistors, *Solid State Technology,* pg33-42.

282. K. Fjeldsted and S. Chase, (2002), Embedded passives: laser trimmed resistors, *CircuiTree*, March 2002, pg70-6.

283. J. Ramirez-Angulo and R. Geiger, (1988), New laser-trimmed film resistor structures for very high stability requirements, *IEEE Transactions on Electronic Devices,* 35 pg516-518.

284. Spectra-Physics, 1335 Terra Bella Avenue, Mountain View, CA., (www.spectra-physics.com)

285. L. Perdieu, W. Teat and B. Marten, (1986), The importance of substrate penetration during resistor laser trimming, *Proceedings of the International Symposium on Microelectronics,* pg88-94.

286. B. Gu, B. Couch, J. Oh and P. Chase, (2003), Comparative study on laser trimming with different wavelengths, *Proceedings of the International Symposium on Microelectronics,* pg672-675.

287. R. Kuehl, (2009), Stability of thin film resistors-Prediction and differences base on time-dependent Arrhenius law, *Microelectronics Reliability,* 49 pg51-58.

288. M. Reid, J. Punch, C. Ryan, J. Franey, G. Derkits, W. Reents and L. Garfias, (2007), The corrosion of electronic resistors, *IEEE Transactions on Components and Packaging Technology,* 30(4) pg666-672.

289. X. Wang and Z. Zhang, (2005), Synthesis of undercoat with high temperature and humidity resistance for resistor, *6th International Conference on Electronics Packaging Technology, 2005,* pg1564620.

290. W. Werner, (2005), High temperature stable thin film resistors, *Capacitor & Resistor Tecnology Symposium CARTS Europe 2005,* pg81-89.

291. C. Pennetta, L. Reggiani and L. Kiss, (1999), Thermal effects on the electrical degradation of thin film resistors, *Physica A; Statistical and Theoretical Physics,* 266 pg214-217.

292. P. Hruska, (1997), Thin film resistor technology and noise reliability indicators, *Proceedings of the 21st International Conference on Microelectronics, MIEL'97,* pg663-666.

293. L. Bos, (1994), Performance of thin film chip resistors, *IEEE Transactions on Components, Packaging and Manufacturing Technology - Part A,* 17(3) pg359-365.

294. A. Dimba, B. Jones and I. Whyte, (1989), The long term stability of some integrated circuit resistors, *Microelectronics and Reliability,* 29(6) pg1035-1038.

295. H. Law, (1980), A rating criterion for film resistors, *Electrocomponent Science and Technology,* 7 pg131-135.

296. A. Van Nie, (1980), Tracking performance of film resistors: definitions and theory, *Microelectronics and Reliability,* 20(4) pg505-508.

297. W. Reiner, (2002), Reliability of thin-film resistors: impact of third harmonic screenings, *Microelectronics and Reliability,* 42 pg807-813.

298. E. Vandamme and L. Vandamme, (2000), Current crowding and its effect on 1/f noise and third harmonic distortion - a case study for quality assessment of resistors, Microelectronics and Reliability, 40 pg1847-1853.

299. S. Hellstrom and H. Wesemeyer, (1977), Nonlinearity measurements of thin films, *Vacuum,* 27(4) pg339-343.

300. W. Roesch, (2008), Forensic characterization of thin film resistor degradation, Microelectronics Reliability, 48 pg958-964.

301. K. Schroeder, (2006), Nichrome resistors deliver reliability at lower cost, *Power Electronics Technology, August 2006,* pg34-36.

302. J. Wang, R. Hilburn and S. Clouser, (2003), Stress effects on thin film nichrome embedded resistor tolerance, *Proceedings of the IPC Annual Meeting,* pgS05-6.

303. W. Cuviello, (2004), Major advancement in the protection of thin film nichrome based resistors with specialised passivation methods (SPM), *Capacitor and Resistor Technology Symposium (CARTS) 2004,* pg307-316.

304. L. Toth, A. Barna and P. Barna, (1983), On the failure mechanism of NiCr thin film resistors under damp heat steady state tests, *Vacuum,* 33 pg53-57.

305. T. Berlicki and E. Prociow, (1982), Allowable power in NiCr film resistors, *Electrocomponent Science and Technology,* 9 pg209-211.

306. W. Keenan, (1976), Pulsed overload tolerance of Si/Cr, Ni/Cr and Mo/Si thin film resistors on integrated circuits, *IEEE Transactions on Reliability,* 25(4) pg248-253.

307. M. Nakabayashi, H. Ohyama, E. Simoen, M. Ikegami, C. Claeys, K. Kobayashi, M. Yoneoka and K. Miyahara, (2001), Reliability of polycrystalline silicone thin film resistors, *Microelectronics and Reliability,* 41 pg1341-1346.

308. B. Jones and E. Mzunzu, (1989), The stability of polycrystalline silicon thin film resistors measured using excess noise, *Microelectronics and Reliability,* 29(4) pg543-544.

309. M. Jadhav, S. Gangal and R. Karekar, (1985), Study of the effect of humidity on AlO-x thin film resistors, *Sensors and Actuators,* 8 pg149-159.

310. Source: WebElements [http://www.webelements.com/].

311. Y. Takizawa and K. Sugahara, (1995), Corrosion resistant Ni-Cr-Mo alloys in hot concentrated sulphuric acid with active carbon, *Materials Science & Engineering,* A198 pg145-152.

312. K. Hashimoto, P. Park, J. Kim, H. Yoshioka, H. Mitsui, E. Akiyama and H. Habazaki, (1995), Recent progress in corrosion resistant metastable alloys, *Materials Science & Engineering,* A198 pg1-10.

313. MIL-PRF-55342 rev.H, (200), Performance specification for fixed film chip resistors, *MIL (military) United states of America, Department of Defence,* pg.1-47.

314. Source: TT Electronics – Welwyn Components Ltd [http://www.welwyn-tt.com], (2005), Current sense resistors application note, pg1-6.

APPENDIX 1 – TARGET SPECIFICATION

TT electronics
Welwyn Components

Low Value AlCuMo Thin Film Chip Resistors

TARGET SPECIFICATION

Extension to PCF Series

- **Precision metal film technology**
- **0805, 1206, 2010 and 2512 sizes**
- **Extended ohmic range >R10 (100mΩ) to 10R (10Ω)**
- **TCR grades 50, 25 and 15ppm/°C**
- **Ideal for current sensing applications**
- **RoHS compliant**

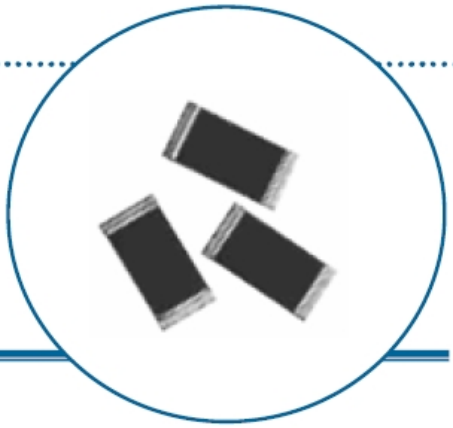

Electrical Data

		0805	1206	2010	2512
Power rating at 70°C	watts	0.1	0.125	0.25	0.5
Resistance range	ohms	R10 to 10R			
Limiting element voltage	volts	100	150	150	150
Typical TCR	ppm/°C	4R7 to 10R = 15 1R0 to 10R = 25 R10 to 10R = 50			
Resistance Tolerance	%	4R7 to 10R = 0.1 1R0 to 10R = 0.25 R47 to 10R = 0.5 R10 to 10R = 1.0			
Standard Values		E24 or E96, Other values available by special request			
Ambient temperature range	°C	-55 to +125			

Performance Data

Test Parameter	Conditions	Maximum Change (ΔR%+0.05Ω)
Load life	1000hrs cyclic load at 70°C	0.25
Humidity	1000hrs at 40°C, 90-95%RH	0.30
Short term overload	6.25 x rated power, or 2 x LEV, for 5sec	0.25
High temperature operation	1000hrs at 125°C	0.25
Temperature cycle	5 cycles -55 to +125°C	0.1
Resistance to solder heat	270°C for 10sec	0.2
Solderability	230°C for 2sec	95% minimum coverage

Issue A – 05.2008

Welwyn Electronics Park, Bedlington, Northumberland, NE22 7AA, England. Tel: 01670 822181 Fax: 01670 829465 Web: www.welwyn-tt.com

APPENDIX 2 – ELECTRICAL TEST PROCEDURES TO BS EN 60115-1

Resistance

Measurements of resistance are be made by using a direct voltage of small magnitude for as short a time as is practicable, in order that the temperature of the resistance element does not rise appreciably during measurement.

Endurance at 70°C

The initial resistance is measured and then the resistors are subjected to an endurance test of 1000 hours at an ambient temperature of 70°C ± 2°C. A dc voltage is applied at full rated power for the duration of the test. For example the voltage applied to a 10Ω resistor with a power rating of 0.125W would be:

$$V = \sqrt{P \times \Omega} \qquad = \sqrt{0.125 \times 10} \qquad = 1.12V$$

After approximately 48, 500 and 1000 hours, the resistors shall be removed from the chamber and allowed to recover, under standard atmospheric conditions for not less than 1 hour and not more than 4 hours. The resistors shall be visually examined. There shall be no visible damage and the marking shall be legible. The final resistance is then measured and the change in resistance, $\Delta\Omega$, is calculated. $\Delta\Omega$ must not exceed the value prescribed in the relevant detailed CECC specification.

Damp heat steady state (DHSS)

The initial resistance is measured and then the resistors are subjected to 56 days of 1000hrs at 40°C and 92% relative humidity. After56 days the resistors shall be removed from the chamber and allowed to recover, under standard atmospheric conditions for not less than 1 hour and not more than 4 hours. The resistors are then visually examined, there must be no visible damage and the marking must be legible. The final resistance is then measured and the change in resistance, $\Delta\Omega$, is calculated. $\Delta\Omega$ must not exceed the value prescribed in the relevant detailed CECC specification.

Short term overload

The initial resistance is measured and then the resistors are mounted horizontally in free air at an ambient temperature between 15°C and 35°C. An overload voltage of 6.25 times the rated power is then be applied to the terminations of the resistor for a period of 5 seconds. For example the overload voltage applied to a 10Ω resistor with a power rating of 0.25W would be:

$$V = \sqrt{6.25P \times \Omega} \qquad = \sqrt{6.25 \times 0.25 \times 10} \qquad = 3.95V$$

After a recovery of not less than 1 hour and not more than 2 hours, the resistors are visually examined. There must be no visible damage and the marking must be legible. The final resistance is then measured and the change in resistance, $\Delta\Omega$, is calculated. $\Delta\Omega$ must not exceed the value prescribed in the relevant detailed CECC specification.

Endurance at the upper category temperature (dry heat)

The initial resistance is measured and then the resistors are subjected to an endurance test of 1000 hours at an ambient temperature of 125°C ± 2°C. The test shall be performed at zero power dissipation.

After approximately 48, 500 and 1000 hours, the resistors shall be removed from the chamber and allowed to recover, under standard atmospheric conditions for not less than 1 hour and not more than 4 hours. The resistors shall be visually examined. There shall be no visible damage and the marking shall be legible. The final resistance is then measured and the change in resistance, $\Delta\Omega$, is calculated. $\Delta\Omega$ must not exceed the value prescribed in the relevant detailed CECC specification.

Rapid change of temperature (TRC)

The initial resistance is measured and then the resistors are subjected to 5 cycles as follows:

Lower temperature:	-55°C
Lower temperature dwell time:	30mins
Temperature transfer time:	<30secs
Upper temperature:	125°C
Upper temperature dwell time:	30mins

On completion of the 5 cycles the resistors are allowed to recover for a period of greater than 1 hour but less than 2 hours, after which the resistors are visually examined. There must be no visible damage. The final resistance is then measured and the change in resistance, $\Delta\Omega$, is calculated. $\Delta\Omega$ must not exceed the value prescribed in the relevant detailed CECC specification

Resistance to soldering heat

The initial resistance is measured and then the test is carried out under the following conditions:

Solder bath temperature:	270°C
Immersion time:	10secs

After recovery the resistors are visually examined, there must be no visible damage and the marking must be legible. The final resistance is then measured 24 hours after the test and the change in resistance, $\Delta\Omega$, is calculated. $\Delta\Omega$ must not exceed the value prescribed in the relevant detailed CECC specification.

Termination solderability

The test is carried out under the following conditions:

Solder bath temperature:	235°C
Immersion time:	2 seconds

Following immersion the terminations shall be examined for good tinning as evidenced by free flowing of the solder with wetting of the terminations.

APPENDIX 3 – PUBLISHED MATERIAL

1. Birkett M, Brooker J, Penlington R, Wilson W, Tan K, (2008), “Electrical Characterisation of AlCuMo Thin Films Prepared by DC Magnetron Sputtering”, *IET Science, Measurement and Technology*, 2 (5), pg304-309.

2. Birkett, M, Brooker, J, Penlington, R, Wilson, A, Tan, K, (2006), “Effects of Annealing on the Electrical Properties of NiCr vs AlCu Thin Film Resistors prepared by DC Magnetron Sputtering”, *Proceedings of the 20th Annual Capacitor and Resistor Technology Symposium, CARTS Europe 2006*, Bad Homburg, Germany, pg307-316.

Published in IET Science, Measurement and Technology
Received on 1st October 2007
Revised on 10th January 2008
doi: 10.1049/iet-smt:20070076

ISSN 1751-8822

Electrical characterisation of AlCuMo thin films prepared by DC magnetron sputtering

M. Birkett[1] *J. Brooker*[1] *R. Penlington*[2] *A. Wilson*[2] *K. Tan*[2]

[1]*TT Electronics Welwyn Components Ltd., Welwyn Electronics Park, Bedlington, Northumberland NE22 7AA, UK*
[2]*School of Computing, Engineering & Information Sciences, Northumbria University, Ellison Building, Newcastle-upon-Tyne NE1 8ST, UK*
E-mail: martin.birkett@welwyn-tt.com

Abstract: Thin film resistors have been manufactured to evaluate the electrical performance characteristics of AlCuMo thin films. The films were prepared on Al_2O_3 substrates at room temperature as a function of Mo concentration by DC magnetron sputtering and were then annealed at various temperatures in air and N_2 atmospheres. The effect of annealing temperature on the electrical properties of the films was systematically investigated. Increase in Mo content produced a decrease in temperature coefficient of resistance (TCR), an increase in resistivity (ρ) and an improvement in long term stability ($\Delta\Omega/\Omega$) of the films. TCR varied from negative to positive and further improvements in resistance stability of the films were also achieved through increasing annealing temperature in both air and N_2 atmospheres. A temperature region is proposed where 'near zero' TCR (ppm/°C) and long term stability of better than 0.2% can be realised.

1 Introduction

Owing to electrical properties such as excellent long term stability ($\Delta\Omega/\Omega$) and low temperature coefficient of resistance (TCR), thin metal alloy films have received much attention in the application of thin film resistors (TFR).

Of the metal alloy systems available for the production of TFR's, NiCr is perhaps the most widely reviewed, either in binary or ternary systems with small additions of doping elements [1–7]. NiCr is generally regarded as a good all-round film as it possesses a resistivity (ρ) of between 150 and 300 $\mu\Omega$ cm, which can cover a wide sheet resistance (R_s) range of $\Omega/\square$ while maintaining excellent electrical properties such as a TCR of less than or equal to ppm/°C and $\Delta\Omega/\Omega$ of less than $\pm 0.1\%$ [8].

However, with ever rising energy prices, the last decade has seen a vast increase in the requirement for TFR's with lower resistivity and equal performance to NiCr, especially in portable devices for the purpose of saving battery power.

It has been previously reported that a binary film system of AlCu ~40/60wt%, produced films with lower resistivity of ~30–40 $\mu\Omega$ cm and similar electrical performance to that of NiCr, however TCR was large and positive [9]. This current study explores the possibility of incorporating a third doping element, molybdenum, within the alloy to produce ternary thin films of AlCuMo, with the aim of reducing and controlling TCR while maintaining a lower resistivity. Molybdenum was chosen as this doping element due to its high chemical affinity with residual oxygen in the deposition chamber. This reaction leads to the formation of thin dielectric layers in the grain boundaries which is seen as a negative TCR and also the formation of a protective oxide layer at the film surface which gives improved protection from the environment and thus enhances electrical stability [10].

Various compositions of AlCuMo were deposited and then compared directly with films of NiCr manufactured under identical conditions. The electrical and structural properties of the films were then investigated as a function of post-deposition annealing temperature and atmosphere, air and N_2.

2 Experimental

2.1 Preparation of resistive films

A summary of the axial TFR manufacturing procedure and barrel-sputtering process conditions are given in Fig. 1 and Table 1, respectively. In general, axial TFRs are manufactured by depositing a sub-micron layer of metal alloy onto a ceramic substrate then heating to give the required pre-value resistance. Termination caps are then fitted before the resistor is adjusted to the target value by removing part of the metal film, usually by a helical cut produced by a laser or cutting wheel. Termination leads are then fitted, before the component is encapsulated in a protective coating.

Substrates used were 1.7 mm in diameter × 3.25 mm long 85% Al_2O_3 rods. The AlCuMo films were deposited at room temperature by the DC magnetron-sputtering technique from 99.99% pure Al, Cu and Mo target pieces. Eighteen of these pieces were assembled to produce a standard target size of 381 mm × 89 mm (15″ × 3.5″) with a composition of AlCuMo 35.7/55/9.3 wt%. The size of the target pieces were then varied to allow different target compositions to be sputtered and subsequently investigated (Table 2).

The vacuum plant employed was a Vac Tec Systems barrel-sputtering plant, which was evacuated to a base pressure of 5×10^{-5} Torr using a combination of a mechanical roughing pump and then a cryo pump. Pure Ar was introduced at a constant flow rate of 35 sccm to achieve the desired sputtering pressure of 3×10^{-3} Torr. Sample batches of 50 kpcs were then sputtered with the various AlCuMo film compositions at a target power of 2 kW DC. Following deposition, the samples were annealed at temperatures of 200, 300, 400 and 500°C in both air and N_2 atmospheres for a period of 5 h. Nickel-plated steel termination caps were then fitted and subsequently resistance welded with 0.6 mm in diameter tin-plated copper termination wire to permit good electrical contact.

2.2 Characterisation of resistive films

Termination caps and leads were fitted and the resistance values of the films at 20°C (R_{20}) and 70°C (R_{70}) were measured in a thermostatically controlled oil bath using a conventional four wire technique in conjunction with a digital multimeter (Agilent 3458A). TCR was then calculated using the following equation

$$\text{TCR (ppm/°C)} = (R_{70} - R_{20})/R_{20}(70 - 20) \times 10^6$$

Film resistivity was calculated from the measured resistance and film dimensions. Film thickness was measured at several points on the cross section of the sputtered rods using a scanning electron microscopy (FEI Quanta200). Stability of resistance of the films was measured after subjection to 1000 h at 155°C in ambient air.

Film composition was calculated from sputtering target weight loss (Salter type 424) and analysed using Energy Dispersive X-ray analysis (EDX).

2.3 Environmental testing

Following initial classification, films containing 5.3 and 9.3 wt% Mo were subjected to a series of environmental tests to check their suitability as TFR's. At this stage films of NiCr were also tested as a control. The tests performed included: voltage load, voltage overload, dry heat, damp

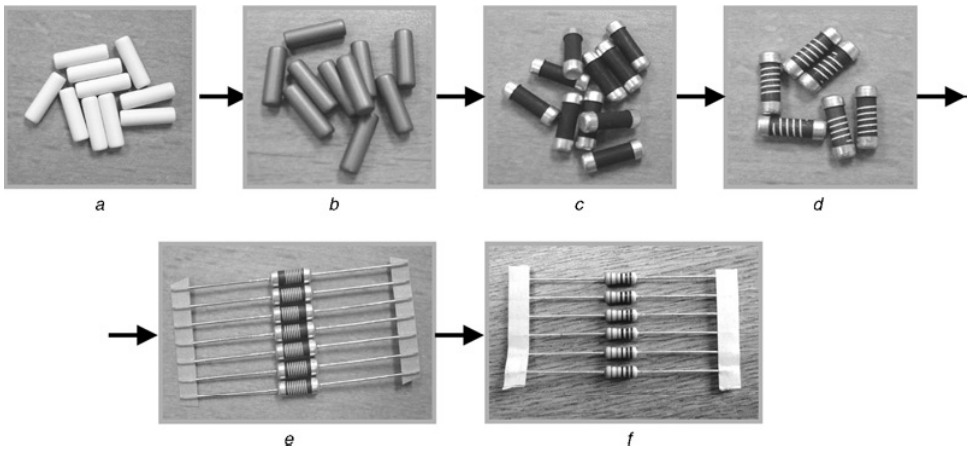

Figure 1 *Sample manufacturing procedure*

a Blank Al_2O_3 rods
b Deposit metal film
c Fit termination caps
d Laser adjust film
e Weld termination leads
f Apply protective coating

Table 1 Sputtering process conditions

base pressure	5×10^{-5} Torr
sputtering pressure	3×10^{-3} Torr
Ar flow rate	35 sccm
barrel rotation speed	3 rpm
deposition time	8 h
deposition power	2 kW
target to substrate distance	250 mm

Table 2 AlCuMo sputtering target compositions

	Wt% of target			
Al	39.1	38.0	36.8	35.7
Cu	57.6	56.7	55.9	55.0
Mo	3.3	5.3	7.3	9.3

heat steady state, temperature rapid change, resistance to solder heat, vibration and bump and climatic cycle.

3 Results and discussion

3.1 Chemical composition of AlCuMo resistive films

EDX analysis of the chemical compositions of the films resulted in a significant shift in comparison to the nominal target compositions (Fig. 2). This discrepancy can be largely explained by the variation in sputter yields of the individual target segments, which were confirmed by measuring the weight lost during sputtering. The sputter ratio of AlCuMo was found to be ~1:2:0.8, which corresponds well with previous data.

3.2 Electrical and structural properties of AlCuMo resistive films

For all compositions the mean film thickness was determined to be ~1100 nm. Thus with a deposition time of 8 h the sputter rate was calculated to be ~2.3 nm/min. This slow deposition rate was related to the large test batch size of 50 000 substrates and also the need to run the sectioned and clamped target arrangement at a reduced power level for cooling purposes. This result suggests that the small changes in Mo content between the four target compositions are not sufficient to affect the overall sputter rate of the alloys.

The effect of Mo content on the resistivity and TCR value of the sputter deposited AlCuMo films is shown in Fig. 3. In general, the addition of Mo to the binary AlCu alloy gives the desired effect of decreasing TCR to a practical level of around ± 50 ppm/°C. However the consequence of this result is an increase in resistivity over that reported for binary films [9]. Variation in Mo content has the effect of decreasing TCR and in turn increasing resistivity from ~25 ppm/°C and 60 μΩ cm at 3.3 wt% Mo, to −60 ppm/°C and 85 μΩ cm at 9.3 wt% Mo. However, the influence of the Mo doping appears to diminish at levels ≤5.3 wt%, where both TCR and resistivity curves begin to flatten off. This suggests that the most useful region is between ~5.3 and 9.3 wt% Mo, where a practical TCR can be achieved while maintaining a lower resistivity. This result is in agreement with the well

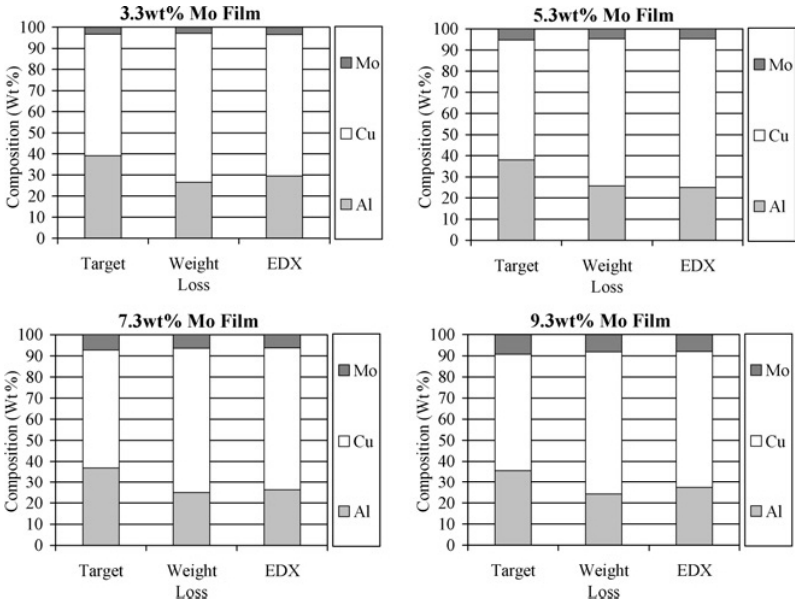

Figure 2 *Sputtering target and film composition, for the AlCuMo films*

doi: 10.1049/iet-smt:20070076

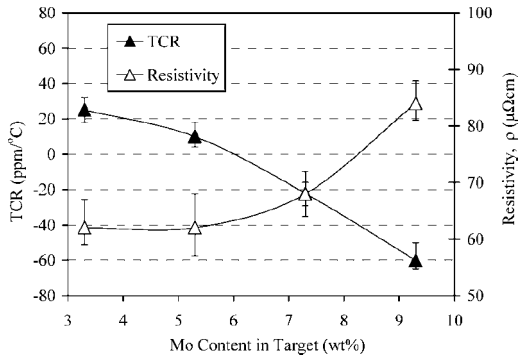

Figure 3 *Sputtered TCR and resistivity, for the AlCuMo films*

documented theory that the introduction of small quantities of doping impurities either in the sputtering gas or target itself can result in more amorphous structures with decreasing conductivity and TCR [10].

The effect of annealing temperature and environment on the TCR and resistivity of the films is shown in Fig. 4. TCR remains relatively unchanged and only increases gradually at temperatures below 300°C, beyond this temperature it rises significantly and after treatment at 500°C, the TCR of all four films is in excess of 200 ppm/°C and hence no longer suitable for use as TFR's. The resistivity of the films demonstrates a similar but inverse trend to that of TCR and decreases with increasing annealing temperature.

On average, resistivity falls by about one third of its original value after treatment at 500°C. Again, the largest value shifts appear to take place at temperatures in excess of 300°C. The most interesting temperature region is that between 300 and 400°C, where TCR appears to be controllable to around ±50 ppm/°C for all except the 3.3wt% Mo film. The best results come from the two films with the highest Mo content, which can both be controlled around the zero TCR line. Of additional benefit is that this region lies beyond the maximum TFR assembly processing

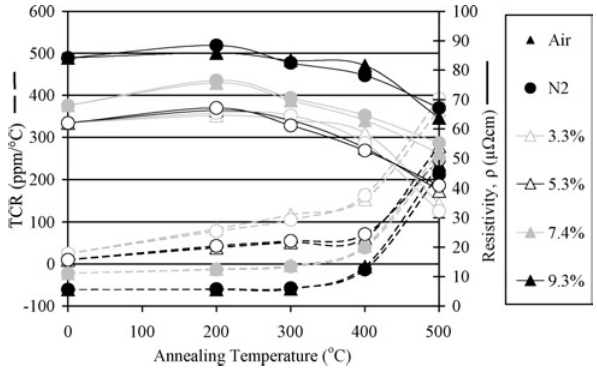

Figure 4 *TCR and resistivity following annealing in air and N2 atmospheres at various temperatures, for the AlCuMo films*

temperature, which is generally accepted to be around 300°C [8], so TCR will be unaffected by subsequent operations.

Perhaps the most striking result is how little influence the annealing atmosphere has on the behaviour of the films. Both TCR and resistivity results for films treated in air and N_2 are virtually identical for all four compositions, thus suggesting that temperature, rather than environment, plays the major role in altering the electrical properties of the films.

These results are in good agreement with previous work, where annealing of films sputtered from mixed composition targets at temperatures in excess of 300°C leads to a positive shift in TCR and indeed follows the general theory of annealing out micro-imperfection and impurities inside grains and recrystallisation of the film leading to a reduction in resistivity [10, 11]. In this investigation, the structural transformation can be distinguished by three annealing states, as illustrated in Fig. 4. At first the sputtered film is in an amorphous state with a negative TCR. At annealing temperatures, below ~400°C crystals with positive TCR are formed and the films are in a metastable state. Here zero TCR can be achieved through careful adjustment of Mo concentration and annealing temperature. At temperatures in excess of 400°C further crystallisation and grain growth takes place leading to a positive shift in TCR and reduction in resistivity towards that of the individual bulk elements [12, 13].

Results for resistance stability of the various film compositions after storage for 1000 h at 155°C in air following stabilisation at 400°C for 5 h in air are given in Fig. 5.

Resistance stability improves quite linearly with increasing Mo content. At 3.3 wt% Mo, the mean change in resistance is ~0.5% and reduces to ~0.15% for the 9.3 wt% Mo film. It can be postulated that the mechanism behind this marked improvement is the reaction of the Mo with oxygen which forms a protective oxide layer [10], both initially in the deposition chamber and annealing furnace and secondly in the environmental test chamber. In future experiments, the oxygen content in the deposition chamber will be

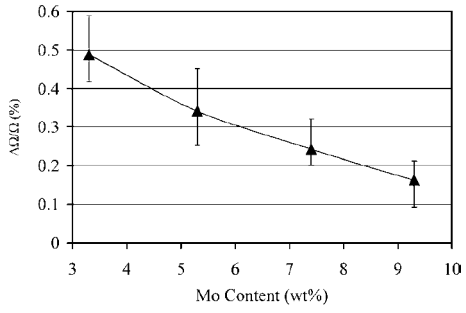

Figure 5 *1000 h resistance stability against Mo content*

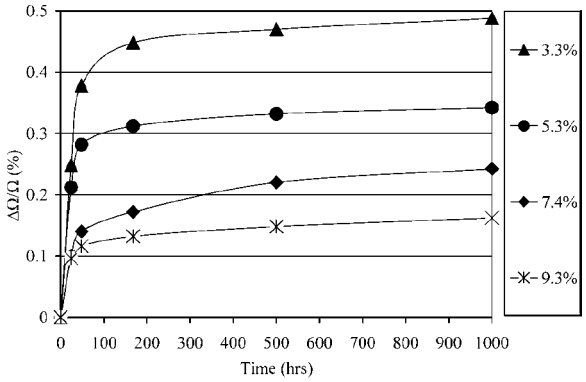

Figure 6 *Resistance stability at 155°C, measurements taken after 24, 48, 168, 500 and 1000 h.*

monitored prior to sputtering, supporting measurement and understanding of the influence of residual oxygen pressure on the electrical properties of the films and ensuring repeatability of the process.

As illustrated in Fig. 6, the vast majority of resistance change takes place in the first 48 h of the stability test. Again this result can be explained by initial oxidation and degradation of the films, followed by stabilisation as the protective oxide layer is formed, retarding the rate of any subsequent changes.

3.3 Environmental testing of AlCuMo and NiCr resistive films

AlCuMo films containing 5.3 and 9.3 wt% Mo were laser adjusted to target value using a Nd:YAG laser (Nohau LSS600) before being encapsulated in a modified epoxy coating. These samples were then subjected to a series of environmental tests in accordance with BS EN 60115-1 [14] together with control standards sputtered form the traditional NiCr resistive film and manufactured under identical conditions. Maximum and typical results of these tests are presented in Table 3.

Again it is clearly evident that an increase in Mo content gives a step improvement in the electrical performance of the AlCuMo film regardless of the test environment and conditions. Results of maximum resistance change ($\Delta\Omega\%$) for the 9.3 wt% Mo film outperforms that of the 5.3 wt%. Mo film for all tests undertaken. Moreover, comparison against the results for the NiCr control film shows a similar performance level. Any minor differences between the results of the two alloy types appear to be attributable to the test conditions. For example, the AlCuMo film gives better results for the lower temperature and load tests, whereas the NiCr performs the best at higher temperatures such as the dry heat test and also the climatic cycle, which contains a 40 h dry heat soak at 155°C. Again this result can be attributed to initial oxidation of the film as highlighted in Fig. 6 and can be further supported by the similarity of the dry heat and climatic cycle results, which suggests that the majority of resistance change is taking place in the first 40–48 h.

4 Conclusion

In order to develop TFR with lower resistivty and equal electrical performance to that of NiCr, the effects of the addition of varying Mo content to AlCu alloy films was studied. The TCR of the films increased and resistivity decreased with reduction in Mo concentration and these changes were further augmented through annealing of the films at temperatures above 300°C. Heat treatment atmosphere, air or N_2 had no significant effect on electrical properties of the films.

Table 3 Environmental test results for AlCuMo and NiCr films

Test specification	Performance ($\Delta\Omega\%$)					
	AlCuMo 38/56.7/5.3		AlCuMo 35.7/55/9.3		NiCr	
	Max.	Typical	Max.	Typical	Max.	Typical
load: 1000 h @ 70°C	0.25	0.2	0.15	0.08	0.3	0.1
short term overload	0.01	0.01	0.01	0.01	0.1	0.02
dry heat: 1000 h @ 155°C	0.6	0.4	0.25	0.2	1	0.15
DHSS: 56 days @ 40°C/93%RH	0.20	0.15	0.12	0.09	0.5	0.1
temperature rapid change	0.33	0.27	0.14	0.05	0.2	0.05
resistance to solder heat	0.03	0.02	0.03	0.01	0.06	0.03
vibration and bump	0.39	0.31	0.1	0.08	0.06	0.02
climatic cycle	0.67	0.35	0.33	0.13	0.3	0.1

doi: 10.1049/iet-smt:20070076

AlCuMo films were characterised by metastable behaviour, which with correct adjustment of Mo concentration and annealing temperature could be utilised to obtain films with near zero TCR, possessing defined electrical properties such as a resistivity of $\sim 80\ \mu\Omega$ cm and a long term stability of $< 0.2\%$.

Thus on the basis of resulting resistivity, thin films of AlCuMo can find use as low ohmic value resistors, whereas offering similar environmental performance to that of the traditional NiCr alloy.

5 Acknowledgments

This work was funded and supported by TT Electronics Welwyn Components Ltd and an Industrial Fellowship awarded by the Royal Commission for the Exhibition of 1851.

6 References

[1] PETROVIC S., BUNDALESKI N., RADOVIC M., *ET AL.*: 'Surface composition and structure of NiCr sputtered coatings exposed in air at room temperature', *Nucl. Instrum. Methods Phys. Res. B*, 2007, **256**, pp. 1–7

[2] SINHA M., MUKHERJEE S., PATHAK B., PAUL R., BARHAI P.: 'Effect of deposition process parameters on the resistivity of metal and alloy films deposited using anodic vacuum arc technique', *Thin Solid Films*, 2006, **515**, pp. 1753–1757

[3] VINYAK S.: 'NiCr thin film resistor fabrication for GaAs monolithic microwave integrated circuits', *Thin Solid Films*, 2006, **514**, pp. 52–57

[4] NGUYEN M., KIM B., KANG B., KIM C., YOON S.: 'Effect of chromium concentration on the electrical properties of NiCr thin film resistors deposited at room temperature by magnetron co-sputtering technique', *J. Electrochem. Soc.*, 2006, **153**, (1), G27–G29

[5] NGUYEN M., YOON S.: 'Effect of deposition temperature on the structural and electrical properties of NiCr thin film resistors by magnetron sputtering', *J. Electrochem. Soc.*, 2006, **153**, (7), G606–G608

[6] KWON Y., KIM N., CHOI G., LEE W., SEO Y., PARK J.: 'Structural and surface properties of NiCr thin films prepared by DC magnetron sputtering under variation of annealing conditions', *Microelectron. Eng.*, 2005, **82**, (3–4), pp. 314–320

[7] LEE B., PARK G., KIM J., LEE D.: 'The effect of the process parameters on the electrical properties of NiCrSi alloy thin film resistors'. Conf. Electrical Insulation and Dielectric Phenomena (CEIDP), Annual Report, 2002, pp. 72–74

[8] VAN DEN BROEK J., DONKERS J., VAN DER RIJT R., JANSSEN J.: 'Metal film precision resistors: resistive metal films and a new resistor concept', *Philips J. Res.*, 1998, **51**, (3), pp. 429–447

[9] BIRKETT M., BROOKER J., PENLINGTON R., WILSON A., TAN K.: 'Effects of annealing on the electrical properties of NiCr vs AlCu thin film resistors prepared by DC magnetron sputtering'. Proc. Capacitor and Resistor Technology Symp., (CARTS), 2006, pp. 307–315

[10] ZHIGAL'SKII G., JONES B.: 'The physical properties of thin metal films', *Electrocompon. Sci. Monogr.*, 2003, **13**, pp. 1–33

[11] WISSMANN P., FINZEL F.: 'Electrical resistivity of thin metal films', *Springer Tracts Mod. Phys.*, 2007, **223**, pp. 9–34

[12] SCHUMANN W., BRUCKNER W., HEINRICH A.: 'Properties and applications of vacuum deposited CuCr films', *Thin Solid Films*, 1993, **228**, (1–2), pp. 44–48

[13] HUR S., KIM D., KANG B., YOON S.: 'Effect of the deposition temperature on temperature co-efficient of resistance in CuNi thin film resistors', *J. Vac. Sci. Technol. B*, 2004, **22**, (6), pp. 2698–2701

[14] BS EN 60115-1: 'Fixed resistors for use in electronic equipment', 2001

Effects of Annealing on the Electrical Properties of NiCr vs AlCu Thin Film Resistors Prepared by DC Magnetron Sputtering

Martin Birkett[1*], Jason Brooker[1], Roger Penlington[2], Alasdair Wilson[2], Kian Tan[2]

[1]TT Electronics Welwyn Components Ltd, Welwyn Electronics Park, Bedlington, Northumberland. NE22 7AA, UK
Tel: +441670 536737, Fax: +441670 821437
martin.birkett@welwyn-tt.com
[*]Corresponding author

[2]Northumbria University, School of Computing, Engineering & Information Sciences, Newcastle-upon-Tyne. NE1 8ST, UK

Abstract

NiCr is widely used in the manufacture of thin metal film resistors (TFR) in the value range 10Ω to 1MΩ because of its relatively large resistivity, low temperature co-efficient of resistance (TCR) and excellent stability of resistance. However the demand for TFR's with ohmic values of less than 10Ω has significantly increased in recent years due to the rising demand for low-loss current sensing in many electronic products. Consequently this trend has highlighted a number of problems associated with the manufacture of lower resistance NiCr films, primarily increased film thickness and hence increase in deposition time.

This paper investigates the electrical properties of AlCu as a replacement for NiCr in this lower resistance range. Films of NiCr and compositions of AlCu were prepared by DC magnetron sputtering in Ar. After deposition the films were annealed in both air and N_2 atmospheres at a range of temperatures. A direct comparison of electrical characteristics of the two film systems was then performed. Results reveal that an increase in Al content produces a decrease in TCR and gives an improvement in resistance stability. A wide region of alloy composition exists where films with equivalent resistance stability and sheet resistance to NiCr can be obtained at lower deposition times.

Introduction

In general thin film axial resistors are manufactured by depositing a sub μm layer of metal onto a ceramic core then heat treated to give a pre-value [1]. The resistor is then adjusted to target value by removing part of this metal film, usually by a helical cut produced by a laser or cutting wheel [2]. Termination leads are then fitted, before the component is encapsulated in a protective coating.

Of the metal alloy systems available for the manufacture of TFR's, NiCr is perhaps the most widely reviewed, either in a binary or ternary system with small additions of doping elements [3-7]. NiCr is widely regarded as good all round film as it can cover a wide pre-value sheet resistance (Rs) range of around 1-1000Ω/□ whilst maintaining excellent electrical properties such as a temperature co-efficient of resistance (TCR) of ≤50ppm/oC and resistance stability (ΔΩ/Ω) of <0.1% [8]. However although this is perfect for values in the middle of the range problems with film thickness can arise at the two extremes, thin film for high resistance values >500Ω/□ and thick film for low resistance values <1Ω/□. Problems associated with thin films can largely be overcome through the use of CrSiO, which has a higher resistivity than NiCr, hence producing a thicker film for the same sheet resistance [9-10]. However at the thicker film low resistance range, there has been little improvement and NiCr remains the preffered film [11]. Currently there exist a number of problems with this range such as long deposition times, and problems with cutting through the thicker film, which is often only achieved through a reduction in machine output speed. Hence, a film system with a lower resistivity than NiCr, which can produce a thinner film for the same sheet resistance, is required for the economic production of pre-value resistors of <1Ω/□. Moreover, with ever increasing energy prices, the demand for lower value resistors in fixed current applications has never been more apparent.

This study explores the possibility of using a binary alloy system of AlCu to try and overcome these problems. Various compositions of AlCu were deposited and then compared directly to films of NiCr manufactured under exacting conditions. Rs, TCR and ΔΩ/Ω were measured as a function of post deposition annealing temperature and environment, Air or N_2.

Experimental

A summary of the manufacturing procedure is given in Figure 1.

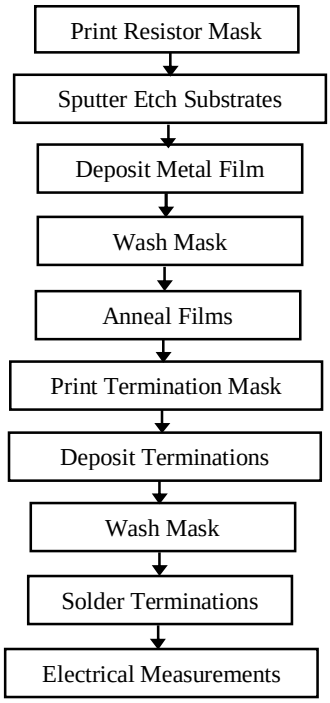

Figure 1: Sample manufacturing procedure

Substrates used were 50.8mm x 50.8mm x 0.635mm thick 93-96% Al_2O_3, which were screen printed with a mask to produce sixteen, 20mm x 4mm resistors patterns. Both the AlCu and NiCr films were deposited at room temperature by DC magnetron sputtering technique. The NiCr samples were sputtered from a 99.999% pure 378mm x 120mm x 8mm target. The AlCu samples were sputtered from 99.99% pure Al and Cu 21mm x 120mm x 8mm pieces. Eighteen of these pieces could be assembled to produce a standard target sizes of which the %area composition could be varied by approx 5.5% to allow for a possible nineteen compositions to be trialled. Of these, the following compositions by %area were investigated (Figure 2):

	% Target surface area						
Cu	100	83	66	50	34	17	0
Al	0	17	34	50	66	83	100

Figure 2 – AlCu sputtering target compositions

The vacuum plant employed was a CPA 9900, which was evacuated to a base pressure using a combination of a mechanical roughing pump and cryo pump. Pure Ar was introduced at a constant flow rate to achieve the desired sputtering pressure. The substrates were then sputtered etched prior to the metal films being deposited. Following deposition, the samples were annealed at temperatures of 200, 300, 400 and 500°C in both air and N_2 atmospheres. The samples were then screen printed with a conductor mask to allow metallic measurement contacts to be sputtered directly on top of the films.

Electrical measurements were then conducted using a four probe measurement system. TCR was measured between 20°C and 70°C and calculated using Equation 1. Resistance stability checks entailed 168 hours at 155°C, with interim measurements being taken after 24 and 48 hours.

$$TCR = \frac{(Rb - Ra) \times 10^6}{Ra\,(Tb - Ta)} \quad ppm/^oC$$

Ra = Ω @ 20°C Rb = Ω @ 70°C Ta = 20°C Tb = 70°C

Equation 1: Calculation of TCR [1]

Results and Discussion

Results of as deposited Rs and TCR are shown in Figure 3. As can be seen a reduction in sheet resistance of between approximately 2 and 35 times that of the NiCr film can be achieved across the range of AlCu compositions. The films sputtered from pure Cu and pure Al gave the lowest sheet resistances of 0.10 and 0.40Ω/□ respectively, that of copper, being lower which compares to the bulk resistivities generally reported for the two elements [12]. However once aluminium is added to the pure copper target to form an alloy the sheet resistance begins to increase. At a composition of Al/Cu 17/83 %area this figure is approximately 0.25Ω/□ and rises quite linearly with increase in Al% to a peak of approximately 1.8Ω/□ at 66%Al. This follows the commonly accepted theory that alloys are always less conductive than the pure metals they are made from, as the presence of solute atoms increases the possibility of collisions between moving electrons and the ions constituting the crystal structure. Hence resistivity rises with increasing impurity concentration, usually reaching a maximum for an alloy composition of approximately 50% "impurity" [1, 12]. However, as the bulk resistivity of Al is significantly greater than that of Cu it follows that the more Al rich alloys have the higher Rs value.

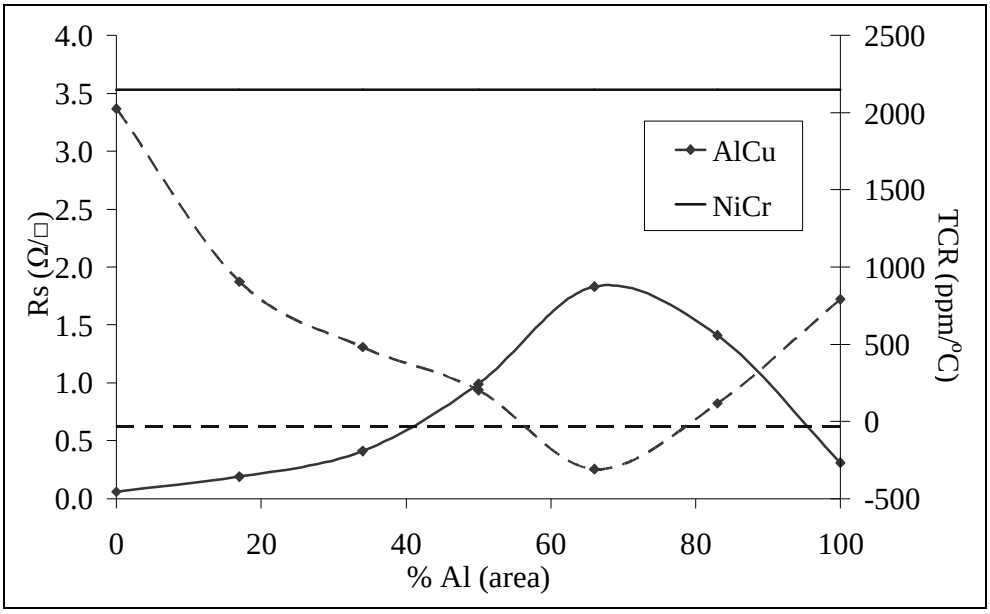

Figure 3 – As deposited Rs and TCR

Results for as deposited TCR produce a plot of virtual mirror image to that produced for sheet resistance (Figure 3). Values for the two elements in bulk are large and positive at around 2000ppm/°C for Cu and 800ppm/°C for Al. This figure then decreases with increase in Al content once in alloy form to a minimum of around –300ppm/°C for the film sputtered from 66%area Al. The TCR value of the NiCr film was around –30ppm/°C. Again, these result correspond quite closely to those published by other researchers [1-8, 13]

Post Annealing

Figures 4 and 5 show results of Rs for the various film compositions following annealing in air and N_2 respectively. In general Rs for the films more rich in Cu appears to remain unchanged with increase in temperature, whereas that for Al rich films tends to decrease. The result for NiCr is similar to that of Cu and does not appear to vary with temperature. A comparison of Rs obtained for films stabilised in Air and N_2 appear to be very similar, hence posing the suggestion that stabilisation environment, whether Air or N_2, has little or no affect on Rs of the films. In terms of relative RS, as both the NiCr and AlCu films decreased by similar amounts during the stabilisation process the advantage is further increased to at least 5 times for the films treated at 500°C.

Figures 6 and 7 show TCR results for the different film compositions following annealing in air and N_2 respectively. It can be clearly seen that increase in stabilisation temperature results in increase in TCR, again regardless of heat treatment environment. This result corresponds to that reported by a number of authors, where heat treatment is used to shift the TCR of a film positive as well as stabilising it and indeed follows the general theory of annealing out impurities in the film leading to properties of that corresponding to the bulk metals themselves [1].

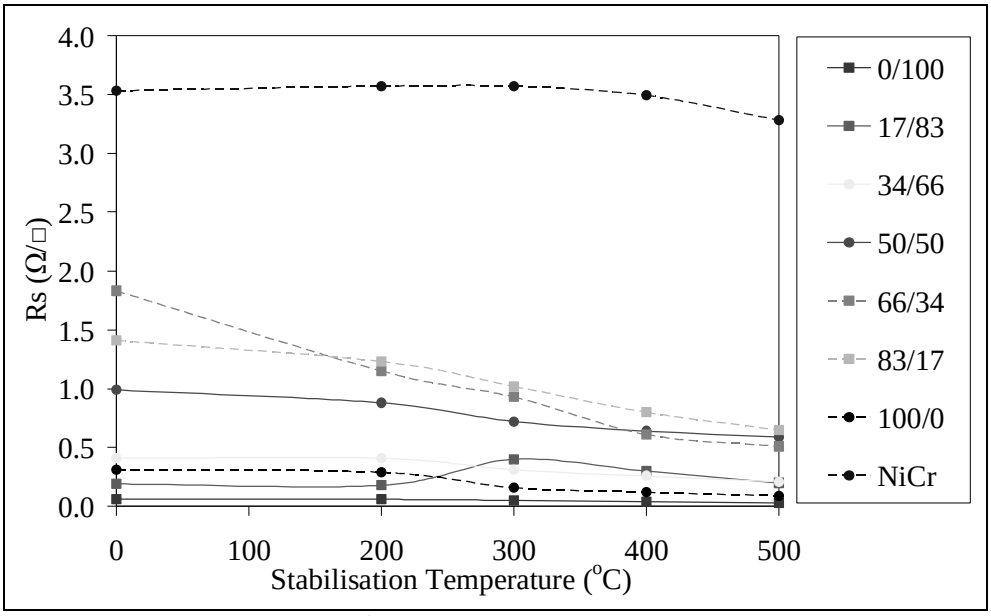

Figure 4: Rs following annealing in air atmosphere

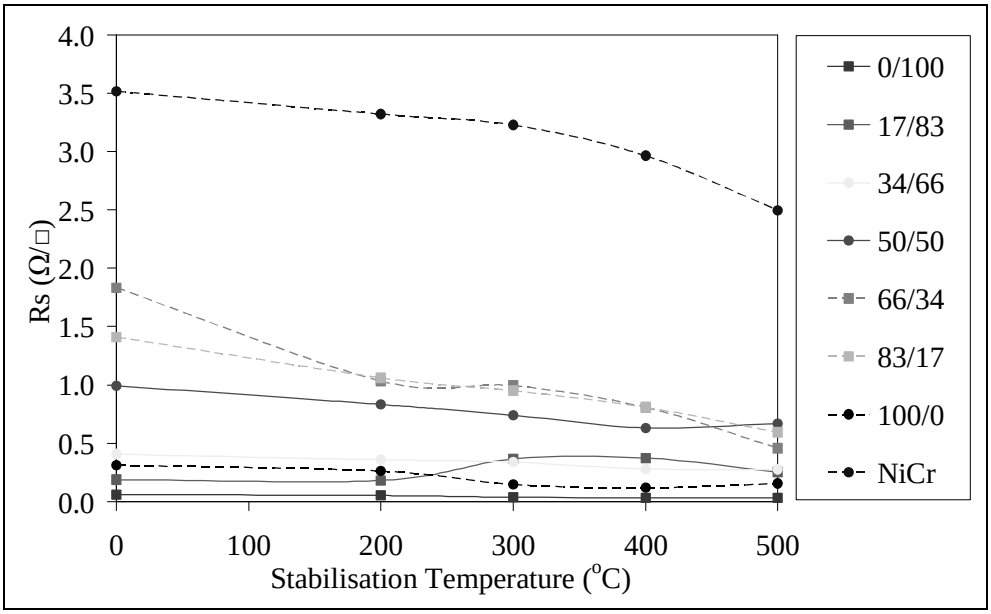

Figure 5: Rs following annealing in N_2 atmosphere

Possibly the most striking area of this result is the difference in TCR response to temperature between the pure elements and the alloys. As can be seen the films of pure Cu and Al rise steeply to peaks of around 4300 and 3500 ppm/°C respectively after stabilisation at 400°C, before decreasing to final values of 4000 and 3000ppm/°C following treatment at 500°C. This positive shift can be explained by the aforementioned theory and perhaps the then negative shift at higher temperatures could be attributed to degradation of the films. Conversely the results obtained for the NiCr and AlCu alloys are relatively stable and TCR increases appear to be more gradual. Further analysis shows that the TCR of the AlCu films move positive quite linearly throughout the temperature range whilst that of NiCr remains unchanged until 300°C where it then begins transition from negative to positive. Again this corresponds closely to results reported for various alloys of NiCr [1-8] and is one of the reasons for its wide spread dominance as the favoured resistive thin film. A further breakdown of the results for the AlCu films shows that they all follow a very similar curvature with the copper rich films always remaining more positive than the Al rich. Perhaps one exception to this observation is the result of the 66% area Al film, which as deposited looked promising with a TCR of around –300ppm/°C. As can be seen this result soon becomes positive with a value approaching 500ppm/°C following stabilisation at 200°C.

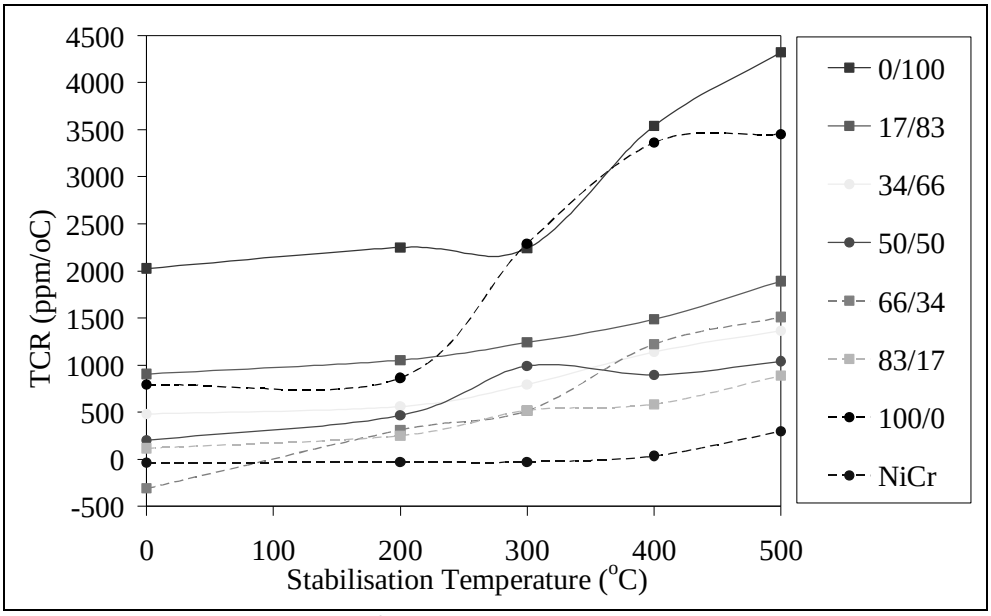

Figure 6: TCR following annealing in air atmosphere

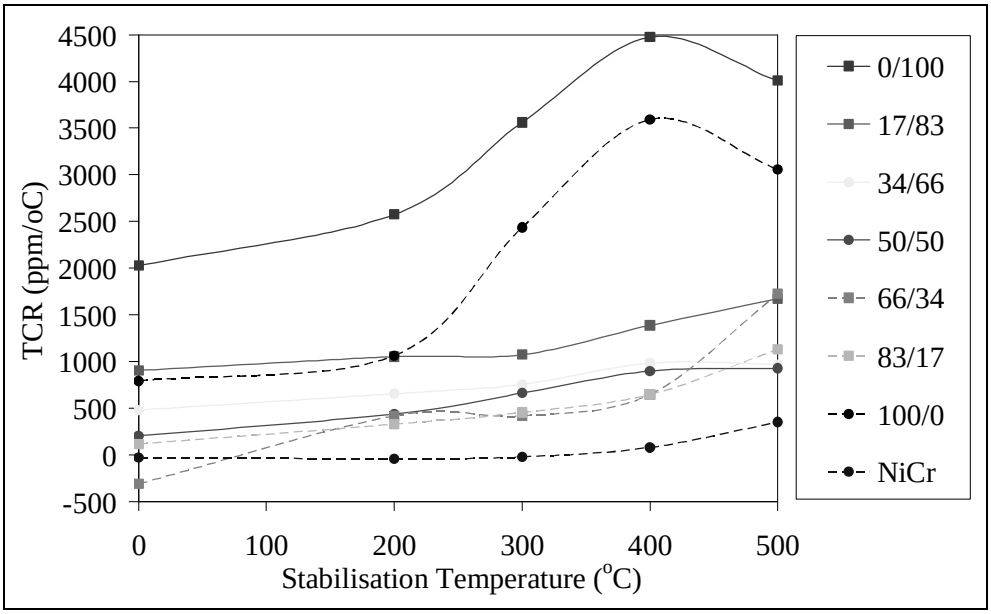

Figure 7: TCR following annealing in N_2 atmosphere

Resistance Stability

Results for mean resistance stability, 168hrs at 155°C, of the various film compositions following stabilisation in Air and N_2 at 200 and 300°C are given in Figure 8. An initial view of the data presented suggests films with an Al content of less than 40% area are very unstable, regardless of stabilisation temperature or environment. The most plausible reason for the huge positive shifts in resistance is oxidation of the Cu rich films. Figure 9 shows the same stability results with the $\Delta\Omega/\Omega$ range tightened. As expected the stability of the NiCr films is better than 0.30% regardless of heat treatment regime. Moreover the most stable of the NiCr samples appears to be that which was annealed in N_2 at 200°C. Changes of around 0.20% were produced for these films, which correlate closely to the findings of other researchers [1-8] who also reported stability results of 0.1-0.3% for NiCr films treated under the same conditions. Of the AlCu films those, which were treated in N_2, appear to be more stable. The most stable of the AlCu samples appears to be 83%area Al stabilised at 200°C in N_2. This film produced a mean change in resistance of approximately 0.1%. However samples annealed at 300°C in N_2 gave more consistent results with stabilities of around 0.3% reported for films with Al contents in the range 33 to 83%. This figure corresponds with the work of Bashev et al [13] who recorded stability figures of no worse than 0.4% for AlCu films containing 46%wt or more Al. For pure Al films treated at both 200 and 300°C the stability increases to around 1%.

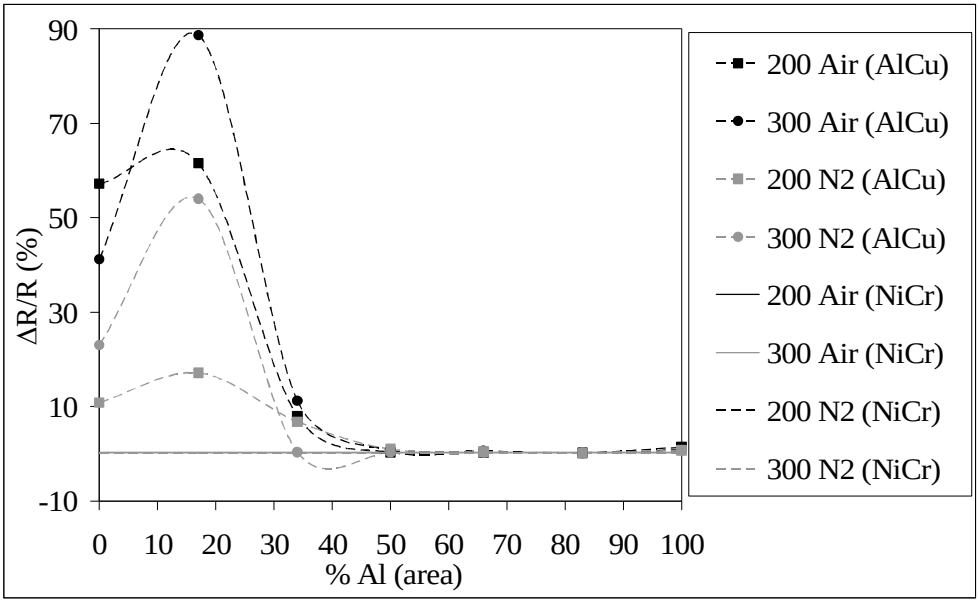

Figure 8: Resistance stability following 168hrs at 155°C

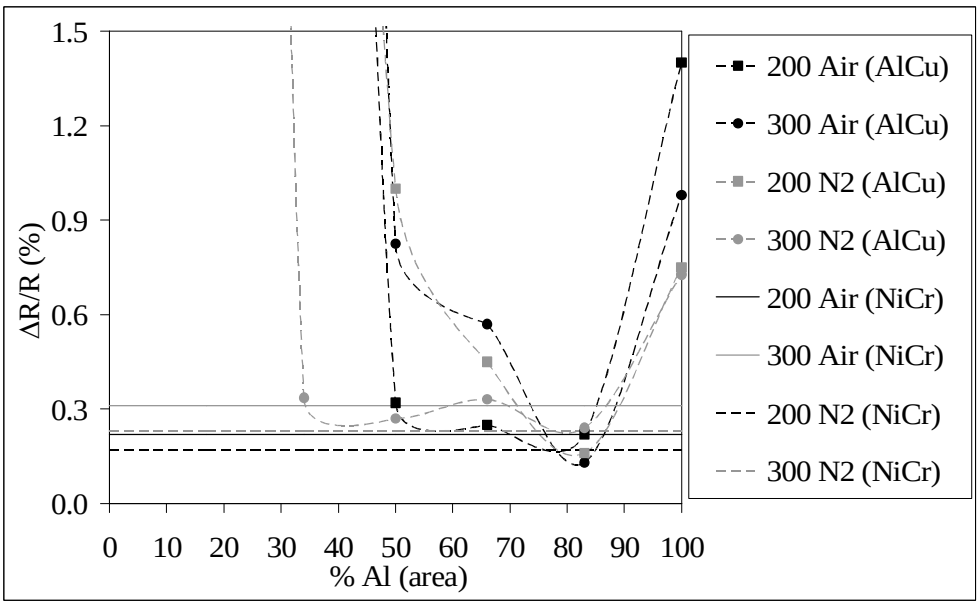

Figure 9: Resistance stability following 168hrs at 155°C - ΔΩ/Ω range tightened

Conclusion

From the work conducted thus far it is quite evident that a binary system of Al and Cu shows much promise in the application of a thin metal film resistor. Ultimately there is a number of detailed specification and criteria to which a component must conform before it can be deemed 'fit for purpose' [14]. However in order to establish an initial impression of a resistors performance, two tests which are more than suitable are that of TCR (20 and 70°C) and also dry heat stability (168 hours at 155°C).

From the results presented for TCR it can be established that only the films with 50% area or more Al have an as deposited value anywhere close to the target of ≤50ppm/°C, whilst that of the Cu rich films and indeed the pure Al and Cu films is large and positive at between 500 and 2000ppm/°C. Furthermore this inadequacy is then amplified following heat treatment stabilisation where TCR is proportional to temperature increase across the composition range and thus the near suitable TCR of the Al rich films soon extends to values of near 500ppm/oC. This trend appears to remain true regardless of heat treatment environment, air or N_2,

A similar result can be concluded for that of resistance stability, where again it appears that a minimum of 33%area Al is required before any sensible figure can be established. On this occasion those films pre heat treated in N_2 atmosphere gave the best results with a consistent figure of 0.3% produced by films annealed at 200°C.

Although at this stage it is still difficult to assess the suitability of AlCu in terms of overall electrical performance it is still useful to compare its fundamental electrical characteristics against those of NiCr, as ultimately it is the performance of this film, which must be met.

	Rs (Ω/□)	TCR (ppm/°C)	ΔR/R (%)
NiCr	3.8	-40	0.17
AlCu (66/34)	1.1	+420	0.10

Figure 11 – Comparison of the fundamental electrical characteristics of NiCr and AlCu thin film resistors stabilised at 200°C in N_2.

Figure 11 shows the best results achieved for an AlCu film compared to that of a NiCr film sputtered and stabilised under identical conditions. As can be seen one major objective can already be satisfied in that the Rs value for the AlCu film is approximately 3.5 lower than that of NiCr, thus lower pre-values could be sputtered at faster rates. Moreover the stability of the AlCu film is also comparable to that of NiCr. However one obvious concern at this stage that must be addressed is the large positive TCR of the AlCu film.

Summary of Conclusions

- Thin metal films of AlCu offer a reduction in Rs of between 2 and 25 times that of NiCr films
- Films rich in Cu have the lowest Rs
- Films rich in Al are the most stable and have the lowest TCR
- A minimum of 33%area Al content is required to produce a film of reasonable stability
- A minimum of 50%area Al content is required to produce a film with reasonable TCR
- Heat treatment stabilisation temperature increase causes decrease in Rs and increase in TCR
- Heat treatment stabilisation environment, air or N2 does not appear have any significant relevance

Recommendations for Further Work

- Conduct further investigations into AlCu films with an Al content of between 50-90%area.
- Investigate performance of AlCu films during further assembly processes
- Investigate structural properties of AlCu films

Acknowledgements

This work was funded and supported by TT Electronics Welwyn Components Ltd and an Industrial Fellowship awarded by the Royal Commission for the Exhibition of 1851

References

[1] Maissel, L & Glang, R (1970), Handbook of Thin Film Technology, McGraw-Hill Publications.
[2] Schultze, V & Fischer, A (1989), *Thin Solid Films*, 182(1-2) pg 23-34
[3] Nocerino, G & Singer, K (1978), *Thin Solid Films*, 57(2) pg 343-348.
[4] Schippel, E (1987), *Thin Solid Films*, 146(2) pg 113-138.
[5] Schippel, E (1984), *Thin Solid Films*, 123(1) pg 57-62.
[6] Schippel, E (1986), *Thin Solid Films*, 144(1) pg 21-28.
[7] Lee, B et al (2002), *Conference on Electrical Insulation and Dielectric Phenomena (CEIDP), Annual Report, 2002*, pg 72-74.
[8] Van Den Broek, J et al (1998), *Philips Journal of Research*, 51(3) pg 429-447.
[9] Jankowski, A (1998), *Thin Solid Films*, 332 pg 272-276.
[10] Dong, X et al (2000), *Shanghai Jiaotong Daxue Xuebao/Journal of Shanghai Jiaotong University*, 34(12) pg 1610-1614.
[11] Kwon, Y et al (2005), *Microelectronic Engineering*, 82 pg 314-320
[12] Higgins, R (1994), Properties of Engineering Materials, Edward Arnold Publications.
[13] Bashev, V et al (1990), *Physics of Metals and Metallography (English translation of Fizika Metallov i Metallovedenie)*, 70(5) pg 203-205.
[14] BS CECC 40101-004/804